Inaugural dissertation

for

obtaining the doctoral degree

of the

Combined Faculty of Mathematics, Engineering and Natural Sciences

of the

Ruprecht - Karls - University

Heidelberg

Presented by

M.Sc. Xin Cheng

born in: Sichuan, China

Oral examination: 27.06.2025

MUTE promotes the development of stomatal subsidiary cells in the succulent model *Kalanchoë laxiflora*

Referees: Prof. Dr. Thomas Greb

Prof. Dr. Michael Raissig

Acknowledgments

At the end of my doctoral study, I would like to thank all the people who have helped me in the past four years, because you make me feel extremely lucky. In addition to a doctoral degree, I have gained more valuable things in these four years, so I believe that these four years are a very precious experience in my life.

First, I thank Prof. Dr. Michael Raissig for allowing me to pursue my doctorate in the best Raissig-Lindner Lab. You let me see for the first time what a scientist who loves science looks like, who does not follow the crowd and has always been firmly engaged in the basic research they love. Thank you for your tireless supervision and help over the past few years and for helping me build my confidence.

Big hug and thanks to Dr. Heike Lindner; I still remember the summer four years ago, when I had just passed the exam of HBIGS and attended the lab party for the first time; you waved and walked towards us, saying to me, "Xin, I am so proud of you." I will never forget this scene in my life, because you were the first person to say this to me besides my parents. It is as warm as spring for someone who has just come to a foreign country. Thank you for supervising, teaching, caring, and encouraging me over the past few years. In the future, I hope to remember your encouragement whenever I have hard times. More importantly, thank you for the positive influence on my life. Because of you, I also want to be a considerate and gentle person.

Thanks to Lea for your company over the past four years. Without your support, it is hard to imagine how I could have persisted in completing my Ph.D. Thank you for your generous and selfless help, encouragement, and care for me. Before this, I never thought I would gain such a precious friendship in a foreign country. You also made me realize that life is not just about chasing fame and paper. Happiness is simple, such as eating ice cream and chatting with friends on a summer afternoon. More importantly, thank you for teaching me how to love and care about others.

Giving a big hug to my brother, Ari. I don't have siblings with the same parents, but thank you for allowing me to feel the love and care of my siblings in this life. It also made me realize that having siblings is more pleasant than growing up alone. Thank you for always being so tolerant of me and generous in helping me. It's a pity we didn't spend much time together, but our friendship will not end here.

Thank you to Tiago and Dan for your help and care when I first arrived. I am also very happy that, in addition to being colleagues, we have also become good friends.
Thanks to all the members of my lab during my four years of Ph.D. study. Big hug and thanks to Roxy. You are always such a nice and sweet person. You helped me generously and encouraged me when I had tough times with my experiments, and I also want to tell you: "Roxy, you are the best!". Big thanks also to Kim; we had a great time working in the lab and hanging out downtown. Huge hug to Lidia; you are always kind and friendly; thank you for hugging me when I was so stressed about my experiments. Thank you, Nastia, for always caring about me and paying attention to whether I am happy. Thank you so much, Paola; you always provide generous and selfless help to members when they need help. Thank you for encouraging me when I was sad. I will never forget the joyful laughter and positive energy you always bring. In addition, thank you to Saiko, Alec, Charlotte, Aurelia, and Pawandeep.
I also appreciate Christopher and Jasmin's generous help caring for our plants at the Institute of Plant Science of the University of Bern. Because of your careful care of the plants, our experiments went so smoothly. I would also like to thank Jasmin for organizing hiking, movie nights, and beer hours at the institute. The most important thing is, thanks for being my friend.
I would like to thank all my TAC members and Thesis committee members. Thank you to Prof. Dr. Thomas Greb and Prof. Dr. Jan Lohmann for your guidance, valuable advice on my project over the past few years, and positive encouragement. Thanks so much to Prof. Dr. Yasin Dagdas and Dr. Kasper van Gelderen for joining my thesis committee.
I would also like to thank my friends I met at the University of Heidelberg. Thank you so much to Penfei and Xiaomin for your encouragement and companionship during my Ph.D.; I will never forget our happy time in Heidelberg.
Ultimately, I want to thank my parents for always loving me, trusting me, supporting me in doing whatever I want, and being proud of me.

Abstract

Stomata, tiny valves in the plant epidermis, regulate the gas exchange for photosynthesis and transpiration, thus playing an essential role in plants' water-use efficiency and stress tolerance. In most land plants, stomata are composed of two kidney-shaped guard cells (GCs) surrounding a central pore. However, novel stomatal morphologies have also been discovered in some species. For example, in grasses, two dumbbell-shaped GCs are flanked by two subsidiary cells (SCs) that contribute to faster stomatal movement and higher water-use efficiency of grasses.

Stomata with SCs are also typical in most succulents. Succulents adopted an innovative photosynthetic lifestyle, where gas exchange occurs at night to avoid severe transpiration during the day to adapt to survival in arid conditions. The stomata in *Kalanchoë laxiflora*, an emerging model system in succulents, include two kidney-shaped GCs surrounded by three unequal-sized, circularly arranged SCs. Research showed that ions shuttle between GCs and SCs in the stomata of *K. laxiflora*, like grasses, suggesting that these SCs might be functionally relevant to stomatal movement. However, the development and function of these anisocytic SCs are unknown. In my study, I focused on the stomatal development in *K. laxiflora*.

Firstly, I established protocols to establish *K. laxiflora* as a model system for stomatal research, including horticultural protocols, tissue culture-based genetic transformation protocols, staining protocols for microscopy imaging, and cloning protocols.

Secondly, based on static imaging, I identified and analyzed each stage of stomatal development of the anisocytic, mesogenous stomatal complex in *K. laxiflora*. In addition, light microscope imaging and quantification in different pairs/sizes of wild type (WT) leaves showed that the stomata on the leaf epidermis gradually develop and differentiate into GCs as the leaves grow. Notably, the 6th pair of leaves are already “mature leaves” for stomatal development.

Thirdly, CRISPR-CAS9-mediated gene editing, reporter lines, and overexpression lines suggested that the two orthologs of the key stomatal transcription factor *AtMUTE*, *KlMUTEs,* promote asymmetric divisions to form SCs in *K. laxiflora*. This is functionally opposite to *AtMUTE*, which terminates the asymmetric divisions and promotes cell fate transition and stomata differentiation in *Arabidopsis thaliana*.

Furthermore, Bulk RNA-sequencing revealed a potential genetic program regulated by *KIMUTE1* for promoting asymmetric divisions during stomatal development.

Overall, this study revealed the development process of a novel stomatal morphotype and a genetic mechanism that regulates the formation of the anisocytic SCs in the succulent model *K. laxiflora*.

Zusammenfassung

Spaltöffnungen (Stomata), kleine Ventile in der Pflanzenepidermis, regulieren den Gasaustausch für Photosynthese und Transpiration, und spielen daher eine essenzielle Rolle für die Wassernutzungseffizienz und Stresstoleranz von Pflanzen. In den meisten Landpflanzen bestehen Stomata aus zwei nierenförmigen Schließzellen (guard cells, GCs), die eine zentrale Pore umgeben. In manchen Spezies wurden aber auch neuere Morphologien von Stomata entdeckt. In Gräsern, beispielsweise, sind zwei hantelförmige GCs flankiert von zwei Nebenzellen (subsidiary cells, SCs), die zu schnelleren stomatalen Bewegungen und höherer Wassernutzungseffizienz von Gräsern beitragen.

Stomata mit SCs sind auch typisch in den meisten Sukkulenten. Sukkulenten haben einen innovativen Lebenszyklus angenommen, bei dem Gasaustausch nachts stattfindet, um starke Transpiration während des Tages zu vermeiden, als Anpassung an aride Bedingungen. Die Stomata in *Kalanchoë laxiflora*, einem sich entwickelnden Modellsystem der Sukkulenten, enthalten zwei nierenförmige GCs, die von drei zirkulär arrangierten SCs umgeben sind. Untersuchungen haben ergeben, dass Ionen, wie auch in den Gräsern, zwischen GCs und SCs in den Stomata von *K. laxiflora* ausgetauscht werden, was darauf hindeutet, dass diese SCs funktionell relevant für die stomatale Bewegung sind. Die Entwicklung und Funktion dieser anisozytischen SCs ist aber bisher unbekannt. In meiner Arbeit habe ich mich auf die stomatale Entwicklung in *K. laxiflora* fokussiert.

Zuerst habe ich Protokolle etabliert, um *K. laxiflora* als Modellsystem für stomatale Forschung auszubauen, inklusive Protokollen für die Gärtnerei, gewebekulturbasierte genetische Transformation, Färbung für Mikroskopie und Protokollen für die Klonierung.

Als zweites habe ich, basierend auf statischer Bildgebung, alle Stufen der stomatalen Entwicklung der anisozytischen, mesogenen stomatalen Komplexe in *K. laxiflora* identifiziert und analysiert. Des Weiteren haben Lichtmikroskopie und Quantifizierung in verschieden Paaren/Größen von Wildtyp (WT)-Blättern gezeigt, dass die Stomata in der Blattepidermis sich graduell entwickeln und zu GCs differenzieren, während die Blätter wachsen. Auffallend ist, dass das sechste Blattpaar bereits „ausgewachsen“ ist im Bezug auf stomatale Entwicklung.

Drittens wiesen CRISPR-CAS9-vermittelte Genmodifizierung, Reporterlinien und Überexpressionslinien darauf hin, dass die zwei Orthologe des Schlüsseltranskriptionsfaktors *AtMUTE*, *KlMUTE*, asymmetrische Zellteilungen unterstützen, die die SCs in *K. laxiflora* formen. Dies ist funktionell gegensätzlich zu *AtMUTE*, das die asymmetrischen Zellteilungen beendet und den Übergang der Zellidentität und stomatalen Differenzierung in *Arabidopsis thaliana* fördert. Zusätzlich hat Bulk RNA-Sequencing ein potenzielles genetisches Programm aufgedeckt, das von *KlMUTE1* reguliert wird und die asymmetrische Zellteilung während der stomatalen Entwicklung unterstützt.

Zusammengefasst hat diese Studie die Entwicklungsprozesse eines neuen stomatalen Morphotypen aufgedeckt, und einen genetischen Mechanismus, der die Formierung von SCs in dem Sukkulentenmodell *K. laxiflora* reguliert.

Abbreviation

ABA	Abscisic acid
ACD	asymmetric cell division
AFB	AUXIN-BINDING F-BOX
ARFs	AUXIN RE SPONSE FACTORs
ARRs	ARABIDOPSIS RESPONSE REGULATORs
Aux/IAA	AUXIN/INDOLEACETIC ACID
AXR3	AUXIN RESISTANT3
BAK	BRIASSOCIATED RECEPTOR KINASE
BASL	BREAKING OF ASYMMETRY IN THE STOMATAL LINEAGE
BDL	BODENLOS
BES1	bri1-EMS SUPPRESSOR1
bHLH	basic helix – loop–helix
BIN2	BRASSINOSTEROID INSENSITIVE 2
BRI	BRASSINOSTEROID INSENSITIVE
BRs	Brassinosteroids
BRXf	BREVIS RADIX family
BZR1	BRASSINAZOLE RESISTANT 1
CAM	Crassulacean Acid Metabolism
C_i	intercellular CO2 concentration
CIM	Callus induction medium
CK	Phytohormone cytokinin

CLL	CHALLAH-LIKE
CO_2	carbon dioxide
COP1	CONSTITUTIVE PHOTOMORPHOGENIC 1
CRY	cryptochrome
DEG	Differentially Expressed Gene
EPFL	EPF-LIKE
EPFs	EPIDERMAL PATTERNING FACTORS
ER	ERECTA
FLP	FOUR LIPS
GA	gibberellin
GCs	guard cells
GMC	guard mother cell
GSK3	GLYCOGEN SYNTHASE KINASE3
HDG	HOMEODOMAIN GLABROUS
H_2S	hydrogen sulfide
HSPs	HEAT SHOCK PROTEINS
ICE1	INDUCER OF CBF EXPRESSION1
JA	jasmonic acid
LRR	leucine-rich repeat
MAPK	mitogen-activated protein kinase
MMC	Meristemoid mother cell
MP	MONOPTEROS

OBG	Oxford Botanical Garden
OPLs	OCTOPUS-LIKES
PC	pavement cell
PCA	Principal Component Analysis
PEP	phosphoenolpyruvate
PEPC	phosphoenolpyruvate carboxylase
phy	phytochromes
PI	propidium iodide
PIFs	phytochrome-interacting factors
POLAR	POLAR LOCALIZATION DURING ASYMMETRIC DIVISION AND REDISTRIBUTION
PPB	preprophase band
RIM	Root induction medium
RLKs	receptor-like kinases
SCRM	SCREAM
SCs	subsidiary cells
SDD1	STOMATAL DENSITY AND DISTRIBUTION1
SERK	SOMATIC EMBRYOGENESIS RECEPTOR KINASE
SIM	Shoot induction medium
SLGC	Stomata lineage ground cell
SMC	subsidiary mother cells
SMR4	SIAMESE-RELATED4

SPCH	SPEECHLESS
TIR1	TRANSPORT INHIBITOR RESPONSE 1
TMM	TOO MANY MOUTHS
VPD	vapor pressure deficit
WT	wild type
YDA	YODA

Table of Contents

Introduction

1. Stomata: gas-exchange gatekeepers in the epidermis

Our lives rely on photosynthesis, which gives us sugar and oxygen. Plant photosynthesis comprises two reactions: the light reactions and the carbon dioxide (CO_2) fixation reaction. How is CO_2 diffused into interior leaves from the atmosphere? Stomata, which originated over 400 million years (Myr) ago, are breathing pores in the leaf epidermis and connect the inside of plants with the outside atmosphere (Harrison et al., 2019; Nunes et al., 2020). Stomata play an essential role in balancing the CO_2 absorption for photosynthesis with water vapor release for transpiration. Therefore, it determines the water-use efficiency and drought tolerance of plants (Cheng & Raissig, 2023). The stomatal pore aperture, number, size, and spacing of stomata are controlled to regulate leaf gas exchange (Franks & Farquhar, 2007; Woodward, 1987). Improving water-use efficiency by manipulating stomata is crucial for future plants and crops to cope with increasingly dry and warm climate change (Haworth et al., 2021). In addition to its physiological significance, stomata are also used as a developmental system to learn developmental biology, since the stomatal development in leaf epidermis of dicot model plants *Arabidopsis thaliana* include lots of fundamental development processes, for example, cell polarity and cell fate specification, cell-cell communication and patterning (Bergmann & Sack, 2007; Lau & Bergmann, 2012; Pillitteri & Torii, 2012). In recent years, there have also been some studies on exploring plant evolution through studying stomata (Veselý et al., 2020).

1.1 Stomatal arrangement and ontogeny among different species

The stomata is usually composed of two GCs, which can open and close by turgor-driven GC movements (Jezek & Blatt, 2017; Lawson & Blatt, 2014), like the stomata in *Arabidopsis thaliana* and a lot of other land plants (Bergmann & Sack, 2007). It is worth noting that, in some plants, GCs can be surrounded by one or more cells that differ in size, shape, arrangement, and sometimes in content from the pavement cells (PCs), so-called SCs (Esau, 2006; Gray et al., 2020). The

arrangements of SCs and stomatal morphology are quite different among species, and the details of the stomatal types classified by the arrangement of stomatal SCs and the ontogeny of GC-surrounding cells (including SCs and PCs) were well described (Rudall et al., 2013).

Stomata in which all neighboring cells stem from different precursor cells than the precursor of the guard mother cell (GMC) belong to perigenous type based on the classifications of ontogenetic stomata types (Pant, 1965), like in grasses (Raissig et al., 2016). Stomata, in which all neighboring cells and GCs are developed from the same precursor cell, are called mesogenous type, like in *Kalanchoë laxiflora* (Nunes et al., 2020; Pant, 1965). Like the stomata in *A. thaliana*, at least one neighboring cell stems from the same precursor cell of the GMC, while all other neighboring cells stem from different precursor cells; thus, the stomata are called mesoperigenous (Pant, 1965).

According to Van Cotthem, eight morphological groups were classified (Van Cotthem, 1973). For example, some plants have paracytic stomata, in which two GCs are surrounded by two parallel SCs (Van Cotthem, 1973), like the stomata in *Portulaca oleracea*; each stomata complex includes two kidney-shaped GCs and two parallel crescent-shaped SCs (Ogburn & Edwards, 2009; Voznesenskaya et al., 2010). The grasses have graminoid stomata, a paracytic type subclass because of the dumbbell-shaped GCs (Franks & Farquhar, 2007; Nunes et al., 2020). Many species of grasses have either dome-shaped or triangular-shaped SCs. For example, Brachypodium, barley, and wheat have dome-shaped SCs (Hughes et al., 2017; Lundgren et al., 2019; McKown & Bergmann, 2018), and stomata in maize and rice have two triangular-shaped SCs (Chaffey, 1983; Wang et al., 2019). In addition, 52 species of herbaceous bamboos of Olyrinae have also been identified to have dome-shaped or triangular-shaped SCs (Lima et al., 2019). Tetracytic stomata show the first pair of SCs stem from the asymmetric division of the neighbor cells from both lateral sides, and the second pair of SCs formed above and below the GCs, like the stomata in Tradescantia (Croxdale et al., 1992; Van Cotthem, 1973). *Sygzgium aromarticum L.* in the family Myrtaceae, for example, has actinocytic stomata surrounded by SCs that are a bit radically elongated (Khan et al., 2014). Diacytic stomata are defined as the stomata that include one or more pair of SCs, and the conjoint cell wall of the adjoining SCs is perpendicular to the GCs, which is found in the family Acanthaceae, for example, *Blepharis sindica* and *Reullia spp*

(Perveen et al., 2008; Prabhakar, 2004). Cyclocytic stomata include at least four SCs that form a ring around GCs (Prabhakar, 2004), which was found in *Ipomoea carnea* (Perveen et al., 2008). The stomata type in *A. thaliana* belongs to anomocytic stomata because it has only two kidney-shaped GCs and no SCs surrounded (Van Cotthem, 1973), and this stomata type is the most dominant since it's found in almost 70 dicot species (Khan et al., 2014). Different from Arabidopsis, in many species of Succulent Kalanchoë family like *K. laxiflora*, *K. fedtschenchoi*, and *K. lativerensis*, stomata is composed of three circular unequal-sized SCs and two kidney-shaped GCs, which is classified as anisocytic stomata (Van Cotthem, 1973). However, even if the morphological definition of SCs and morphological classes of stomata were given many years ago (Esau, 2006; Van Cotthem, 1973), there is still a lack of functional definition of SCs. Studies in grasses revealed that the SCs on both sides could help GCs open and close faster to respond to environmental changes, suggesting that the SCs are physiologically functional (Raissig et al., 2017). Except for grasses stomata, it is still uncertain whether these neighboring cells surrounding stomatal GCs, which have different morphologies from PCs, are functionally relevant in other species.

In summary, the stomatal SCs arrangement presents various types. However, from an evolutionary perspective, the evolution time and frequency of SCs are unknown. In the moss *Physcomitrium patens*, stomata are directly formed by an incomplete symmetric division of the protodermal cell (Chater et al., 2016). Therefore, the appearance of stomatal SCs means a more complex division pattern, which may adapt to higher plants' complex growth and development process (Cheng & Raissig, 2023). In the future, except for grasses, it is also necessary to study the development and function of SCs in other stomatal morphological types in other species to further explore the effects of SCs on stomatal function and plant development and growth.

2. Stomatal development in dicot model *Arabidopsis thaliana*

Arabidopsis thaliana, a model organism of plant biology, is the most thoroughly studied compared to all the known species of flowering plants (Koornneef & Meinke, 2010). It has a short life cycle, small size, small genome, and yields many seeds through self-pollination, making it useful for genetic research (Meyerowitz, 2001;

Ochatt & Sangwan, 2008). In addition, More than 10,000 scientists and 4,000 research institutions are involved in the study of Arabidopsis, which has also led to rapid development of research on plant molecular biology, biochemistry, genetics, and physiology in *A. thaliana* (Rhee et al., 2003). Currently, there are highly efficient genetic transformation methods and shared and accessible resources for genome analysis, including updated Locus information and genome annotation, etc (Meinke et al., 1998; Rhee et al., 2003).

Unsurprisingly, the stomatal development in *A. thaliana* has been extensively studied in the last few decades (Bergmann & Sack, 2007; Pillitteri & Torii, 2012). Studying the stomatal development in *A. thaliana* and learning the fundamental developmental processes of developmental biology also has excellent reference significance for exploring the stomatal development in other species.

2.1 Overview of stomatal development

Once the stomatal lineage is established on the epidermis of *Arabidopsis thaliana*, the stomatal lineage precursor cell undergoes several cell divisions, cell identity transition, and cell differentiation to produce a stomata (Pillitteri & Dong, 2013). Core basic helix – loop–helix (bHLH) transcription factors control the continuous development processes by regulating the expression of downstream genes, such as cell cycle regulators and transcription factors (Han et al., 2018, 2022; MacAlister et al., 2007). Stomata are evenly distributed on epidermis to improve gas exchange (Geisler et al., 2000). The spacing of stomata is regulated by cell-cell signaling, mediated by secreted peptide ligands from epidermal cells and mesophyll cells, cell surface receptors and intracellular mitogen-activated protein kinase (MAPK) cascade (and/or other unknown signaling components), to regulate the core bHLH transcription factors and control the stomatal initiation and spacing divisions (Qi et al., 2017; Tameshige et al., 2017). Environmental factors and plant hormones also significantly affect stomatal development through crosstalk in signal transduction pathways (Qi & Torii, 2018). In addition, a set of polarity proteins polarize to the plasma membrane of meristemoid mother cell (MMC) or meristemoid before mitosis to regulate the cell divisions and fate specification (Kim et al., 2023; Wallner et al., 2023).

2.2 Stages in stomatal development

During stomatal development, some protodermal cells acquire the MMC identity (Bergmann & Sack, 2007; Pillitteri & Dong, 2013; Pillitteri & Torii, 2012). The MMC undergoes the first asymmetric cell division (ACD), which is also called “Entry division”, to create two unequal-sized daughter cells; the smaller one is meristemoid, and the larger one is stomatal lineage ground cell (SLGC) (Lau & Bergmann, 2012). The meristemoid is like a “stem cell” and can continue to make ACDs; these self-renewal divisions are called “amplifying divisions”, since these divisions increase the number of SLGCs in a single lineage (Geisler et al., 2000; Von Groll et al., 2002). The amplifying divisions can occur up to three times, although most meristemoids only undergo one or two amplifying divisions or directly transit into GMC (Gong et al., 2023). The SLGC can either directly differentiate into a lobed PC or get MMC identity and initiate an ACD to produce a meristemoid positioned away from an existing meristemoid/GMC called “spacing division”(Torii, 2021). The GMC is finally divided symmetrically into two young GCs, which are differentiated into stomata (Pillitteri & Dong, 2013) (Fig.1).

2.3 Core bHLH transcription factors control the organized stomatal development

Many studies uncovered that the conserved key bHLH transcription factors SPEECHLESS (SPCH), MUTE, and FAMA, together with their combined bHLH heterodimers, SCREAM (also known as INDUCER OF CBF EXPRESSION1) (SCRM/ICE1) and SCRM2 (Kanaoka et al., 2008), are crucial for stomata initiation and differentiation (Han & Torii, 2016; Kim & Torii, 2024; Lampard & Bergmann, 2007; Lau & Bergmann, 2012).

Firstly, SPCH accumulates in the protodermal cell and establishes the MMC identity. Then *AtSPCH* promotes ACDs by upregulating a set of cyclins (D-type), including CYCD3;1 and CYCD3;2 (MacAlister et al., 2007; Vatén et al., 2018), for the entry division, amplifying divisions and spacing divisions (MacAlister et al., 2007). The DREAM complex is activated for mitosis(Simmons et al., 2019). The *atspch* showed the absence of stomata in the whole leaf epidermis (MacAlister et al., 2007) (Fig.1).

Next, *MUTE* terminates ACD(s) of the meristemoid and differentiates the meristemoid into GMC (Pillitteri, Sloan, et al., 2007). During the process, AtMUTE can recruit trans-acting factors BPC1 and BPC2, which recruit PRC2 to repress the

expression of *AtSPCH* (Kim et al., 2022). In addition, *AtMUTE* induces cyclin-dependent kinase inhibitor, SIAMESE-RELATED4 (SMR4), which can directly interact with AtCYCD3;1 (and probably AtCYCD3;2) and terminate the ACDs, at the same time, *AtMUTE* induce GMC specific G1 cyclin CYCD5;1, which don't interact with SMR4 and thus promote the symmetric division of the GMC (Han et al., 2018, 2022; Pillitteri, Sloan, et al., 2007). After this, *AtMUTE* upregulates *AtFAMA* and *At(FOUR LIPS)FLP* for inhibiting excess symmetric cell division by directly suppressing cell cycle regulators, for example, CYCD5;1 and CYCD7;1, to promote the GCs differentiation (Hachez et al., 2011; Han et al., 2018; Xie et al., 2010; Zuch et al., 2023). The *atmute* mutant showed the arrested meristemoid and no GCs differentiation (Pillitteri, Sloan, et al., 2007) (Fig.1).

In the end, *AtFAMA,* together with MYB transcription factors *AtFLP* and *MYB88*, regulates the transition from division to differentiation in GMC to produce functional stomata (Bergmann et al., 2004; Lai et al., 2005; Ohashi-Ito & Bergmann, 2006). The *atfama* mutant showed epidermal cell proliferation in the stomata location instead of proper GCs differentiation (Lee et al., 2014; Ohashi-Ito & Bergmann, 2006) (Fig.1).

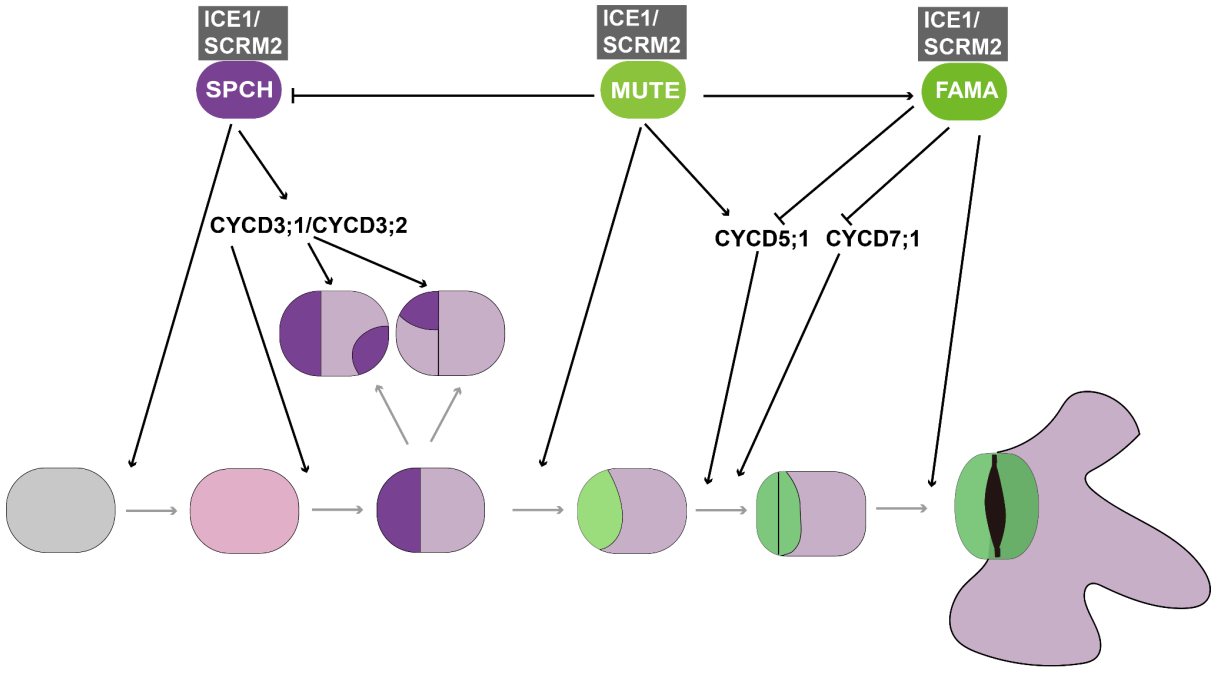

Figure 1. Stomatal development in *Arabidopsis thaliana*.
Key stomatal transcription factors SPCH, MUTE, and FAMA, their heterodimers ICE1/SCRM2, and their downstream main cell cycle regulators are indicated. Cell types are displayed in different colors. Protodermal cell is in grey, MMC is in pink, meristemoid is in

dark purple, SLGC and PC are in light purple, GMC is in light green, and GCs are in darker green.

2.4 Stomatal patterning

2.4.1 Ligand-receptor signaling contributes to stomata distribution

In *Arabidopsis thaliana*, stomatal patterning and stomatal density are strictly regulated for proper stomatal movement and efficient gas exchange. For instance, when two MMC next to each other, one of the MMC will either undergo a spacing division and yield a meristemoid away from the existing stomata or stomata precursor cell, or differentiate into a pavement cell, rather than having two stomata adjacent to each other, suggesting that the spacing division is oriented (Geisler et al., 2000; Lucas et al., 2006). The stomata pattern is achieved by ligand-receptor signaling. Cysteine-rich peptide ligands from EPIDERMAL PATTERNING FACTORS (EPFs) family, EPF1 (Hara et al., 2007) and EPF2 (Hara et al., 2009; Hunt & Gray, 2009; Torii, 2012), are secreted by stomatal precursors/ stomatal lineage cells and perceived by the receptors on the cell surface of the neighboring cells which have extracellular leucine-rich repeat (LRR) domain (Qi et al., 2017). The cell surface receptors complex are composed of three ERECTA (ER)-family receptor-like kinases (RLKs), including ER, ERECTA LIKE 1 (ERL1), and ERECTA LIKE2 (ERL2) (Shpak et al., 2005); a signal modulator, LRR receptor-like protein TOO MANY MOUTHS (TMM) (Nadeau & Sack, 2002a); SOMATIC EMBRYOGENESIS RECEPTOR KINASE (SERK) family RLKs (Meng et al., 2015). Although both EPF1 and EPF2 are negative regulators of stomata patterning, it is worth noting that EPF1 and EPF2 have distinct function for regulating stomatal patterning, EPF2 functions earlier than EPF1 and inhibits the entry division of the MMC initiating stomatal lineage, while EPF1 expresses later, orients spacing division and prevents stomata clustering (Hara et al., 2007, 2009; Hunt & Gray, 2009). EPF2 is secreted by MMCs and meristemoids and bind to ER in neighboring protodermal cells (Lee et al., 2012; Tameshige et al., 2017), then the signals are transduced from intercellular to intracellular and mediated by the downstream MAPKs signaling cascade, including the MPK3 and MPK6, their upstream MAPK kinases, MKK4, MKK5, MKK7, and MKK9, and upstream MAPKK kinase, YODA(YDA) (Bergmann et al., 2004; Lampard et al., 2009; Wang et al., 2007). Finally, SPCH is phosphorylated and degraded; thus, establishing MMC cell fate is inhibited (Lampard et al., 2008). EPF1 is secreted by

late meristemoids and GMCs and is recognized and binds with ERL1 in neighboring meristemoids (Lee et al., 2012; Tameshige et al., 2017). The EPF1-ERL1 signaling pathway inhibits MUTE, thus preventing the meristemoid from stomata formation and inhibiting stomata pairing, although the downstream signaling components involved are not known yet (Qi et al., 2017; Tameshige et al., 2017). However, EPF-LIKE9 (EPFL9/Stomagen), which is produced in mesophyll cells and functions as a positive regulator, was found to compete with EPF2 to bind with ER; thus, the EPF2 signaling is disrupted, and the downstream SPCH inhibition is released (Lee et al., 2015; Takata et al., 2013). Different from the stomatal patterning regulation in cotyledon and leaves, in hypocotyl, the signals from EPFL6/CHALLAH subfamily, including EPFL4 (*CHALLAH-LIKE2* (*CLL2*)) /5(*CHALLAH-LIKE1)*/6, are also mediated by the ER family to regulate stomata formation negatively, but the signal from EPFL4/5/6 is disrupted by TMM (Abrash et al., 2011; Abrash & Bergmann, 2010). Except for the ligand-receptor signaling modules, STOMATAL DENSITY AND DISTRIBUTION1 (SDD1), which is expressed in meristemoids/GMCs, negatively regulate stomata density by extracellular signaling (Berger & Altmann, 2000; Hara et al., 2007; Von Groll et al., 2002).

Former studies proved negative feedback loops between the receptor-ligands signaling components and their target downstream transcription factors for proper spacing and stomata distribution. SPCH directly targets and activates peptide ligand EPF2 and the signal modulator TMM, which, in turn, inhibit the SPCH expression level in the neighboring protodermol cells for stomatal cell lineage specification (Horst et al., 2015; Lau et al., 2014). Similarly, receptor kinase ERL1 is directly targeted by MUTE and upregulated when the meristemoid transit into GMC, and EPF1 peptide bind to ERL1 and, in turn, inhibit the MUTE activity via an autocrine inhibition mechanism for ensuring that the symmetric cell division only happen once and proper stomata patterning (Qi et al., 2017).

2.4.2 Environmental factors and hormones affect stomatal development through signaling cross-talk

Light promotes stomatal formation (Boccalandro et al., 2009; Casson et al., 2009; Casson & Hetherington, 2014; Hronková et al., 2015; Kang et al., 2009; Klermund et al., 2016; Qi & Torii, 2018). In *Arabidopsis thaliana*, light signals are perceived by the photoreceptors, including phytochromes (phy) family (phyA-phyE) for red/far-red light

and cryptochrome (CRY) for blue/ UV-A light (Cantón & Quail, 1999; Cashmore et al., 1999; Li & Yang, 2007). Among them, phyA is mainly responsible for perceiving far-red light, whereas phyB is mainly responsible for perceiving red light (Casson et al., 2009; Kang et al., 2009). phyA, phyB and CRY downregulate E3 ubiquitin ligase CONSTITUTIVE PHOTOMORPHOGENIC 1(COP1), which is a light signaling inhibitor, COP1 promote the expression of downstream YDA (Kang et al., 2009). However, in the dark, COP1 can directly interact with and degrade SCRM/SCRM2, thus inhibiting stomatal differentiation (Chen et al., 2020; Lee et al., 2017). phyB also inhibit photomorphogensis negative regulator, phytochrome-interacting factors (PIFs), which suppress GATA factors of the B-subfamily transcription factors (B-GATAs), thus promote the expression of bHLH transcription factors SPCH and promote stomatal development in hypocotyls (Huq et al., 2004; Klermund et al., 2016; Ni et al., 1999; Richter et al., 2010). In mesophyll cells, while COP1 is inhibited in light signaling, the downstream of COP1, HY5, can directly bind and activate the expression of STOMAGEN (Hronková et al., 2015; S. Wang et al., 2021).

In *A. thaliana*, increased CO_2 reduces stomatal density (Qi & Torii, 2018). CO_2 induces the subtilisin-like serine protease CRSP, which could activate EPF2; thus, it promotes the EPF2-mediated signaling pathway and inhibits stomata development (Ohki et al., 2011; Qi & Torii, 2018). Opposite to CO_2 regulation, CO could increase stomata density by upregulating STOMAGEN and downregulating EPF2 (Weng et al., 2022).

Under higher temperature, the bHLH transcription factor PHYTOCHROME-INTERACTING FACTOR 4 (PIF4) is accumulated, the induced PIF4 directly inhibit the expression of stomatal regulater SPCH and cause lower stomatal density, in turn, SPCH could also negatively regulate the expression of PIF4, thus form a negative feedback-loop (Lau et al., 2018). Another study showed that under heat stress, HEAT SHOCK PROTEINS 90s (HSP90s), including HSP90.1 and HSP90.2, are induced and interact with YDA to activate the MAPK cascade, thus decreasing the activity of downstream SPCH and inhibiting stomata formation (Samakovli et al., 2020).

It is poorly understood how water conditions affect stomatal development (Qi & Torii, 2018). Drought and osmotic stress downregulate the expression of SPCH through the YDA/MAPKK/MAPK signaling pathway, thus inhibiting stomata formation and reducing the stomata density (Kumari et al., 2014).

The signals from plant hormone Brassinosteroids (BRs) are perceived by the receptor BRASSINOSTEROID INSENSITIVE 1 (BRI1), once BRs bind to BRI1, the receptor will recruit BRIASSOCIATED RECEPTOR KINASE (BAK1)/SERK3 to inhibit the downstream regulator, GLYCOGEN SYNTHASE KINASE3 (GSK3)/SHAGGY-like kinase BRASSINOSTEROID INSENSITIVE 2 (BIN2) (Qi & Torii, 2018; Zoulias et al., 2018). BIN2 downregulate the expression of downstream genes in BRs-mediated signaling, for example, the BRASSINAZOLE RESISTANT 1 (BZR1) and bri1-EMS SUPPRESSOR1 (BES1), which could directly promote MKK9 and inhibit FAMA, to repress the stomata formation (Belkhadir & Chory, 2006; Kim & Wang, 2010; S. Li et al., 2024). Some studies have shown that BIN2 can specifically phosphorylate and degrade both YDA and MKK4; thus, the MAPK cascade signaling is disrupted, and it is claimed that BRs negatively regulate stomatal development (Khan et al., 2013; Kim et al., 2012). Interestingly, studies revealed that BIN2 is regulated by scaffold protein POLAR LOCALIZATION DURING ASYMMETRIC DIVISION AND REDISTRIBUTION (POLAR) and its closest homolog POLAR-LIKE1 to ensure the cell type specificity of BR response for stomatal development (Kim et al., 2023). However, different from the regulation in cytoledon, in hypocotyls, BIN2 could phosphorylate and degrade SPCH, therefore, stomata formation is promoted by BRs mediated signaling (Gudesblat et al., 2012; Yang et al., 2015), indicating that the effect of BRs on stomatal development might be tissue specific (Qi & Torii, 2018).

Auxins negatively regulate stomatal development (Balcerowicz et al., 2014; Le et al., 2014; Qi & Torii, 2018; Zhang et al., 2014). Auxin is perceived by the receptor TRANSPORT INHIBITOR RESPONSE 1 (TIR1)/AUXIN-BINDING F-BOX(AFB), then the receptor bind and degrade the downstream AUXIN/INDOLEACETIC ACID (Aux/IAA) protein, BODENLOS (BDL/IAA12), therefore, one of the downstream transcription factors AUXIN RE SPONSE FACTORs (ARFs), the Stomagen negative regulator MONOPTEROS (MP)/ARF5 is released, thus inhibit the expression of Stomagen and supress the stomata formation (Balcerowicz et al., 2014; Schlereth et al., 2010; Yamaguchi et al., 2013; Zhang et al., 2014). In the dark, TIR1/AFB receptor also inhibits AUXIN RESISTANT3 (AXR3/IAA17), which might upregulate EPFs to inhibit the stomata formation, but the downstream ARF is unknown (Balcerowicz et al., 2014).

In *A. thaliana*, Abscisic acid (ABA) negatively affects stomatal density (Chater et al., 2015; Qi & Torii, 2018; Tanaka et al., 2013). The former studies revealed that ABA

could inhibit SPCH, and the ABA positive regulator HOMEODOMAIN GLABROUS11 (HDG11) can repress stomatal development by promoting the expression of ER (Tanaka et al., 2013; Yu et al., 2008).

Some other plant hormones, for example, are also found to regulate stomata development in *A. thaliana* (Qi & Torii, 2018). In hypocotyls, gibberellin (GA) increases stomatal density (Saibo et al., 2003). Ethylene also positively regulates stomatal density(Serna & Fenoll, 1996). Phytohormone cytokinin (CK) promote stomata formation by activating SPCH for spacing divisions, whereas, SPCH could also induce cell type specific type-A ARABIDOPSIS RESPONSE REGULATORs (ARRs), ARR16 and ARR17, to inhibit the spacing divisions and in turn suppress CK signaling, to ensure the precise CK signaling regulation (Vatén et al., 2018). In addition, jasmonic acid (JA) negatively regulates the stomata development by activating hydrogen sulfide (H_2S), which is upstream of SPCH and inhibits the stomatal initiation (Deng et al., 2020; Han et al., 2018; Pillitteri et al., 2011).

2.5 Polarity crescent orients ACDs and specifies distinct cell fates

Cell polarity is essential for guiding ACDs and cell fate specification in multicellular organisms. During stomatal development, proper stomatal patterning for efficient stomata function is regulated by cell-cell signaling, environmental factors, and plant hormones. However, the intracellular mechanism that orients ACDs is cell polarity. In *Arabidopsis thaliana*, before the ACDs, the polarity proteins, including BREAKING OF ASYMMETRY IN THE STOMATAL LINEAGE (BASL) and BREVIS RADIX family (BRXf) (Dong et al., 2009; Rowe et al., 2019) which polarize at the plasma membrane of the cell and form a cortical polarity crescent (Muroyama et al., 2023). The polarization of BASL is regulated by the phosphorylation of MPK3/6, then the phosphorylated BASL recruits YODA and MPK3/6 for spatially signaling at the plasma membrane (Zhang et al., 2015). In addition, BASL/BRXf complexes also recruit POLAR and POLAR-LIKE 1, which regulate the oriented ACD by “sequestering” BIN2 (Houbaert et al., 2018; Kim et al., 2023). Once POLAR (together with POLAR-LIKE1) and BIN2 are polarized with BASL/BRXf, BIN2 phosphorylate and degrade YDA; thus, the MAPK signaling is attenuated, and SPCH could be accumulated in the MMC or meristemid (Houbaert et al., 2018; Kim et al., 2023; Yang et al., 2020). BIN2 also phosphorylates BES1 to suppress the BR signaling

(Kim et al., 2023). Then the BASL/BRXf complex regulates the microtubules-dependent nucleus migration away from the BASL/BRXf polarity domain before the ACD (Muroyama et al., 2020). Studies showed that another polarity protein, OCTOPUS-LIKES (OPLs), oppositely polarized to the plasma membrane before ACD (Wallner et al., 2023). During the ACD, when the preprophase band (PPB) is formed, the phosphatase BSL1 binds to the polarized domain and mediates BIN2 to release from POLAR (Kim et al., 2023). After the ACD, two unequal-sized daughter cells are produced; the bigger daughter cell inherits the BASL/BRXf/POLAR crescent, which then orients the actin-dependent nucleus migration by regulating MYOXI-I (Muroyama et al., 2020). BIN2 is redistributed in the nucleus and then YDA in the polarized domain phosphorylate and degrade SPCH; thus, the activity of SPCH is strongly inhibited (Kim et al., 2023; Muroyama et al., 2023). At the same time, BIN2 is sensitive to BR-mediated inhibition, and BES1 is dephosphorylated and moves into the nucleus to activate the BR signaling (Kim et al., 2023). BIN2 also phosphorylate and degrade POLAR, the polarity domain is dissoluted and this daughter cell is differentiated into SLGC (Houbaert et al., 2018; Wallner et al., 2023). The BASL/BRXf/POLAR might be repolarized at another domain for spacing divisions; otherwise, the SLGC will be differentiated into a PC (Muroyama et al., 2020). OPLs crescent is inherited by the smaller daughter cell, which becomes a meristemoid, then OPLs might repolarize at another domain of this meristemoid, together with oppositely polarized BASL/BRXf/POLAR, orient amplifying divisions (Wallner et al., 2023). Once the meristemoid transits into GMC, the OPLs domain will be depolarized from the cell cortex (Wallner et al., 2023). After the symmetric cell division, OPLs polarize at the new cell plate of both young GCs, endowed with the same cell fate (Wallner et al., 2023).

3. Stomatal development and function in monocot model *Brachypodium distachyon*

Except for the studies of the developmental mechanism of the anomocytic, mesoperigenous stomata in the dicot model plant *Arabidopsis thaliana*, the development of the paracytic, perigenous stomata in grasses was also widely studied in recent years. *Brachypodium distachyon*, relative of cereal crops wheat and barley, was established as a monocot model, since it has common characteristics in other model plants, for example, short life cycle, small plant size, small genome,

community resources, etc, making it useful for plant biology research (Kellogg, 2015; Raissig & Woods, 2022; Scholthof et al., 2018).

Unlike the stomata in *A. thaliana,* which only have kidney-shaped GCs, the stomata in *B. distachyon* have dumbbell-shaped GCs and lateral SCs (Nunes et al., 2020). Strikingly, studies on this stomata, which have novel morphology, uncovered that the specialized guard cell morphology and the stomatal SCs can help stomata faster breathing response to environmental changes (Franks & Farquhar, 2007; Raissig et al., 2017; Spiegelhalder et al., 2024), suggesting that further exploring the development and function of stomata in grasses will help improve the water use efficiency of crops facing climate change.

3.1 Stages in stomatal development

The stomata in dicots have random orientation, and the stomata at different developmental stages are dispersed throughout the whole leaf epidermis; however, all the stomata in the leaf epidermis of grasses follow linear development patterns and have the same orientation (Raissig et al., 2016). Developing stomata are present at the base of the leaf, while differentiated and mature stomata are present at the leaf tip (Liu et al., 2009; Raissig et al., 2016).

Some of the cells at the leaf base acquire stomatal cell file identity (Nunes et al., 2020; Raissig et al., 2016; Stebbins & Shah, 1960) and initiate a transverse ACD, which produces a large SLGC and a small GMC (Cheng & Raissig, 2023; Raissig et al., 2016). After the GMC matures, it induces subsidiary mother cells (SMC) identity in both lateral cells (Cheng & Raissig, 2023). Then the SMCs divide asymmetrically and longitudinally to produce two SCs adjacent to the GMC (Spiegelhalder et al., 2024). Afterward, the GMC divides symmetrically into two young GCs (Spiegelhalder et al., 2024). Finally, the two young GCs and two SCs differentiate into mature stomata complexes (Cheng & Raissig, 2023; Spiegelhalder et al., 2024; Spiegelhalder & Raissig, 2021).

3.2 Stomatal bHLH transcription factors are rewired for novel stomatal morphology in grasses

Stomatal core transcription factors SPCH, MUTE, and FAMA are conserved in all land plants (Chater et al., 2017). However, in the grass model *Brachypodium distachyon*, the orthologs of Arabidopsis stomatal key bHLHs have diverged to

regulate the novel stomatal morphology and patterning (Raissig et al., 2016, 2017). *BdSPCHs* (including *BdSPCH1* and *BdSPCH2*, which are partially redundant) and their heterodimer *BdSCRM/BdICE1* establish stomata identity in particular protodermal cells and drive a transverse ACD to form a GMC and an SLGC (Raissig et al., 2016). The SPCH orthologs in rice have similar functions (Wu et al., 2019). Different from *AtMUTE* in *Arabidopsis thaliana,* which terminates ACDs and establishes GMC identity (Pillitteri et al., 2007), *BdMUTE* expresses in GMC, and then the MUTE protein moves to lateral neighboring cells to establish SMCs identity (Raissig et al., 2017; Spiegelhalder et al., 2024). Similar to MUTE in *B. distachyon*, the MUTE ortholog in maize is also mobile and recruits SMCs in lateral non-stomatal cell files (Wang et al., 2019). After the SMCs are longitudinally and asymmetrically divided to produce two SCs, and the GMC divide longitudinally and symmetrically into two young GCs, *BdFAMA* and its heterodimer *BdSCRM2* are required for the GCs' differentiation (Cheng & Raissig, 2023; McKown et al., 2023; Raissig et al., 2016), this is similar to *OSFAMA* in rice (Wu et al., 2019). In addition, *BdFAMA* also has an overlapping function with *BdMUTE* and can rescue the SCs defects phenotype in *bdmute* (McKown et al., 2023).

3.3 Novel stomatal morphology conveys rapid stomatal movements and high water-use efficiency in grasses

Studies from almost sixty years ago already showed that while the stomata in maize is open, osmolytes potassium (K^+) and chloride(Cl^-) accumulate in GCs, and when the stomata is closed, K^+ and Cl^- accumulate in SCs, implying that the differential distribution of osmolytes between GCs and SCs during stomatal opening and closing might be responsible for faster gas exchange in grasses (Raschke & Fellows, 1971). In 2007, a “see-sawing’’ model was proposed, where ion shuttling and turgor pressure exchange between GCs and SCs in grasses is required to overcome the mechanical advantage of SCs, thus accelerating the stomata movement rate (Franks & Farquhar, 2007). Strikingly, this proposal was confirmed in 2017; the *bdmute* plants that have stomatal SCs defects can still survive, however, the stomata have smaller stomatal pores and much slower opening and closing rate response to the environmental changes, suggesting that the stomatal SCs are functionally relevant for stomatal physiology in grasses (Raissig et al., 2017).

4. Stomatal development in Crassulaceae succulents

4.1 Most succulents adopt Crassulacean Acid Metabolism (CAM) to achieve drought resistance

In the plant Kingdom, approximately 3–5% of flowering plants, which are called “succulents”, adapt to drought conditions and maintain normal physiological and growth activities by storing water in large cells of specific tissues or organs (Eggli & Nyffeler, 2009; Willert et al., 1990), including roots, stems, and leaves (Griffiths & Males, 2017; Pérez-López et al., 2023). Major succulents are from 35 families within Angiospermae, for example, Crassulaceae, Orchidaceae, Euphorbiaceae, Asphodelaceae, Asparagaceae, Aizoaceae, Cactaceae, Apocynaceae, etc. (Cushman, 2001; Griffiths & Males, 2017; Winter & Smith, 1996). Succulents are annual or perennial and have also evolved different forms to adapt to their living environment (Griffiths & Males, 2017). For example, columnar and opuntioid stem succulents, massive-leaf succulents are found in semi-desert areas (Griffiths & Males, 2017); in some desert and semi-desert regions, succulents are also miniaturised (Griffiths & Males, 2017); succulents are also found in epiphytes, for example, orchids, bromeliads, and some ferns, which contribute to the tropical forest (Griffiths & Males, 2017).

Most succulents employ CAM photosynthesis instead of C3 and C4 photosynthesis, first described for species of the family Crassulaceae (Lüttge, 2004). The stomata are open at night, and CO_2 is uptaken from the atmosphere (Lee, 2010). Under the catalysis of phosphoenolpyruvate carboxylase (PEPC), CO_2 reacts with phosphoenolpyruvate (PEP) to generate oxaloacetic acid, which is then stored in the vacuole as malic acid; the next day, stomata are closed during the day, malic acid extrusion from the vacuole and CO_2 is released into cytoplasm through decarboxylation, finally, CO_2 is fixed in the Calvin-Benson-Bassham cycle (Borland et al., 2014). Due to this evolutionary adaptation of photosynthesis, the stomata of plants are closed during the day to avoid intense transpiration and a large amount of water loss, while at night, when the air humidity is relatively high, the stomata are open to absorb CO_2 (Estrella et al., 2012). This photosynthesis strategy reduces water loss and improves water use efficiency (Males & Griffiths, 2017). Coupled with the feature of succulence, succulent CAM plants can survive in highly arid conditions (Griffiths & Males, 2017; Heyduk, 2022; Sage et al., 2023).

CAM plants that always perform CAM and can't switch to other ways of photosynthesis are called "Constitutive CAM" or "Obligate CAM"; the plants that induce CAM photosynthesis under water-limited conditions and reversibly switch to C3 or C4 photosynthesis under well-watered conditions are called "Facultative CAM" (Winter, 2019).

4.2 *Kalanchoe laxiflora*: an emerging model system for CAM research

Exploring the CAM mechanism will provide insights into the evolution of CAM and future induction of CAM in C3 crops to meet climate change; therefore, research on CAM has been increasing in recent years (Borland et al., 2011, 2014; Yang et al., 2015). In order to study the molecular basis of CAM physiology, some emerging model systems have been established (Males & Griffiths, 2017). Some species from the family Crassulaceae, genus Kalanchoë, have been regarded as critical model systems for CAM research (Cushman & Bohnert, 1999; Garcês & Sinha, 2009; Hartwell, 2007; Kluge et al., 1991). Kalanchoë has over 100 succulent species, which are found in Africa, Madagascar, and Asia, and most of the Kalanchoë species are found in Madagascar (Vargas et al., 2022). Representative model CAM species in genus Kalanchoë include *Kalanchoe gracilipes*, *Kalanchoe fedtschenkoi*, *Kalanchoe laxiflora*, *Kalanchoe daigremontiana*, *Kalanchoe rhombopilosa,* etc (Hartwell et al., 2016). Among them, *K. fedtschenkoi* and *K. laxiflora* have assembled and annotated genome sequences and transcriptome sequences (Borland et al., 2009; Cheng et al., 2024; Moseley et al., 2019; Yang et al., 2015). In addition, *K. fedtschenkoi*, *K. laxiflora,* and *K. daigremontiana* have already been reported to be genetically modified for research (Boxall et al., 2020; Dever et al., 2015; Garcês et al., 2014).

K. laxiflora are diploid or tetraploid, have small genomes, and yield thousands of seeds; thus, this species is fit for genetic research, for example, genetic crossing and mutagenesis(Hartwell et al., 2016). *K. laxiflora* also reproduces asexually through plantlets that grow from the edges of leaves (Barlow, 2009). In addition, a simple and highly efficient tissue-culture based genetic transformation protocol has already been established and T0 transgenic plants are regenerated around 5~6 months after transformation (Hartwell et al., 2016; Wang et al., 2019). Despite this, *K. laxiflora* still has many shortcomings compared with *Arabidopsis thaliana* (Hartwell et al., 2016). For example, the entire life cycle from seed to seed takes one year (Hartwell et al.,

2016). In addition, after obtaining transgenic seedlings, several months are required for the plants to grow to a suitable size for subsequent experiments (Dever et al., 2015). Therefore, research using this model species is very time-consuming, and the plants are large and take up space (Hartwell et al., 2016). In the future, the protocols to establish *K. laxiflora* as an emerging model species are expected to be further improved.

4.3 Stomata biology in CAM plants

Corresponding to the physiological characteristics of CAM, succulents generally have an inverse stomatal movement rhythm (Males & Griffiths, 2017), low stomatal density, low maximum conductance, and high stomatal sensitivity to environmental changes compared to C3 species (Zambrano et al., 2014; Griffiths & Males, 2017). However, there are few publications on stomatal biology in succulent CAM plants. Compared to the stomata in C3 species, the stomatal GCs in CAM species have less sensitivity to blue light (Tallman et al., 1997) and circadian oscillator (von Caemmerer & Griffiths, 2009), but more sensitivity to leaf-air vapor pressure deficit (VPD) (Lange & Medina, 1979) and ABA-dependent water status response (Jewer et al., 1981). In addition, stomatal conductance is also regulated by temperature, while 15–25°C is the optimal range for CAM activities during the night (Yamori et al., 2014). It is worth noting that intercellular CO_2 concentration(C_i) is considered to be the most crucial factor in regulating the stomatal aperture in CAM plants (Wyka et al., 2005). In the morning, CO_2 accumulates in cytoplasm through decarboxylation of malic acid, coupled with respiration, the dramatically increased Ci induces stomatal closure; while in dusk, the CO_2 released by malic acid is gradually consumed and reduced Ci drives stomatal opening (Cockburn, 1979; Griffiths et al., 2007; Males & Griffiths, 2017; Spalding et al., 1979; von Caemmerer & Griffiths, 2009; Wyka et al., 2005). However, a clear understanding of how stomata conduct sensing of Ci and metabolites is still lacking in CAM plants (Males & Griffiths, 2017).

Some studies suggest that the metabolism of guard cells in CAM plants plays a vital role in CAM physiology. For example, the photosynthesis in stomatal GCs might contribute to stomatal closure during the day (Lind et al., 2015). In addition, the circadian expression profiles of key ion channels in constitutive CAM species *Agave*

americana are also shifted compared to C3 model species *A. thaliana* (Abraham et al., 2016).

Strikingly, there are also significant differences in the proportions of stomatal complexes of different morphologies between CAM and C3 species (Males & Griffiths, 2017). Stomata in all monocot CAM species have SCs; this proportion in monocot C3 species is only around 70% (Males & Griffiths, 2017). In addition, the number of CAM species with Tetracytic stomata is almost twice that of C3 species (Males & Griffiths, 2017). Among dicot CAM species, it is also rare to find that stomata lack SCs, and many species have paracytic SCs in their stomata (Males & Griffiths, 2017). Interestingly, stomatal SCs are also found in a few fern lineages that have evolved CAM (Males & Griffiths, 2017; Patel et al., 1975). SCs appear to be overrepresented among CAM species, suggesting that these stomatal SCs might have functional relevance to CAM physiology. Still, no studies have yet confirmed the specific function of the SCs (Males & Griffiths, 2017). Given that the SCs are adjacent to the GCs, they may be involved in the perception of C_i and transduce signals to the GCs, thus regulating the stomatal aperture (Cheng & Raissig, 2023). Stomatal SCs in grasses are confirmed to enhance the stomatal kinetics (Franks & Farquhar, 2007; Raissig et al., 2017). Like the stomata in grasses, there might be “see-sawing” osmotic and turgor pressure exchange between GCs and SCs to facilitate stomatal physiology in CAM plants (Cheng & Raissig, 2023). For example, during the day, turgor pressure increases in SCs, and it decreases in GCs, promoting further closing of stomata and reducing transpiration, while at dusk, turgor pressure increases in GCs, causing stomata to open to absorb CO_2 rapidly (Cheng & Raissig, 2023; Dodd et al., 2002).

4.4 Anisocytic stomata in *Kalanchoë laxiflora*

In the CAM model species *Kalanchoë laxiflora*, kidney-shaped GCs are surrounded by three circular unequal-sized subsidiary-like cells (Cheng & Raissig, 2023; Nunes et al., 2020). The stomatal development, the genetic modules that contribute to it, and the function of SCs are entirely unknown (Cheng & Raissig, 2023).

Relevance and impact

Compared with the stomata of the C3 dicot model *Arabidopsis thaliana*, the innovative stomatal morphology in the C3 monocot model *Brachypodium distachyon* facilitates faster gas exchange and higher water use efficiency (Franks & Farquhar, 2007; Raissig et al., 2017). However, in the succulent CAM species with the highest water use efficiency (Hatfield & Dold, 2019), the unique stomatal development and function are poorly studied (Males & Griffiths, 2017). Studying the stomatal development of CAM plants will reveal the developmental process of unknown anisocytic stomata and how stomatal morphology evolves in different species to adapt to the environment. Future exploration of the functions of stomatal SCs in succulent CAM plants may reveal new stomatal physiological mechanisms and specific mechanisms of the functional relevance of stomata in CAM physiology. In addition, the functions of stomatal SCs may provide a new physiological mechanism for the extremely high water use efficiency of succulents, thus also providing ideas and a molecular/physiological basis for crop drought resistance breeding in response to climate change in the future.

Scope and aims of the thesis

In my thesis, I will work on the stomatal development in the succulent model species, *Kalanchoe laxiflora*. Specifically, it will include the following three aspects:

Firstly, I will establish *K. laxiflora* as a model system for stomatal research. Including establishing horticultural protocols, tissue-culture based genetic transformation protocol, staining protocols, and cloning protocols.

Secondly, to learn the stomatal development of *K. laxiflora*, I will analyze and summarize each stage of stomatal development by static imaging and analyzing the changes and characteristics in the stomatal development on the leaf epidermis as the leaves grow by imaging and quantification.

Thirdly, I will analyze the development of stomatal SCs in *K. laxiflora*. Stomatal key bHLH transcription factors SPCH, MUTE, and FAMA are conserved in land plants (Chang et al., 2023; Ran et al., 2013). Notably, the neofunctionalization of MUTE in *Brachypodium distachyon* contributes to the novel stomatal morphology (Raissig et al., 2017). Therefore, the homologs of MUTE in *K. laxiflora* are essential candidates for studying the development of stomatal SCs in *K. laxiflora*. I will analyze the

function of MUTEs in the stomatal development of *K. laxiflora* by gene editing and reporter gene analysis. In addition, I will also explore the potential downstream programme of MUTE by bulk RNA sequencing.

Results

1. Establishing *Kalanchoë laxiflora* as a model system for stomatal research

To explore the stomatal development in *Kalanchoë laxiflora*, I first established *K. laxiflora* as a model system, including the establishment of horticultural protocols, tissue-culture-based genetic transformation protocols, staining protocols for imaging, and cloning protocols.

1.1 Tissue-culture-based genetic transformation shows high transformation efficiency

To better understand and learn stomatal development in *Kalanchoë laxiflora*, it's necessary to get transgenic lines of genes of interest for further research. Therefore,I established a tissue-culture-based transformation protocol in Prof. Dr. Michael Raissig and Dr. Heike Lindner's lab (University of Bern, Bern) by adapting the well-established protocol from Dr. James Hartwell's lab (University of Liverpool, Liverpool) (Boxall et al., 2020). The detail of this protocol is described below:

I. 4-6 weeks wild-type seedlings were prepared for transformation

A. ½ MS medium was prepared for seedlings' growth:

2.2 g/L MS (Gamborg B5 vitamins)+30 g/L sucrose+8 g/L phyto agar. NaOH was used to adjust the pH to 5.8.

B. Seeds sterilization protocol:

a. A small amount of seeds were put into a 1.5 mL Eppendorf tube and seeds were incubated with 1 mL 70% EtOH for 5 min. During this time, the tube was shaked upside down to ensure that the seeds and EtOH are fully mixed.

b. EtOH was discarded and seeds were resuspended with 1 mL sterile water, the rest of the liquid was discarded, and this step was repeated twice.

c. Seeds were resuspended in 0.1% agarose.

d. 6-8 seeds were sowed one by one on the seedlings' growth medium.

e. Seeds were grown in the Perceval with 16 h light/8 h dark (45-50 µmol PAR m^{-2} s^{-1}; day temperature = 22°C, night temperature = 18°C).

II. Agrobacterium was prepared 1 d before transformation

A. *Agrobacterium tumefaciens* GV3101 was inoculated from glycerol stock with 4 mL fresh LB medium (+50 mg/L Rifampicin + 25 mg/L Gentamicin +

antibiotics corresponding to the resistance tag in the construct carried in Agrobacterium (For example, in my project, I used 50 mg/L Spectinomycin)).

B. Agrobacterium was cultured in a shaker, 180 rpm and 28℃ overnight.

III. Transformation

A. All LB with bacteria was poured into a new 50 mL Eppendorf tube.

B. The tube was put into a centrifuge, and centrifuged 10 min at 4000 rpm.

C. The supernatant was discarded carefully and the pellet was resuspended in the bottom of the tube with about 20 mL MS liquid (4.4 g/L MS (Gamborg B5 vitamins) + 30 g/L sucrose, autoclaved before use).

D. OD_{600} was measured and bacteria with MS liquid was diluted to OD_{600} = 0.1. Usually, around 40 mL of MS liquid with bacteria is enough for transformation.

E. Acetosyringone was added to the bacteria to a final concentration of 100 μM, the whole tube was wrapped with aluminum paper, and left in a shaker (continuously shaking at slow speed) at room temperature for at least 2 h to allow the induction of *Agrobacterium vir* genes.

F. During this 2 h, plant materials for transformation were prepared in the laminar flow hood. Seedlings that were green and looked healthy from at least 4 plates were used for transformation for 1 construct. For each seedling, from around 2^{nd} to 4^{th} pairs, over 1 cm leaves were cut off by sterile scissors (Fig. 2A). All the leaves were moved into a sterile petri dish using a tweezer (Fig. 2B-2C), and each leaf was chopped into 2-3 small pieces by sterile scalpel and tweezers (Fig. 2D-2E). The minimum size for leaf pieces was approximately 2 – 3 mm (Fig. 2F); if they are smaller than that, they will turn brown and die very rapidly on medium.

G. In the laminar flow hood, all leaf pieces was carefully poured into MS liquid with Agrobacterium (Fig. 2G) and the tube was left on the shaker (continuously shaking slowly) for around 1 h.

H. All liquid from the tube was discarded and all leaf pieces were moved onto 2-3 layers of sterile filter paper in a sterile petri dish to remove most of the bacteria from the surface of the leaf tissues (Fig. 2H).

IV. Co-culture

All leaf tissues were placed onto fresh Callus induction medium (CIM) plates (4.4 g/L MS (Gamborg B5 vitamins)+ + 30 g/L Sucrose + 8 g/L phyto agar + 1 mg/L TDZ + 0.2 mg/L IAA, adjust pH to 5.7 using 1M NaOH) +100 μM acetosyringone without

any antibiotics (Fig. 2I), the plates were covered with aluminum foil and Agrobacterium was co-cultured with leaf pieces for 48 h at 22ºC day temperature for 16 h, 18ºC night temperature for 8 h in the dark.

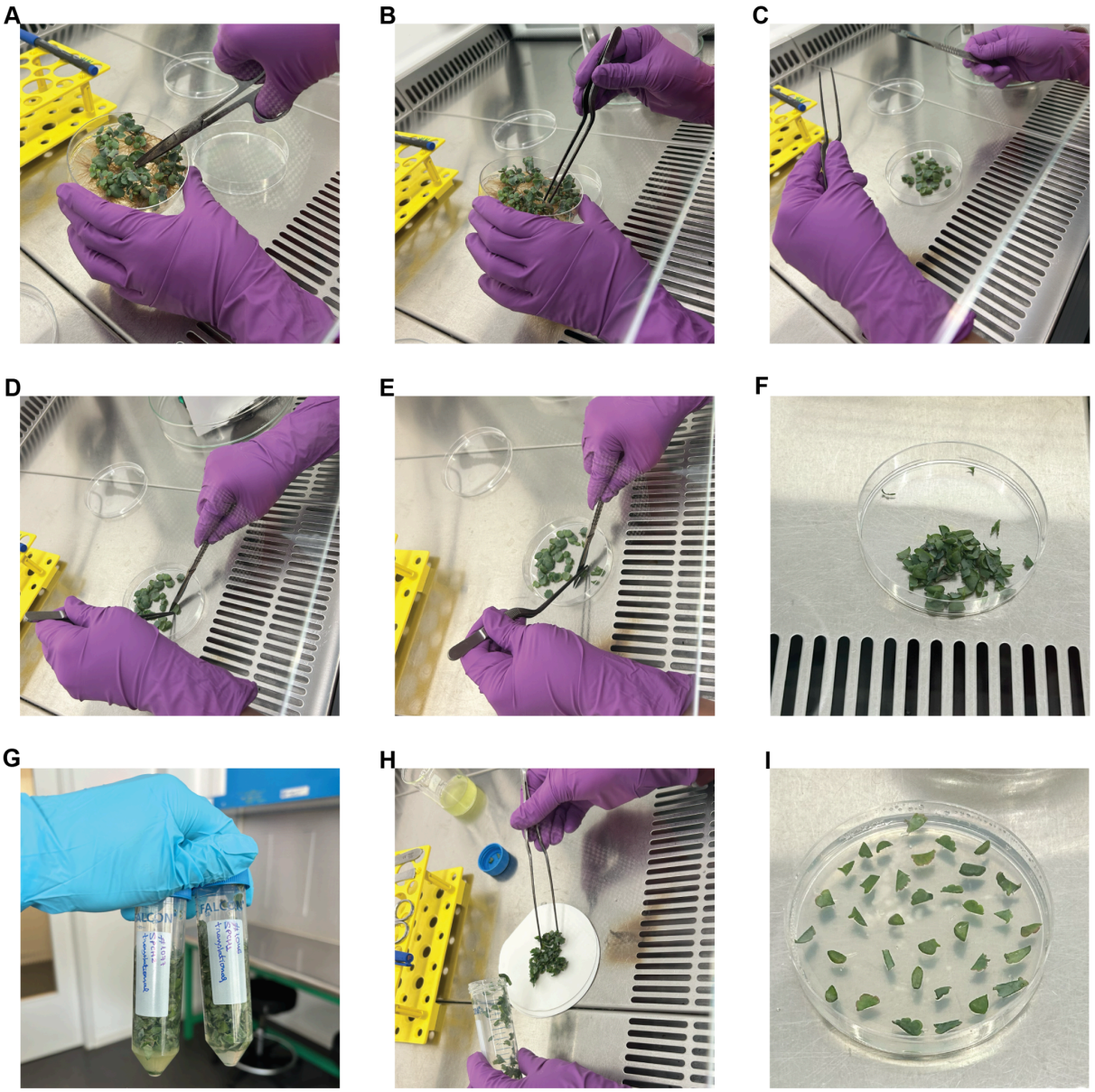

Figure 2. Tissue-culture-based transformation of *Kalanchoë laxiflora*.
(A) Around 1 cm of leaves from sterile plants were cut using scissors. (B-C). Moving leaves onto another sterile petri dish. (D-E). Two different ways to cut the leaves into small pieces. (F). Around 0.5 cm of leaf pieces were prepared for transformation. (G). Leaf pieces were incubated with Agrobacterium. (H). Most of the Agrobacterium was removed from the leaf surface using filter paper. (I). Moving leaf pieces onto CIM with 100 µM acetosyringone.

V. CIM stage

After 2 days of co-culture, all leaf pieces were transferred onto CIM plates (4.4 g/L MS (Gamborg B5 vitamins)+ 30 g/L Sucrose + 8 g/L phyto agar + 1 mg/L TDZ + 0.2 mg/L IAA + 300 mg/L Timentin + antibiotics corresponding to the resistance tag in the construct carried in Agrobacterium (For example, in my project, I used 100 mg/L Kanamycin), adjust pH to 5.3 using 1 M NaOH) (Fig. 3). All leaf tissues onto fresh CIM were transferred every two weeks. This stage will last 2-3 months. During tissue culture, new plantlets grown from leaf edges and brown tissues could be removed.

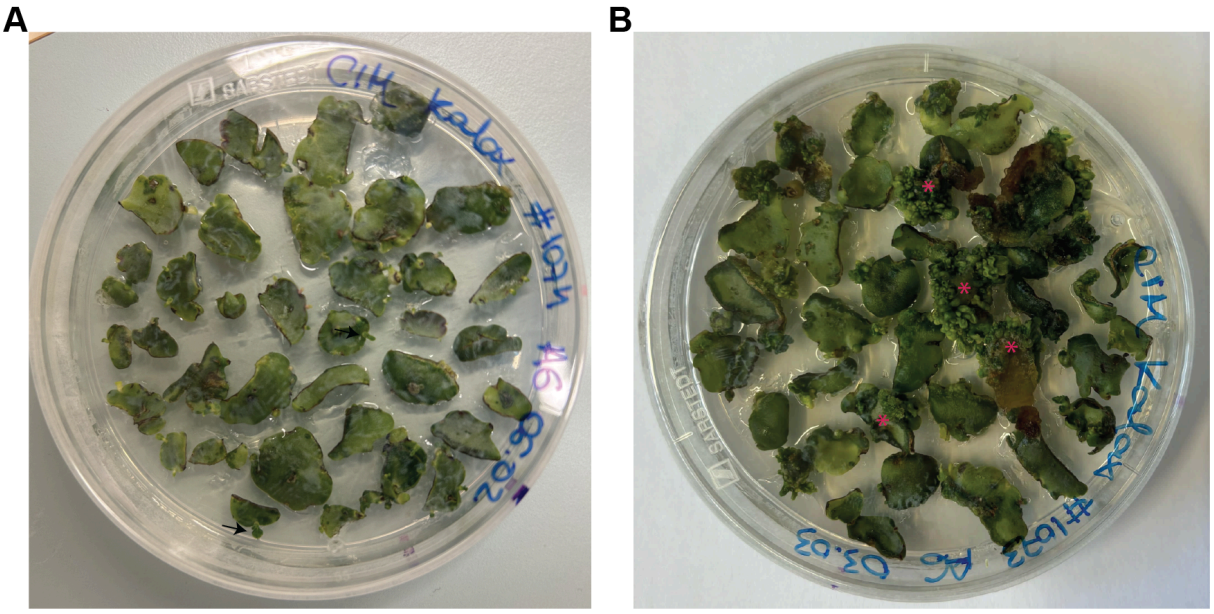

Figure 3. Calli were induced from the cutting edge of the leaf pieces on CIM.
(A). Leaf pieces were moved from CIM with 100 μM acetosyringone to CIM with antibiotics and moved to fresh CIM with antibiotics plates every two weeks. During this stage, the little shoots that growed at the leaf edges (shown in the black arrow) were non-transgenic and could be removed. (B). Calli started to grow from the cutting side of some leaf pieces. Red asterisks showed the calli.

VI. Shoot induced medium (SIM) stage

When substantial calli have grown from the cutting edge of most leaf pieces (Fig. 4A), the calli were cut off from the leaf piece and moved onto SIM plates (4.4g/L MS (Gamborg B5 vitamins)+ + 30 g/L Sucrose + 8 g/L phyto agar + 1 mg/L BAP + 0.2 mg/L IAA +100 mg/L Kanamycin + 300 mg/L Timentin, adjust pH to 5.1 using 1M NaOH). Leaf pieces which didn't have calli yet were continued to be cultured on CIM. To ensure that the calli can fully contact the SIM, they were chopped into small pieces (Fig. 4B). Calli from different leaf pieces belong to independent lines,

therefore, each independent line needed to be labeled at this stage. Calli were transferred onto fresh SIM every two weeks for about 2 months.

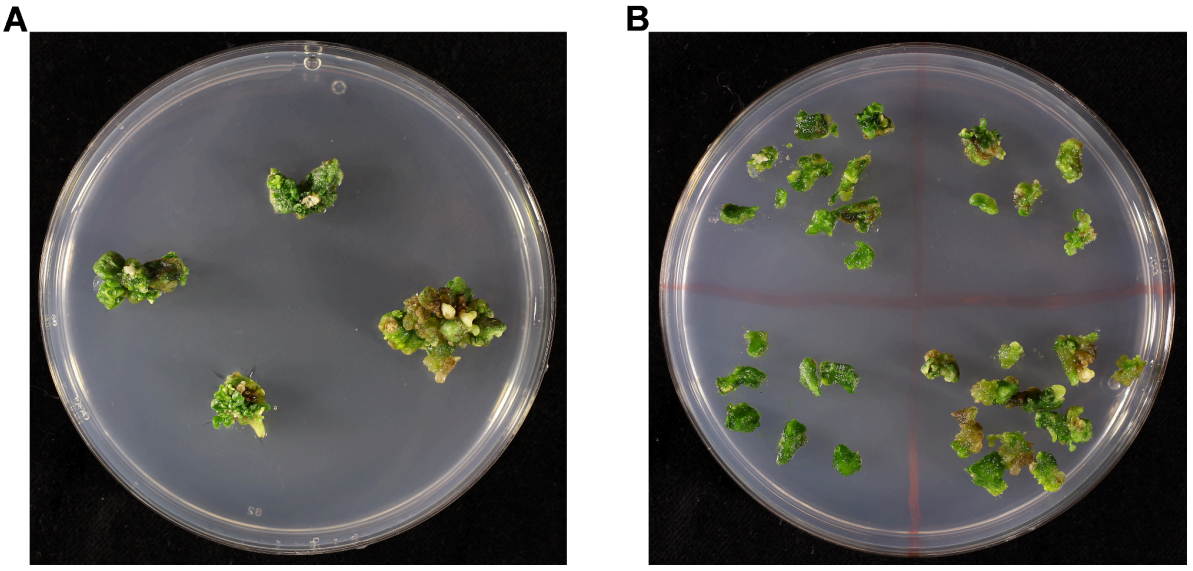

Figure 4. Calli at the CIM-SIM transition stage.
(A). Green calluses grow fully on the edge of the leaves on the CIM plate and were ready to move onto SIM plates. (B). Calli (together with leaves) were cut into small pieces and then moved onto SIM plates; calli from different lines would be distinguished at this stage.

VII. Root induction medium (RIM)

When the calli were getting bigger and clusters of shoots were clearly visible Fig. 5A), all the calli from one line (from the same leaf piece) were transferred onto RIM (4.4g/L MS (Gamborg B5 vitamins)+ 30 g/L Sucrose + 8 g/L phyto agar + 50 mg/L Kanamycin + 300 mg/L Timentin, adjust pH to 5.2 using 1M NaOH) and separated from other lines. While the shoots were big enough to handle (could be easily cut off from the bottom without hurting the whole plant) (Fig. 5B), the shoots were cut off close to the surface of the callus with tweezers, and each individual was separated and transferred to a new plate (Fig. 5C). After 1-2 months the plants have grown roots of 1-2 cm (Fig. 5D). At this point the transgenic plants could be transferred to soil for any further experiments.

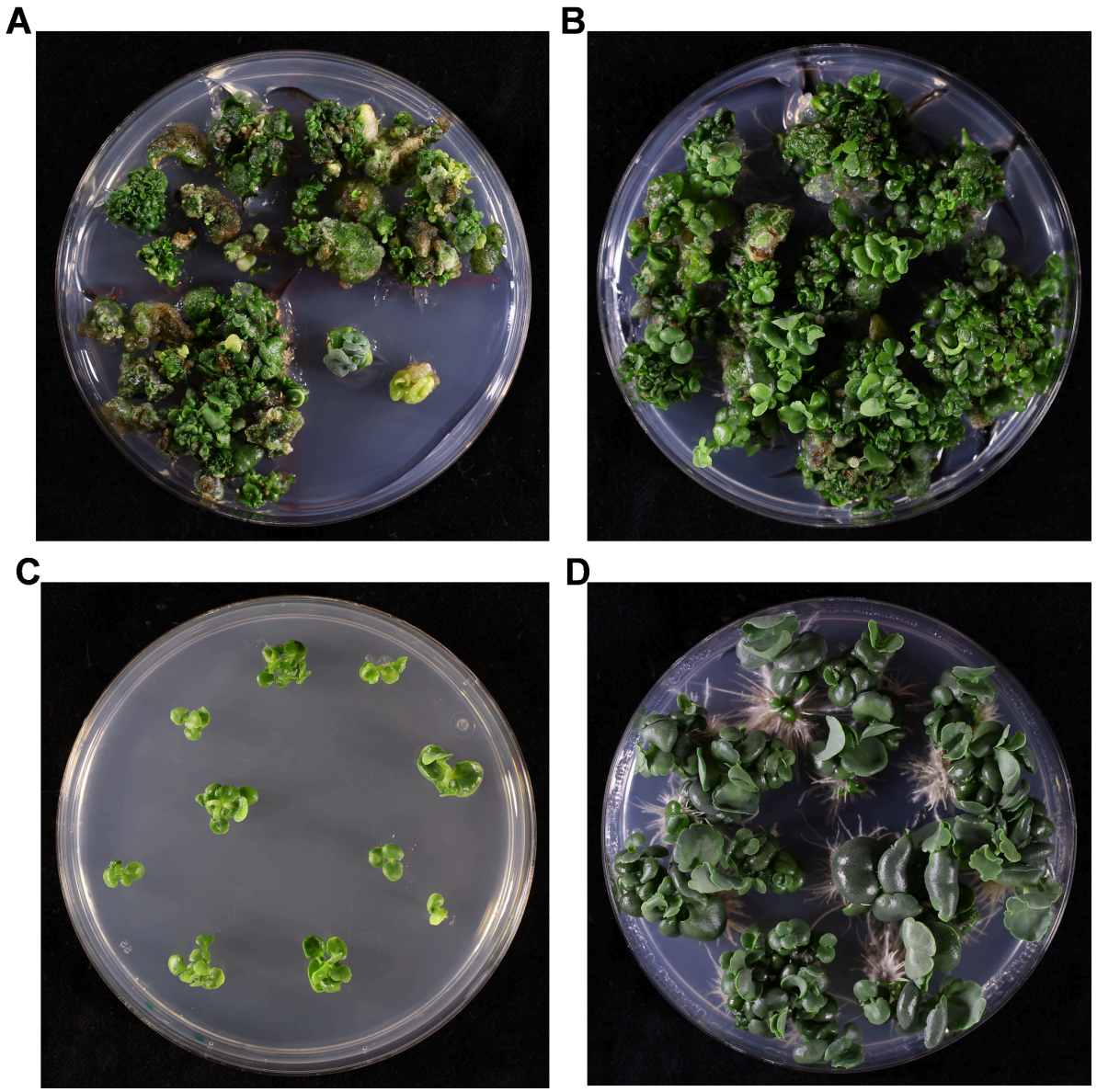

Figure 5. Transgenic shoots were regenerated from calli and transferred separately onto RIM.
(A). Plenty of shoots were regenerated from calli on SIM and ready to transfer to RIM. (B). Shoots grew bigger on RIM. (C). Individuals from the same transgenic line were separated and continued growing on RIM. (D). When the roots grew to around 1~2 cm, transgenic plants were ready to be transferred to soil from RIM.

During my Ph.D., I transformed 22 constructs into WT *K. laxiflora* (Table. 1), and obtained positive transgenic lines from 18 constructs. Apart from this, *KlSPCH1* and *KlSPCH2* translational reporter constructs didn't show any signal. This might be because the promoters cloned before were too short, and the important elements in the promoters were missing. Therefore, new constructs with longer promoters were rebuilt for transformation again. For *KlFAMA1a* transcriptional and translational

reporters, Ph.D student Lidia Hoffmann (University of Bern, Bern) didn't find any signal. At the same time, I didn't find *KlFAMA1a* expressed in WT mature leaves of *K. laxiflora* based on bulk RNA-seq data, indicating that either *KlFAMA1a* doesn't express in mature leaves, or *KlFAMA1a* was wrongly annotated and doesn't exist in the *K. laxiflora* genome, resulting in no signal from the reporters.

Full name
pGGZ003_35S_mCherry-GSL_AtPIP1;4_KanR
p01178-AtCAS9-AtU6_26-KlMUTE1
p01178-AtCAS9-AtU6_26-KlMUTE2
p01178-AtCAS9-AtU6_26-KlMUTE
pK7GWIWG2(II)-KlMUTE1-F1
pK7GWIWG2(II)-KlMUTE1-F2
KlMUTE1 pro-mCitrine linker-KlMUTE1(genomic)-dummy-rbcsT-kan
KlMUTE2 pro-mCitrine linker-KlMUTE2 (genomic)-dummy-rbcsT-kan
KlMUTE1 pro-mCitrine linker-GFP_NLS-dummy-rbcsT-kan
35S::mCitrine-KlMUTE1
35S::mCitrine-KlMUTE2
35S::mCitrine-AtMUTE
KlMUTE2 pro-mCitrine linker-GFP_NLS-dummy-rbcsT-kan
p[KlSPCH1]: mCitrine-Ala-Linker:eGFP-NLS:D-dummy:t[rbcs]:Kan
p[KlFAMA2]: mCitrine-Ala-Linker:eGF-NLSP:D-dummy:t[rbcs]:Kan
p[KlFAMA1a]: mCitrine-Ala-Linker:eGFP-NLS:D-dummy:t[rbcs]:Kan
p[KlSPCH2]: mCitrine-Ala-Linker:eGFP-NLS:D-dummy:t[rbcs]:Kan
p[KlFAMA1b]: B-dummy:CDS-FAMA1b(genomic):GSL-mCitrine:t[rbcs]:KanR
p[KlFAMA1a]: B-dummy:CDS-FAMA1a(genomic):GSL-mCitrine:t[rbcs]:KanR
p[KlSPCH1]: B-dummy:CDS-SPCH1(genomic):GSL-mCitrine:t[rbcs]:KanR
p[KlSPCH2]: B-dummy:CDS-SPCH2(genomic):GSL-mCitrine:t[rbcs]:KanR
p[KlFAMA1b]: mCitrine-Ala-Linker:eGFP-NLS:D-dummy:t[rbcs]:Kan

Table 1. Constructs transformed during my Ph.D.

Constructs that didn't get positive transgenic lines were marked in red.

For most constructs that have positive transgenic lines, I got over ten independent lines for each construct, and at least three independent lines were positive, indicating that the transformation efficiency is high.

1.2 Establishing protocols for light microscopy imaging

1.2.1 Toluidine blue staining protocol

To image the stomata of *Kalanchoë laxiflora* under the light microscope, with the help of Yiğit Berkay Gündoğmuş, a former master student in Prof.Dr.Michael Raissig's lab, I established the light microscope imaging protocol by using Toluidine blue O staining. The detail of this protocol is described below:

I. Prepare Acetate buffer

0.01g pectolyase was dissolved in 84.7 mL 1M Acetic acid, then distilled water was added up to 100 mL.

II. Prepare Toluidine Blue O staining solution

0.2 g Toluidine Blue O was dissolved in 40 mL Acetate Buffer.

III. Staining

A. The leaf was folded in half from the adaxial side, then the epidermis on the abaxial of the leaf was gently torn along the crease in the middle (Fig. 6A), then the epidermis was separated from the remaining leaves with a blade, and then the complete piece of epidermis was placed on a microscopy slide (Fig. 6B). If the epidermis is not flat, flatten it with tweezers, or drop a few drops of water on the surface of the epidermis and use the tension of the water to spread it out. Then, discard the water.

B. 1~2 drops of Toluidine Blue O staining solution was added onto the leaf epidermis (Fig. 6C), after a few seconds, the dye was discarded, and the leaf epidermis was washed with water until the water on the slide was transparent.

C. The epidermis was mounted onto the slide in 50% glycerol. the coverslip was carefully placed over the sample, and then tweezers were used to gently squeeze the coverslip to eliminate air bubbles (Fig. 6D).

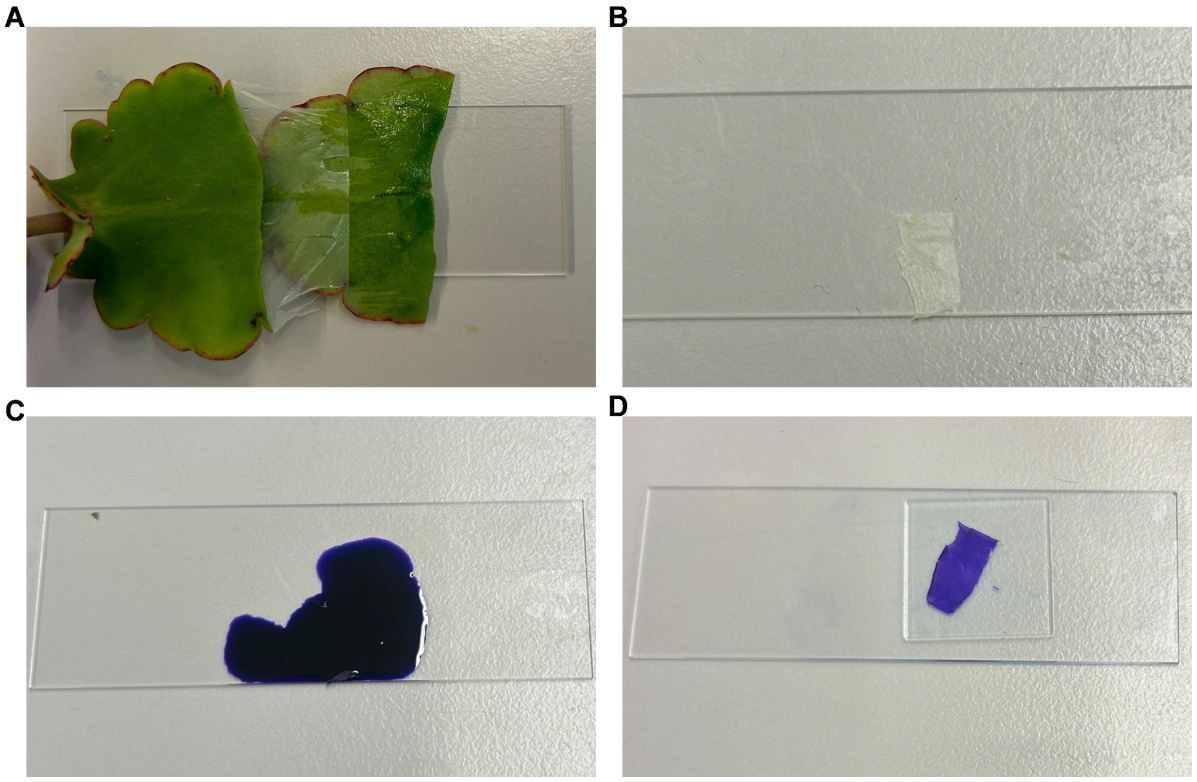

Figure 6. Toluidine blue staining of leaf epidermis of *Kalanchoë laxiflora*.
(A). The adaxial side of the leaf was gently broken in the middle and the epidermis on the abaxial side of the leaf was peeled off. (B). A small piece of the entire leaf epidermis was left on the microscope slide. (C). 1~2 drops of Toluidine blue staining solution was dropped onto the leaf piece and the solution was risen off after a few seconds. (D) The sample was mounted in 50% glycerol and it was covered with a coverslip before imaging.

1.2.2 Protocols tested for light microscopy imaging cotyledons

For imaging the cotyledons of *Kalanchoë laxiflora*, I first tested the same protocol as used for imaging *Arabidopsis thaliana* (Pillitteri, Bemis, et al., 2007). Images showed that the leaf epidermis was blurred, and I could not see the entire stomatal morphology in *klmute1;klmute2* mutants (Fig. 7). I think this is because, compared to the cotyledons of Arabidopsis, the cotyledons of Kalanchoë are thicker and have more mesophyll cells.

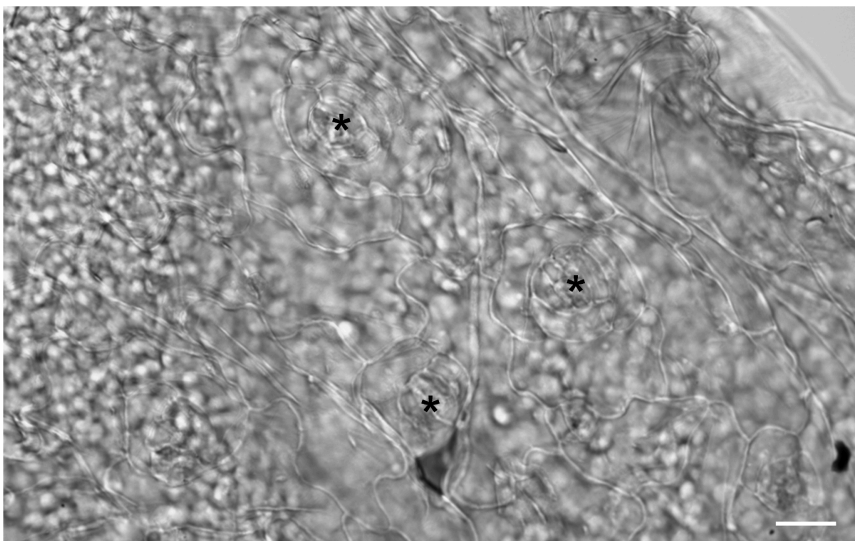

Figure 7. Imaging the cotyledon of *klmute1;klmute2* mutants under the light microscope using the same protocol as in *Arabidopsis thaliana*.
Black asterisks indicate the stomata. Scale bar, 20 μm.

Therefore, I tried another protocol that improved from the protocol for DIC imaging stomata in *A. thaliana* (Sharma, 2017). For testing the best conditions for imaging cotyledons of *K. laxiflora*, firstly, I incubated WT cotyledon materials in 7:1 95% ethanol: acetic acid overnight at room temperature (each cotyledon incubated in 1 mL 7:1 95% ethanol: acetic acid in a 1.5 mL Eppendorf centrifuge tube), the next day I removed 7:1 95% ethanol: acetic acid and incubated cotyledons with 1 mL 1N Potassium hydroxide (KOH) for 0.5 h/1 h/2 h/3 h/4 h) / without KOH (incubated in water), rinsed leaves with water after incubating with KOH (wash the leaves for only 1 time is enough), then I mounted the materials onto slides with Hoyer's solution(1 X or 0.5 X), left slides on bench and kept them at room temperature overnight. Finally, I did the light microscope imaging 1 d and 2 d after mounting slides separately.

Images I took 1 d after mounting samples with Hoyer's solution showed that compared to samples incubated with KOH, the samples incubated without KOH were uneven (Fig. 8), suggesting that KOH might help flatten the leaf tissue. Images showed that incubating leaf samples with KOH for 0.5 h is already good enough for imaging (Fig. 8). In addition, compared to the leaf samples that were treated with / without KOH for the same time, the images from the leaves that were mounted in 1 X Hoyer's solution were much better than the images from leaves that were mounted in 0.5 X Hoyer's solution (Fig. 8). This might be because Hoyer's solution can help clear the leaf tissue.

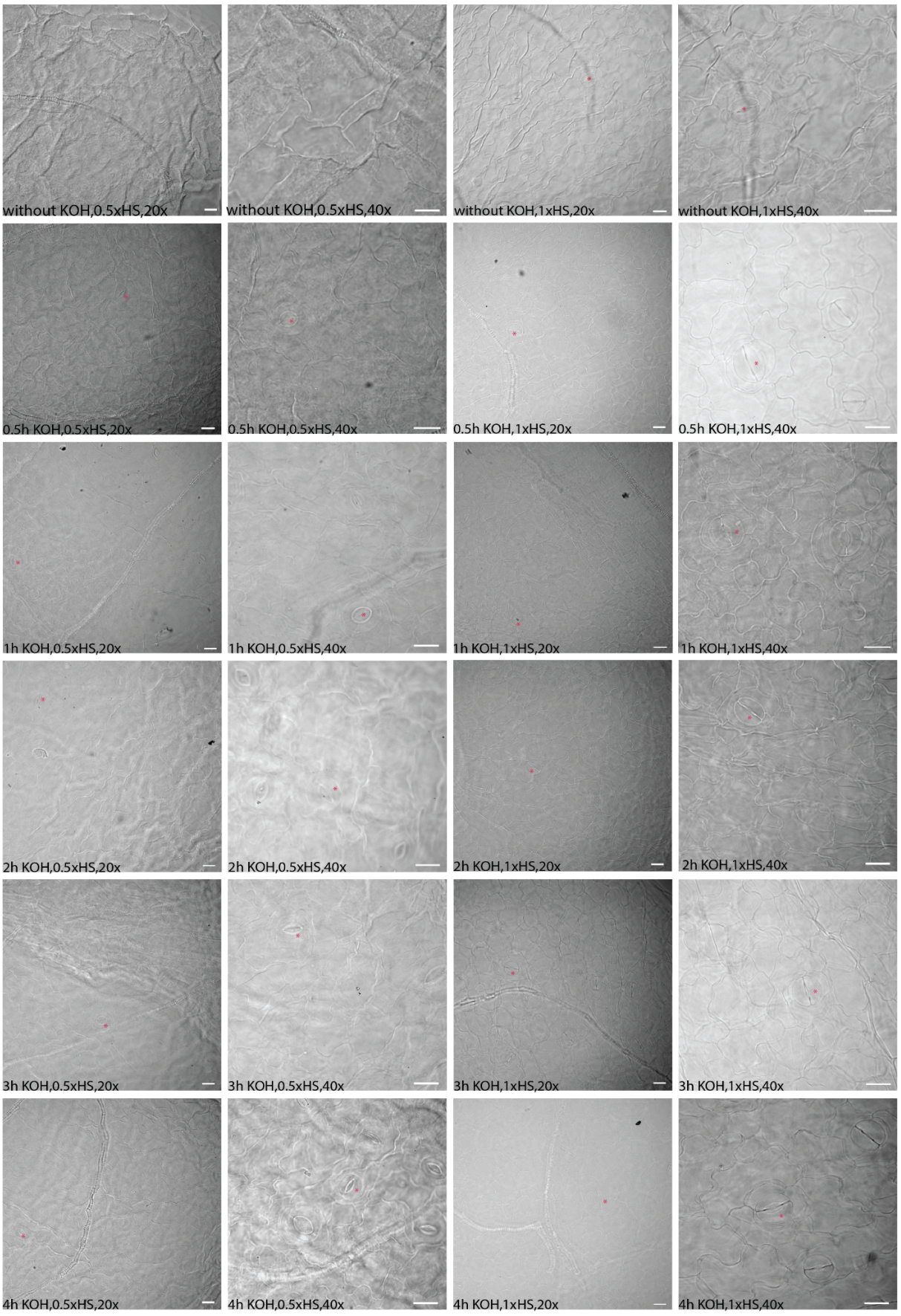
without KOH,0.5xHS,20x
without KOH,0.5xHS,40x
without KOH,1xHS,20x
without KOH,1xHS,40x
0.5h KOH,0.5xHS,20x
0.5h KOH,0.5xHS,40x
0.5h KOH,1xHS,20x
0.5h KOH,1xHS,40x
1h KOH,0.5xHS,20x
1h KOH,0.5xHS,40x
1h KOH,1xHS,20x
1h KOH,1xHS,40x
2h KOH,0.5xHS,20x
2h KOH,0.5xHS,40x
2h KOH,1xHS,20x
2h KOH,1xHS,40x
3h KOH,0.5xHS,20x
3h KOH,0.5xHS,40x
3h KOH,1xHS,20x
3h KOH,1xHS,40x
4h KOH,0.5xHS,20x
4h KOH,0.5xHS,40x
4h KOH,1xHS,20x
4h KOH,1xHS,40x

Figure 8. Light microscope imaging of WT cotyledons of *Kalanchoë laxiflora* after 1d of Hoyer's solution incubation.
The abaxial side of WT cotyledons was imaged under the light microscope. Different conditions (including different KOH treatment times, different HS concentrations, and microscope magnifications) were indicated in each image. Red asterisks indicated the stomata. Scale bars, 20 μm.

Images I took after 2 d showed that leaf tissues were clearer compared to the leaf samples mounted in Hoyer's solution for only 1 d (Fig. 9). In some samples, cell walls were hard to see because the tissue was too clear. Across all samples the ones incubated with KOH for half an hour and mounted with 1x Hoyer's solution have resulted in better images, compared to the other approaches.

Overall, this experiment suggested that incubating cotyledons with KOH for 0.5 h, then mounting materials onto slides with 1x Hoyer's solution and imaging the slide the next day can get better images for light microscope imaging cotyledons of *K. laxiflora*. The details of this protocol are as follows:

I. The cotyledon was incubated overnight in a 1.5 mL Eppendorf centrifuge tube containing 1 mL 7:1 95% ethanol: acetic acid mixture.
II. 7:1 95% ethanol: acetic acid was discarded and the cotyledon was incubated with 1 mL 1N KOH for 0.5h.
III. KOH was removed and the cotyledon was resuspended with 1 mL ddH_2O.
IV. The cotyledon was mounted onto a slide with 1~2 drops of 1X Hoyer's solution, and a coverslip was carefully placed over the cotyledon, and then tweezers were used to gently squeeze the coverslip to eliminate air bubbles. the slide was left at room temperature overnight.
V. Imaging this slide the next day.

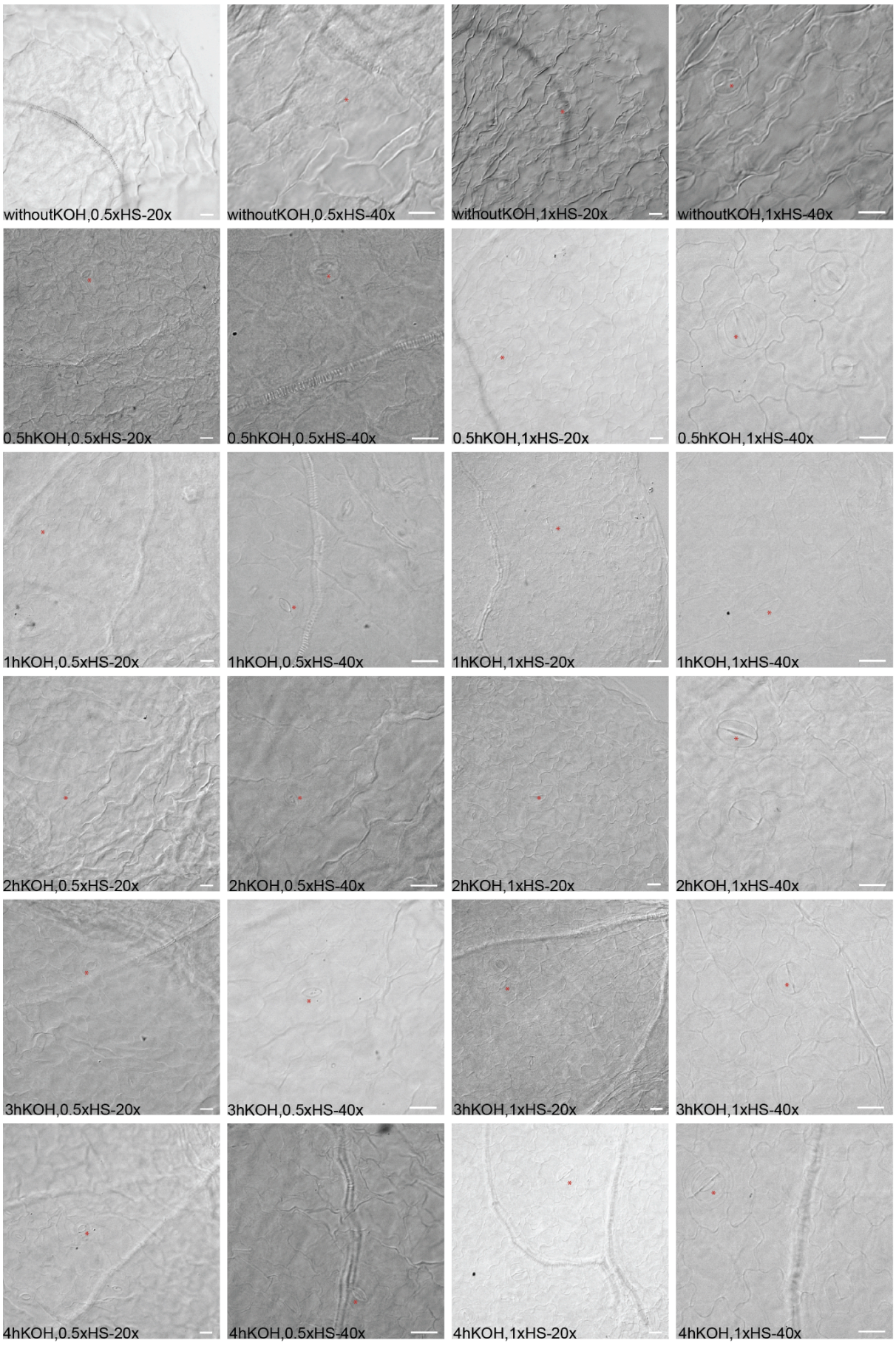
withoutKOH,0.5xHS-20x
withoutKOH,0.5xHS-40x
withoutKOH,1xHS-20x
withoutKOH,1xHS-40x
0.5hKOH,0.5xHS-20x
0.5hKOH,0.5xHS-40x
0.5hKOH,1xHS-20x
0.5hKOH,1xHS-40x
1hKOH,0.5xHS-20x
1hKOH,0.5xHS-40x
1hKOH,1xHS-20x
1hKOH,1xHS-40x
2hKOH,0.5xHS-20x
2hKOH,0.5xHS-40x
2hKOH,1xHS-20x
2hKOH,1xHS-40x
3hKOH,0.5xHS-20x
3hKOH,0.5xHS-40x
3hKOH,1xHS-20x
3hKOH,1xHS-40x
4hKOH,0.5xHS-20x
4hKOH,0.5xHS-40x
4hKOH,1xHS-20x
4hKOH,1xHS-40x

Figure 9. Light microscope imaging of WT cotyledons of *Kalanchoë laxiflora* after 2d of Hoyer's solution incubation.
The abaxial side of WT cotyledons was imaged under the light microscope. Different conditions (including different KOH treatment times, different HS concentrations, and microscope magnifications) were indicated in each image. Red asterisks indicated the stomata. Scale bars, 20 μm.

1.3 FM4-64 fluorescence staining shows the best effect under confocal microscopy

1.3.1 FM4-64 staining protocol

To detect the signal emitted by the fluorescent protein expressed by the fluorescent tag on the vector in transgenic plants under a confocal microscopy, I established a staining protocol for confocal microscopy imaging. The detail of this protocol is described below:

I. 10 μL 0.1 mM FM4-64 stock was diluted into 90 μL water for staining
II. Staining
   A. The whole leaf was cut in half along the middle vein with a blade. One half was taken and it was cut in half again from the middle (crosswise). The veins and leaf edges were removed, and then it was trimmed into a square shape (Fig. 10A).
   B. The leaf was rubbed gently with some water containing hand sanitizer or soap to remove the cuticular wax.
   C. The leaf piece was Incubated in 0.01 mM FM4-64 for 5 min.
   D. The leaf piece was taken out from FM4-64 and put into water for several seconds.
   E. The leaf piece was mounted onto a microscope slide in water. If the leaf piece is big and thick, Vaseline could be applied evenly around the leaves (Fig. 10B), water was added, and a coverslip was covered with the sample. Tweezers were used to gently squeeze the coverslip to remove the bubbles (Fig. 10C).

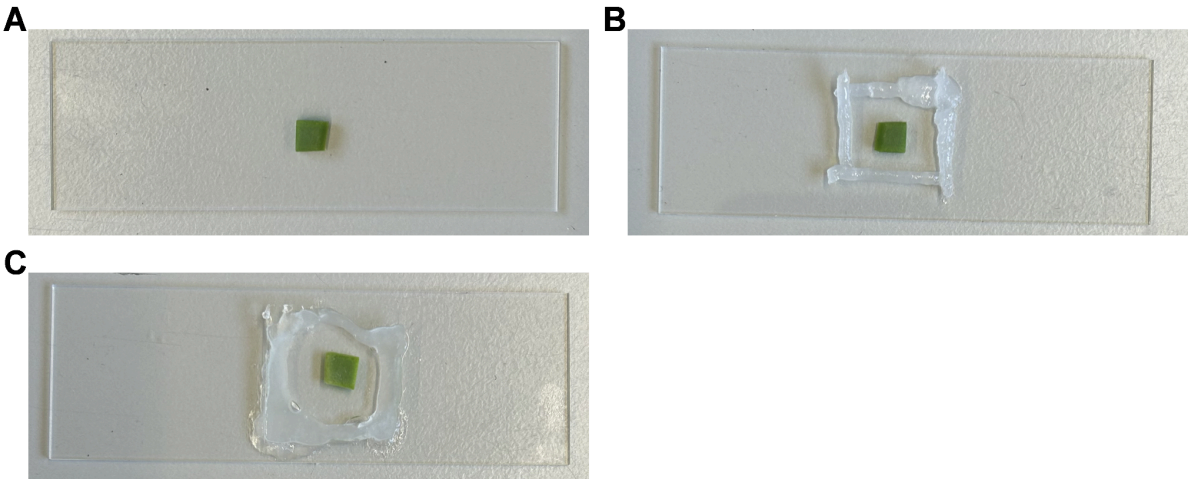

Figure 10. Sample preparation for FM4-64 staining and confocal microscopy imaging. (A). The leaf sample was cut into appropriate size and shape for FM4-64 staining. (B). The sample was surrounded by evenly applied Vaseline. (C). The sample was mounted in water for confocal microscopy imaging.

1.3.2 Other stainings tested for confocal microscopy imaging cotyledons

To image cotyledons of *Kalanchoë laxiflora* under the confocal microscopy, I tested propidium iodide (PI), Calcofluor white, Direct Red 23, and FM4-64, four different fluorescence stainings. Results showed that Calcofluor white and Direct Red 23 didn't work well in cotyledons of *K. laxiflora* (Fig. 11A and 11B). Images of cotyledon stained with Calcofluor white showed that, except for the cell wall, Calcofluor white also stained the cytoplasm (Fig. 11A), indicating that the concentration of Calcofluor white might be too high or the cotyledon was stained for too long. Images of cotyledon stained with Direct Red 23 showed that the staining didn't work at all; the cell wall of epidermal cells was not stained (Fig. 11B). Images of cotyledon stained with PI showed clear cell wall outlines of epidermal cells, but the signal from chloroplasts, especially the chloroplasts from GCs, were also detected (Fig. 11C). Compared to other stainings, FM4-64 stained better, and the images from FM4-64 staining showed good and clear signals from the plasma membrane of epidermal cells (Fig. 11D).

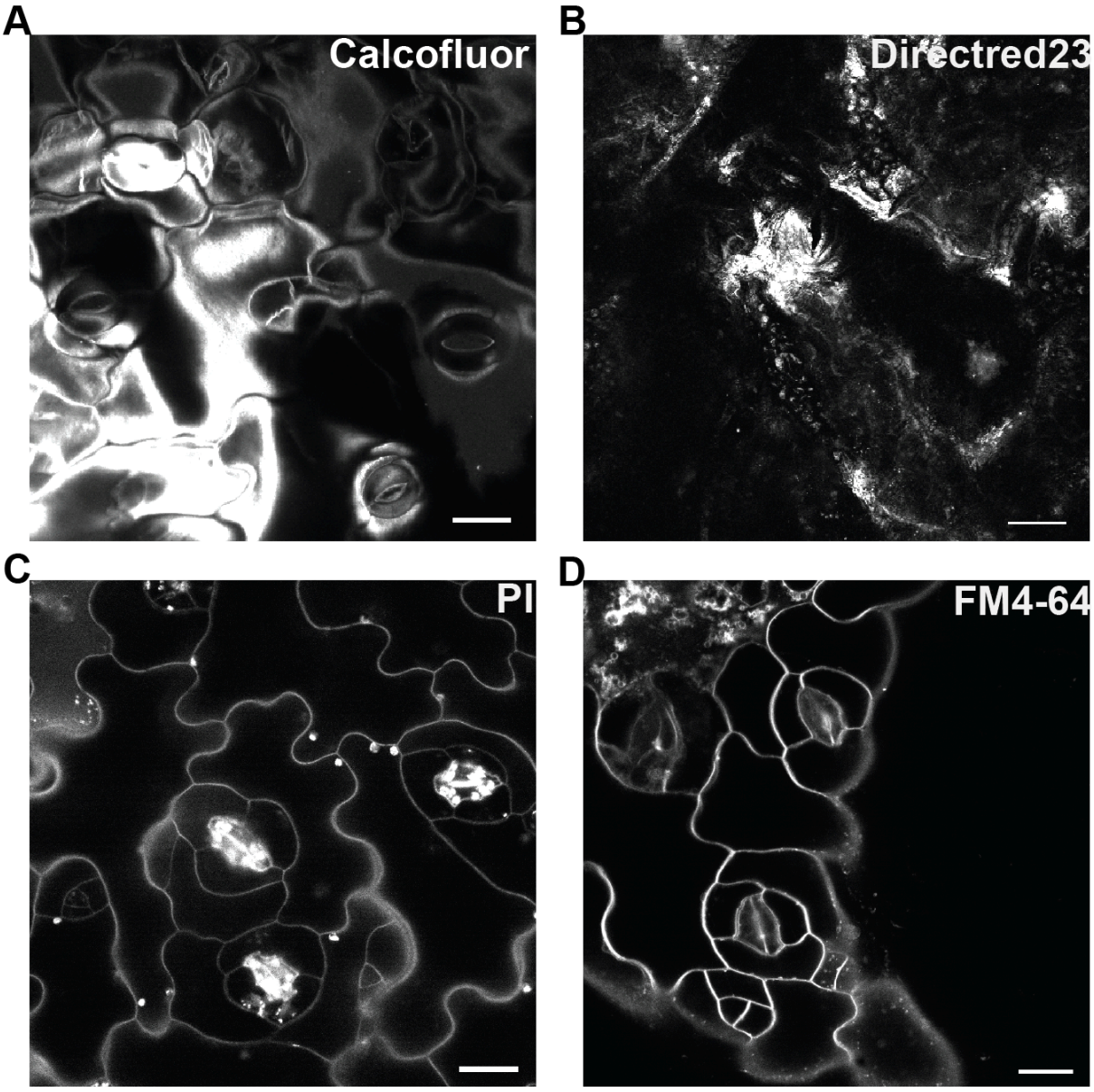

Figure 11. Confocal microscopy imaging of WT cotyledons of *Kalanchoë laxiflora* by using different fluorescence dyes.
(A). 0.01% Calcofluor white staining. (B). 0.1% Direct Red 23 staining. (C). 0.01 mg/mL PI staining. (D). 0.01 mM FM4-64 staining. Scale bars, 20 μm.

1.4 CRISPR CAS9-mediated gene editing is feasible in *Kalanchoë laxiflora*

To analyze the function of stomatal genes in *Kalanchoë laxiflora*, I also tried to clone the CRISPR CAS9 construct and transform it into WT *K. laxiflora*. Firstly, I used Geneious(Geneious | Bioinformatics Software for Sequence Data Analysis) to choose guide RNA. When I was choosing the guide RNAs, I preferred to choose the guide with a high on-target score and low off-target score and target the first or

second exon to obtain shorter amino acid residues. The CRISPR CAS9 cloning protocol I used was modified from former Ph.D student Dan Zhang's protocol (based on CRISPRcloning_HigheffPlasmid from Daniel Woods and modified). Finally, the genotyping of transgenic lines showed the expected mutation around the target site, this means that this plasmid can successfully perform gene-editing in *K. laxiflora*. The detail of this cloning protocol is described below:

I. Phosphorylating the oligos
   A. 3 µL 100 uM sense gRNA, 3 µL 100 µM antisense gRNA, 3 µL T4 ligase buffer (contains ATP), 2 µL T4PNK, and 19 µL H_2O were sequentially added into a PCR tube.
   B. Setting up the PCR machine to:
   a. Incubating 1h at 37°C
   b. 95°C/5 min + ramping to down to 85°C at -2°C/second + ramping down to 25°C at -.1°C/sec + 4°C hold.

II. Digesting and dephosphorylating the backbone

Plasmid:

pFASTRK-PcUBIP-AtCas9-NLS-P2A-mCherry-G7T-AtU6-BsaI-CmR-ccdB-BsaI scaffold (p01178) was used as the backbone for gene-editing in *K. laxiflora* (Fig. 12). In this backbone, Arabidopsis AtU6-26 promoter drive the single guide, and AtCAS9-mCherry was driven by eukaryotic promoter PcUBIP.

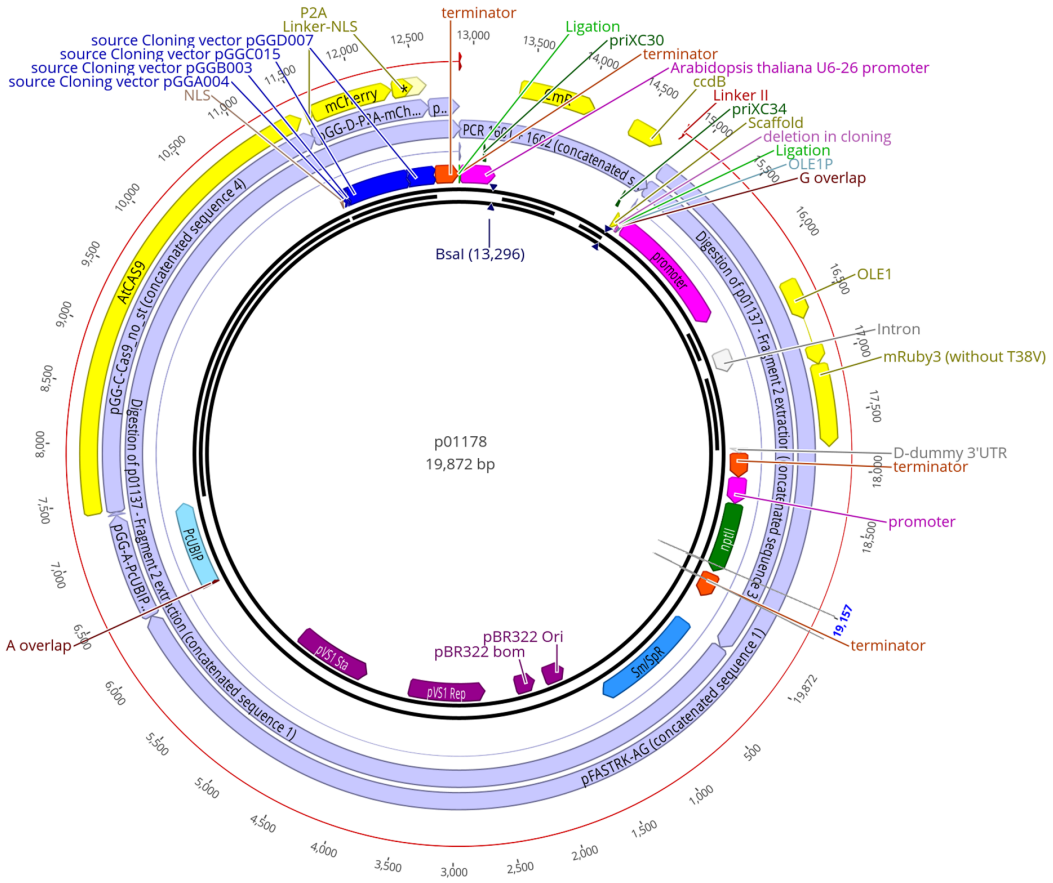

Figure 12. The plasmid map of the CRISPR CAS9 construct pFASTRK-PcUBIP-AtCas9-NLS-P2A-mCherry-G7T-AtU6-BsaI-CmR-ccdB-BsaI scaffold (p01178) used for gene-editing in *Kalanchoë laxiflora*.

A. Plasmid Prepartion

a. Inoculating E.coli from glycerol stock with 4 mL fresh LB (50 mg/L Spectinomycin).

b. Bacteria was cultured in a shaker, 180 rpm and 37℃ overnight.

c. Plasmid was extracted from bacteria and the concentration was measured using the nano-drop.

B. Enzyme digestion

a. Around 5 μg plasmid, 5 μL digestion buffer, and 5 μL Eco31I/BsaI were sequentially added to a PCR tube, and water was added until the total is 50 μL.

b. The PCR tube was left in PCR thermocycler at 37℃ for 2.5 h.

c. The digestion enzyme was inactivated at 65℃, 20 min.

d. The concentration was measured for dephosphorylation.

C. Digested p01178 backbone dephosphorylation.

a. The backbone was diluted with water to around 90 ng/μL.

b. 15 μL backbone, 2 μL Antarctic phosphatase buffer, 2 μL Antarctic phosphatase, and 1 μL H_2O were added to a PCR tube.

c. Incubation: at 37℃, 30min

d. The Antarctic phosphatase was inactivated at 80℃, 2min.

III. Annealed oligos were ligated into digested and dephosphorylated backbone p01178:

A. 1 μL digested and dephosphorylated p01178 (50~100 ng/μL), 1 μL annealed oligo(1:25 dilution), 1 μL T4 buffer, 1 μL T4 ligase, and 6 μL ddH_2O were added into a PCR tube.

B. 16 ℃, overnight

IV. 10 μL ligation products were transformed into NEB DH5a.

V. Colony PCR: priXC30 and gRNA-specific reward primer were used. The size of the band was around 170 bp.

VI. Enzyme digestion: NcoI was used, and the digestion protocol is the same as above.

VII. Sequencing: priXC30 was used.

1.5 Efficient flower induction and crossing protocol

To better understand the life cycle of *Kalanchoë laxiflora* and start genetic breeding, Dr.Heike Lindner and I established flower induction and crossing protocol for *K. laxiflora*.

I. Flower induction

A. The seedlings, which were at least 10 cm in height, were transferred to a short-day chamber or Perceval with 22°C, 8 hr light: 18°C, 16 hr dark cycle (light intensity:130-150 μmol PAR m^{-2} s^{-1}).

B. Flower hooks were formed after around 4 weeks in short-day conditions. After the flower hooks were visible, the plants were transferred back to a long-day greenhouse with 24°C,16 hr light: 18°C, 8 hr dark cycle (light intensity: 300 μmol PAR m^{-2} s^{-1}).

II. Crossing

A. Plants started to flower around 4 weeks after being moved back to the long-day greenhouse.
B. Flower buds whose petals were more than 5 cm away from the receptacle but have not yet opened were chosen (Fig. 13A, indicated by number “1”). A small pair of tweezers was used to carefully remove the petals of the flowers whose pollen has not yet matured and dispersed (Fig. 13B), then the filaments and anthers were removed (Fig. 13C). Emasculated flowers could be labeled with tape. Before the next emasculation, the tweezer is supposed to be sterilized by 75% ethanol in case of cross-pollination.
C. After 2 d, the four stigmas of the emasculated flowers were mature (Fig. 13D). Flowers from the father parent that were fully open with ruptured anthers and mature pollen were selected (Fig. 13E). The pollen was applied evenly on the mature stigma from the mother plant.
D. The seeds were harvested after 1 month.

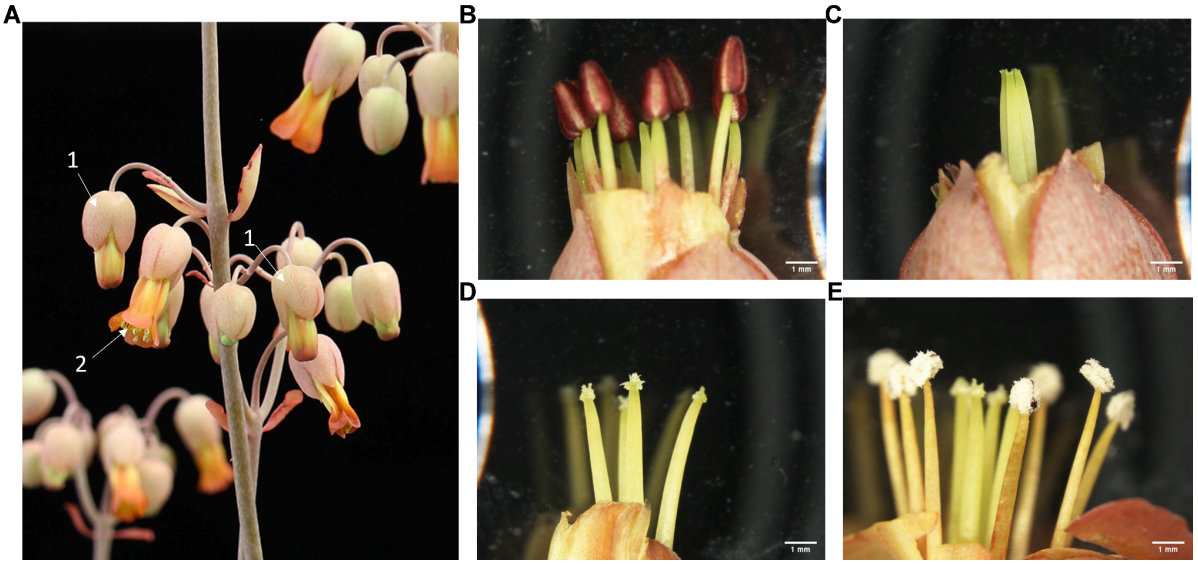

Figure 13. Crossing of *Kalanchoë laxiflora*.
(A). Flowers from the mother plant that were ready for emasculation. Number “1” indicated the best condition of the flowers that could be emasculated for crossing. Number “2” indicated the open flower that might be already self-pollinated. (B). The petals of flowers from mother plants were removed before emasculation. (C). The emasculation of the flowers from the mother plants. (D). After around 2 d, the stigmas of the emasculated flowers were in the best condition for crossing. (E). The flowers from the father plants, which were fully open with ruptured anthers and mature pollen, were selected for crossing. Scale bars were indicated in the photos.

2. Stomatal development in *Kalanchoë laxiflora*

2.1 GCs are surrounded by three anisocytic SCs

Compared to stomata, which only have two kidney-shaped GCs in *Arabidopsis thaliana*, in *Kalanchoë laxiflora*, three circular arranged cells that look different and smaller than PCs surround two kidney-shaped GCs (Fig. 14). According to the morphological definition of SCs and morphological classes of stomata (Evert, 2006; Pant, 1965; Van Cotthem, 1973), these three unequal-sized, circular arranged cells are anisocytic SCs. To explore whether other species of Kalanchoë have the same stomatal morphology, except *K. laxiflora*, I went to Dr. James Hartwell's lab, which cultures various Kalanchoë species. During the visit, I tried to peel the epidermis and stain it with Toluidine blue, followed by light microscope imaging. I was ableto stain and image the stomata of 9 different Kalanchoë species and confirmed that they also have anisocytic stomata like observed in *K. laxiflora*. (Fig. S1).

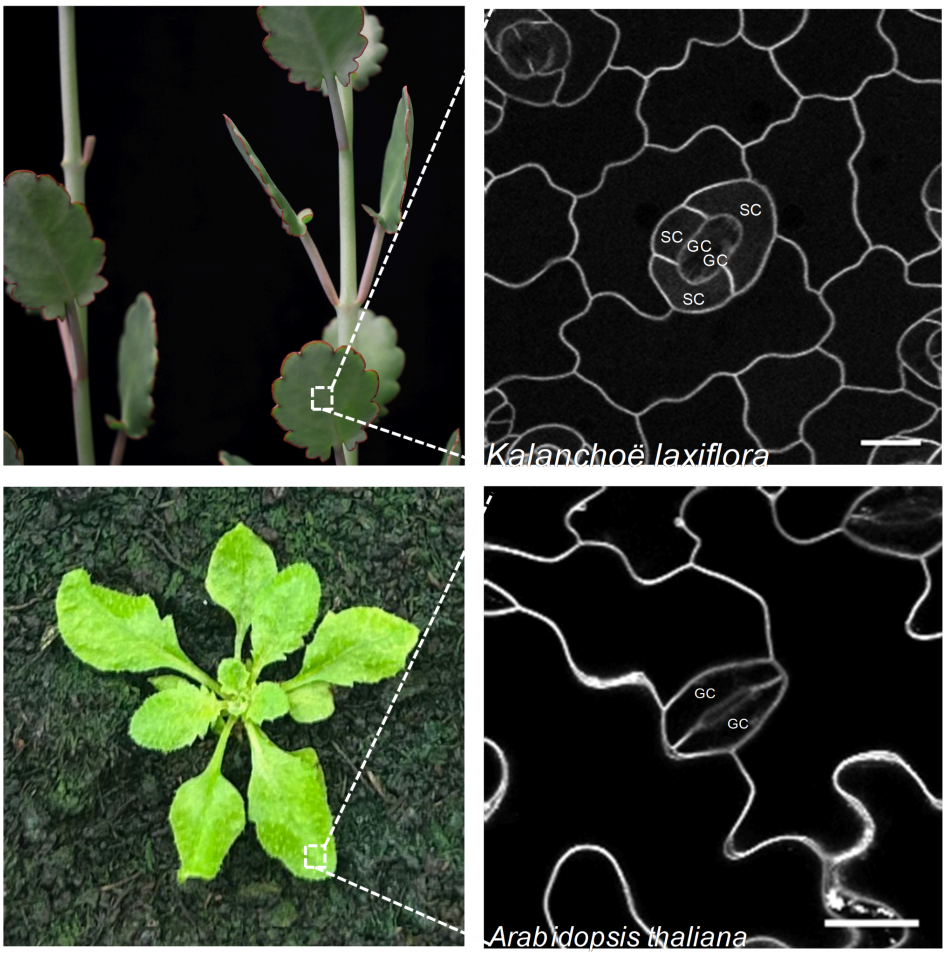

Figure 14. Comparison of stomata morphology between *Kalanchoë laxiflora* and *Arabidopsis thaliana*.

The abaxial side of the leaves from *Kalanchoë laxiflora* and *Arabidopsis thaliana* were imaged under confocal microscopy. The stomata in *Kalanchoë laxiflora* included two GCs and three anisocytic SCs, and the stomata in *Arabidopsis thaliana* only included two GCs. GCs and SCs were indicated in the images. Scale bars, 20 μm.

2.2 The stomatal SCs are mesogenous

To explore the the developmental trajectory of stomata in *Kalanchoë laxiflora*, I imaged the leaves using confocal microscopy. Results showed that different from the stomatal development in *Brachypodium distachyon*, which has clear developing zone and developed zone (Raissig et al., 2016), I can see developing stomata at different stages and mature stomata in the same zone in one leaf of *K.laxiflora* (Fig. 15A). Based on static imaging, Prof. Dr. Michael Raissig and I established the first model to speculate how the stomata are developed in *K. laxiflora* (Fig. 15B). In my hypothesis, a cell acquires meristemoid mother cell (MMC) identity. It undergoes the first asymmetric cell division (ACD) to produce a smaller cell (meristemoid1) and a bigger cell (stomata lineage ground cell (SLGC)), then the meristemoid1 undergoes another two ACDs to produce two SLGCs. After the first three ACDs, it yields three SLGCs, which will develop into PCs (Fig. 15B, a-c). Next we speculate that the meristemoid transitions to another cell type: from meristemoid 1 to meristemoid 2 (Fig. 15B, c), and undergoes another three ACDs to produce three SCs instead of PCs (Fig. 15B, d-f). Finally, the meristemoid2 transits into GMC (Fig. 15B, g) and divides symmetrically into two GCs (Fig. 15B, h); in the end, the stomatal complex includes two GCs and three SCs (Fig. 15B, i).

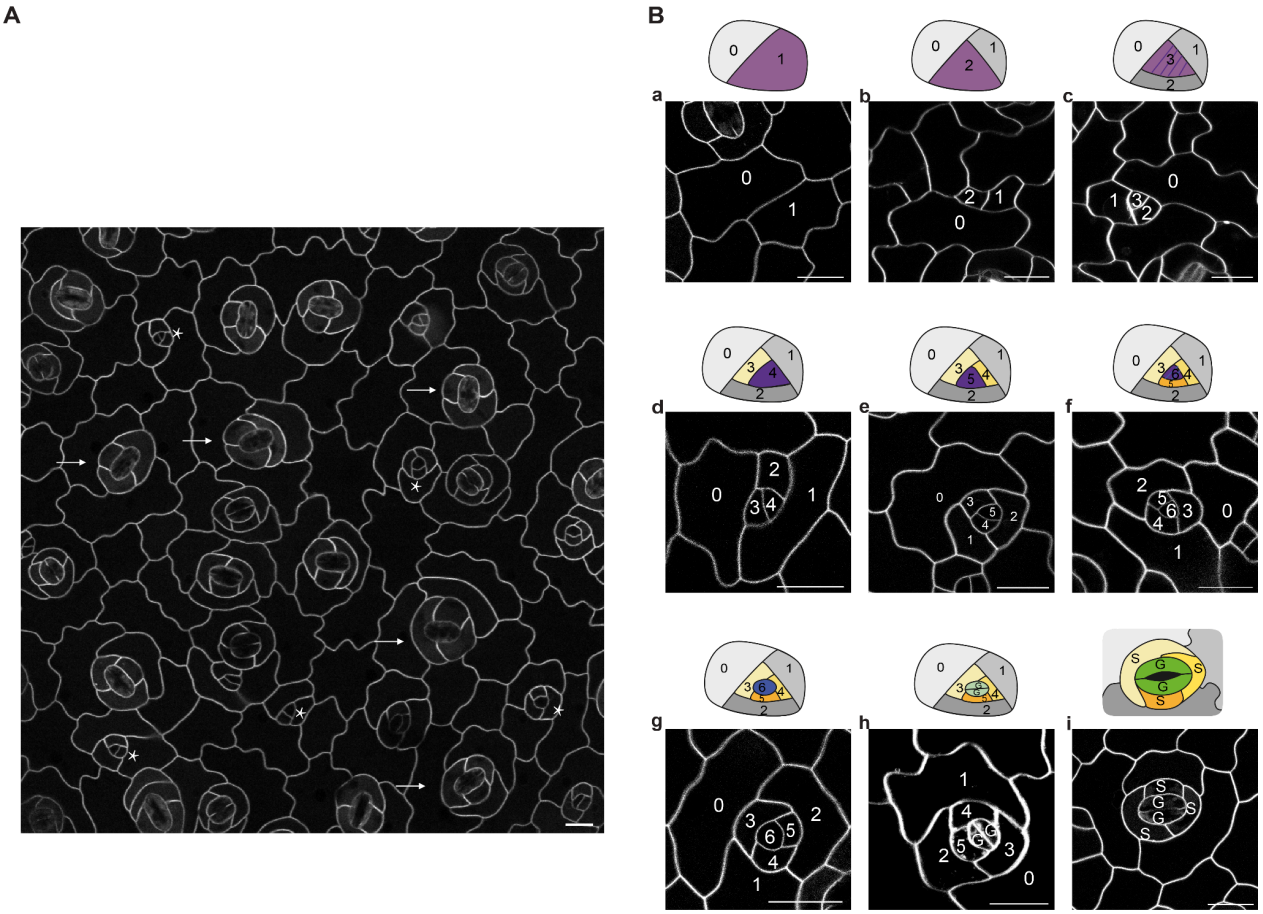

Figure 15. Different stages of stomatal development in *Kalanchoë laxiflora*.
(A). Confocal microscopy imaging of a 1.4 cm, abaxial side of a leaf of plasma membrane marker line. White arrows indicated the mature stomatal complexes, and white asterisks indicated the developing stomata. (B). The proposed model of stomatal development in *Kalanchoë laxiflora* based on static imaging. For each stage, the scheme is above, and the corresponding confocal microscopy image is below. (a)-(c). The first three ACDs yield three SLGCs. SLGCs are in grey, the meristemoid1 is in light purple, and the purple shade in (c) indicates the transition from meristemoid1 to meristemoid2. (d)-(f). The second three ACDs yield three SCs. SCs are in yellow, and the meristemoid2 is in dark purple. (g)-(i). Meristemoid2 transits into GMC, and the GMC divides symmetrically and finally differentiates into two GCs. The GMC is blue, the young GCs are light green, and the differentiated GCs are dark green. Scale bars, 20 μm. This scheme was created by Prof.Dr.Michael Raissig and myself, and is published in a review article in *New Phytologist* (Cheng & Raissig, 2023) (https://doi.org/10.1111/nph.18951), and revised by myself.

2.3 Stomatal development changes with leaf growth in *Kalanchoë laxiflora*

To better understand differences in stomatal development between different ages and sizes of leaves, I imaged leaves from the 2nd pair to the 4th pair (count the first visible leaf pair from the top as the 1st leaf pair) by confocal microscopy. Additionally, I also peeled the leaves from the 4th pair to the 6th pair and stained them with Toluidine blue, followed by DIC imaging. Results showed that, while the leaf was still

small and young, most epidermal cells were square (Fig. 16A), a lot of developing stomata were in the early stage of stomatal development (Fig. 16A, indicated by arrows), and only few mature stomata with GCs had formed (Fig. 16A, indicated by asterisks). While the leaf was getting bigger, more stomata were developing into mature complexes (Fig. 16B). The PCs were becoming puzzle-like through lobing while the leaf was growing until around 1.2 cm (Fig. 16C and 16D). At this stage, in addition to a large number of mature complexes, most of the remaining stomata in the leaf epidermis were already in the late stages of stomatal development (Fig. 16C and 16D, indicated by arrows). In leaves of around 2 cm, the epidermal cells were already much bigger than those in 1 cm (Fig. 16E). At this stage, most stomata already differentiated into GCs, and only a few developing stomata were in the later stages of stomatal development (Fig. 16E). In addition, the shape of PCs looked like puzzles, which were easy to identify (Fig. 16E). PCs continued expanding and were becoming bigger in the 4th pair leaves (Fig. 16F). However, comparing confocal and light microscopy images of the same pair, similar size of leaves, I found that the shape of the PCs in the light microscopy images looked less puzzle-like than those in the confocal microscopy images (Fig. 16F and 16G). This might be caused by peeling as this damages the cells, which in turn can affect the morphology. PCs continued to expand in older leaves (Fig. 16H and 16I), except for differentiated GCs and PCs; there were few developing stomata, and most of them were undergoing spacing divisions (Fig. 16H and 16I).

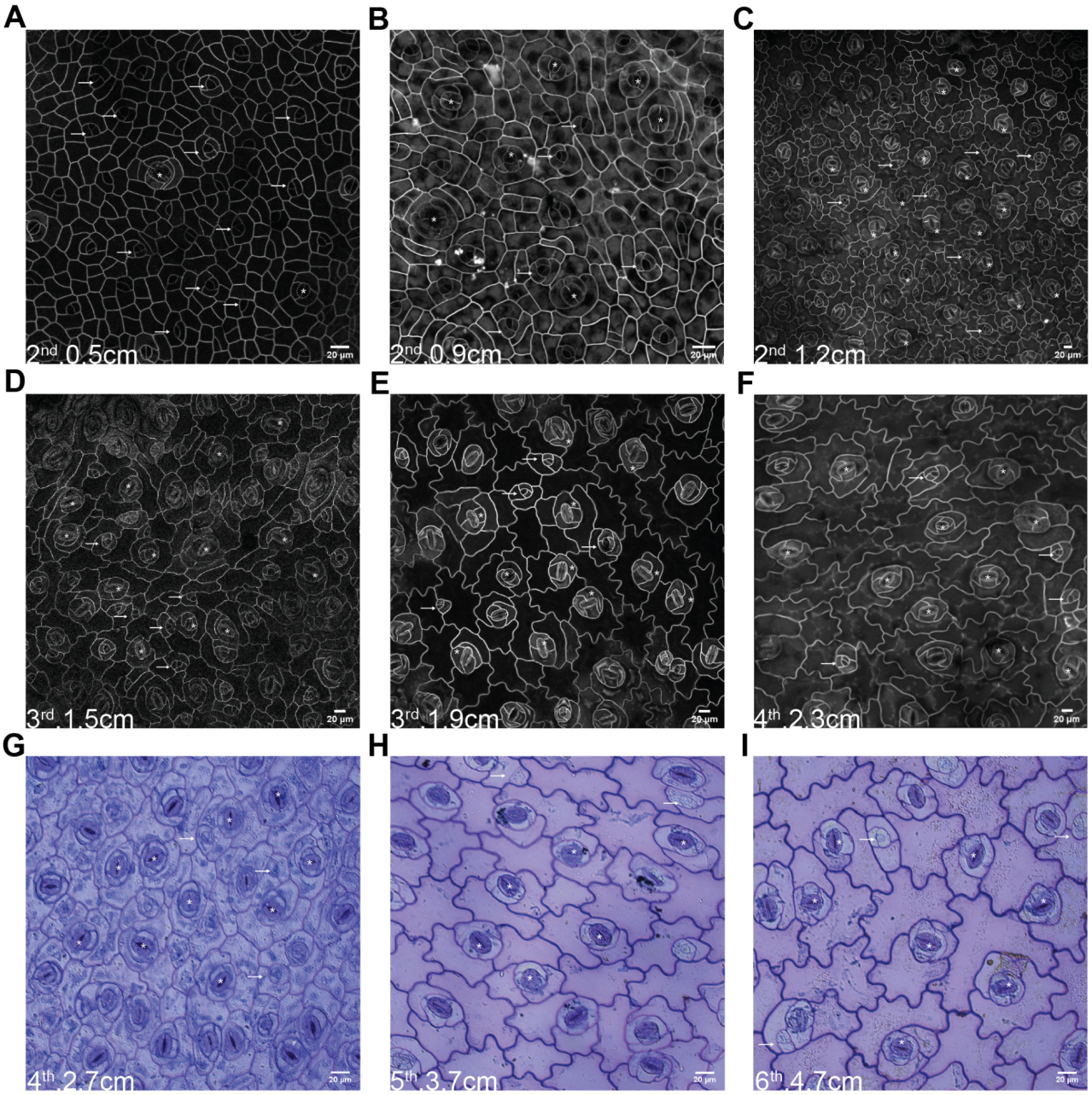

Figure 16. The development of stomata changes as the leaves grow older.
(A)-(F). Confocal microscopy images of the abaxial side of the leaves from the 2nd pair to the 4th pair of the plasma membrane marker line. (G)-(I). Toluidine blue staining and light microscope images of the abaxial side of the leaves from the 4th pair to the 6th pair of WT plants. The leaf pair and the leaf size were indicated in each image. White asterisks indicated the mature stomatal complexes, and white arrows indicated the developing stomata. Scale bars, 20 μm.

To quantify the difference in stomatal development across the plants develoment, I imaged the abaxial side of leaves from the 4th pair until the 15th pair from three WT

individuals (Fig. 17A). Interestingly, I found that except for in young leaves (Fig. 17B), developing stomata could still be observed in the 15th pair (Fig. 17C). In addition, I also observed that in the images from the older leaves like Fig. 17C, PCs were stained in light purple while GCs were stained in dark purple, but SCs were still in white. The difference in color between PCs and SCs suggested that the PCs and SCs might belong to different cell types and have different functions.

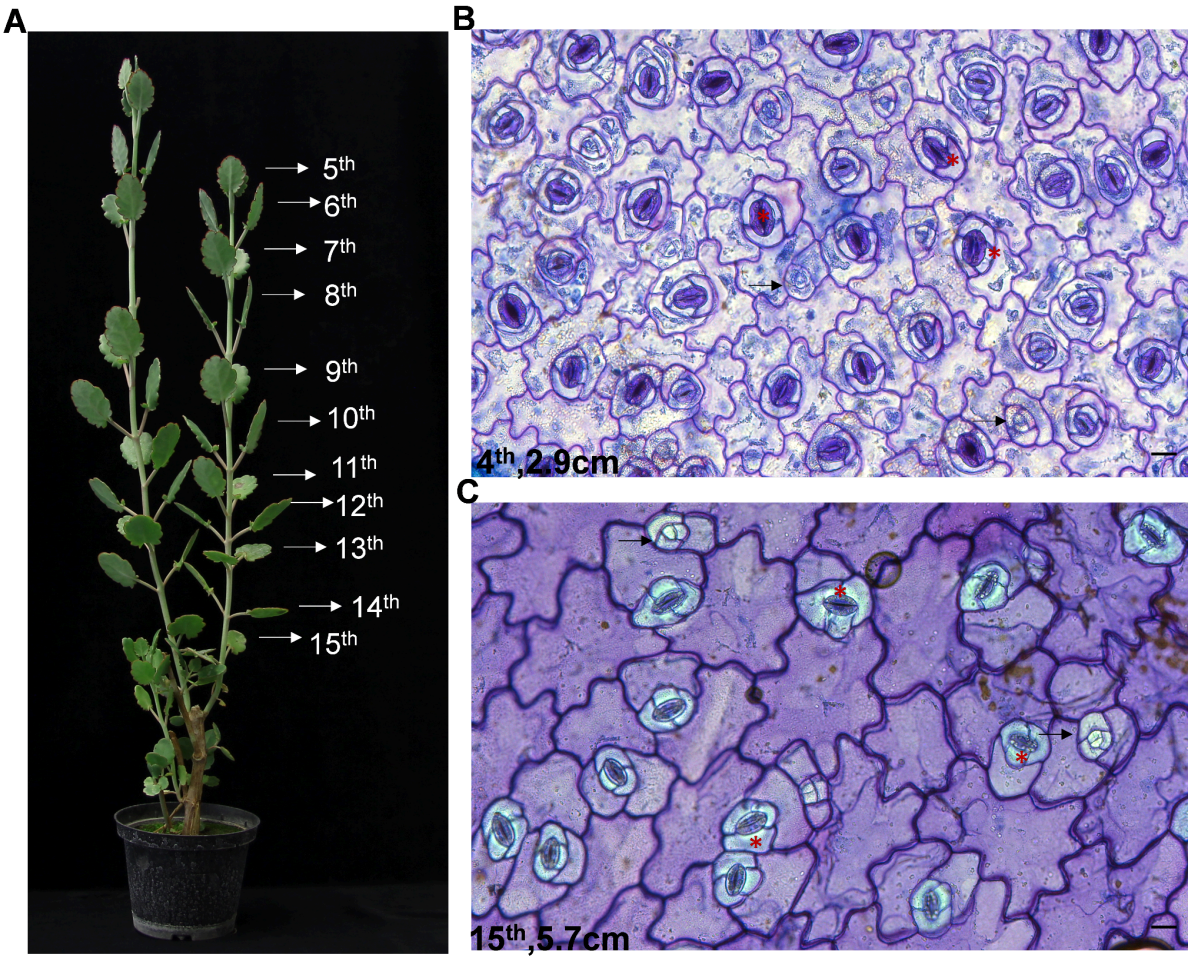

Figure 17. Light microscope imaging from the 4th pair of leaves to the 15th pair of leaves of WT *Kalanchoë laxiflora*.
(A). The leaves from the 4th pair to the 15th pair were harvested and peeled, and the abaxial side of leaves were stained with Toluidine blue staining for light microscope imaging. (B). Light microscopy image of the 4th, 2.9 cm leaf. (C). Light microscopy image of the 15th, 5.7 cm leaf. The stomatal SCs were stained white, while PCs and GCs were purple. The red asterisks indicate the mature stomatal complexes. Scale bars, 20 μm.

Quantification showed that cell density (Fig. 18A), developing stomata density (Fig. 18B), and stomatal density (Fig. 18C) decreased dramatically from the 4th pair to the

5th pair; the density tended to be relatively stable from the 6th pair to the 15th pair. Surprisingly, I also found that the stomata index didn't change significantly from the 4th pair to the 15th pair (Fig. 18D); this indicated that the proportion of cells that developed into GCs during the whole leaf epidermis development is always stable. In general, there was no significant change in developing stomata density, stomatal density, and stomata index from the 6th pair to the 15th pair, suggesting that the 6th pair of leaves can be considered "mature leaves" for stomatal development.

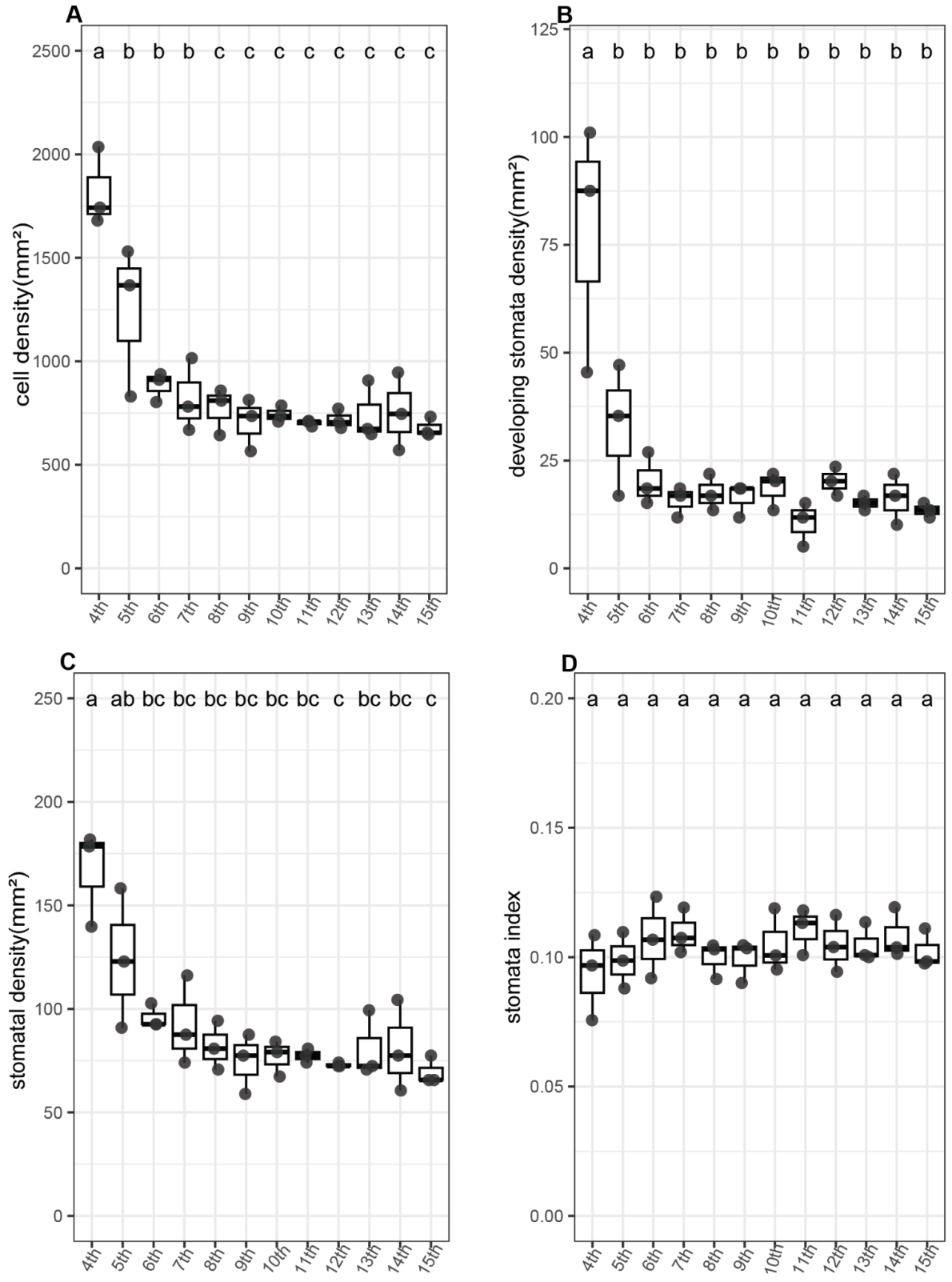

Figure 18. Quantification of the stomatal development from the 4th pair of leaves to the 15th pair of leaves of *Kalanchoë laxiflora*.
(A). The cell density of the leaf epidermis significantly decreased from the 4th pair to the 7th pair and became stable from the 8th pair. (B). Developing stomata density and (C). Stomatal density decreased dramatically from the 4th pair and tended to be stable from the 6th pair of

leaves. (D) The stomatal index did not change significantly while the leaf was growing bigger. Three WT individuals were counted. One-way ANOVA and Tukey posthoc test were used to compare multiple samples; letters indicated significance groups (pValue<0.05 was considered significant).

2.4 The stomata show the same morphology but different development in plantlets

Similar to other succulents, which can vegetatively propagate easily by producing plantlets from leaf margins (Garcês et al., 2007), leaves from *Kalanchoë laxiflora* also made plantlets from leaf edges (Fig. 19A). To investigate whether the stomatal development in leaves of plantlets is different from that in leaves of plants germinated from seeds or cuttings, I imaged the abaxial side of the 1st, 2nd, and 3rd pairs of leaves from plantlets which had 4 pairs of leaves in total (count the first visible leaf pair from the top as the 1st leaf pair). Interestingly, I found that the leaf epidermis from the bottom of the 1st pair had the “developing zone” which only had a few GCs and most stomatal complexes were still dividing (developing stomata were indicated by arrows, Fig. 19B), while the leaf epidermis from the tip of the 1st pair had the “developed zone”, where the PCs looked puzzles-like, even if there were still some developing stomata, more stomatal complexes have reached the GC stage (Fig. 19C), this is similar to the linear stomatal development in *Brachypodium distachyon* (Raissig et al., 2016). Different from the 2nd pair, 0.5 cm leaf of plants germinated from seeds which showed square PCs and a lot of developing stomata in the early stages of stomatal development (Fig. 16A), many GCs and puzzles-like, differentiated PCs were observed in the epidermis of the 2nd pair, 0.4 cm leaf from plantlets(Fig. 19D), which is similar to the stomatal development in the same pair (the 2nd pair), but bigger leaves (1.2 cm) of plants germinated from seeds (Fig. 16C). While the leaf of plantlets was getting older (the 3rd pair, 1.3 cm), PCs were expanding and getting bigger, most stomata differentiated into GCs and only a few remaining stomata were in the later stage of stomatal development (Fig. 19E). This is similar to the stomatal development from the same pair (the 3rd pair), around 2 cm leaves of plants germinated from seeds (Fig. 16E), but different from that in the similar size (1.2 cm) of leaf from plants germinated from seeds (Fig. 16C).

Images from the leaf epidermis of plantlets showed that the stomatal development in plantlets is different from that in plants germinated from seeds or cuttings. Leaf pair rather than leaf size decides the stomatal development in leaves of plantlets.

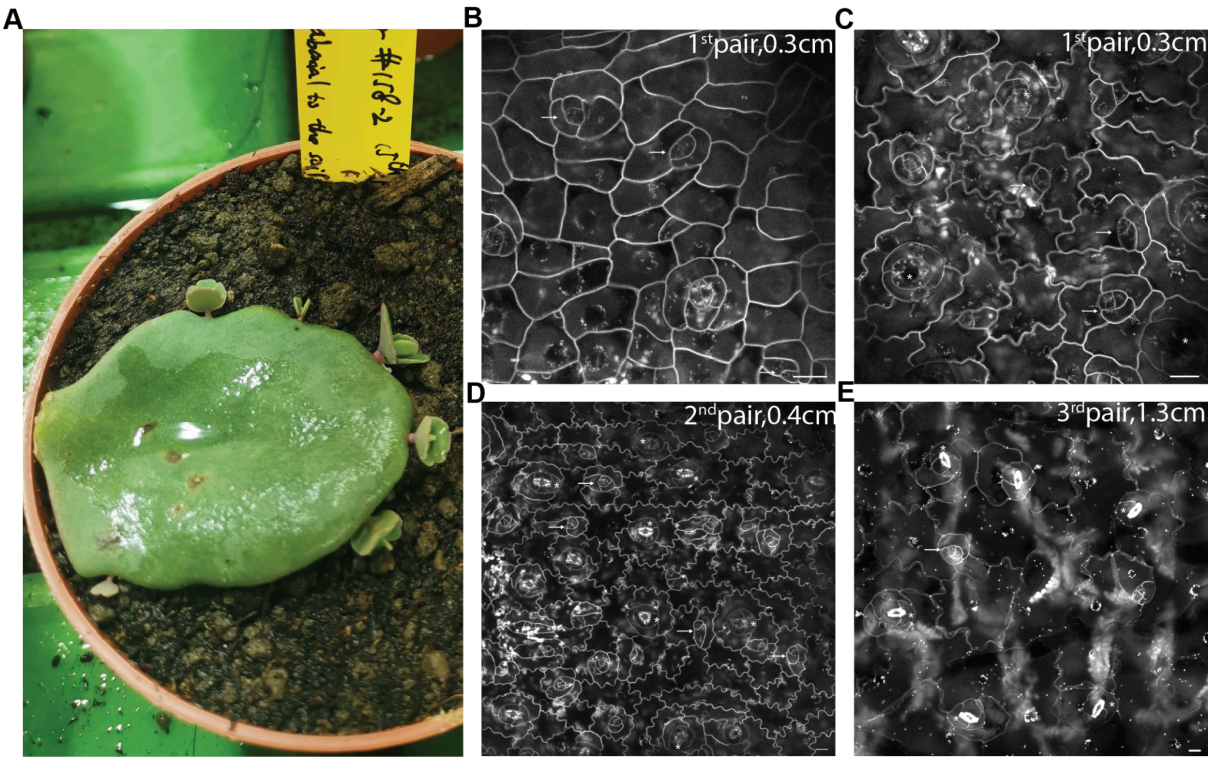

Figure 19. Confocal microscopy imaging of the leaf epidermis from the plantlets of Kalanchoë laxiflora.
(A). The plantlets grow from the edges of the detached mother leaf. (B)-(E). Confocal microscopy images of the abaxial sides of leaves from the plantlets of plasma membrane marker lines. Leaf pairs and leaf size were indicated in each image. White asterisks indicated the mature stomatal complexes, and white arrows indicated the developing stomata. Scale bars, 20 μm.

3. *MUTE* drives asymmetric divisions to form stomatal SCs in *Kalanchoë laxiflora*

Based on my proposed model of stomatal development in *Kalanchoë laxiflora*, the meristemoid undergoes more ACDs than in *Arabidopsis thaliana* (Gong et al., 2023), suggesting that the meristemoids in *K. laxiflora* have higher division capacity and are more precisely regulated. Moreover, the daughter cells from the first three ACDs are different cell types compared to those from the second three ACDs, indicating that the meristemoid transitions from meristemoid 1 to meristemoid 2 (Fig. 15B, c). However, the genetic program that controls this transition and allows the higher division capacity is unknown.

3.1 Identifying *KlMUTEs* in *Kalanchoë laxiflora*

The conserved key stomatal bHLH transcription factors SPCH, MUTE, and FAMA are important for stomatal development across different species (C. C. Chater et al., 2016; Chua & Lau, 2024; Ortega et al., 2019; Serna, 2020). In *Arabidopsis thaliana*, stomata consist of only two kidney-shaped GCs. *AtMUTE* terminates ACDs of the meristemoid, drives the meristemoid to GMC transition, and promotes a symmetric cell division of the GMC (S.-K. Han et al., 2018). However, the ortholog of *AtMUTE* in the grass model *Brachypodium distachyon*, whose stomata include two dumbbell-shaped GCs and two lateral dome-shaped SCs, BdMUTE is required for the recruitment of subsidiary mother cells from neighbouring cell rows, and *bdmute* shows SC defects in stomata (Raissig et al., 2017). This implies that MUTE might have diverged functions for diverse stomatal morphology in different species. Similar to the stomata in *B. distachyon*, the stomata in *Kalanchoë laxiflora* also have SCs. To explore whether the orthologs of MUTE in *K. laxiflora* also contribute to the stomatal SC development, I decided to investigate MUTE as a crucial candidate gene for studying this process.

Through homologs amino acid sequence alignment analysis, I found two homologs of *AtMUTE* in *K. laxiflora* and named them *KlMUTE1* and *KlMUTE2* (Fig. 20A). Then, I did the MUTE alignment with *K. laxiflora* and five representative monocot grass species and five dicots (Fig. 20B). The results showed that the C-terminus of MUTE in five dicots whose stomata do not have SCs are shorter than in grasses whose stomata include SCs. Interestingly, I found that both KlMUTE have longer C-terminus compared to MUTE in other dicots, similar to MUTE in grasses. Combined with the fact that the stomata in *K. laxiflora* also have SCs, this implies that the C-terminus of MUTE might be functionally relevant to the development of stomatal SCs.

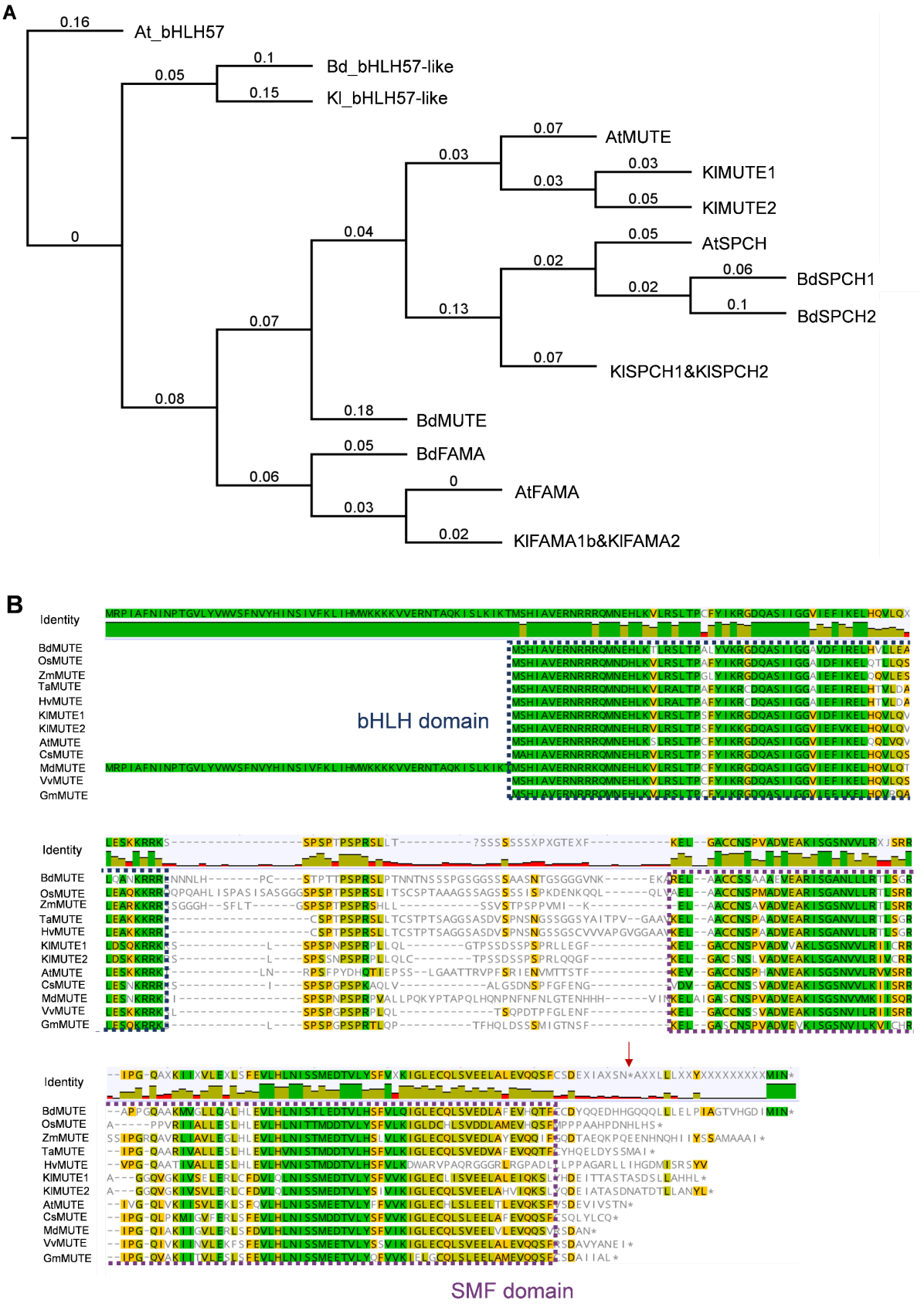
A
0.16
At_bHLH57
0.05
0.1
Bd_bHLH57-like
0.15
Kl_bHLH57-like
0.07
AtMUTE
0.03
0.03
KlMUTE1
0.03
0.05
KlMUTE2
0.05
AtSPCH
0.02
0.06
BdSPCH1
0.02
0.1
BdSPCH2
0.07
KlSPCH1&KlSPCH2
0
0.04
0.13
0.07
0.08
0.18
BdMUTE
0.05
BdFAMA
0.06
0
AtFAMA
0.03
0.02
KlFAMA1b&KlFAMA2
B
Identity
BdMUTE
OsMUTE
ZmMUTE
TaMUTE
HvMUTE
KlMUTE1
KlMUTE2
AtMUTE
CsMUTE
MdMUTE
VvMUTE
GmMUTE
bHLH domain
SMF domain

Figure 20. Phylogenetic tree of conserved stomatal transcription factors and MUTE alignment among different species.

(A). Phylogenetic tree of stomatal transcription factors SPCH, MUTE, and FAMA (with their sister gene bHLH57) in *Kalanchoë. laxiflora*, *Brachypodium. distachyon* and *Arabidopsis. thaliana*. Each gene's bHLH domain (63 amino acids) was extracted from the whole amino acid sequence for the alignment. The phylogenetic tree was built by neighbor-joining and set up the At_bHLH57 bHLH domain as an outgroup in Geneious. Sequences are from: *Kalanchoë. laxiflora*, (KlSPCH1 = KlGene017537, KlSPCH2 = KlGene027982, KlMUTE1 = KlGene012921, KlMUTE2 = KlGene023418, KlFAMA1b = KlGene012763, KlFAMA2 = KlOBG012781), the Kl_bHLH57-like (=Kalaxd.09G089900) is from *Kalanchoë. laxiflora var FTBG2000359A*, *Arabidopsis. thaliana* (AtSPCH =AT5G53210.1, AtMUTE = At3G06120, AtFAMA = AT3G24140.1, At_bHLH57 = AT2G46810.1), *Brachypodium. distachyon* (BdSPCH1 = Bradi1g38650.1, BdSPCH2 = Bradi3g09670.1, BdMUTE = Bradi1g18400, BdFAMA = Bradi2g22810.1, Bd_bHLH57-like = Bradi1g71990.2). (B). MUTE protein alignment from five grass species and six dicot species. Including *Brachypodium. distachyon* (BdMUTE=Bradi1g18400), *Oryza sativa* (OsMUTE=Os05g51820.1), *Zea mays* (ZmMUTE=Zm00001d009778_P001), *Triticum aestivum* (TaMUTE=Traes_2BS_EE97B0B15.1), *Hordeum vulgare* (HvMUTE=HORVU2Hr1G020990.3), *Kalanchoë. laxiflora* (KlMUTE1 = KlGene012921, KlMUTE2 = KlGene023418), *Arabidopsis. thaliana* (AtMUTE=AT3G06120), *Cucumis sativus* (CsMUTE=Cucsa.254010.1), *Malus domestica* (MdMUTE=MD13G1184300), *Vitis. vinifera* (VvMUTE=GSVIVT01017892001), *Glycine max* (GmMUTE=Glyma.13G208300.1).

3.2 *KlMUTE1* and *KlMUTE2* might have redundant functions

To explore the function of *KlMUTEs* in the stomatal development of *Kalanchoë laxiflora*, I started using CRISPR-CAS9-mediated gene editing and RNA interference to analyze their function.

To knock out KlMUTEs in *K. laxiflora*, I designed a specific guide for knocking out *KlMUTE1* (Fig. 21A, guide1) and *KlMUTE2* (Fig. 21A, guide2), respectively, and one guide for knocking out both KlMUTEs simultaneously (Fig. 21A, guide3). The three guide RNAs were cloned into the final pFASTRK-PcUBIP-AtCas9-NLS-P2A-mCherry-G7T-AtU6-BsaI-CmR-ccdB-BsaI scaffold (p01178) backbone separately, and I transformed these three constructs into WT *K. laxiflora* individually. Finally, I got transgenic lines from three constructs. Among these transgenic lines, I only got *klmute1* single mutant from guide 3 instead of double mutants, so I decided to work with *klmute1* from guide 3 and *klmute2* from guide 2. *klmute1* had a homozygous “T” insertion close to the PAM site, which caused a shift in the open reading frame leading to an early stop. This mutation resulted in a protein which was only 56 amino acids long instead of 207 amino acids (Fig. 21B). *klmute2* had a “T” insertion and a “T” deletion (heteroallelic) close to the PAM site, causing a shift in the open reading frame. The “T” insertion produced a protein which had 145 amino acids instead of 208 amino acids, while the “T” deletion

produced a protein which had 121 amino acids instead of 208 amino acid (Fig. 21C). By comparing the 7th leaf pair (ca. 4 cm) of WT plants with the single mutants, no phenotype in stomatal morphology was observed (Fig. 21D), suggesting that *KIMUTE1* and *KIMUTE2* might have a redundant function.

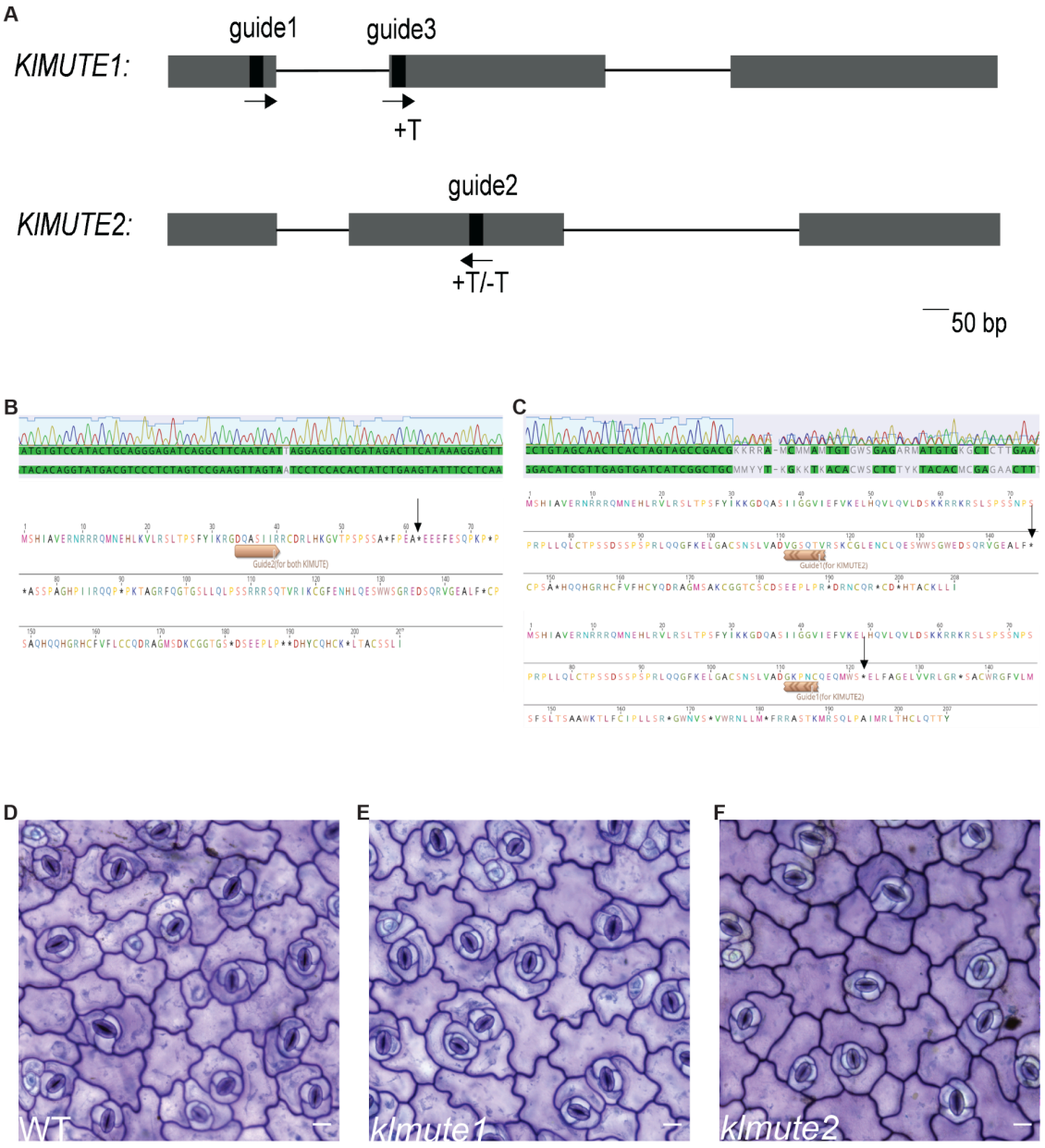

Figure 21. *KIMUTE1* and *KIMUTE2* might have redundant functions.
(A). Locations of the gene editing sites in *KIMUTEs*. Guides were indicated. (B)-(C). Amino acid sequence of *klmute1* single homozygous mutants (B) and *klmute2* single homozygous mutants(C). The black arrow indicated the site of premature termination of protein translation. (D)-(F) Toluidine blue staining and light microscope imaging of the abaxial side of the 7th, around 4 cm leaves of WT (D), *klmute1* (E) and *klmute2* (F). Scale bars, 20 μm.

To obtain double mutants for further analyzing the function of *KlMUTEs* and explore whether *KlMUTE1* and *KlMUTE2* have slight differences in function, I crossed the single *klmute1* mutants with single *klmute2* mutants. For crossing, I pollinated the stigma from *klmute1* with the pollen from *klmute2* (Fig. 22A) and vice versa (Fig. 22B). In the next generation, except double mutants, I also harvested seeds of *klmute1/klmute1;klmute2/+*, *klmute1/+;klmute2/klmute2* and *klmute1/+;klmute2/+*. After the self-pollination of *klmute1/klmute1;klmute2/+* and *klmute1/+;klmute2/klmute2*, I sowed the seeds from the mutants and WT at the same time. After the genotyping of seedlings, I got three individuals of each genotype: *klmute1/klmute1;klmute2/+*, *klmute1/+;klmute2/klmute2*, *klmute1/klmute1;+/+* and *+/+;klmute2/klmute2*. Then I chosen the 7th pair, roughly 4 cm leaves from WT, *klmute1/klmute1;klmute2/+*, *klmute1/+;klmute2/klmute2*, *klmute1/klmute1;+/+* and *+/+;klmute2/klmute2*, and performed toluidine blue staining of epidermal peels. DIC imaging showed that similar to *klmute1* single mutants and *klmute2* single mutants (Fig. 22E and 22F), *klmute1/klmute1;klmute2/+* and *klmute1/+;klmute2/klmute2* didn't show any stomatal morphology phenotype compared with WT (Fig. 22C to 22E). The quantification results showed that there was no significant difference in cell density (Fig. 22F) and stomatal density (Fig. 22G) between the mutants and WT, and also there was no significant difference between the mutants, suggesting that *KlMUTE1* and *KlMUTE2* have redundant functions. For stomata index (Fig. 22H), *klmute1/klmute1;klmute2/+*, *klmute1/+;klmute2/klmute2*, *klmute1/klmute1;+/+* and *+/+;klmute2/klmute2* didn't show significant difference compared with WT. However, *klmute1* single mutant (*klmute1/klmute1;+/+*) showed a significantly higher stomata index compared to *klmute1/+;klmute2/klmute2*. The stomata index of *klmute1/klmute1;klmute2/+* on the other hand is slightly lower than in *klmute1/klmute1;+/+* but higher than in *klmute1/+;klmute2/klmute2*, suggesting that *KlMUTE2* is important for the GC divisions. Combined to the data showed that the stomata index of *klmute1/klmute1;klmute2/+* is similar as that in *klmute2* single mutants (*+/+;klmute2/klmute2*), implying that even if *KlMUTE1* and *KlMUTE2* have redundant function, KlMUTE2 might play a more important role in GCs divisions.

A

mute1/mute1;MUTE2/MUTE2;CAS9^{MUTE1}/-
X
MUTE1/MUTE1;mute2/mute2;CAS9^{MUTE2}/-

♀ \ ♂	***MUTE1;mute2***	***MUTE1;mute2;CAS9^{MUTE2}***
mute1;MUTE2	*mute1/MUTE1;MUTE2/mute2;-/-;-/-*	*mute1/MUTE1;mute2/mute2;-/-;-/CAS9^{MUTE2}*
mute1;MUTE2;CAS9^{MUTE1}	*mute1/mute1;MUTE2/mute2;CAS9^{MUTE1}/-;-/-*	*mute1/mute1;mute2/mute2;CAS9^{MUTE1}/-;-/CAS9^{MUTE2}*

B

MUTE1/MUTE1;mute2/mute2;CAS9^{MUTE2}/-
X
mute1/mute1;MUTE2/MUTE2;CAS9^{MUTE1}/-

♀ \ ♂	***mute1;MUTE2***	***mute1;MUTE2;CAS9^{MUTE1}***
MUTE1;mute2	*MUTE1/mute1;mute2/MUTE2;-/-;-/-*	*mute1/mute1;mute2/MUTE2;-/CAS9^{MUTE1};-/-*
MUTE1;mute2;CAS9^{MUTE2}	*MUTE1/mute1;mute2/mute2;-/-;CAS9^{MUTE2}/-*	*mute1/mute1;mute2/mute2;-/CAS9^{MUTE1};CAS9^{MUTE2}/-*

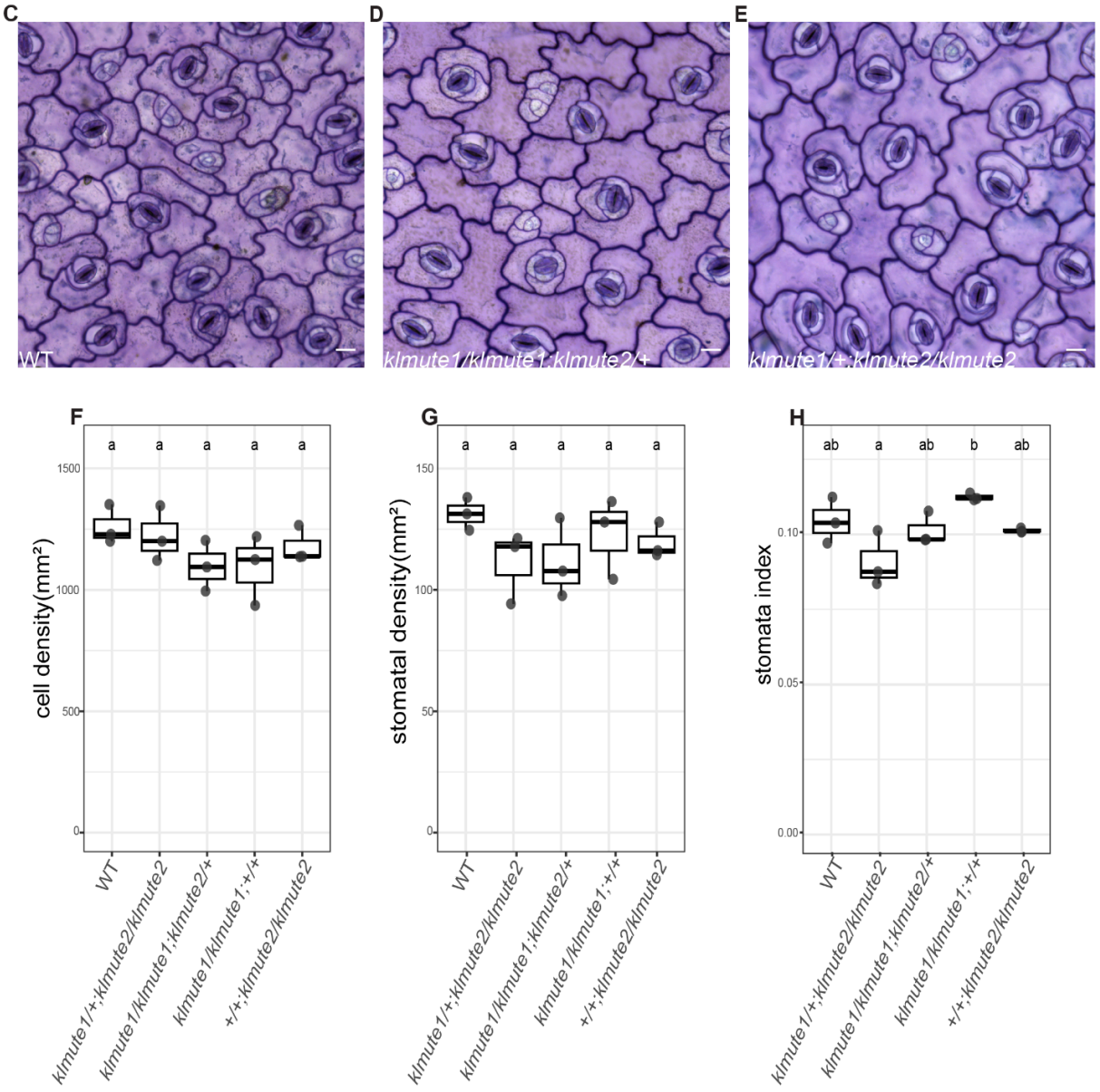

Figure 22. *KlMUTE1* and *KlMUTE2* might have slight differences in the preference of gene functions.
(A)-(B). Crossing schemes for obtaining different genotypes of *KlMUTEs* mutants. (C)- (E). Light microscope imaging of the abaxial side of the 7th, around 4 cm leaves of WT(C), *klmute1/klmute1;klmute2/+* (D) and *klmute1/+;klmute2/klmute2* (E). Scale bars, 20 μm. (F)-(H) Quantification of cell density (F), stomatal density (G), and stomata index (H) between WT and different genotypes of *KlMUTEs* mutants. For each genotype, three individuals were counted. One-way ANOVA and Tukey posthoc test were used for comparison between multiple samples, letters indicated significance groups (pValue<0.05 was considered as significant).

3.3 *klmute1;klmute2* show aberrant asymmetric divisions and don't have GCs

From the crossing (Fig. 22A and 22B), I got double mutants, compared to the WT seedlings (Fig. 23A), *klmute1;klmute2* have severe growth phenotypes (Fig. 23B). The seedlings arrested very early in development and only had two young cotyledons (they can be kept for a while on the plates with sugar, but can't survive on the plates without sugar). Then, I did confocal microscopy imaging using 14d-after-sowing cotyledons of seedlings of WT and double mutants. Compared with WT which has properly developing stomata (Fig. 23C) and mature stomatal complex (Fig. 23D); in *klmute1;klmute2*, instead of proper ACDs, the stomata show parallel divisions (Fig. 23E) or divisions at the wrong division plane (Fig. 23F). In addition, the stomata also show divisions in neighbor cells (white arrow in Fig. 23E and 23F), which does not happen in SCs of developing stomata in WT (Fig. 23C). The whole leaf epidermis does not have any GCs, suggesting that *KlMUTEs* might function in the early ACDs before the GMC transition.

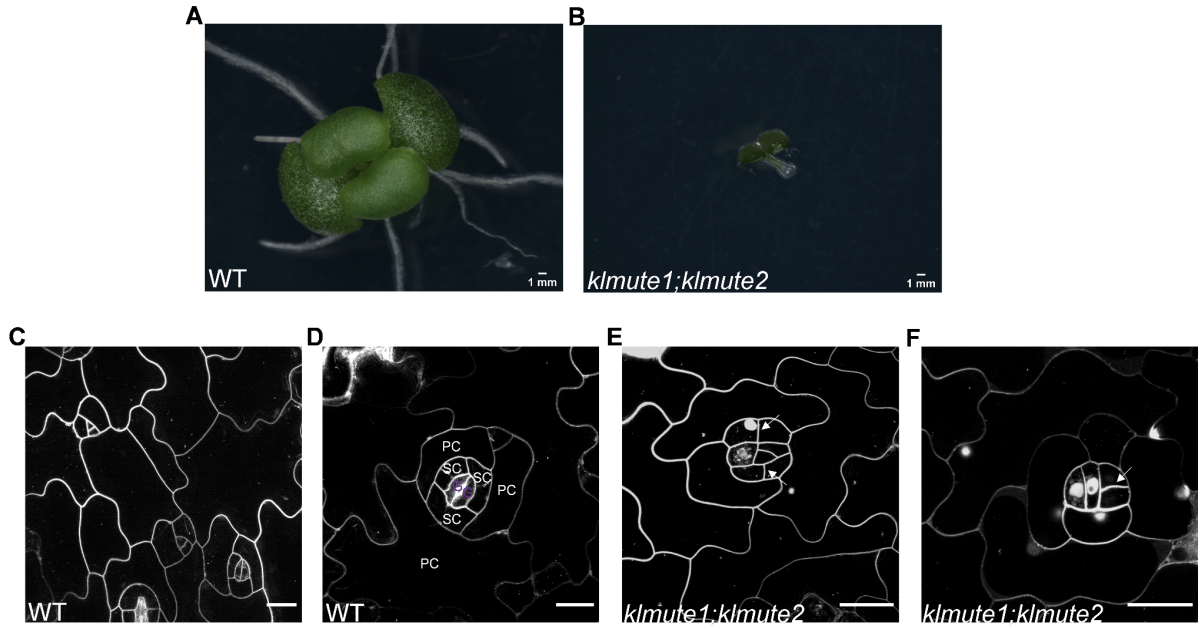

Figure 23. *klmute1;klmute2* show aberrant asymmetric divisions and don't have guard cells.
(A)-(B). Compared to WT (A), the growth of *klmute1;klmute2* was stuck in two cotyledons (B). Scale bars were indicated. (C)- (F). Confocal microscopy images from the abaxial side of 14d-after-sowing cotyledons from WT (C)- (D) and *klmute1;klmute2* (E)-(F). White arrows indicated the extra divisions in neighboring cells. Scale bars, 20 μm. Plasma membranes were stained with FM4-64.

3.4 KlMUTEs RNAi lines show excess asymmetric division and GC defects

MUTE mutants in other species like *Arabidopsis thaliana*, *Zea mays,* and *Oryza sativa (Pillitteri, Sloan, et al., 2007; H. Wang et al., 2019; Wu et al., 2019)* show GCs defects and thus have seedling lethality. Therefore, given that the same situation may also occur in *Kalanchoë laxiflora*, I might not be able to analyze the stomata phenotype, so in addition to gene-editing (CRISPR-CAS9), I also cloned two RNAi constructs, both RNAi constructs are used for knocking down both KlMUTEs in *K. laxiflora*. For cloning, I used the KlMUTE1 coding sequence (CDS) as a template, and then aligned the KlMUTE1 CDS with the KlMUTE2 CDS, the KlSPCH1 CDS, the KlSPCH2 CDS, the KlFAMA1a CDS, the KlFAMA1b CDS and the KlFAMA2 CDS. Finally, I chose two highly specific fragments which include consecutive 21 bp matched in KlMUTE1 and KlMUTE2 but not in the CDS of other genes (Fig. 24A). I cloned these two fragments separately from KlMUTE1 CDS and produced the final constructs. In the end, I generated transgenic lines for both constructs. The T0 lines

from both constructs have the same phenotype. Since fragment 2 (F2) is longer than fragment 1 (F1), I expected it to have higher efficiency in simultaneously knocking down KIMUTE1 and KIMUTE2, so I finally decided to use the transgenic lines that carried fragment 2 in the construct. Compared with WT, *KIMUTE*^{RNAi} lines show growth defects, grow much slower than WT, and the leaf edges turn yellow. In addition, *KIMUTE*^{RNAi} lines also have smaller leaves than WT (Fig. 24B).

Next, I did DIC imaging of the abaxial side of 3rd leaf pair, 2 cm leaves from WT and *KIMUTE*^{RNAi} lines. The results showed that compared to WT, which has mostly mature stomatal complexes and only a few developing stomata (Fig. 24C), *KIMUTE*^{RNAi} lines only have very few mature stomata (Fig. 24D). Instead of proper ACDs and GCs differentiation (Fig. 24E), some stomata show parallel divisions (Fig. 24F), this phenotype is similar to the stomata in *klmute1;klmute2* (Fig. 23E). Some stomata also show continuous ACDs and arrested meristemoids (Fig. 24G), this phenotype is similar to stomata in *atmute* in *A. thaliana* (Pillitteri, Sloan, et al., 2007). Other than these two major abnormalitiesin *KIMUTE*^{RNAi} lines, a few stomata also show GC defects (Fig. 24H).

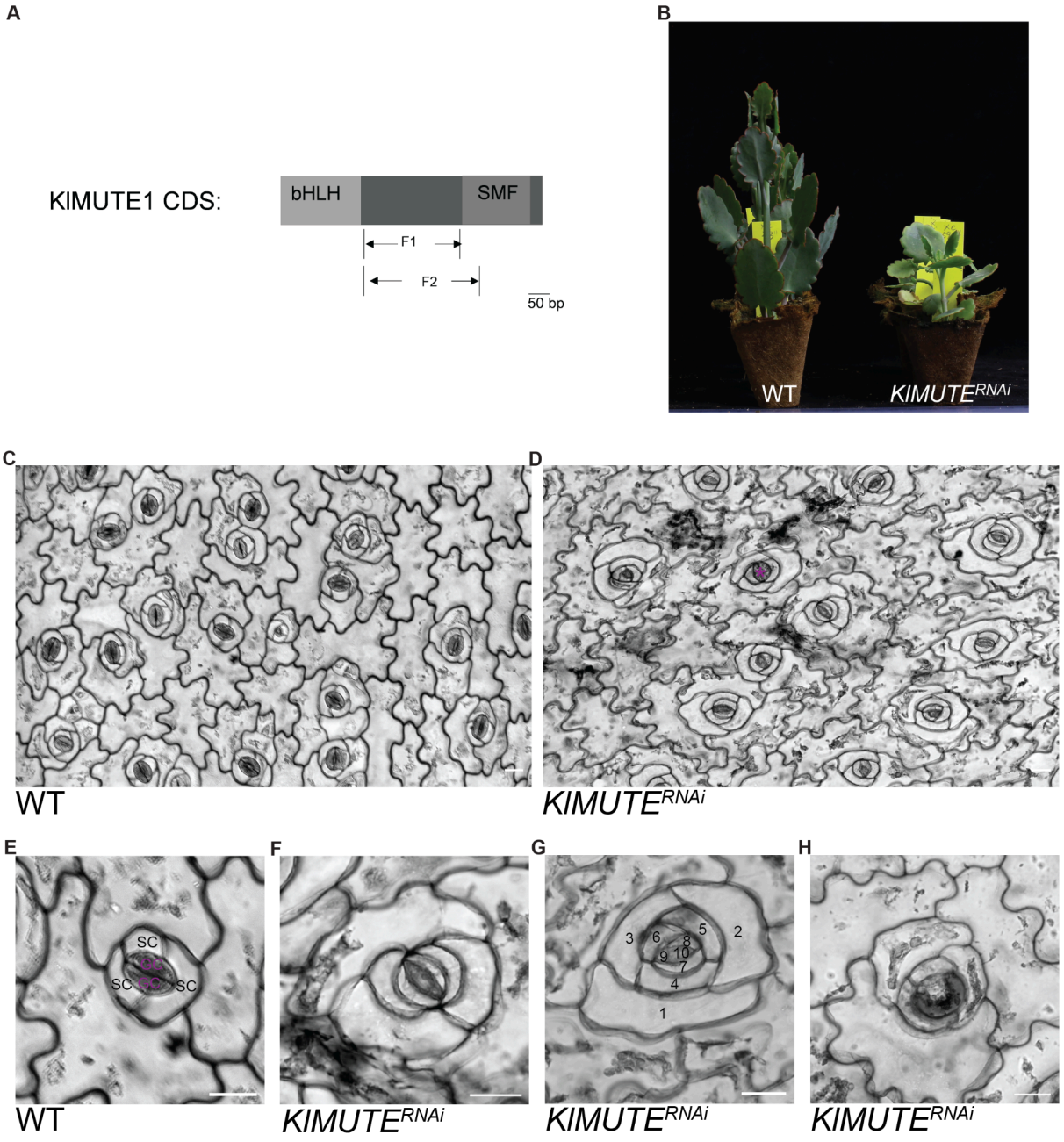

Figure 24. KlMUTEs RNAi lines show excess asymmetric division and GC defects. (A). Scheme of knocking down both KlMUTEs in *Kalanchoë laxiflora*. (B). Comparison of the plant growth between WT and KlMUTEs RNAi lines. (C)- (D). Light microscope imaging the abaxial side of the 3rd, 2 cm leaves from WT (C) and KlMUTEs RNAi lines (D). GCs were indicated in red asterisk in (D). (E)-(H). Compared to WT (E), the stomatal phenotype in KlMUTEs RNAi lines is different (F)-(H). Scale bars, 20 μm. Cell types were labeled in (E). SLGCs and the meristemoid in one stomatal complex were numbered in (G).

To further quantify the stomata phenotype in *KlMUTE*^{RNAi} lines, I screened three lines that had a strong phenotype (Fig. 25A to 25D), and I peeled the abaxial side of the 3rd, 2 cm leaves from WT and T0 *KlMUTE*^{RNAi} lines: *KlMUTE*^{RNAi}*-1*, *KlMUTE*^{RNAi}*-2* and *KlMUTE*^{RNAi}*-3* and stained them with Toluidine blue. DIC imaging and quantification

showed that while WT has roughly 70% mature stomata, *KlMUTE^{RNAi}-1* and *KlMUTE^{RNAi}-3* don't have mature stomata, and *KlMUTE^{RNAi}-2* only has around 10% mature stomata (Fig. 25E), suggesting that similarly as in *klmute1;klmute2*, *KlMUTE^{RNAi}* lines have defects in GC formation. In addition, compared to the developing stomata in WT, which have around 4 SLGCs (including the meristemoid), the developing stomata in three *KlMUTE^{RNAi}* lines have around 7-8 SLGCs (including the meristemoid) (Fig. 25F), implying that stomata in *KlMUTE^{RNAi}* lines undergo more divisions.

In summary, the stomata in *KlMUTE^{RNAi}* lines show excessive divisions and GC defects, similar to the stomatal phenotype in *atmute (Pillitteri, Sloan, et al., 2007)*, suggesting that *KlMUTEs* and *AtMUTE* might have a similar function in GMC transition.

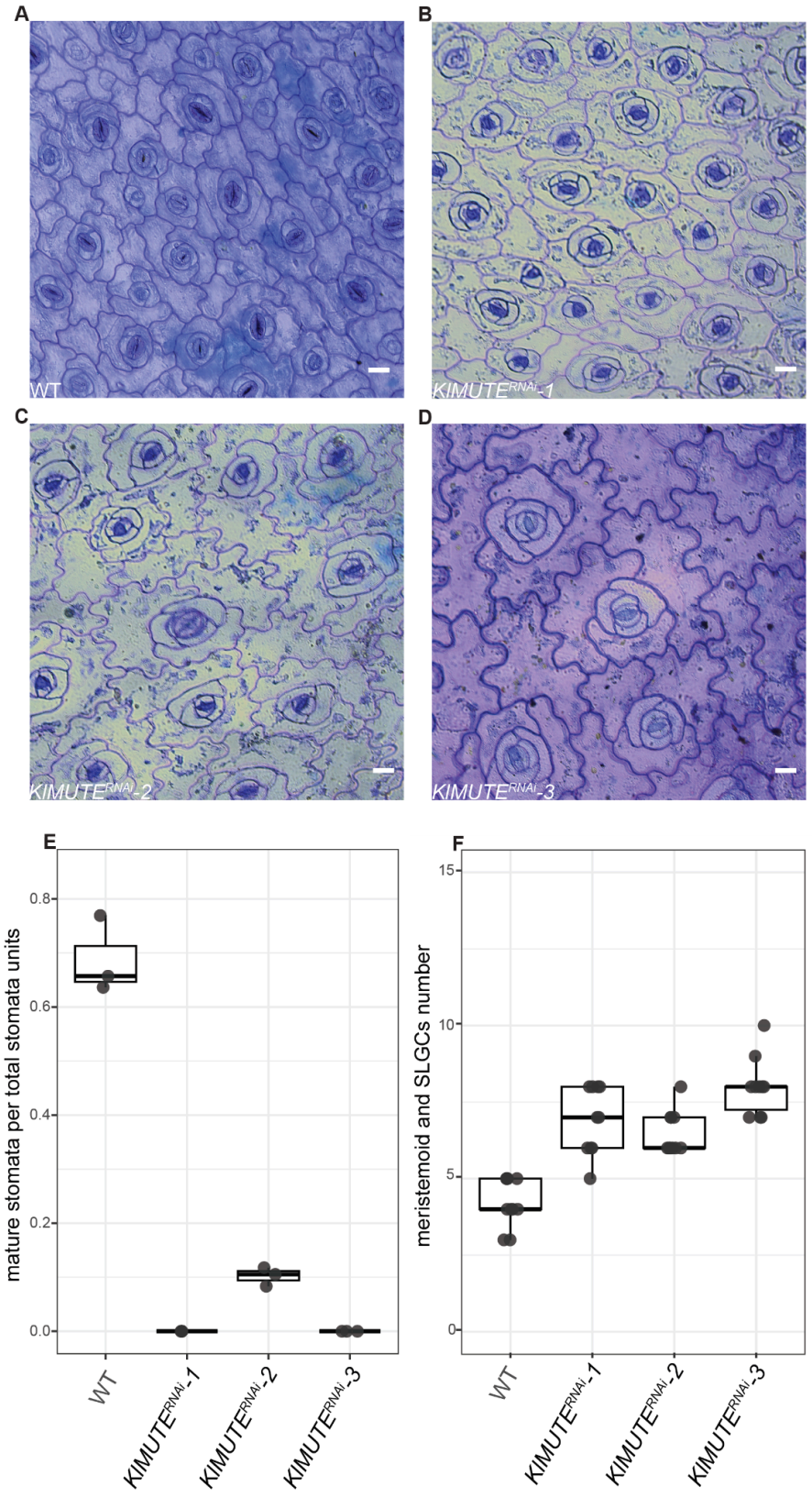

Figure 25. KIMUTEs RNAi lines showed arrested meristemoids instead of GC formation.
(A)-(D). Light microscope imaging of the abaxial side of the 3rd, 2cm leaves from WT (A) and three KIMUTE RNAi lines (B)-(D). Scale bars, 20 μm. (E). Quantification of mature stomata

per total stomata units between WT and three KlMUTEs RNAi lines. Only one individual was used for each genotype, and three fields of view were counted for plotting. (F). Quantification of meristemoid and SLGCs number per stomatal complex between WT and three KlMUTEs RNAi lines. Only one individual was used for each genotype, and ten stomatal complexes were counted for plotting.

To test the expression level of *KlMUTEs* in the *KlMUTE*^{RNAi} lines, I did semi-quantitative RT-PCR. The results showed that *KlMUTE1* might be slightly knocked down, but the expression of *KlMUTE2* didn't show a significant difference compared with WT (Fig. 26A). Similarly, KlSPCHs didn't show a difference in expression level compared to WT (Fig. 26B). However, KlFAMA1a and KlFAMA1b were significantly knocked down compared to WT (Fig. 26C), suggesting that KlMUTE1 might promote KlFAMA1a/KlFAMA1b expression in *K. laxiflora*. In some of the lines of *KlMUTE*^{RNAi}, KlFAMA2 was also down-regulated compared to WT (Fig. 26D). Since I could not confirm by semi-quantitative RT-PCR that the construct sufficiently knocked out both KlMUTEs, I decided to use CRISPR-CAS9 mutants for further gene function analysis.

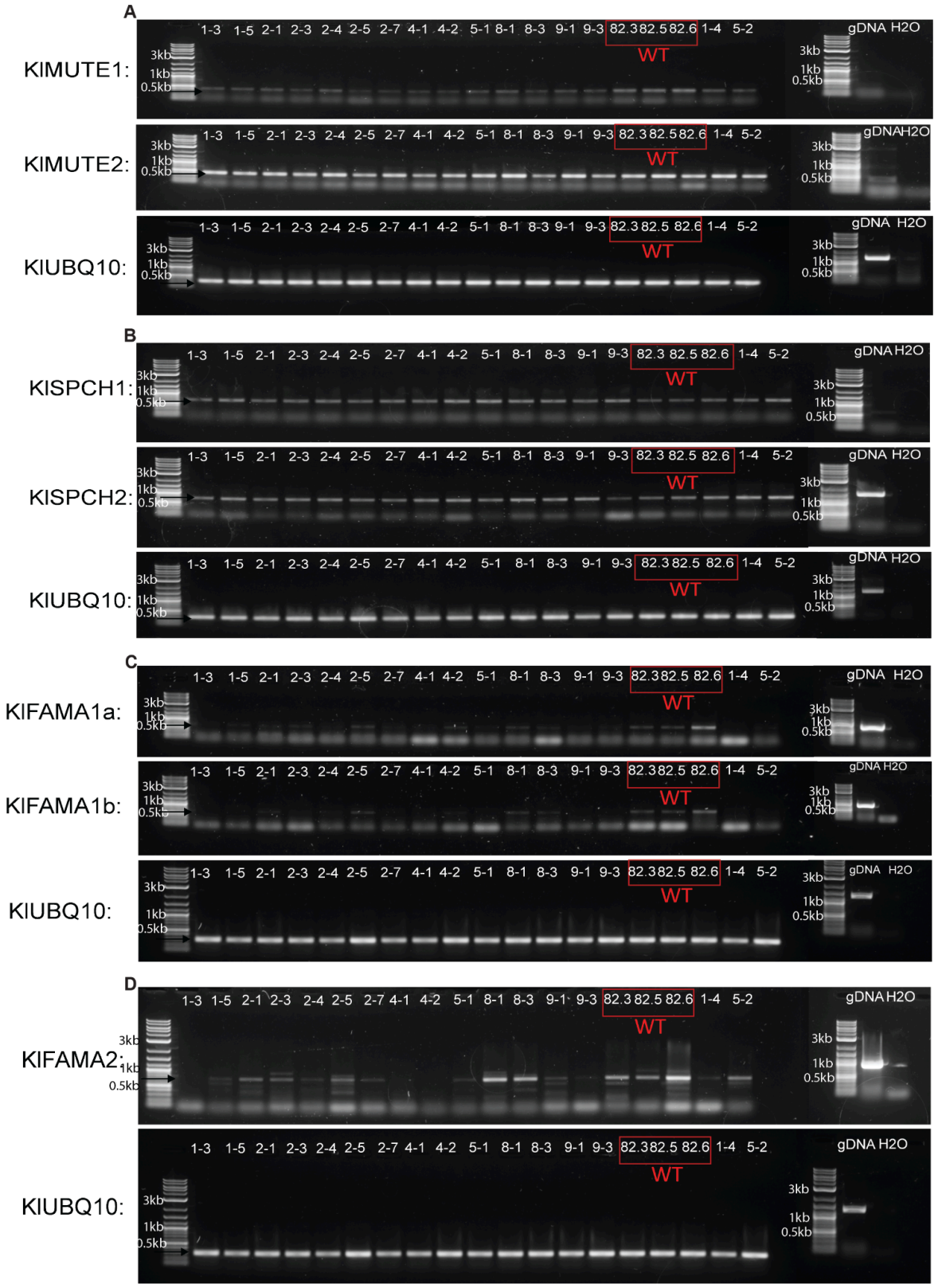

Figure 26. Semi-quantitative RT-PCR of stomatal key transcription factors in WT and KIMUTEs RNAi lines.
The expression levels of KIMUTEs, KISPCHs, and KIFAMAs in WT and individuals from different KIMUTE RNAi lines were tested by Semi-quantitative RT-PCR. KIUBQ10 was

regarded as a reference gene. Black arrows indicate target bands. WT samples and the main bands of DNA markers were also indicated in the images.

3.5 *KlMUTEs* are expressed during SCs divisions

To explore the expression of *KlMUTEs* during stomatal development and better understand the function of *KlMUTEs*, I cloned transcriptional reporters *KlMUTE1:mCitrine-eGFP*^{NLS} and *KlMUTE2:mCitrine-eGFP*^{NLS} and transformed them into WT of *Kalanchoë laxiflora*. The results showed that both *KlMUTE1* (Fig. 27) and *KlMUTE2* (Fig. 28) were first expressed in stage 3, and then persisted duirng all SC divisions (stage 4 to stage 6). During the SC divisions, the signal in the meristemoid 2 got stronger after each division and had the strongest signal in the GMC in stage 7; after the GC division, the signal became weaker (stage 8). The signal in SCs and GCs was still maintained after GC differentiation (stage 9).

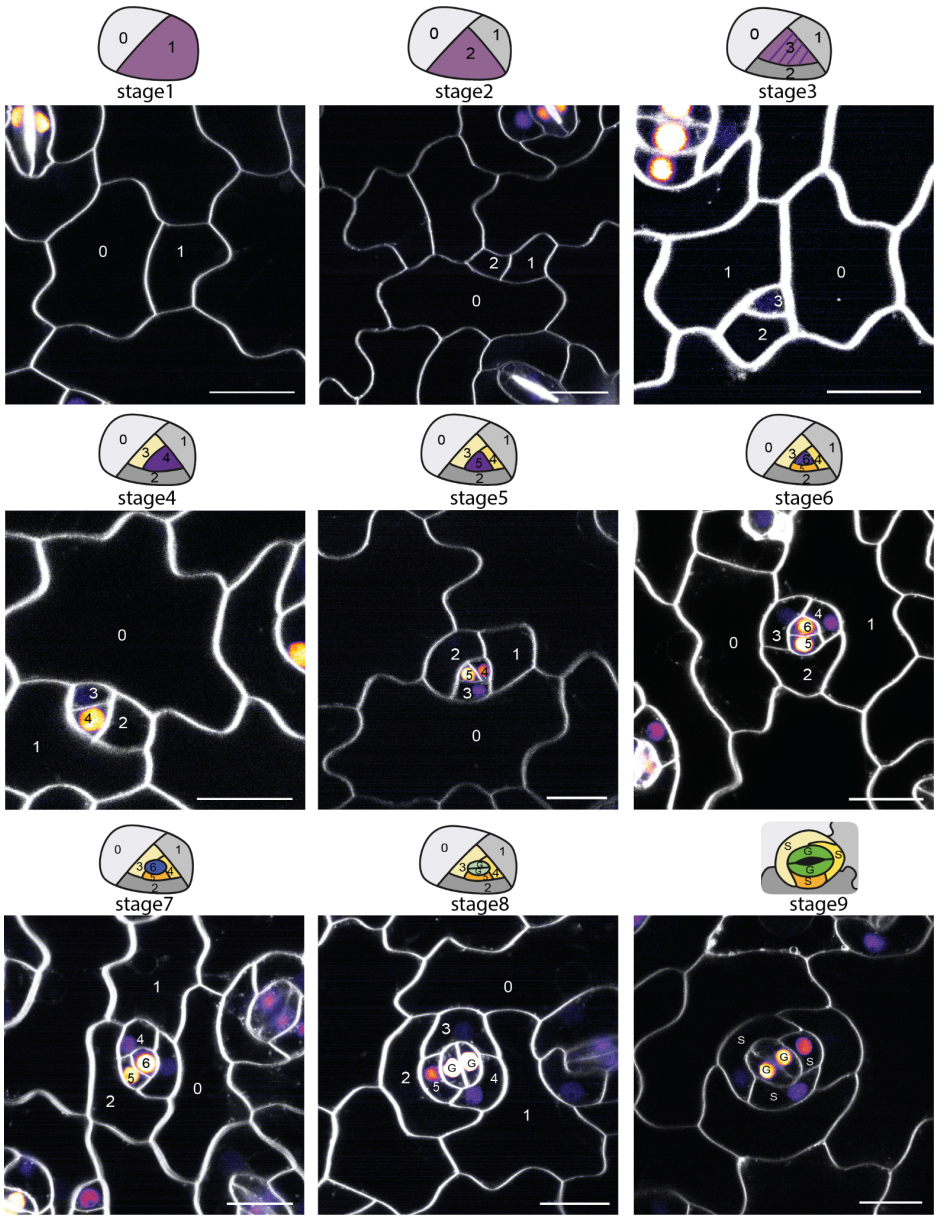

Figure 27. *KIMUTE1* is expressed in all SC divisions.
Confocal microscopy imaging of *KIMUTE1* transcriptional reporter *KIMUTE1:mCitrine-eGFP*^{NLS}. The scheme of each stomatal development stage was indicated above the corresponding confocal microscopy image. Plasma membranes were stained with FM4-64. Scale bars, 20 μm. This scheme was created by Prof.Dr.Michael Raissig and myself, and is published in a review article in *New Phytologist* (Cheng & Raissig, 2023) (https://doi.org/10.1111/nph.18951), and revised by myself.

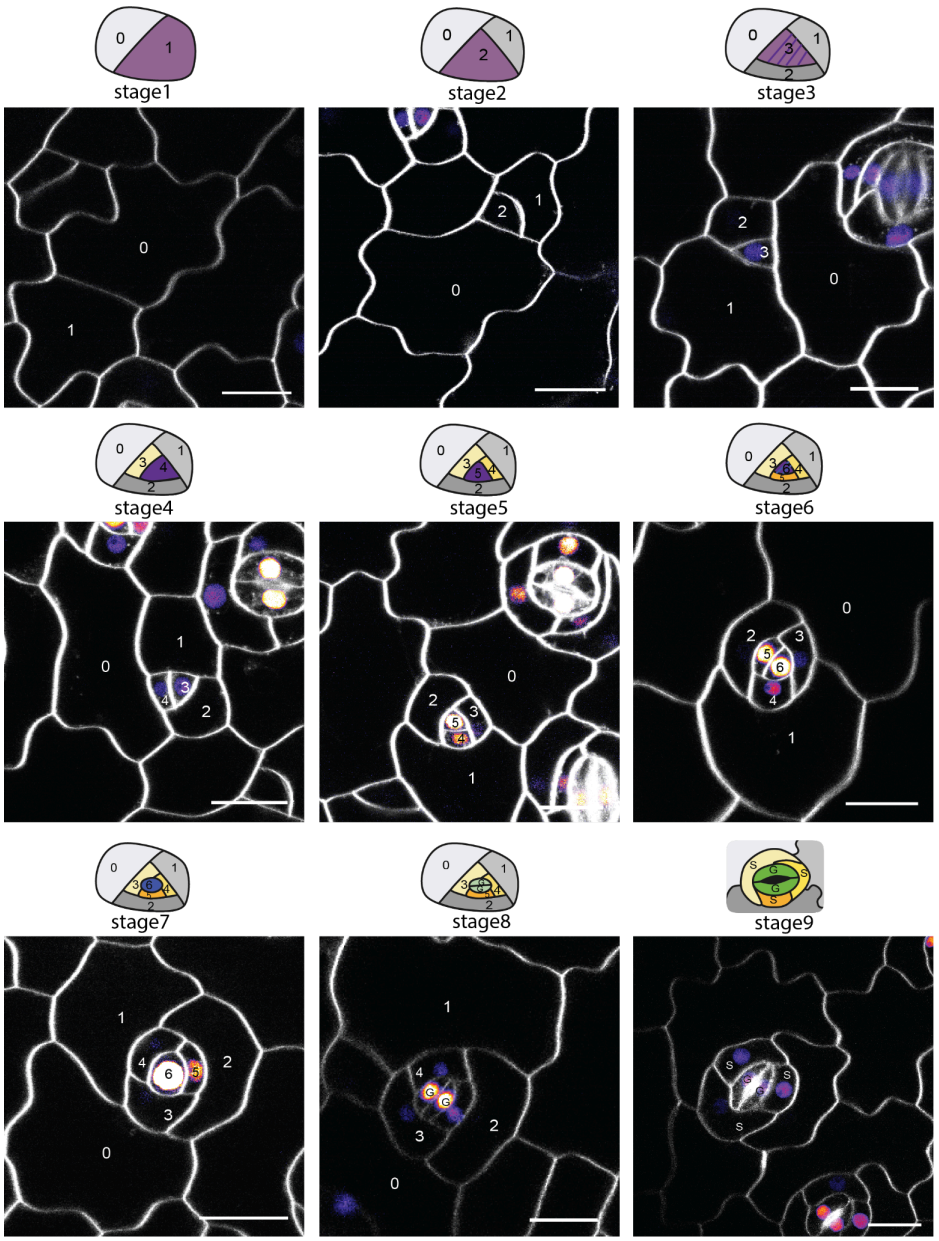

Figure 28. *KlMUTE2* is expressed in all SC divisions.
Confocal microscopy imaging of *KlMUTE2* transcriptional reporter *KlMUTE2:mCitrine-eGFP*^{NLS}. The scheme of each stomatal development stage was indicated above the corresponding confocal microscopy image. Plasma membranes were stained with FM4-64. Scale bars, 20 μm. This scheme was created by Prof.Dr.Michael Raissig and myself, and is published in a review article in *New Phytologist* (Cheng & Raissig, 2023) (https://doi.org/10.1111/nph.18951), and revised by myself.

3.6 KlMUTEs protein localized in meristemoid2 and SCs during SCs divisions

Except for transcriptional reporters, I also cloned KlMUTEs translational reporters *KlMUTE1::mCitrine-KlMUTE1* and *KlMUTE2::mCitrine-KlMUTE2* and transformed them into WT to explore the location of the KlMUTEs proteins during the stomatal

development. After I generated thetransgenic lines, I crossed KlMUTEs translational reporter lines with plasma membrane marker lines (*35S::mCherry-AtPIP1;4*) for higher imaging quality. Confocal microscopy imaging showed that similar as KlMUTEs transcriptional reporters, KlMUTE1 (Fig. 29) and KlMUTE2 (Fig. 30) started to show very weak signals in stage 3. Then the signal became stronger during the SC divisions of the meristemoid 2 (stage 4 to stage 6) and the strongest signal was observed in the GMC stage (stage 7). After the GMC divided into two GCs, the signal became weaker (stage 8) and by stage 9 there was no signal anymore. In general, the signal at early stages was weaker in the *KlMUTE2* translational reporters than in the *KlMUTE1* translational reporters. Compared to the transcriptional reporters, the signal in SCs was weaker during SC divisions, and there was no signal after the GMC division, suggesting that the KlMUTEs protein might be highly regulated during stomatal divisions for proper function. In addition, I also found that although the signal in SCs was weak during SC divisions, it got stronger again at the GMC stage. implying that KlMUTE might be mobile and moved from the GMC to SCs at the GMC stage. This is similar to BdMUTE in *Brachypodium distachyon* (Raissig et al., 2017). Interestingly, I also found that although there is no signal in SCs after the GMC division (stage 8), sometimes some signal was detected in the smallest SC after GC differentiation (stage 9).

KlMUTEs transcriptional and translational reporters suggest that both *KlMUTEs* are expressed in all SC divisions and thus might function in SCs development.

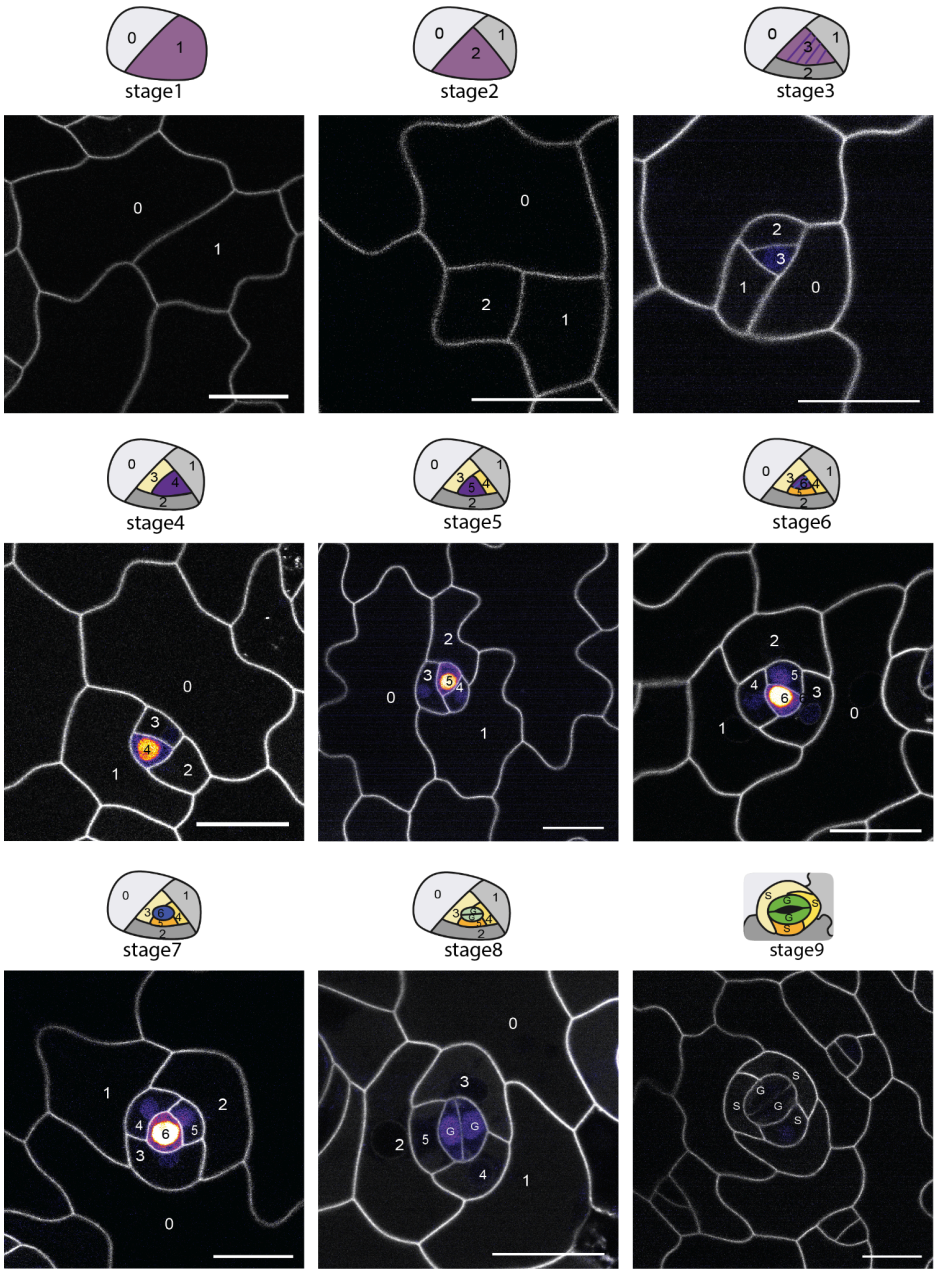

Figure 29. KIMUTE1 localized in meristemoid2 and SCs during SCs divisions. Confocal microscopy imaging of *KIMUTE1* translational reporter *KIMUTE1::mCitrine-KIMUTE1*. The scheme of each stomatal development stage was indicated above the corresponding confocal microscopy image. Cell membranes were indicated by plasma membrane marker *35S:mCherry-AtPIP1;4*. Scale bars, 20 μm. This scheme was created by Prof.Dr.Michael Raissig and myself, and is published in a review article in *New Phytologist* (Cheng & Raissig, 2023) (https://doi.org/10.1111/nph.18951), and revised by myself.

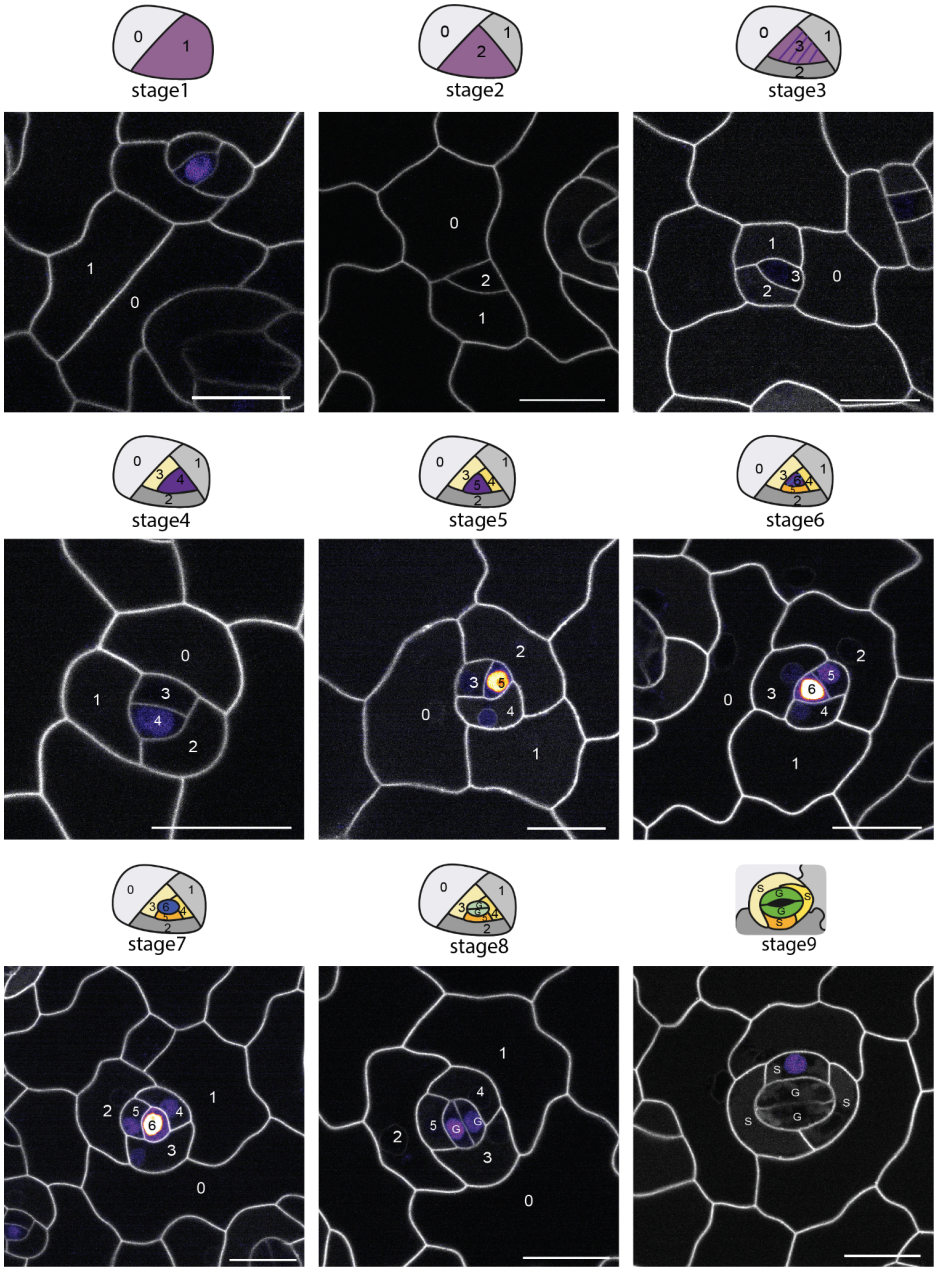

Figure 30. KIMUTE2 localized in meristemoid2 and SCs during SCs divisions. Confocal microscopy imaging of *KIMUTE2* translational reporter *KIMUTE2::mCitrine-KIMUTE2*. The scheme of each stomatal development stage was indicated above the corresponding confocal microscopy image. Cell membranes were indicated by plasma membrane marker *35S:mCherry-AtPIP1;4*. Scale bars, 20 μm. This scheme was created by Prof.Dr.Michael Raissig and myself, and is published in a review article in *New Phytologist* (Cheng & Raissig, 2023) (https://doi.org/10.1111/nph.18951), and revised by myself.

3.7 Overexpression of *KlMUTEs* induces ectopic asymmetric divisions

The phenotype of *klmute1;klmute2* showed aberrant divisions before GMC transition. *KlMUTE1* and *KlMUTE2* transcriptional and translational reporters also showed that *KlMUTE1* and *KlMUTE2* were expressed during SC divisions before the GMC stage. These data implied that *KlMUTEs* might function in the SCs divisions. To further confirm the function of *KlMUTEs*, I cloned overexpression constructs to express *KlMUTE1* and *KlMUTE2* under the 35S promoter. Then, I transformed these two overexpression constructs separately into WT *Kalanchoë laxiflora*. Confocal microscopy imaging of the same size of leaves of plasma membrane marker lines and KlMUTEs overexpression lines showed that, compared to the stomatal phenotype in plasma membrane marker which was regarded as WT (Fig. 31A), *35S::mcitrine-KlMUTE1* and *35S::mcitrine-KlMUTE2* showed more ACDs and had more and smaller cells (Fig. 31B and C).

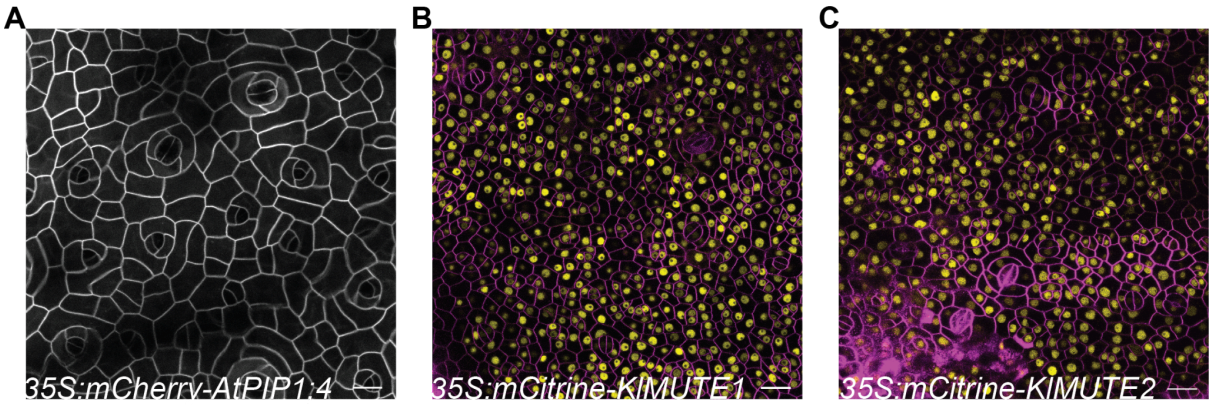

Figure 31. Overexpression of *KlMUTEs* induces ectopic asymmetric divisions in young leaf epidermis.
Confocal microscopy images of 0.5 cm leaves from plasma membrane marker *35S:mCherry-AtPIP1;4* (A), *KlMUTE1* overexpression line *35S::mcitrine-KlMUTE1* (B), and *KlMUTE2* overexpression line *35S::mcitrine-KlMUTE2* (C). In (B) and (C), plasma membranes were stained with FM4-64. Scale bars, 20 μm.

To explore the stomatal phenotype in mature leaves of *KlMUTEs* overexpression lines, I did the DIC imaging of the 8th pair, around 3 cm leaves from WT and *KlMUTEs* overexpression lines. The images showed similar results. Compared to the WT epidermis, which had big differentiated PCs (puzzle-shaped) and only a few developing stomata (Fig. 32A), *KlMUTE1* (Fig. 32B) and *KlMUTE2* (Fig. 32C) overexpression lines showed more ACDs, thus having more and smaller cells. This

phenotype is different from overexpressing *AtMUTE* in *Arabidopsis thaliana* (S.-K. Han et al., 2018; Pillitteri, Sloan, et al., 2007), indicating that different from *AtMUTE,* which terminates ACDs and promotes symmetric cell divisions in *A. thaliana*, *KlMUTEs* promote ACDs during stomatal development in *K. laxiflora*. In addition, different from stomata in WT, which mostly only had three SCs, some stomata in *KlMUTEs* overexpression lines had more than three SCs (indicated by red asterisks in Fig. 32B).

To further quantify the phenotype of *KlMUTEs* overexpression lines, I screened three independent lines from *35S::mcitrine-KlMUTE1* and *35S::mcitrine-KlMUTE2*. Rotation master student Miro Läderach (University of Bern, Bern) harvested the 5th pair, around 3 cm leaves from three individuals (from three independent lines) of WT, *35S::mcitrine-KlMUTE1* and *35S::mcitrine-KlMUTE2*. Then he stained the leaf epidermis with Toluidine blue, and took the images from a DIC microscope. Miro Läderach and I counted the stomata and total number of cells from selected images, and I plotted the data. Results showed that, compared with WT, *KlMUTE1* overexpression lines had over four times the number of cells than WT, and *KlMUTE2* overexpression lines had around three times the number of cells than WT (Fig. 32D). *KlMUTE1* overexpression lines also had significantly higher cell density than *KlMUTE2* overexpression lines (Fig. 32D). In addition, *KlMUTE1* overexpression lines also had significantly higher stomatal density than WT and *KlMUTE2* overexpression lines (Fig. 32E). *KlMUTE2* overexpression lines had lower stomatal density than WT, but there is no significant difference (Fig. 32E). *KlMUTE1* overexpression lines and *KlMUTE2* overexpression lines had significantly higher percentages of stomata with more than three SCs than stomata in WT, especially *KlMUTE1* overexpression lines (Fig. 32F). *KlMUTE1* overexpression lines and *KlMUTE2* overexpression lines had similar stomata index, significantly lower than WT (Fig. 32G).

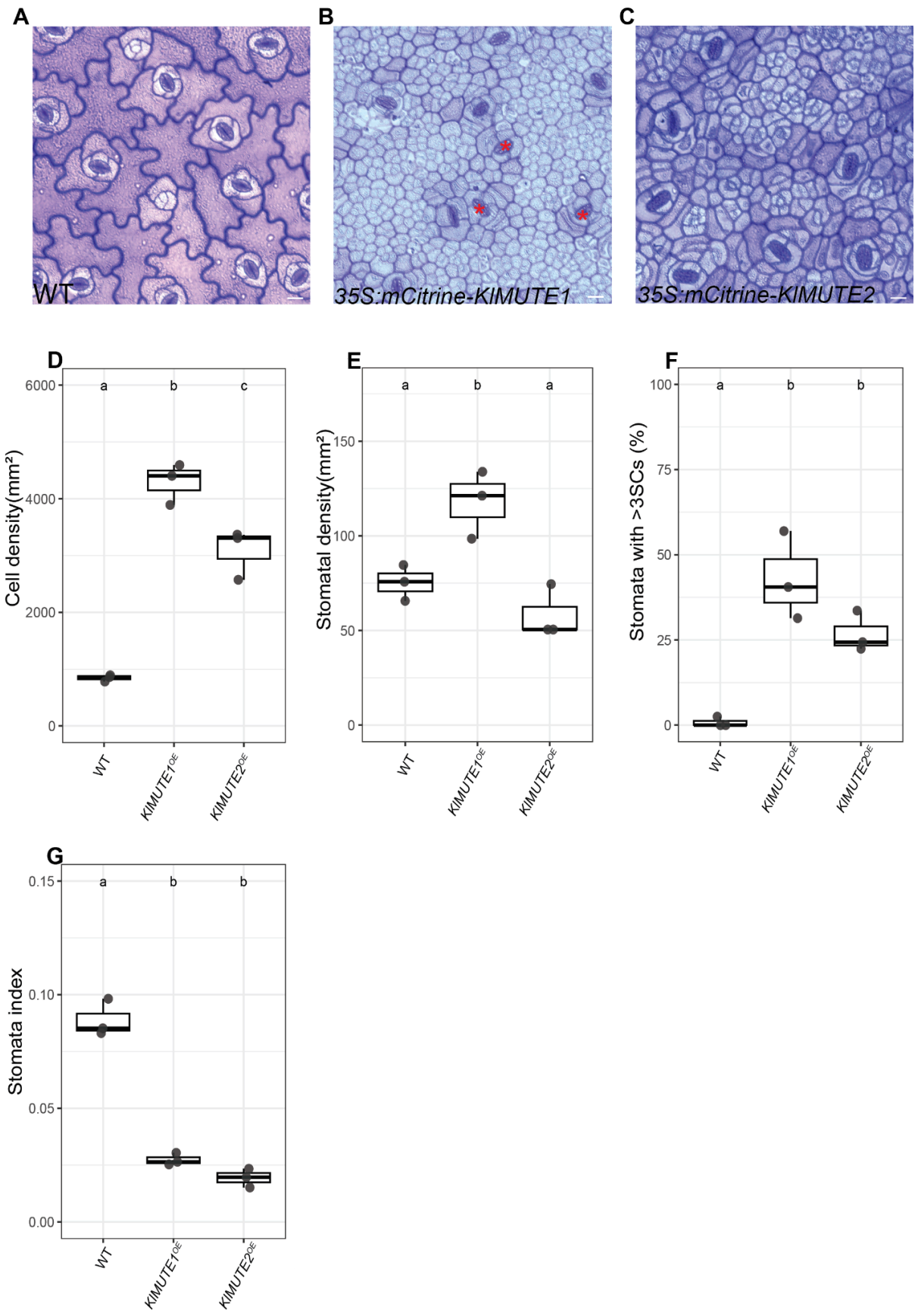
A
B
C
WT
35S:mCitrine-KlMUTE1
35S:mCitrine-KlMUTE2
D
Cell density(mm²)
6000
4000
2000
0
a
b
c
WT
KlMUTE1OE
KlMUTE2OE
E
Stomatal density(mm²)
150
100
50
0
a
b
a
F
Stomata with >3SCs (%)
100
75
50
25
0
a
b
b
G
Stomata index
0.15
0.10
0.05
0.00
a
b
b

Figure 32. Overexpression of *KlMUTEs* induces ectopic asymmetric divisions in mature leaf epidermis.
(A)-(C). Light microscope imaging of the abaxial side of the 8th, 3 cm leaves of WT (A), *KlMUTE1* overexpression lines *35S::mcitrine-KlMUTE1* (B), and *KlMUTE2* overexpression lines *35S::mcitrine-KlMUTE2* (C). Scale bars, 20 μm. Stomata with more than three SCs were indicated in red asterisks. (D)-(G). Quantification of cell density (D), stomatal density (E), the percentage of stomata with more than three SCs (F), and stomata index (G). For each genotype, three individuals were counted. One-way ANOVA and Tukey posthoc test were used for comparison between multiple samples, letters indicated significance groups (pValue<0.05 was considered as significant).

Except for the stomata phenotype, I also found that compared with the leaves from WT plants, leaves from *KlMUTEs* overexpression lines had more wax on the leaf surface, and the leaves were bent towards the abaxial or adaxial of the leaves (Fig.S2). This might be because the ectopic expression of *KlMUTE*s disrupted the development of the leaf epidermis, especially the PCs, leading to changes in the leaf epidermal barrier and asymmetric mechanical tension on both sides of the leaf epidermis.

In summary, *KlMUTEs* overexpression lines of *K. laxiflora* showed more ACDs on leaf epidermis than WT, indicating that *KlMUTEs* promote ACDs during stomatal development in *K. laxiflora*.

3.8 The function of *KlMUTEs* for promoting asymmetric divisions is species context-dependent

To explore whether the function of *KlMUTEs* for promoting ACDs resulted from either the difference between KMUTE and AtMUTE or species context, I built *35S::mCitrine-AtMUTE* and transformed *35S::mCitrine-AtMUTE*, *35S::mCitrine-KlMUTE1,* and *35S::mCitrine-KlMUTE2* into WT *Arabidopsis thaliana*. Confocal microscopy imaging showed that similar to overexpressing *AtMUTE* in *A. thaliana* (Fig. 33A), overexpressing *KlMUTE1* and *KlMUTE2* in *A. thaliana* resulted in all epidermal cells acquired GMC identity and divided symmetrically into GCs (Fig. 33B and 33C).

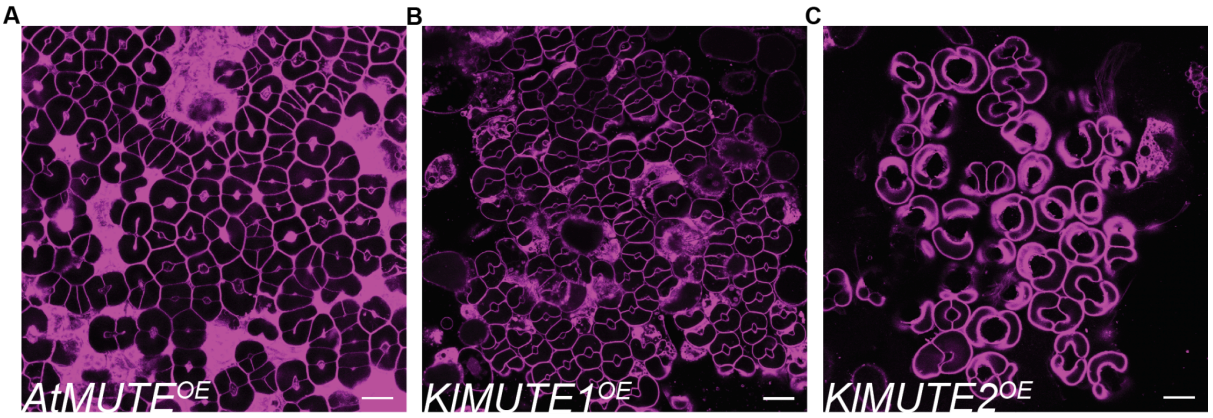

Figure 33. Overexpressing *KlMUTEs* into *Arabidopsis thaliana* induced all epidermal cells to divide into GCs.
Confocal microscopy imaging of cotyledons from *AtMUTE* overexpression lines *35S::mCitrine-AtMUTE* (A), *KlMUTE1* overexpression lines *35S::mCitrine-KlMUTE1* (B), and *KlMUTE2* overexpression lines *35S::mCitrine-KlMUTE2* (C) in *Arabidopsis thaliana*. Plasma membranes were stained with FM4-64. Scale bars, 20 μm.

On the contrary, I also transformed *35S::mCitrine-AtMUTE* into WT *Kalanchoë laxiflora*. Compared to the stomatal phenotype of plasma membrane maker line *35S:mCherry-AtPIP1;4* which was regarded as WT (Fig. 34A), overexpressing *AtMUTE* in *K. laxiflora* caused a lot of ACDs (Fig. 34B). This phenotype is different from overexpressing *AtMUTE* in *A. thaliana* (Pillitteri, Sloan, et al., 2007), and is similar to overexpressing *KlMUTEs* in *K. laxiflora*. Although compared to *KlMUTEs* overexpression lines(especially *KlMUTE1* overexpression lines), overexpressing *AtMUTE* in *K. laxiflora* induced more symmetric cell divisions.
Overall, the results showed that *KlMUTEs* in promoting ACDs in *K. laxiflora* are species context-dependent.

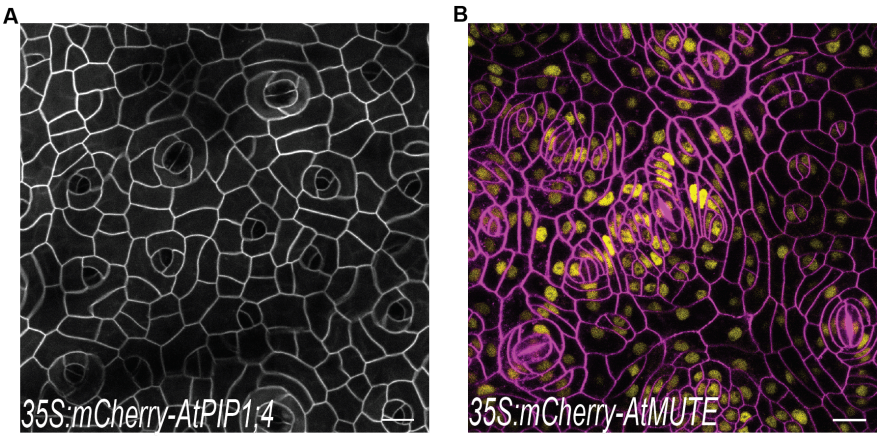

Figure 34. Overexpressing *AtMUTE* in *Kalanchoë laxiflora* induced ectopic asymmetric divisions.
Confocal microscopy imaging of the 2nd, 0.5 cm leaves from plasma membrane marker *35S:mCherry-AtPIP1;4* (A), and *AtMUTE* overexpression lines in *Kalanchoë laxiflora* (B). Plasma membranes in (B) were stained with FM4-64. Scale bars, 20 μm.

3.9 Bulk RNA-seq revealed a potential genetic program regulated by *KlMUTE1*

To further elucidate the mechanism of *KlMUTEs* promoting ACDs and explore the candidate downstream genes regulated by *KlMUTEs*, I collected the 7th pair of leaves from four WT individuals and three independent *KlMUTE1* overexpression lines, followed up by RNA extraction and bulk RNA-sequencing (Fig. 35A). To analyze the sequencing data quality, I did the Principal Component Analysis (PCA) test and Sample Distance Heatmap based on DESeq2 normalized counts (Fig. S3). PCA test showed that four WT samples were clustering very well, while three *KlMUTE1* overexpression samples were separated because these three samples were from three different lines. No extreme outliers among these samples was observed from the Sample Distance Heatmap, indicating that this RNA-seq data was reliable.

Differential Expressed Gene (DEG) analysis was performed by DESeq2. Compared to the mature leaves of WT, 2943 genes were significantly upregulated (log2FoldChange>1 and padj<0.05), and 1817 genes were significantly downregulated (log2FoldChange<-1 and padj<0.05) in the mature leaves of *KlMUTE1* overexpression lines.

To explore the differentially expressed key transcription factors involved in stomatal development in *Kalanchoë laxiflora*, firstly, I blasted and identified the homologs of key transcription factors reported in *Arabidopsis thaliana* (Table. S1). Except for *KlSPCHs*, *KlMUTEs,* and *KlFAMAs,* which were identified before (Fig. 20A), I also identified two homologs of *AtSCRM*, which were named *KlSCRM1* and *KlSCRM2* (Fig.S4), and one homolog of *AtFOUR-LIPs* (*AtFLP*). Significant expressed transcription factors (padj<0.05, the same as below) were marked in the volcano plot (Fig. 35B). The results showed that *KlMUTE1* was upregulated most among all the upregulated genes. *KlMUTE2* was also upregulated by overexpressing *KlMUTE1*. *AtFAMA* and *AtFLP* were upregulated by overexpressing *AtMUTE* to inhibit the symmetric cell division and promote GC differentiation in *A. thaliana* (S.-K. Han et al., 2018). Strikingly, I found that *KlFAMA2* and *KlFLP* were significantly

downregulated by overexpressing *KlMUTE1* in *K. laxiflora*. This opposite regulation in overexpressing *KlMUTE1* lines indicated that *KlMUTE1* might promote ACDs by delaying GC commitment. Similar to overexpressing *AtMUTE*, *KlSCRM2* was also upregulated in overexpressing *KlMUTE1*.

Except for key transcription factors, I also identified homologs of key genes involved in cell polarity and cell divisions during stomatal development described in *A. thaliana*, including *AtCYCD3;1*, *AtCYCD3;2, AtCYCD3;3*, *AtCYCD5;1*, *AtPOLAR*, *AtPOLARlike1*, and *AtBRXL2* (Table. S2). Instead of only three CYCD3 subgroup members in *A. thaliana* (Dewitte et al., 2007), I found nine homologs in *K. laxiflora* (Fig.S5). During stomatal development in *A. thaliana*, *AtCYCD3;1* and *AtCYCD3;2* function in ACDs of a meristemoid and are induced by *AtSPCH* and inhibited by *AtMUTE*-induced CYCDK inhibitor *SMR4* (S.-K. Han et al., 2022; MacAlister et al., 2007; Vatén et al., 2018). Except for CYCD3 homologs, I identified four homologs of *AtCYCD5;1* (Fig. S6), which is induced by *AtMUTE* and promotes a symmetric cell division of the GMC (S.-K. Han et al., 2018; Pillitteri, Sloan, et al., 2007). Differentially regulated key cell polarity and cell division factors homologs in overexpressing *KlMUTE1* mature leaves were marked in the volcano plot (Fig. 35C). Surprisingly, I found that the *KlCYCD3like2*, which is the homolog of *AtCYCD3* subgroup members, diverged even earlier than all other homologs (Fig. S5) and was significantly upregulated by overexpressing *KlMUTE1* (Fig. 35C), suggesting that *KlCYCD3like2* might be a crucial candidate gene downstream of *KlMUTE1* for promoting ACDs. Similar to overexpressing *AtMUTE*, *KlCYCD5;1like2a*, *KlCYCD5;1like2b* and *KlPOLARlike1* were upregulated by overexpressing *KlMUTE1*.

To explore the differentially expressed genes involved in stomatal patterning, I identified the homologs of ligands, receptors, and downstream modules of stomatal signaling and other genes described in *A. thaliana*, including *AtSTOMAGEN*, *AtCHALLAH*, *AtEPF1*, *AtEPF2*, *AtERECTA* (*AtER*), *AtERlike1*, *AtERlike2*, *AtTMM*, *AtYDA*, and *AtSDD* (Table. S3). I identified two *KlSTOMAGENs* (Fig. S7), four *KlEPF1likes* (Fig. S8), and two *KlYDAs* (Fig. S9) in *K. laxiflora*. However, I only found the same homolog of *AtERL1* and *AtERL2-KlERLike* in *K. laxiflora* (Fig. S10). Significantly expressed genes involved in stomatal patterning were marked in the volcano plot (Fig. 35D). While *KlER*, *KlCHALLAH,* and *KlYDA2* were upregulated, *KlEPF1like1b* was downregulated by overexpressing *KlMUTE1*, similar to overexpressing *AtMUTE1(S.-K. Han et al., 2018)*. However, *KlSDD* was significantly

downregulated by overexpressing *KlMUTE1* in *K. laxiflora*, of which the homolog was oppositely regulated by overexpressing *AtMUTE* in *A. thaliana*.

In conclusion, most of the crucial genes for stomatal development have more than one homolog in *K. laxiflora*, indicating that this might offer more possibilities for the neofunctionalization of these genes for novel functions. In addition, some genes were oppositely regulated compared to their homologs in *A. thaliana*, suggesting that KlMUTE1 might regulate different downstream programs to promote ACDs.

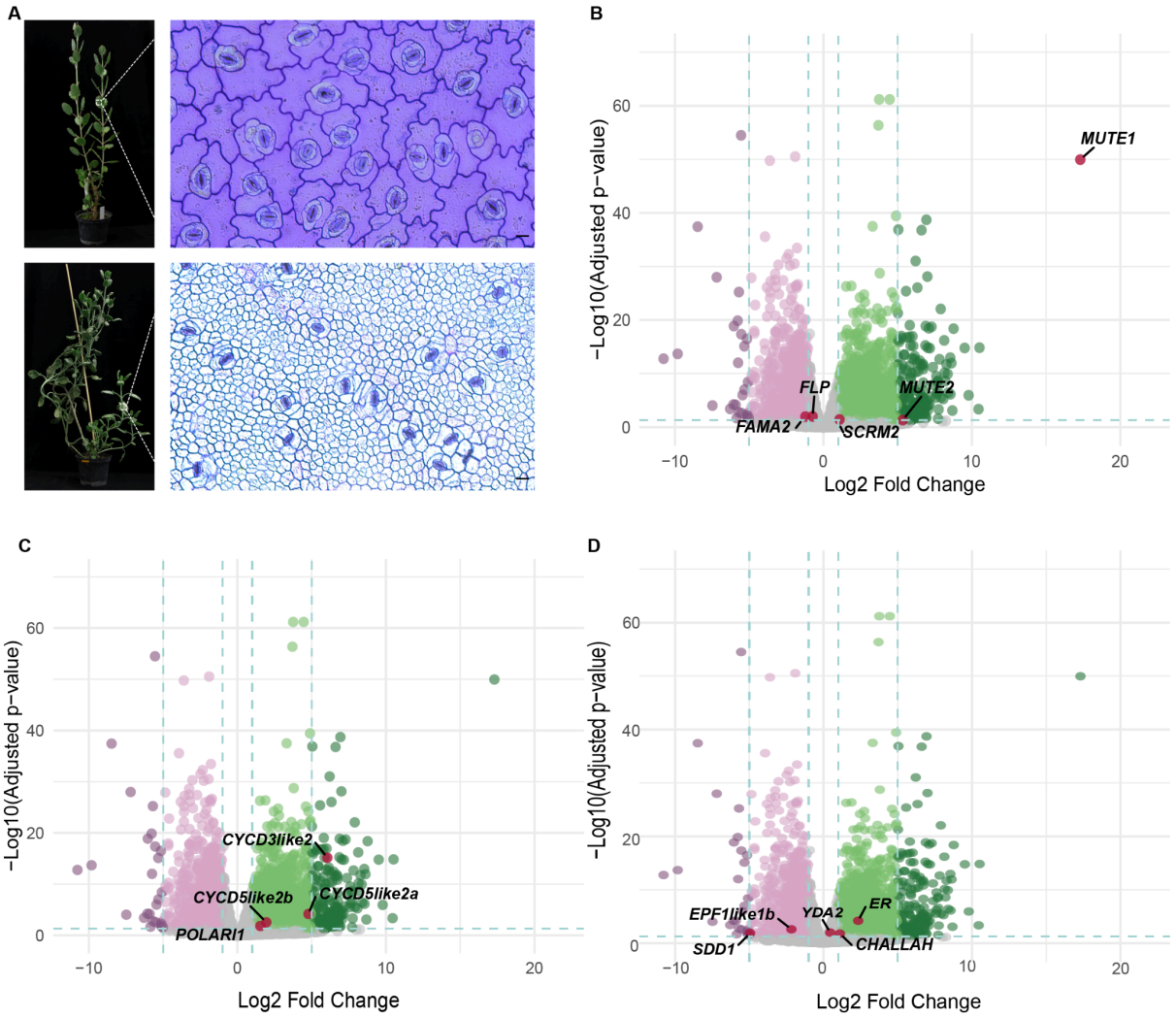

Figure 35. Bulk RNA-seq revealed a potential genetic program regulated by KlMUTE1. (A). Light microscope imaging of the 7th pair of leaves from WT and *KlMUTE1* overexpression lines. Scale bars, 20 µm. (B)-(D). Significantly differentially expressed genes involved in stomatal development. Including the main stomatal transcription factors (B), genes involved in cell polarity and cell divisions during stomatal development (C), and genes involved in stomatal patterning (D). Genes with log2FoldChange>1 and padj<0.05 were considered significantly upregulated, genes with log2FoldChange<-1 and padj<0.05 were considered significantly downregulated.

Discussion

1. Establishing *Kalanchoë laxiflora* as a model system for stomatal research

In addition to using sterile seedlings (grown from seeds on ½ MS medium) for tissue-culture-based transformation, I also tried to use plantlets as transformation materials. I sterilized mature leaves from the greenhouse, put the leaves onto ½ MS medium, and induced the plantlets from leaf margins based on the protocol for *Kalanchoë fedtschenkoi* (Liu et al., 2019). Results showed that this method is also feasible for *Kalanchoë laxiflora*. I got transgenic lines after transforming the first construct into plantlet leaf pieces. In addition, I also tried to harvest the plantlets directly grown from the greenhouse and then sterilized the plantlets in a sterile bench for transformation. However, this method did not work well; most leaves had fungal contamination from the petiole. Even if I tried to incubate the leaves with ethanol and bleach solution for longer, I could not resolve this issue.

Whether using sterile plantlets or seedlings, robust and healthy plant materials are the most important step for transformation; around 50 µmol PAR m −2 s–1 light intensity and around 40% relative humidity are enough for seedlings. If the plates are placed in dry condition, using higher Petri dishes (8.5 cm x 2 cm) and pouring more medium into each plate is recommended. In addition, Micropore is much better than Parafilm for sealing the plates.

For most of the constructs I transformed during my Ph. D., I got over 10 independent lines, each line had many individuals (Fig. 5B), and I had at least three positive lines, indicating that this tissue culture-based genetic transformation protocol for *K. laxiflora* is very stable and efficient. However, this protocol also contains some apparent disadvantages.

In the tissue-culture-based transformation protocol for *Brachypodium distachyon*, embryonic callus induced from isolated embryos are used for transformation (Spiegelhalder et al., 2024; Zhang et al., 2022), thus single cell proliferates and differentiates into an individual, this way of plant regeneration is also called “Somatic embryogenesis” (Ikeuchi et al., 2019). This regeneration method is widely used in tissue culture and transformation of many plant species (Kamle et al., 2011; Soulhat et al., 2023). In the tissue-culture-based transformation protocol for *K. laxiflora*, I induced callus from the cutting edges of leaf pieces, which are regarded as explants,

followed by shoot induction. This way of regeneration is called “De novo shoot organogenesis”, which is also widely used (Duclercq et al., 2011). However, since genetically modified plants are generated from callus, this regeneration pathway is more likely to produce chimeras than Somatic embryogenesis (Rout et al., 1991). Therefore, it is necessary to establish a somatic embryo-based genetic transformation protocol for *K. laxiflora* in the future. Since the seeds of *K. laxiflora* are tiny, inducing somatic embryos directly from tissues might be easier than from immature zygotic embryos. In addition to the potential risk of chimerism, the whole transformation period (from transformation experiment to transgenic plants moving to soil) takes around 6 months; thus, it is also necessary to establish new protocols for accelerating genetically modified plant production in the future.

Except for the agrobacterium-mediated stable genetic transformation, I think it might be useful for developing the transient transformation protocol of *K. laxiflora* since the stable transformation takes too long. Thus, we can transiently transform recombination vectors fused with fluorescence tags into *K. laxiflora* and test whether the fluorescence signal can be detected before we produce genetically modified plants carrying these recombination vectors. This method can avoid the failure to obtain stably transformed transgenic plants due to cloning errors and thus save plenty of time. Although the transient transformation protocol of *Nicotiana tabacum* is well established (Sparkes et al., 2006), it might be better to transiently transform the constructs into *K. laxiflora* instead of *N. tabacum* since *K. laxiflora* and *N. tabacum* are distantly related in evolution.

Toluidine blue staining solution stains plant cell walls (O’Brien et al., 1964), and it works well in *K. laxiflora*, but peeling the epidermis is required for this staining protocol. However, peeling the epidermis from the first three leaf pairs (count the first visible leaf pair from the top as the 1st leaf pair) (smaller than 2 cm) is very difficult; thus, I only chose to peel and stain the epidermis from the 4th leaf pair or the elder leaf pairs. Therefore, it is necessary to establish a new protocol for peeling very young leaves in the future.

Due to the leaves of *K. laxiflora* being very thick and having many mesophyll cells, directly imaging the whole leaf under a light microscope is very tricky. For the whole cotyledon light microscope imaging, I improved a protocol for DIC imaging stomata in *Arabidopsis thaliana* (Sharma, 2017). The image of the treatment “0.5 h KOH, 1x HS, 40X” showed apparent cell outlines of stomata and PCs in the epidermis (Fig.

8). However, DIC imaging should be tested in the future; it might give better resolution and contrast than brightfield.

FM4-64 stain plasma membrane (Fischer-Parton et al., 2000). Bigger leaves are easier to peel for Toluidine blue staining; however, for FM4-64 fluorescence staining, smaller leaves are easier to be stained and mounted onto slides. For better staining, the maximum leaf size I selected for imaging is around 2 cm; therefore, in the future, the FM4-64 fluorescence staining protocol should also be improved to stain bigger leaves. Except for plasma membrane staining, other cell wall stainings should be continuously tested in the future. Calcofluor white, Direct Red 23, and PI are common fluorescent dyes for plant cell wall staining (Redkar et al., 2018; Ursache et al., 2018). Results showed that Calcofluor white might stain too long or the concentration of the Calcofluor white is too high (Fig. 11A), indicating that for the Calcofluor white staining test the next time, the concentration of Calcofluor white should be lower than 0.01% or stain shorter than 10 min. For the Direct Red 23 staining, which did not work at all (Fig. 11B), higher concentration (higher than 0.1%) and longer incubation time (longer than 10 min) are recommended for the test experiment in the future. Besides this, incubating leaf tissue with a staining solution in a vacuum might also help. PI stained the cotyledon very well (Fig. 11C); however, the chloroplasts, especially in the nucleus, also caused strong interference to the imaging, indicating that PI is not a perfect cell wall stain for *K. laxiflora*. Except for the fluorescence dyes mentioned above, other commonly used fluorescent dyes, for example, Pontamine Fast Scarlet 4B, Direct Yellow 96, Basic Fuchsin, Acriflavine, and Fluorol Yellow might be also important candidates for testing staining in *K. laxiflora* (Bidhendi et al., 2020; Piccinini et al., 2024; Ursache et al., 2018).

During my Ph.D, I tested the first CRISPR CAS9 construct applying to *K. laxiflora*: pFASTRK-PcUBIP-AtCas9-NLS-P2A-mCherry-G7T-AtU6-BsaI-CmR-ccdB-BsaI scaffold (p01178). I transformed three single guide RNA (sgRNA) (3 constructs) into WT *Kalanchoë laxiflora* separately, and I got regenerants from all three guides. Regenerants from two guides were genotyped and sequenced, and I got homozygous from T0 regenerants, indicating that this CRISPR CAS9 system worked well in *K. laxiflora*. In addition, because of the mCherry tag fused with the backbone, I can directly screen mutants under a fluorescence microscope 3 weeks after sowing the seeds onto ½ MS plates. This helped to speed up the screening process. However, this construct only allows the insertion of one sgRNA into the backbone,

although other CRISPR CAS9 constructs carrying multiple sgRNAs to target multiple genes or multiple sites of one gene have been widely used in well-established dicot model *A. thaliana* (Li et al., 2024; Raitskin & Patron, 2016). Therefore, it is necessary to select other constructs that could carry multiple sgRNAs or modify this existing backbone for carrying multiple sgRNAs and test whether these constructs would work in *K. laxiflora* in the future.

It takes around 3 months from inducing flowers to harvesting seeds, much longer than other model species like *A. thaliana* or *B. distachyon* (Draper et al., 2001; Krämer, 2015). Despite this, *K. laxiflora* can easily produce at least 50-60 flowers on one individual (cutting the main branch and inducing side branches before moving into short-day chambers could produce more flowers), and the flowers are big. This makes emasculation and pollination relatively easy, and the crossing has very high efficiency. In addition, flowering time is not synchronized, and it takes around 2 weeks, making it easier for me to find the flowers that are in the perfect stage for pollination and cross with different individuals with different genotypes. The state of the stigma during pollination is a key step in crossing. When the surface of the stigma looks moist, it is in the best condition for pollination. It is worth noting that the stigma dries quickly in summer, especially in the afternoon. In the future, the horticulture protocols might be improved to shorten the time before harvest. For example, research shows that seeds lose water during development (Leprince et al., 2017); this might suggest that at the late maturation stage, plants might not need too much water for the seeds' maturation. Therefore, we could test to directly harvest and dry the seeds at different stages of late seed maturation, or stop watering the whole plants and harvest the seeds after maturation, then, we can test the germination rate of these seeds and whether it affects the seed lifespan, to shorten the time it takes for the overall seeds maturation.

In summary, to establish *K. laxiflora* as a model system for stomatal research, I developed tissue culture-based transformation protocol, staining protocols for light and confocal microscopy imaging. Besides these, I also established the CRISPR CAS9 cloning protocol and flower induction and crossing protocol. These protocols worked well in *K. laxiflora*. However, in the future, these protocols could still be further optimized or test other protocols to achieve better results or shorten the time.

Although the life cycle of *K. laxiflora* is very long (seeds from seeds takes around 6 months), and the genetic transformation also takes long, the small genome of *K.*

laxiflora is fully sequenced and annotated, and the vegetative propagation strategies are very simple (both cuttings and plantlets induction work well), except for these, flowers also yield thousands of dust-like seeds in single plant, these make *K. laxiflora* is becoming a good model system.

2. Stomatal development in *Kalanchoë laxiflora*

In the plant kingdom, stomata in most plants consist of two kidney-shaped GCs with a central pore, like the stomata in the dicot model *Arabidopsis thaliana* (Franks & Farquhar, 2007; Nunes et al., 2020). Fossil remains of this stomatal morphology date back to the Lower Devonian (Franks & Farquhar, 2007; Stubblefield & Banks, 1978; Sun et al., 2005). However, I found that in the succulent CAM model plant *Kalanchoë laxiflora* (Hartwell et al., 2016), except for two kidney-shaped GCs, stomata also include three circular arranged, unequal-sized SCs surrounding the GCs (Fig.14), the same stomata morphology are found in some other species of Kalanchoë family (Fig. S1). In the future, it will be necessary to observe the stomata of different species in Kalanchoë and other succulent (CAM) families, to determine whether their stomata morphology is consistent with the stomata in *K. laxiflora*, and explore the evolution of stomatal morphology in different succulent (CAM) species, as well as explore its functional relevance and adaptation to the living environment.

Except for the anisocytic SCs in succulents, grasses recruit paracytic SCs on both sides of GCs (Cheng & Raissig, 2023; Nunes et al., 2020; Rudall et al., 2013). In the grass model *Brachypodium distachyon*, stomata feature dumbbell-shaped GCs and dome-shaped SCs (Cheng & Raissig, 2023; Nunes et al., 2020). Unlike the unknown function of stomatal SCs in succulents, the function of stomatal SCs in grasses has been well studied (Franks & Farquhar, 2007; Raissig et al., 2017; Wang et al., 2019). The unique morphology of dumbbell-shaped GCs and the “see-sawing” opposite exchanges in osmotic and turgor pressure between GCs and SCs during stomatal opening and closing allow grasses stomata faster opening and closing to cope with environmental changes than other species (Franks & Farquhar, 2007; McAusland et al., 2016). Stomata in *bdmute* have SCs defects and show slower stomatal opening and closing in *B. distachyon* (Raissig et al., 2017; Spiegelhalder et al., 2024). Strikingly, similar to grasses (Raschke & Fellows, 1971), Ph.D student Antonio Aristides Pereira Gomes Filho (University of Bern, Bern) also found that there is a

potassium shuttle between GCs and three SCs during stomatal opening and closing in *K. laxiflora* (Cheng et al., 2024), suggesting that the SCs in succulents might also be functionally related. Since most succulents are CAM plants, it is interesting to explore whether the SCs contribute to CAM physiology. For instance, the SCs might sense the change of the Ci in mesophyll cells and transduce the signal to GCs for stomata opening and closing, alternatively, push the GCs open more during the night to absorb more CO_2 and close more tightly during the day to minimize the transpiration and water loss (Cheng & Raissig, 2023; Males & Griffiths, 2017). Therefore, producing mutants with fewer SCs or without SCs and performing physiology experiments, for example, measuring stomatal conductance, might help explore the function of SCs in succulents in the future.

Static imaging of plasma membrane marker lines showed that different stages of developing stomata and mature stomata were found in the same zone of a leaf, and the orientation of stomata are random in *K. laxiflora* (Fig. 15A), this is similar to the stomatal pattern in *A. thaliana* (Zhao & Sack, 1999) but is different from *B. distachyon* which has linear stomatal development and all stomata are uniformly orientated (Raissig et al., 2016).

Based on the static imaging of plasma membrane marker lines, Prof. Dr. Michael Raissig and I established the proposed stomatal development model in *Kalanchoë laxiflora* (Fig. 15B). This model is confirmed by manual time-lapse imaging performed by Ph.D student Lidia Holfmann (University of Bern, Bern) (Cheng et al., 2024). At the beginning of stomatal development, the protodermal cell (stage “P”) established the MMC identity (stage 0), and underwent the first ACD to yield two unequal-sized cells, the bigger one was SLGC and the smaller one was meristemoid (stage 1) (Cheng et al., 2024). The meristemoid continued to make another two ACDs and yield another two SLGCs (stage 2 - stage 3), until this stage (stage 3), the meristemoid was surrounded by three SLGCs (Cheng et al., 2024). Next, the central smallest cell underwent another three ACDs to produce three SCs instead of SLGCs (stage 4 - stage 6)(Cheng et al., 2024). After this, the meristemoid tranformed into GMC (stage 7) and divided symmetrically and differentiated into two GCs (stage 8) (Cheng et al., 2024). Compared to the first three ACDs which yielded three SLGCs, the second three ACDs produced three cells which are different cell types from SLGCs, indicating that the meristemoid that drived the first three ACDs (is also called “meristemoid1”) might be different from the meristemoid which drived the

second three ACDs (is also called “meristemoid2”), thus there might be a transition from meristemoid 1 to meristemoid 2 during stomatal development (Cheng et al., 2024). In the future, it will be interesting to explore which gene(s) control this important cell type transition. The ACDs during stomatal development in *K. laxiflora* are similar to the “amplifying divisions” of stomatal development in *A. thaliana* (Bergmann & Sack, 2007; Pillitteri & Dong, 2013; Pillitteri & Torii, 2012). However, compared to most meristemoids, which are directly differentiated into GMCs or only undergo 1-2 ACDs during stomatal development in *A. thaliana* (Gong et al., 2023*)*, meristemoids in *K. laxiflora* undergo more ACDs (Cheng et al., 2024). This hints that there might be a more complicated and delicate molecular regulatory mechanism behind this complicated stomatal development process of *K. laxiflora* compared with that in *A. thaliana.* In addition, manual time-lapse imaging showed that in some conditions, the SLGC next to a developing stomata complex got MMC identity and underwent another two ACDs to yield two SLGCs (Cheng et al., 2024). Then, the meristemoid underwent another three ACDs to make three SCs, followed by the GMC transition, GC division, and differentiation (Cheng et al., 2024). Finally, a stomata was produced away from an existing stoma (Cheng et al., 2024). In this case, only five ACDs instead of six ACDs happened during stomatal development. This spacing division is similar to that in *A. thalianana* (Nadeau & Sack, 2002a, 2002b*)*. In the future, it is expected that manual time-lapse imaging, together with quantification, will provide a more comprehensive understanding of stomatal development and patterning in *K. laxiflora*.

Static and manual time-lapse imaging revealed that in *K. laxiflora*, SCs and GCs stem from one cell, called mesogenous stomata (Pant, 1965). In *B. distachyon*, however, SCs are recruited from lateral neighboring cells of GMC (Nunes et al., 2020; Raissig et al., 2017); thus, GCs and SCs stem from the different mother cells, called perigenous stomata (Pant, 1965). This indicates that the different stomatal morphotypes could result from diverged ontogeny.

Figure 16 showed the development of epidermal cells during leaf growth. During the development from 0.5 cm leaf to 5 cm leaf, the leaf epidermal cells underwent divisions, differentiation, and expansion. The leaf epidermal cells underwent most of the divisions and differentiation from 0.5 cm leaf to 2 cm leaf, while the leaf grew until 2 cm, most of the stomata differentiated into mature stomata complex, and the PCs

also differentiated (look like puzzle-like cells). After the leaf grows over 2 cm, PCs were still expanding due to leaf growth.

For a better understanding of the development of epidermal cells, especially stomata development during leaf growth, I stained and imaged the peels from the 4th leaf to the 15th leaf from three individuals and quantified the cell density, developing stomata density, stomatal density, and stomata index. Quantification results showed that the cell density (Fig. 18A) decreased dramatically from the 4th pair to the 6th pair, implying that this might be the result of PC expansion. The stomatal density and developing stomatal density showed a similar pattern as well as cell density. However, while the cell density was significantly decreased from the 6th pair to the 8th pair, the stomatal density and the developing stomatal density were very stable. These results indicated that during this stage, except for the PCs expansion, some developing stomata might initiate stomatal divisions and some developing stomata which were at the latter stages of stomatal development differentiated into GCs when the leaf was getting bigger. The results from Figure 18B to Figure 18D showed that the stomatal development trend was stable from the 6th pair to the 15th pair, suggesting that the 6th pair is considered to be “mature leaves” for stomatal development. Full CAM photosynthesis also starts from leaf pair 6 (Boxall et al., 2020), implying that the stomatal development might be crucial for CAM physiology.

Since the first three pairs of leaves are relatively thin and difficult to peel, I chose to peel from the 4th pair for quantification. However, Figure 16 showed that most of developing stomata underwent divisions and differentiated into GCs before the leaf growth until 2 cm (the 3rd pair), this means that the stomata development changes dramatically before leaves reach 2 cm (the 3rd pair), thus it is necessary to quantify the stomatal development in the first three pairs of leaves in the future.

In rice, the Toluidine blue staining solution stains stomatal SCs in pink, different from other cells, and thus is used as an SCs cell identity indicator (Gallagher & Smith, 2000; Lu et al., 2019). Like rice, I also found that Toluidine blue stains stomatal SCs in different colors than other epidermal cells in *K. laxiflora*. While PCs are stained in light purple and GCs are stained in dark purple, SCs are in white (Fig. 17), suggesting that in *Kalanchoë laxiflora*, these three unequal-sized cells surrounding GCs might have a different cell identity compared to PCs and might be “real” SCs, like the stomatal SCs in rice.

Stomata are distributed on either one side of leaves (abaxial or adaxial) or both sides of leaves, which is common in different plant species (Parkhurst, 1978). Even if the stomata are distributed on both sides of the leaf, it does not mean they are always evenly distributed on both sides (Taylor et al., 2012; Willmer & Fricker, 1996). In most cases, there are more stomata on the abaxial side of leaves than on the adaxial side (Mott et al., 1982; Pemadasa, 1979; Willmer & Fricker, 1996). except for in some species, for example, wheat, more stomata are on the adaxial side (Wall et al., 2022). In my thesis, I only imaged and quantified the stomata from the abaxial side. Therefore, in the future, it is necessary to image and quantify the stomata from the adaxial side and compare with the stomatal density and stomata index of the abaxial side.

I found the same stomatal morphotype in the leaves of plantlets grown from the leaf margins compared to the stomata in the leaves of plants grown from seeds or cuttings (Fig. 19). However, different from the stomatal development in the leaves of plants grown from seeds or cuttings which largely depends on leaf size, I think the stomatal development in the leaves of plantlets mainly depends on leaf pair (leaf age), and I think the reason is that the plantlets grow very slowly, especially from the beginning, thus the leaf size between each pair is not changed significantly. However, the stomatal development between each pair is already dramatically changed.

3. MUTE drives asymmetric divisions to form stomatal SCs in *Kalanchoë laxiflora*

SPCH, MUTE, and FAMA are conserved core bHLH transcription factors that regulate stomatal development among species (Nunes et al., 2020; Peterson et al., 2010). In *Kalanchoë laxiflora*, there are two *KlSPCHs*, two *KlMUTEs*, and three *KlFAMAs* (there are *KlFAMA1a*, *KlFAMA1b*, and *KlFAMA2* in the genome based on the annotations, but *KlFAMA1a* didn't show any expression in mature WT leaves in the bulk RNA-seq dataset, so indicating that either *KlFAMA1a* does not express in the mature leaves or there might be only *KlFAMA1b* and *KlFAMA2* exist in the genome). The number of these stomatal transcription factors is doubled compared to that in *Arabidopsis thaliana*, indicating that subfunctionalization and neofunctionalization of these amplified key bHLHs might contribute to the more intricate meristemoid divisions and more complicated stomata morphotype compared

to the stomatal development in *A. thaliana* (Cheng & Raissig, 2023). Therefore, except for *KlMUTEs*, the analysis of the function and expression (for example, manual time-lapse imaging) of other stomatal conserved bHLH transcription factors SPCH, FAMA, and their potential heterodimers SCRM will further help to understand the entire stomatal development in *K. laxiflora* in the future.

bHLH transcription factors have been widely identified in some model plants and crops and are one of the largest transcription factor families in plants (Gao et al., 2018). As bHLH transcription factors, the bHLH domain consists of around 60 bp amino acid, which is highly conserved and important for DNA binding (Blanc-Mathieu et al., 2024; Carretero-Paulet et al., 2010; Pires & Dolan, 2010). However, except for the bHLH domain, bHLH transcription factors might have other domains for the specificity of DNA binding and/or modulating the activity (Heim et al., 2003; Toledo-Ortiz et al., 2003). For stomatal key bHLH transcription factors SPCH, MUTE, and FAMA, except the bHLH domain, they also have a plant-specific “SMF” (Abbreviation of SPCH, MUTE, FAMA) domain in the C-terminus of the protein (Heim et al., 2003; MacAlister & Bergmann, 2011). The results of MUTE alignment among different species showed that KlMUTEs also have bHLH domain and SMF domain like MUTE in other species.

Spiegelhalder et al found that C-terminus tagged BdMUTE (BdMUTEp: BdMUTE-mCitrine) is non-functional while N-terminus tagged BdMUTE (BdMUTEp:mCitrine-BdMUTE) is fully functional (Raissig et al., 2017; Spiegelhalder et al., 2024), suggesting that even if the conserved bHLH domain is at the N-terminus, the C-terminus might be more important for the specific function of MUTE protein. The MUTE alignment showed that compared to *A. thaliana* and other dicots, which only have two GCs stomata, the MUTE amino acid sequence in some common grass species that have paracytic SCs and both MUTE in *K. laxiflora* that have anisocytic SCs have longer C-terminus, suggesting that this longer C-terminus might be crucial for the stomatal SCs development. Therefore, it might be essential to analyze the potential elements in this longer C-terminus and identify the amino acid(s) crucial for SCs development by cutting the C-terminus into fragments of different lengths for complementation experiments.

Similar to the stomata in *atmute* mutants (Pillitteri, Sloan, et al., 2007), I found stomata in *klmute1;klmute2* mutants also didn’t form any GCs. However, the stomata in *klmute1;klmute2* mutants also showed misoriented ACDs, indicating that different

from *AtMUTE* in *A. thaliana*(Pillitteri, Sloan, et al., 2007), KlMUTE might function in the proper ACDs before the GMC transition. In addition, the extra divisions in the neighboring cells suggested that while the meristemoid could not undergo correct ACDs and GC division, the stomatal division program restarted again in the adjacent cell(s), indicating that *KlMUTEs* are not the only genes that regulate ACDs during the whole stomatal development in *K. laxiflora*.

KlMUTE1 and *KlMUTE2* started to be expressed in stage 3, while both KlMUTE proteins only showed very weak signal in stage 3 but began to show good signal from stage 4, suggesting that KlMUTEs might function in the transition from meristemoid 1 to meristemoid 2. Different from the *KlMUTEs* transcriptional reporters and translational reporters, which show signal in all daughter cells during SC divisions, in *A. thaliana*, *AtMUTE* only starts to be expressed in late meristemoid, while AtMUTE protein is mainly located in GMC (MacAlister et al., 2007; Mahoney et al., 2016). The differences in gene expression and protein localization suggest this may be due to different functions between *KlMUTEs* and *AtMUTE*. Compared to *KlMUTEs* transcriptional reporters which still showed strong signals in both GCs and SCs after GC division (stage 8) and GC differentiation (stage 9), in both *KlMUTEs* translational reporters, the signal in GCs were much weaker than that in GMC and no signal is detected in SCs after GC division (stage 8), suggesting that both KlMUTEs are quickly degraded in GCs and SCs after GCs division, thus means transcription factors KlMUTEs are strictly regulated post translation. Studies about the regulation of MUTE post translation could help to better understand the neofuctionalization of this protein in succulent plants.

Overexpressing *KlMUTEs* in WT *K. laxiflora* induced more ectopic ACDs in leaf epidermis, which is different from overexpressing *AtMUTE* in *A. thaliana* (MacAlister et al., 2007). However, whether these smaller cells are SCs is still unclear. Combined with the *klmute1;klmute2* phenotype, the expression of *KlMUTEs* in the transcriptional reporters, and the location of KlMUTEs in the translational reporters, it is confirmed that *KlMUTEs* promote SC divisions during the stomatal development in *K. laxiflora*.

Overall, all my experiments showed that *KlMUTEs* function in the transition from meristemoid 1 to meristemoid 2 and the SC divisions of stomatal development (Fig. 36). This is similar to the function of *BdMUTE* in promoting ACDs of the subsidiary mother cell (Raissig et al., 2017; Spiegelhalder et al., 2024) but different from

AtMUTE, which terminates ACDs and promotes GC division and differentiation (Pillitteri, Sloan, et al., 2007). Although stomata in grasses and succulents have distinct ontogeny of SCs (perigenous SCs in grasses while mesogenous SCs in succulents), my results showed that there might be a convergent genetic mechanism of MUTE between monocots and dicots.

Despite this, the novel function of MUTE in *K. laxiflora* does not result from the MUTE protein itself; however, it is context-dependent. Since overexpressing *KlMUTEs* into *A. thaliana* resulted in all epidermal cells acquired the GMC identity and differentiated into GCs, while overexpressing *AtMUTE* in *K. laxiflora* induced ectopic ACDs in epidermis. To explore the potential context-dependent downstream program of KlMUTEs for regulating stomatal ACDs, I did Bulk RNA-sequencing of mature leaves from WT and *KlMUTE1* overexpression lines. Before further interpreting the bulk RNA-seq data, firstly, I blasted and identified homologs of key factors function in stomatal development described in *A. thaliana*, including crucial stomatal transcription factors, key genes involved in cell polarity, cell divisions, and stomata patterning. Most of these genes have more than one homolog in *K. laxiflora*, suggesting that there might be more possibilities of neofunctionalization and subfunctionalization of these genes, which might contribute to the intricate stomatal ACDs or SCs identity establishment (Cheng & Raissig, 2023). It is noteworthy that compared to the bHLH transcription factors, receptors, and peptide ligands which have relatively conserved amino acid sequences compared to *A. thaliana*, the homologs of cyclin D type, including AtCYCD3 three subgroup members, and AtCYCD5;1 have rather divergent amino acid sequence, suggesting that these cyclins might have distinct function compared to the homologs in *A. thaliana*. In addition, In Figure 35C, I only displayed the significantly expressed genes from KlCYCD3 and KlCYCD5;1 family in the volcano plot in which padj value >0.05. However, if the threshold of the padj is >0.1, I found that there were two *KlCYCD5;1likes* were upregulated and one *KlCYCD5;1like* was downregulated. In addition, *KlCYCD3like2* and *KlCYCD3;1* were upregulated and *KlCYCD3;2/3c* were downregulated by overexpressing *KlMUTE1*, indicating that the function of these cyclins from the same family might be diversified for differentially regulating cell divisions in *K. laxiflora*. Therefore, these differentially expressed cyclins could be important candidate genes for further stomatal research. In *A. thaliana*, *AtSPCH* induced the expression of *AtCYCD3;1* and *AtCYCD3;2* for promoting ACDs of the

meristemoid (Han et al., 2022; MacAlister et al., 2007; Vatén et al., 2018), However, *AtMUTE* could induce cyclin-dependent kinase inhibitor, SIAMESE-RELATED4 (SMR4) to directly interact with AtCYCD3;1 (and probably AtCYCD3;2) to terminate the amplifying ACDs. At the same time, *AtMUTE* induce CYCD5;1 for the symmetric division of the GMC(Han et al., 2018, 2022; Pillitteri, Sloan, et al., 2007). After this, *AtMUTE* upregulates *AtFAMA* and *AtFLP* to inhibit excess symmetric cell division and promote the GC differentiation (Hachez et al., 2011; Han et al., 2018; Xie et al., 2010). Oppositely, I found that in *K. laxiflora*, *KlMUTE1* upregulated two *KlCYCD3* genes, but KlFAMA2 and KlFLP were inhibited by overexpressing *KlMUTE1*, suggesting that *KlMUTE1* might promote ACDs to form stomatal SCs by inducing specific *KlCYCD3* genes and inhibit GCs differentiation by downregulating *KlFAMA2* and *KlFLP* (Fig. 36).

Stomata in *klmute1;klmute2* didn't form any GCs, this could due to either the misoriented stomatal ACDs or the possible role of KlMUTEs in GMC transition (Fig. 36). Therefore, until now, it is still unclear how the intricate ACDs end and how the GMC is established in *K. laxiflora*. When I imaged different lines of *KlMUTEs* and *AtMUTE* overexpression lines in *K. laxiflora*, I noticed that compared to *KlMUTE1* overexpression lines which always showed ectopic asymmetric divisions at different expression levels, some symmetric cell divisions were also observed in strong expression lines of overexpressing *KlMUTE2* and *AtMUTE*. This indicated that *KlMUTE2* might also function in the GMC establishment. Since the stomatal phenotype in lines with different overexpression levels was slightly different, this implies that the function of *KlMUTE2* in promoting stomatal ACDs and establishing GMC identity might be dosage-dependent.

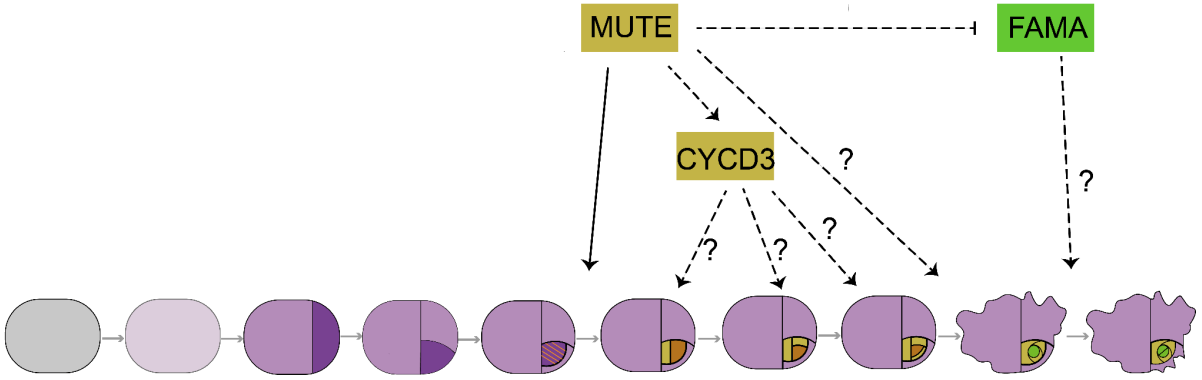

Figure 36. Proposed model of stomatal development in *K.laxiflora*.
During the stomatal development, KlMUTEs transit meristemoid1 into meristemoid2 and promote the whole SCs divisions by upregulating relative cell cycle regulators, and inhibiting GCs differentiation. Cell types were indicated in different color.

klmute1 and *klmute2* single mutants did not show phenotype in stomatal morphology, suggesting that *KlMUTE1* and *KlMUTE2* have a redundant function. However, except for the stomatal phenotype, which was slightly different between *KlMUTE1* and *KlMUTE2* strong overexpression lines of *K. laxiflora* mentioned above, quantification results also showed that *KlMUTE2* overexpression lines had lower cell density and stomatal density compared to *KlMUTE1* overexpression lines. Relative experiment showed that the epidermal peels of *KlMUTE1* overexpression lines had lower ploidy; however, the *KlMUTE2* overexpression lines had similar ploidy compared to WT (Cheng et al., 2024), suggesting that the function of *KlMUTE1* and *KlMUTE2* might be slightly different. In addition, the *KlMUTE2* translational reporter showed weaker signal in stage 3 than the *KlMUTE1* translational reporter. Bulk RNA-seq data also showed that KlMUTE2 was upregulated by overexpressing *KlMUTE1* in mature leaves, indicating that *KlMUTE2* might function slightly later than *KlMUTE1*. Quantification of KlMUTE mutants of different genotypes showed that

klmute1/klmute1;klmute2/+ had similar stomata index compared to *+/+;klmute2/klmute2*, while *klmute1/klmute1;+/+* had higher stomatal index, implying that *KlMUTE2* might function more in GMC transition compared to *KlMUTE1*. My data suggested that *KlMUTE1* might function earlier in stomatal ACDs and then activate *KlMUTE2* for GMC transition.

Meristemoid 2 undergoes three ACDs, which are called SC divisions. The SC identity might be established after the ACD. However, I also noticed that the signal was detected in all three SCs and the GMC at the GMC stage in *KlMUTEs* translational reporters, suggesting that KlMUTEs in SCs at the GMC stage might help to establish the SC identity, the strongest signal was detected in the GMC, suggesting that the GMC might be important for the SCs identity establishment by for example, cell signaling. Therefore, whether the SC's identity is established after the ACD of meristemoid 2 or at the GMC stage is unclear. It is worth noting that the signal in SCs was stronger at the GMC stage than during the ACDs of the meristemoid 2, indicating that either *KlMUTEs* are expressed more in the SCs at the GMC stage, or KlMUTEs might be mobile and can move from the GMC to the SCs at this stage. The signal was detected in both nucleus and cytoplasm in the GMC, this might support the latter proposal. This is simiar to BdMUTE in *Brachypodium distachyon*, which is mobile and moves from GMC to lateral cells to establish the subsidiary mother cell identity (Raissig et al., 2017).

In the future, differentially expressed genes analysis of bulk RNA-sequencing data of overexpressing *KlMUTE1* and *KlMUTE2* compared to WT, together with Chip-seq and protein interaction validation assay, for example, pull-down or Co-Immunoprecipitation (Co-IP), can help to screen candidate downstream genes of KlMUTEs. In addition, further analysis, for example, mutants and transcriptional/translational reporters of these downstream genes will validate the function of these (novel) genes and reveal the species-specific downstream genetic program of KlMUTEs in promoting the stomatal SC divisions in *K. laxiflora*.

Since the *klmute1;klmute2* did not form GCs, it is impossible to analyze the function of SCs by using this mutant. Therefore, it is necessary to explore other mutants with proper GCs with SC defects in the future, for example, by forward screening or expressing KlFAMA under KlMUTE promoter in *klmute1;klmute2* background or KlFAMA under KlSPCH promoter in *klmute1;klmute2* background.

Materials and methods

1. Plant material and growth conditions

Genotype Oxford Botanical Garden (OBG) was used as WT for the research of *Kalanchoë laxiflora* in my thesis. For *K. laxiflora*, seeds can be directly used for germination without vernalization after harvest. For seed germination on medium, an appropriate amount of seeds was filled in a 1.5 mL Eppendorf tube. Then the tube was filled with 1 mL 70% Ethanol (v/v) for 5 min. The seeds were rinsed with 1 mL water three times, followed by resuspending the seeds with 1 mL 0.1% agarose. Around 20 (4x5) seeds were sowed on each 1/2MS plate. The seeds were germinated in a plant growth chamber where the growth condition was 16 h light (22℃,45 - 50 μmol PAR m −2 s–1): 8 h dark (18℃). Except for the seeds germinated on medium, all calli, shoots, and transformants produced from tissue culture also grew in the same conditions as the seeds in the growth chamber. When the sterile plants had over 1-2 cm roots, they were transferred from medium to the “seedling substrate”, or the seeds were directly sowed on the surface of the “seedling substrate”, after two weeks grew in a walk-in growth chamber where the growth condition was 12 h light(24℃,300 μmol PAR m −2 s–1;): 12 h dark (18℃), plants were transferred to bigger pots containing “Kalanchoë soil” and started to grow in the greenhouse where the growth condition was 16 h light (24℃,300 μmol PAR m −2 s–1): 8 h dark (18℃).

Arabidopsis thaliana Col-0 plants used for floral dip transformation were grown in a greenhouse where the growth condition was 16 h light (22℃,130-150 μmol PAR m −2 s–1): 8 h dark (18℃). Around 20~30 Arabidopsis seedlings that were grown in the “seedling substrate” were used for transformation. For seed sterilization, an appropriate amount of seeds were placed in a 15 mL falcon tube, 70% ethanol was filled in the tube, followed by upside down about 10 times. The ethanol was discarded and this step was repeated another two times. Then, the tube was filled in 5 ml 100% ethanol and the seeds with ethanol were poured onto filter paper on a sterile bench. After the seeds were dried out thoroughly, they were spreaded evenly on the 12 cm x 12 cm square plates with ½ MS(+50 mg/L Kanamycin).

The details of the recipe of mediums were listed in Supplementary Table 4.

The details of the soil recipe used for plant growth were listed in Supplementary Table 5.

2. Vegetative growth of *Kalanchoë laxiflora*

Kalanchoë laxiflora can easily grow from cuttings or margins of detached leaves. For making cuttings, the branch with the first 4-5 leaf pairs was cut from the stem and planted in Kalanchoë soil. Cuttings grew in the greenhouse where the growth condition was 16 h light (24℃,300 µmol PAR m −2 s–1): 8 h dark (18℃) and were transferred to bigger pots after two weeks. For plantlet growth, a mature leaf(at least 4~5cm) was detached from the mother plant and placed adaxial side up on the Kalanchoë soil. While the plantlets grown from the margin were around 5 cm in height, they were separated and placed individually in pots. Once the plantlets grew to 10 cm in height, they were transferred to bigger pots containing the same soil.

3. Molecular cloning

3.1 CRISPR/CAS9 cloning

Guide RNA sequences that showed high on-target activity scores and overall off-target scores were selected in Geneious (Geneious | Bioinformatics Software for Sequence Data Analysis) for CRISPR/Cas9 knockouts against *KlMUTE1* and *KlMUTE2*. To produce the CRISPR/CAS9 constructs, double-strand guide RNA was made by hybridizing and phosphorylating the oligo duplexes (priXC24 and priXC25 for CRISPR guide target KlMUTE1:KlMUTEs-gRNA-2; priXC14 and priXC15 for CRISPR guide target KlMUTE1:KlMUTE1-gRNA-2; priXC18 and priXC19 for CRISPR guide target KlMUTE2:KlMUTE2-gRNA-1), ligated into the BsaI digested and dephosphorylated p01178 vector (pFASTRK-PcUBIP-AtCas9-NLS-P2A-mCherry-G7T-AtU6-BsaI-CmR-ccdB-BsaI scaffold, from VIB). CRISPR guide KlMUTEs-gRNA-2 was also designed to target KlMUTE2, but only *klmute1* single mutant lines were screened. CRISPR guide KlMUTE2-gRNA-1 was intended to target KlMUTE2 specifically.

3.2 RNAi cloning

3.2.1 RNA extraction and cDNA synthesis

RNA was extracted from young WT leaves of *Kalanchoë laxiflora* (OBG) using the RNeasy Plant Mini Kit. In addition to following the manufacturer's protocol, 3%(v/v) PEG20.000 was used to mix with the RLC buffer. The RNA was reverse transcribed into cDNA using PrimeScript RT Master Mix and following the manufacturer's instructions. cDNA was used as a template for RNAi cloning.

3.2.2 Entry clone

Gateway cloning was used for RNAi cloning in *Kalanchoë laxiflora*. For specifically knocking down both KlMUTEs, priXC1 and priXC2 were used for amplifying a 233 bp fragment from KlMUTE1 CDS; priXC1 and priXC3 were used for amplifying a 280 bp fragment from KlMUTE1 CDS. Align these two fragments with the CDS of KlSPCHs and KlFAMAs to promise that no consecutive 21 bp can be matched in the cDNA of other genes. For the entry clone, the pENTR ™ /D-TOPO ® Cloning Kit was used. The two fragments were amplified from KlMUTE1 CDS by PCR reaction, and the size of the fragments was confirmed by running in a 2% agarose gel. Then the two fragments were inserted separately into the pENTR ™ /D-TOPO ® vector by TOPO cloning reaction (details for the TOPO cloning reaction:topota_man.pdf). E.coli transformation and colony PCR were followed by enzyme digestion and Sanger sequencing.

3.2.3 Destination vector cloning

For inserting the fragment into the destination vector pK7GWIWG2(II) (from VIB), the LR reaction was set up catalyzed by LR Clonase ™ enzyme mix (details for the LR reaction: gatewayman.pdf). E.coli transformation and colony PCR were followed by enzyme digestion and Sanger sequencing.

3.3 Reporters cloning

All the reporters and overexpression constructs were built based on the GreenGate system (Lampropoulos et al., 2013). *KlMUTEs* promoter and coding sequence (including introns) were amplified by Q5 High-Fidelity DNA Polymerase from the genomic DNA of WT *Kalanchoë laxiflora* (OBG) extracted by a modified CTAB protocol (Raissig et al., 2016). The *AtMUTE* coding sequence (CDS) was amplified from *Arabidopsis thaliana* Col-0 WT cDNA synthesized with the PrimeScript RT Master Mix from RNA extracted with the RNeasy Plant Mini Kit, following the manufacturer's instructions.

3.3.1 DNA extraction

DNA was extracted by a modified CTAB protocol (Raissig et al., 2016). First, around 0.5~1cm leaf was collected and quickly frozen in liquid nitrogen with a 2 mm bead in a 1.5 mL Eppendorf tube. Then, the sample was ground into fine powder by using a grinder. 300 µL 2 x CTAB buffer was added into the tube, and the sample was incubated with the buffer at 65°C for at least 15 min. After cooling down, 300 µL chloroform was added to the tube under the fume hood and thoroughly vortexed the sample. Five minutes of full-speed spinning was performed to separate the components in the sample. 300 µL 2-Propanol was added to a new 2.0 mL Eppendorf tube with the supernatant, then the DNA in the supernatant was pelleted by spinning the sample for 5 min at 12,000 rpm. The liquid was removed carefully and the pellet was purified with 500 µL 70% ethanol. The DNA was spinned again for 5 min at full speed. Finally, the pellet was air dried and dissolved into 100 µL water. 1-2 µL DNA was used for PCR amplification. The receipe of 2X CTAB buffer preparation was listed in the supplementary table 6.

3.3.2 Transcriptional and translational reporter cloning

To create the entry module pGGA_KlMUTE1pro (pXC10), 1313 bp upstream of *KlMUTE1* was amplified using the forward primer priXC6 and reward primer priXC7. To create the entry module pGGA_KlMUTE2pro (pXC12), 2109 bp upstream of *KlMUTE2* was amplified using the forward primer priXC59 and the reward primer priXC11. To get a linearized backbone with proper overhang, the empty pGGA000 backbone was digested by BsaI and then dephosphorylated by Antarctic phosphatase. The PCR products of the *KlMUTEs* promoter were also digested by BsaI, and then T4 DNA ligase ligated the PCR products into the linearized pGGA000 backbone. To produce the entry module pGGC_KlMUTE1 (with STOP codon)(pXC11), the *KlMUTE1* genomic sequence was amplified by using the forward primer priXC4 and the reward primer priXC5. To get a linearized backbone with proper overhang, the empty pGGC000 backbone was digested by BsaI and then dephosphorylated by Antarctic phosphatase. The PCR product of the *KlMUTE1* genomic sequence was also digested by BsaI, and then T4 DNA ligase catalyzed the ligation reaction between the amplicon and the linearized pGGC000 backbone. To produce the entry module pGGC_KlMUTE2 (with STOP codon) (pXC13), primers

priXC12 and priXC13 were used to mutate the BsaI site in the second intron of the *KlMUTE2* genomic DNA sequence. Forward primer priXC8 and reward primer priXC12 were used to amplify one fragment, while forward primer priXC13 and reward primer priXC9 were used to amplify another fragment. Both fragments were digested by BsaI at the same time, and then T4 DNA ligase catalyzed the ligation reaction between the two fragments and the linearized pGGC000 backbone. After the ligation reaction, the E.coli transformation and colony PCR (using Taq DNA polymerase) were followed by enzyme test digestion and Sanger sequencing.

To build *pGGZ004_KlMUTE1pro:mCitrine-eGFP^{nls}* expression vector, pGGA_KlMUTE1 pro(pXC10), pGGB_mCitrine_IPK_Ala-linker(pMTR84), pGGC_eGFP_NLS (pGGC012), pGGD_Dummy (pGGD002), pGGE_rbcsTerminator(pGGE001) and pGGF_NOSpro-KanR (pGGF007) were orderly ligated by overhangs and introduced into pGGZ004 by GreenGate reaction. To produce the transcriptional reporter *pGGZ004_KlMUTE2pro:mCitrine-eGFP^{nls}*, pGGA_KlMUTE2 pro (pXC12), pGGB_mCitrine_IPK_Ala-linker(pMTR84), pGGC_eGFP_NLS (pGGC012), pGGD_Dummy (pGGD002), pGGE_rbcsTerminator(pGGE001) and pGGF_NOSpro-KanR (pGGF007) were orderly ligated by overhangs and assembled into the final construct pGGZ004 by GreenGate reaction. To generate *pGGZ004_KlMUTE1pro:mCitrine-KlMUTE1*, pGGA_KlMUTE1 pro(pXC10), pGGB_mCitrine_IPK_Ala-linker(pMTR84), pGGC_KlMUTE1 (with STOP codon)(pXC11), pGGD_Dummy (pGGD002), pGGE_rbcsTerminator(pGGE001) and pGGF_NOSpro-KanR (pGGF007) were orderly ligated by overhangs and introduced into pGGZ004 by GreenGate reaction. For producing the expression vector *pGGZ004_KlMUTE2pro:mCitrine-KlMUTE2,* pGGA_KlMUTE2 pro(pXC12), pGGB_mCitrine_IPK_Ala-linker(pMTR84), pGGC_KlMUTE2 (with STOP codon)(pXC13), pGGD_Dummy (pGGD002), pGGE_rbcsTerminator(pGGE001) and pGGF_NOSpro-KanR (pGGF007) were orderly ligated by overhangs and assembled into the final construct pGGZ004 by GreenGate reaction. All the assembled constructs from the GreenGate reaction were tested by enzyme digestion followed by whole-plasmid Sanger sequencing or sequencing of the overhang sites between each module.

The empty entry modules pGGA000, pGGC000, pGGC012, pGGD002, pGGE001, and pGGF007 were previously described in (Lampropoulos et al., 2013). pGGZ004

was described in (Lupanga et al., 2020). pGGB_mCitrine_IPK_Ala-linker was cloned by Prof. Dr. Michael Raissig.
The details of Q5 PCR amplification set-up and thermocycling conditions were listed in supplementary table 7.

3.3.3 Overexpression constructs cloning

To produce the overexpression construct *pGGZ004_35Spro:mCitrine-KIMUTE1:* six different modules pGGA_35Spro(pGGA004), pGGB_mCitrine_IPK_Ala-linker(pMTR84), pGGC_KIMUTE1 (with STOP codon)(pXC11), pGGD_Dummy (pGGD002), pGGE_rbcsTerminator(pGGE001) and pGGF_NOSpro-KanR(pGGF007) were digested by BsaI and orderly ligated by overhangs and assembled into BsaI digested final destination construct pGGZ004 by GreenGate reaction. To build the overexpression construct *pGGZ004_35Spro:mCitrine-KIMUTE2:* six different modules pGGA_35Spro(pGGA004), pGGB_mCitrine_IPK_Ala-linker(pMTR84), pGGC_KIMUTE2 (with STOP codon)(pXC13), pGGD_Dummy(pGGD002), pGGE_rbcsTerminator(pGGE001) and pGGF_NOSpro-KanR(pGGF007) were digested by BsaI and orderly ligated by overhangs and assembled into BsaI digested final destination construct pGGZ004 by GreenGate reaction. To build the overexpression construct *pGGZ004_35Spro:mCitrine-AtMUTE(CDS)*, first, primers priTN63 and priTN94 were used to amplify the *AtMUTE* coding sequence from the cDNA of *Arabidopsis thaliana* Col-0 plants. Next, to produce the entry module pGGC_AtMUTE(CDS, with stop codon), the fragment was digested by BsaI and then ligated into the pGGC000 backbone (pGGC000 was digested by BsaI and dephosphorylated by antarctic phosphatase) by T4 DNA ligase. Finally, six entry modules: pGGA_35Spro(pGGA004), pGGB_mCitrine_IPK_Ala-linker(pMTR84), pGGC_AtMUTE(CDS, with stop codon), pGGD_Dummy(pGGD002), pGGE_rbcsTerminator(pGGE001) and pGGF_NOSpro-KanR(pGGF007) were digested by BsaI and orderly ligated by overhangs and assembled into BsaI digested final destination construct pGGZ004 by GreenGate reaction.
The entry module pGGA004 was previously described in (Lampropoulos et al., 2013).

3.3.4 Plasma membrane marker cloning

Former MSc student in Prof.Dr.Michael Raissig's lab, Yiğit Berkay Gündoğmuş cloned the plasma membrane marker construct *pGGZ003_35Spro:mCherry-AtPIP1;4*. To build this construct, pGGA_35Spro(pGGA004), pGGB_mCherry-GSL, pGGC_AtPIP1;4, pGGD_Dummy(pGGD002), pGGE_rbcsTerminator(pGGE001), pGGF_NOSpro-KanR(pGGF007) and pGGZ003 were used for the GreenGate assembly. The pGGB_mCherry-GSL was generously provided by Karin Schumacher's group(COS, Heidelberg University, Germany). The pGGC_AtPIP1;4 was generously provided by Alexis Maizel (COS, Heidelberg University, Germany). Destination vector pGGZ003 was previously described in (Lampropoulos et al., 2013).

The details of Taq PCR amplification set-up and thermocycling conditions were listed in supplementary Table 8.

The details of the Greengate reaction were listed in supplementary Table 9.

The details of the plasmids used in my thesis were listed in supplementary Table 10.

4. Genetic transformation of *Arabidopsis thaliana*

pGGZ004_35Spro:mCitrine-KIMUTE1, *pGGZ004_35Spro:mCitrine-KIMUTE2* and *pGGZ004_35Spro:mCitrine-AtMUTE* were transformed into *Arabidopsis thaliana* Col-0 WT(separately) by *Agrobacterium tumefaciens* strain GV3101 mediated floral dip-based transformation (Clough & Bent, 1998).

5. Genetic transformation of *Kalanchoë laxiflora*

All the constructs above were transformed into *Agrobacterium tumefaciens* strain GV3101 by heat-shock, and then transformed into *Kalanchoë laxiflora*. The details of the tissue-culture-based transformation protocol of *Kalanchoë laxiflora* and the list of constructs transformed into *Kalanchoë laxiflora* were described in results "1.1 Establish tissue-culture-based genetic transformation protocol for *Kalanchoë laxiflora*".

The details of antibiotics and plant hormones used in my thesis were listed in supplementary Table 11.

The details of the organisms used in my thesis were listed in supplementary Table 12.

6. Genotyping

For genotyping, DNA from around 0.5cm of leaf tissue was extracted by a modified CTAB protocol (Raissig et al., 2016).

Genotyping of *klmute1* single mutants (containing CRISPR guide KlMUTEs-gRNA-2) was performed by amplifying 1033 bp, including the mutated region using priXC61 and priYBG4. Genotyping of *klmute2* single mutants (containing CRISPR guide KlMUTE2-gRNA-1) was performed by amplifying 399 bp, including the mutated region using priXC122 and priXC123. PCR products were sequenced using Sanger sequencing. Genotyping the mutation sites of *klmute1;klmute2* double mutants produced from crossing used the same primers as single mutants.

7. SemiRT-PCR

SemiRT-PCR was performed to test the expression level of *KlMUTEs*, *KlSPCHs*, and *KlFAMAs* in KlMUTE RNAi lines. The same pair and the same size (around 0.5 cm) of leaves from WT and KlMUTE RNAi lines were selected for RNA extraction. RNA was extracted by the RNeasy Plant Mini Kit, and DNA contamination from RNA was removed by on-column DNAseI treatment or by following the protocol (Lindner et al., 2015). The concentration of RNA in each sample was measured by Qubit. Then, the RNA was reverse transcribed into cDNA using PrimeScript RT Master Mix. cDNA was used as a template for semiRT-PCR. KlUBQ10 was used as a reference gene. Taq DNA polymerase was used for PCR amplification. priXC94/priXC87 were used for amplifying *KlMUTE1* (30 thermo cycles, annealing temperature 58℃); priXC95/priXC86 were used for amplifying *KlMUTE2* (32 thermo cycles, annealing temperature 56.5℃); priXC90/priXC85 were used for amplifying *KlUBQ10* (26 thermo cycles, annealing temperature 58℃); priYBG7a/priYBG10 were used for amplifying *KlFAMA1a*, priYBG7b/priYBG8 were used for amplifying *KlFAMA1b*, priYBG9/priYBG8 were used for amplifying *KlFAMA2*; priXC96/priXC89 were used for amplifying *KlSPCH1* (29 thermo cycles, annealing temperature 52℃); priXC98/priXC74 were used for amplifying *KlSPCH2* (32 thermo cycles, annealing temperature 58℃).

The details of the primers used in my thesis were listed in supplementary Table 13.

8. Flower induction and crossing

The details of flower induction and crossing of *Kalanchoë laxiflora* were described in results “1.5 Establish flower induction and crossing protocol for *Kalanchoë laxiflora*”.
For acquiring *klmute1;klmute2* double mutants, 4 *klmute1* homozygous and 2 *klmute2* homozygous were selected for crossing. Stigmas of *klmute1* were pollinated with the pollen from *klmute2* and vice versa.
For crossing the *KlMUTEs* translational reporter lines *KlMUTE1:mCitrine-KlMUTE1*, *KlMUTE2:mCitrine-KlMUTE2* with the plasma membrane marker line *35S:mCherry-AtPIP1;4*, 4 individuals from 3 independent lines of *KlMUTE1:mCitrine-KlMUTE1* and one individual of *KlMUTE2:mCitrine-KlMUTE2* and several individuals of *35S:mCherry-AtPIP1;4* with good signal were selected for crossing. Stigmas of *KlMUTE1:mCitrine-KlMUTE1* and *KlMUTE2:mCitrine-KlMUTE2* were pollinated with pollen from *35S:mCherry-AtPIP1;4*.

9. Light microscopy

Details of staining protocol and sample preparation for light microscope imaging were described in the results “1.2 Establish staining protocol for light microscope imaging of *Kalanchoë laxiflora*”.
To quantify the stomatal development between different size of leaf pairs, the abaxial side of leaves from the 4th pair (count the first visible leaf pair from the top as the 1st leaf pair) to the 15th pair of three around 4 months-old WT plants were peeled and stained with Toluidine blue solution. The samples were mounted onto slides and imaged under a Leica DM2000LED (Leica Microsystems) light microscope. 5-10 brightfield images were taken randomly from each sample under the 20X objective. Three images from each sample were chosen for counting mature stomata complexes, developing stomata complexes, and the total number of cells per field of view in Fiji. Cell density was calculated by the total number of cells per field of view divided by the size of the field of view (20X:0.198mm^2). Stomatal density was calculated by the number of mature stomatal complexes divided by the size of the field of view (20X:0.198mm^2). Developing stomatal density was calculated by the number of developing stomatal complexes (all the developing stages could be

identified from the images) divided by the size of the field of view (20X:0.198mm^2). The stomata index was calculated by dividing the number of mature stomatal complexes by the total number of cells. Values from three fields of view per individual were averaged, and the data were plotted in R.

To image and compare the stomatal development between *klmute1/klmute1;klmute2/+*, *klmute1/+;klmute2/klmute2*, *klmute1/klmute1;+/+*, *+/+;klmute2/klmute2* and WT, the abaxial side of the 7th leaf pair (around 4 cm) from three individuals per each genotype was carefully peeled and stained with Toluidine Blue solution. The samples were mounted onto slides and imaged under a Leica DM2000LED (Leica Microsystems) light microscope. Five fields of view of each sample were randomly taken under the 20X objective for phenotyping, and three fields of view were selected for quantification. Cell density, stomatal density, and stomata index were quantified as described above. Values from three fields of view per individual were averaged, and the data were plotted in R.

Toluidine blue staining and light microscopy were also used to phenotype the *KIMUTE^{RNAi}* lines. For quantification, the abaxial side of the 3rd, 2cm leaf from three independent *KIMUTE^{RNAi}* lines and WT (one individual per genotype) were peeled and stained with Toluidine blue staining solution. The samples were mounted onto slides and imaged under a Leica DM2000LED (Leica Microsystems) light microscope. 5-10 brightfield images were taken randomly from each sample (including all genotypes) under the 20X objective, and three images were selected to quantify mature stomata per total stomata units. For quantifying mature stomata per total stomata units, the number of mature stomata complexes and the total number of cells were counted in each image using Fiji, and the number of mature stomata complexes was divided by the total number of cells per field of view. Around 20 images were taken randomly from each sample of the three *KIMUTE^{RNAi}* lines under the 40X objective. 10 (arrested) developing stomatal complexes of each genotype(one individual per genotype) from the images taken under the 20X or 40X objective were selected for counting the total number of meristemoid and stomata lineage ground cells in one (arrested) developing stomata. The data were plotted in R.

To image and quantify the stomatal development between the *35Sp:mCitrine-KIMUTE1*, *35Sp:mCitrine-KIMUTE2* overexpression lines and WT, the abaxial side of the 5th pair of leaves (around 3 cm) from three individuals per

genotype were peeled and stained with Toluidine Blue staining solution. The samples were mounted onto slides and imaged under a Leica DM2000LED (Leica Microsystems) light microscope. Five brightfield images were taken randomly from each sample under the 20X objective, and four images were selected for quantification. WT-like mature stomata (GCs surrounded by three SCs), mature stomata with more than three SCs, and the total number of cells per field of view were counted in each image using Fiji. Stomatal density, cell density, and stomata index were quantified as described above. To calculate the percentage of mature stomata with more than three SCs. The number of mature stomata with more than three SCs was divided by the total number of mature stomata in each image. Values from four fields of view per individual were averaged, and the data were plotted in R. The receipe of the Toluidine blue staining solution was listed in the supplementary Table 14.

10. Confocal microscopy

For test imaging the cotyledon of *Kalanchoë laxiflora* under a confocal microscopy, propidium iodide (PI), Calcofluor white, Direct Red 23, and FM4-64 were used. The protocol of Calcofluor white staining used in this thesis was from Prof.Dr.Alexander Betekhtin (University of Silesia in Katowice): the sample was incubated in 0.01% calcofluor in PBS for 10 min, followed by rinsing in PBS for 5 min for 3 times, and the sample was rinsed in ddH_2O for 5 min for 3 times. The sample was mounted onto a slide with water and imaged under the confocal microscopy. For Calcofluor white fluorescence excitation, "Alexa 405" was selected. The PI staining protocol used in this thesis was from Dr. Paola Ruiz Duarte (University of Bern): the leaf sample was gently rubbed in water with soap and then rinsed with ddH_2O. Afterward, the sample was incubated in 0.01 mg/mL PI staining solution in a 2 mL Eppendorf tube. Leaving the Eppendorf tube in the vacuum and incubating for 30 min, followed by rinsing the sample with clean water. The sample was mounted onto a slide with water or glycerol and imaged under the confocal microscopy. For PI fluorescence excitation, the wavelength of a 549 nm laser with around 10-20% intensity and around 100% signal gain was used. The Direct Red 23 staining protocol used in this thesis was from Antonio Aristides Pereira Gomes Filho (University of Bern): the sample was incubated in 0.1% Direct Red 23 in PBS for 10 min, then the sample was rinsed in

PBS for 5 min for 3 times, followed up by rinsing in ddH_2O for 5 min for 3 times. The sample was mounted onto a slide with water and imaged under the confocal microscopy. For Direct Red 23 fluorescence excitation, the wavelength of a 561 nm laser with around 10-20% intensity and around 100% signal gain was used. The FM4-64 staining protocol was described in results “1.3.1 FM4-64 staining protocol”. For FM4-64 fluorescence excitation, the wavelength of a 549 nm laser with around 10-20% intensity and around 100% signal gain was used. Images from the stainings mentioned above were acquired under a 63X glycerol immersion objective; the setting of images was 1024×1024 pixels or 512×512 pixels.

For imaging the leaves from the plasma membrane marker *35Spro:mCherry-AtPIP1;4*, for mCherry fluorescence excitation, the wavelength of a 549 nm laser with around 10-20% intensity and around 100% signal gain was used. Images were acquired under a 63X glycerol immersion objective; the setting of images was 1024×1024 pixels or 512×512 pixels.

For phenotyping double mutants *klmute1;klmute2*, cotyledons of plate-grown *klmute1;klmute2* and WT seedlings 14 days after sowing were carefully collected, 0.01mM FM4-64 fluorescence stain was used to stain the cell membrane of the leaf epidermis. For FM4-64 fluorescence excitation, the wavelength of a 549 nm laser with around 10-20% intensity and around 100% signal gain was used. Images were acquired under a 63X glycerol immersion objective; the setting of images was 1024×1024 pixels.

To image the overexpression lines of *KlMUTEs* and *AtMUTE*: *35Sp:mCitrine-KlMUTE1*, *35Sp:mCitrine-KlMUTE2,* and *35Sp:mCitrine-AtMUTE* in *Arabidopsis thaliana*, seeds were germinated on ½ MS(+50 mg/L Kanamycin), after around 11 days of sowing, cotyledons of seedlings were picked with tweezers and stained with 0.01 mM FM4-64 fluorescence stain as described above. To image the overexpression lines of *KlMUTEs* and *AtMUTE*: *35Sp:mCitrine-KlMUTE1*, *35Sp:mCitrine-KlMUTE2,* and *35Sp:mCitrine-AtMUTE* in *Kalanchoë laxiflora*, around 0.5 cm leaves from the 2nd leaf pair were selected and stained with 0.01 mM FM4-64 fluorescence stain as described above. For mCitrine fluorescence excitation, the wavelength of a 515 nm laser with around 10% intensity and around 100% signal gain was used. For FM4-64 fluorescence excitation, the wavelength of a 549 nm laser with around 10-20% intensity and around 100% signal gain was used. Images

were acquired under a 63X glycerol immersion objective; the setting of images was 1024×1024 pixels or 512×512 pixels.

To image transcriptional reporter *KlMUTE1p:mCitrine-eGFP^{nls}*, translational reporter *KlMUTE1p:mCitrine-KlMUTE1* and *KlMUTE2p:mCitrine-KlMUTE2*, around 1-2 cm (primarily the 2nd or 3rd leaf pair) leaves were used. To image transcriptional reporter *KlMUTE2p:mCitrine-eGFP^{nls}*, around 0.5-1 cm leaves (primarily the 2nd or 3rd leaf pair) were collected from soil-grown plants. For imaging transcriptional reporters, the sample was stained with 0.01 mM FM4-64 fluorescence stain as described above. For imaging translational reporters, the sample was directly imaged under a microscope. For mCitrine fluorescence excitation, the wavelength of a 515 nm laser with around 10% intensity was used. Around 100% signal gain was used for imaging transcriptional reporters, and 150% signal gain was used for imaging translational reporters. For mCherry or FM4-64 fluorescence excitation, the wavelength of a 549 nm laser with around 10-20% intensity and around 100% signal gain was used. Images were acquired under a 63X glycerol immersion objective; the setting of images was 1024×1024 pixels or 512×512 pixels.

All images were acquired under a Leica Stellaris 5 confocal microscopy (Leica Microsystems).

The details of the emission and excitation wavelength used for confocal microscopy were listed in the supplementary Table 15.

11. Bulk RNA-sequencing analysis

For bulk RNA sequencing, the 7th pair of leaves (count the first visible pair as the 1st pair) from four WT and three independent *KlMUTE1* overexpression lines were harvested in the greenhouse. RNA was extracted from these samples using Qiagen Rneasy Plant Mini Kit, and DNA was removed by on-column DNAseI treatment. The concentration of RNA was measured by Qubit 4 Fluorometer (Thermo Fisher Scientific) and Qubit™ RNA Broad Range (BR) Assay Kits. Then, the RNA from these samples was sent to the Next Generation Sequencing Platform at the University of Bern. 500 ng RNA for each sample was reverse transcribed into cDNA and sequenced on an Illumina NovaSeq 6000 instrument. The quality control of all sequencing runs was tested by FASTQ, HISAT2 was used for mapping the sequencing reads to the *Kalanchoë laxiflora* genome (OBG accession), and

HTSeq-count was used to count the number of reads mapped to each gene. Raw counts were normalized by DESeq2 for PCA analysis and Sample Distance Heatmap to visualize the dataset. Differentially expressed genes were identified using DESeq2 in R (Love et al., 2014). Genes with Log2FoldChange>1 and padj<0.05 were considered significantly upregulated, while genes with Log2FoldChange<-1 and padj<0.05 were considered significantly downregulated. The homologs of stomatal key genes in *Arabidopsis thaliana* were identified in *K. laxiflora* by blasting the amino acid sequence of the gene against the proteome in a local NCBI blast installed on Windows.

Appendix

1. Supplementary Figures

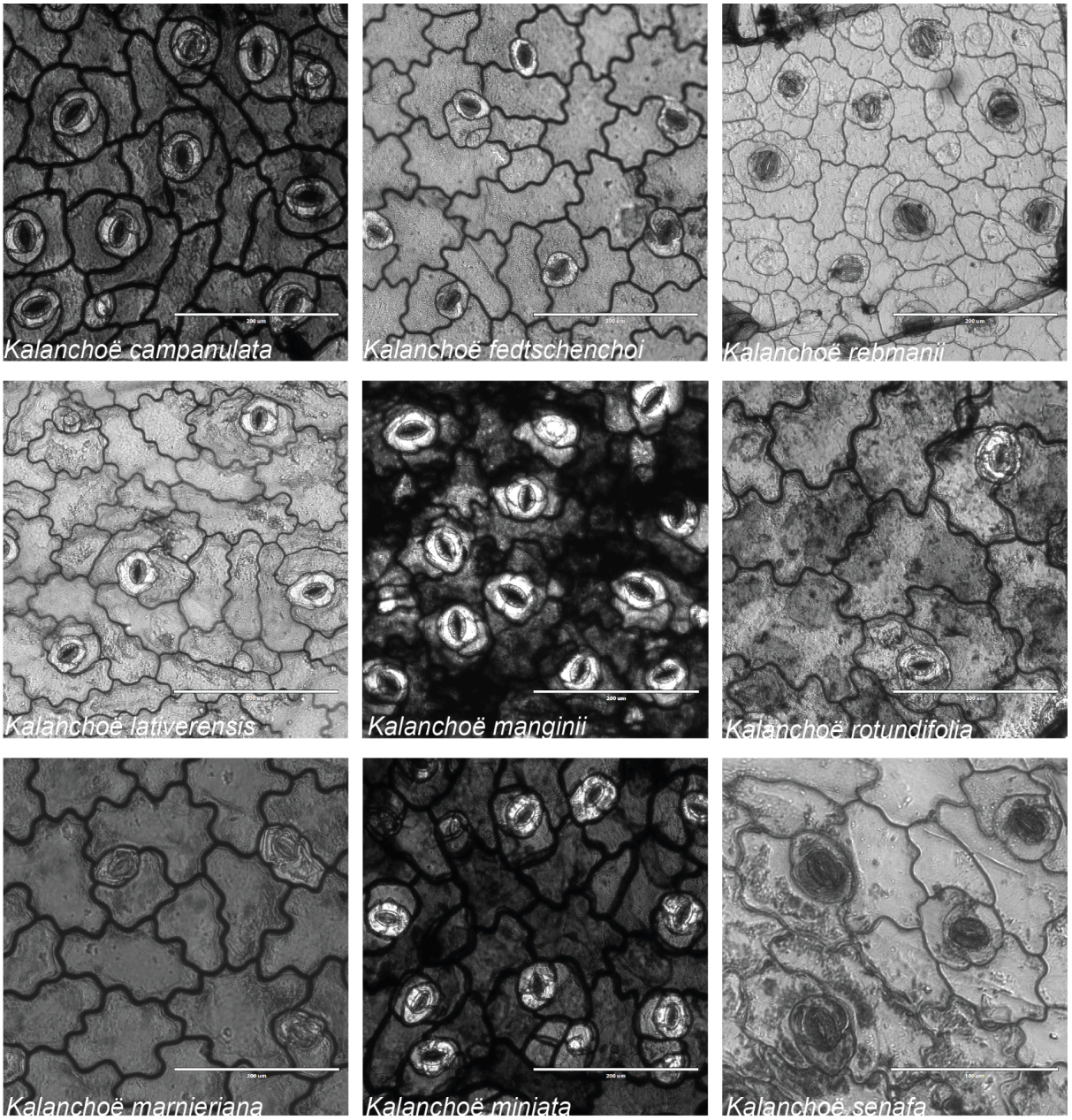

Figure S1. Some other species in the Kalanchoë family showed the same stomatal morphotype as *Kalanchoë laxiflora*.
Toluidine blue staining and light microscope imaging of the leaf epidermis from *Kalanchoë campanulata, Kalanchoë fedtschenchoi*, *Kalanchoë rebmanii*, *Kalanchoë lativerensis*, *Kalanchoë manginii*, *Kalanchoë rotundifolia*, *Kalanchoë marnieriana*, *Kalanchoë miniata*, *Kalanchoë senefa*. Scale bars were indicated.

Figure S2. The leaves of the *KIMUTEs* overexpression lines are bent toward the abaxial or adaxial side, showing a "spoon shape".
(A). The plants of WT (the left side) and KIMUTE2 overexpression lines (the right side). (B). The adaxial side of the detached leaves from WT, KIMUTE1 overexpression lines, and KIMUTE2 overexpression lines. (C). The abaxial side of the detached leaves from WT, KIMUTE1 overexpression lines, and KIMUTE2 overexpression lines. Scale bars, 20 μm.

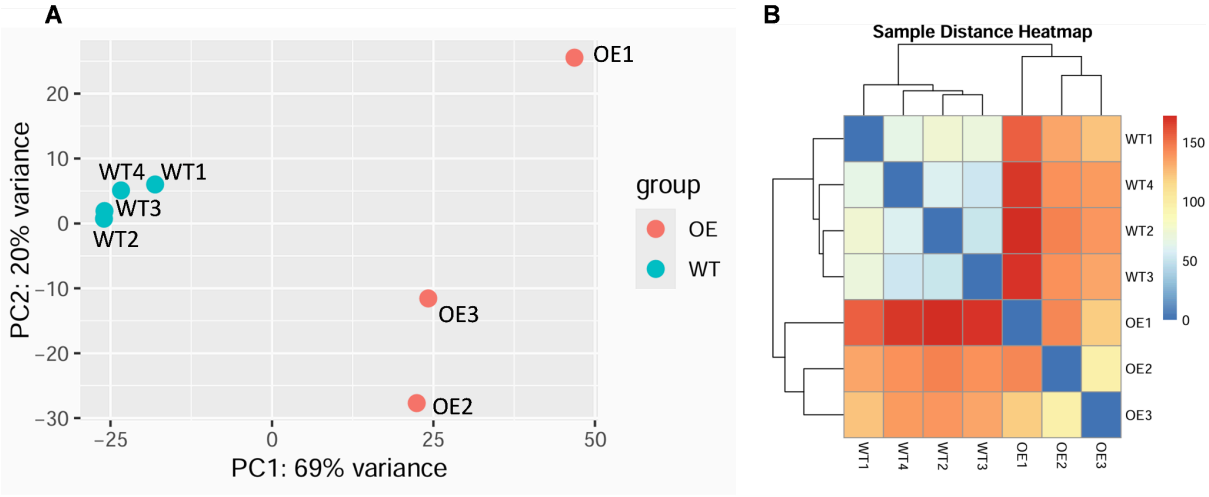

Figure S3. Visualization of bulk RNA-seq dataset of KIMUTE1 overexpression lines and WT.
(A). Principal Component Analysis and (B). Sample Distance Heatmap were used for quality control of bulk RNA-seq data of *KIMUTE1* overexpression lines and WT.

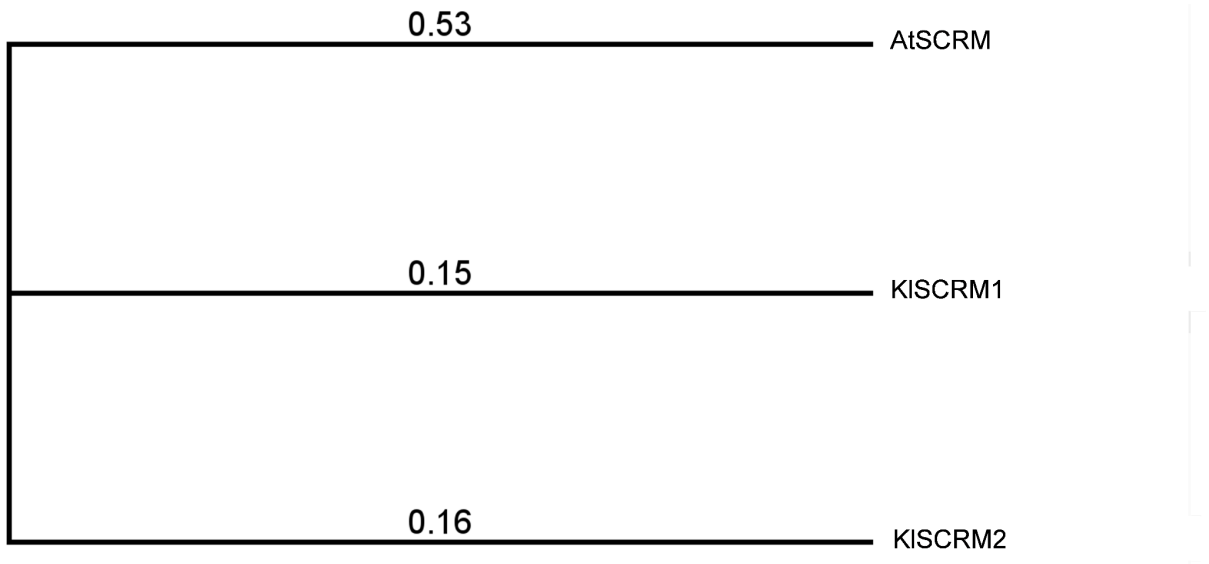

Figure S4. Phylogenetic tree of stomatal transcription factor SCRM in *Kalanchoë laxiflora* and *Arabidopsis thaliana*.

The whole amino acid sequence of each gene was used for the alignment. The phylogenetic tree was built by neighbor-joining, and no outgroup was set up. Sequences are from Kalanchoë laxiflora (KlSCRM1 = KlGene000465, KlSCRM2 = KlGene009864) and *Arabidopsis thaliana* (AtSCRM = AT3G26744).

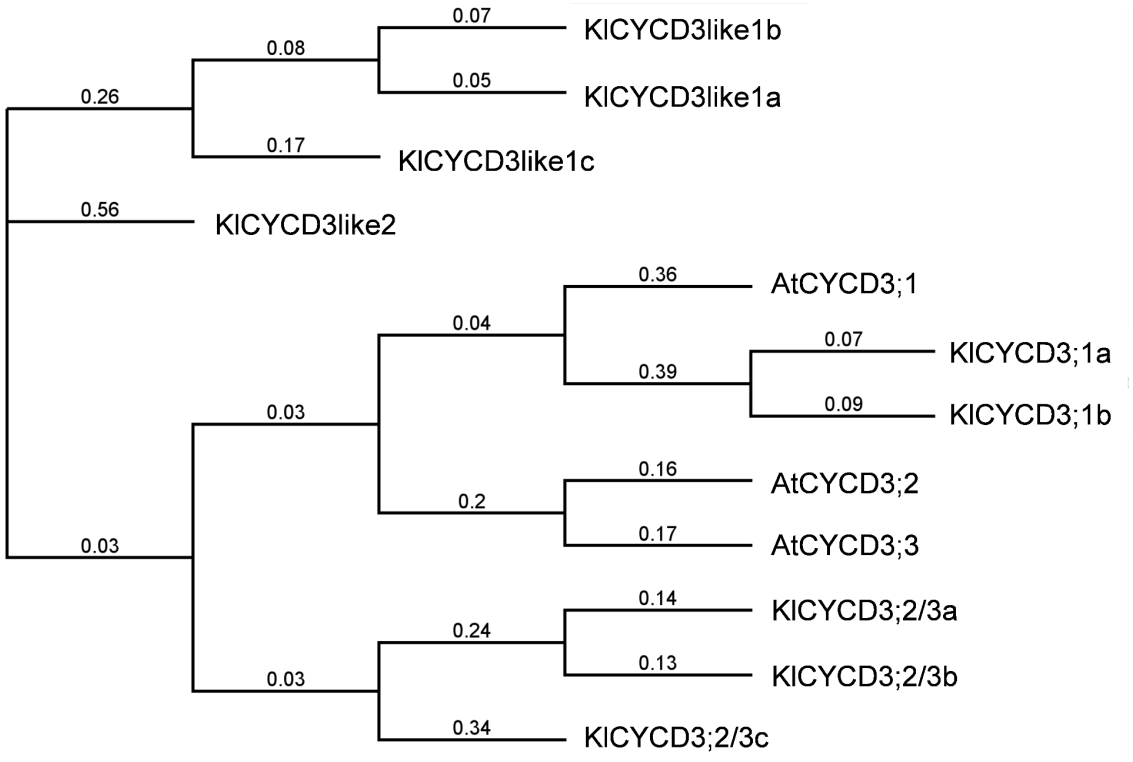

Figure S5. Phylogenetic tree of cyclin-D3 members in *Kalanchoë laxiflora* and *Arabidopsis thaliana*.
The whole amino acid sequence of each gene was used for the alignment. The phylogenetic tree was built by neighbor-joining, and no outgroup was set up. Sequences are from: *Kalanchoë laxiflora*(KlCYCD3like1b = KlGene001946, KlCYCD3like1a = KlGene025540, KlCYCD3like1c = KlGene008989, KlCYCD3like2 = KlGene000830, KlCYCD3;1a = KlGene007307, KlCYCD3;1b = KlGene029624, KlCYCD3;2/3a = KlGene012173, KlCYCD3;2/3b = KlGene019573, KlCYCD3;2/3c = KlGene015034) and *Arabidopsis thaliana* (AtCYCD3;1 = AT4G34160, AtCYCD3;2 = AT5G67260, AtCYCD3;3 = AT3G50070).

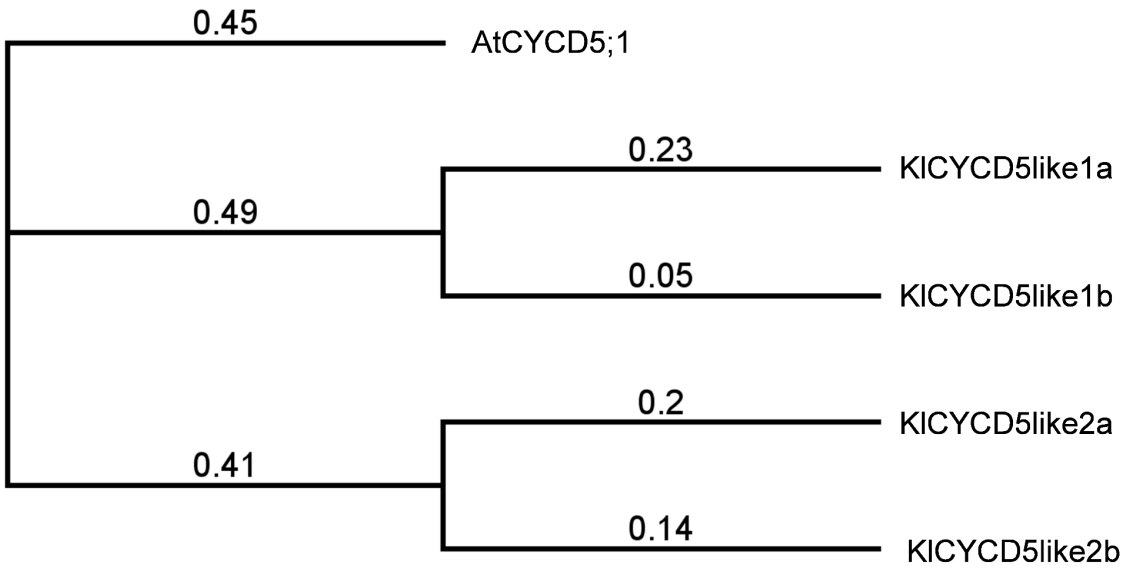

Figure S6. Phylogenetic tree of CYCD5;1 in *Kalanchoë laxiflora* and *Arabidopsis thaliana*.
The whole amino acid sequence of each gene was used for the alignment. The phylogenetic tree was built by neighbor-joining, and no outgroup was set up. Sequences are from: *Kalanchoë laxiflora*, (KlCYCD5like1a = KlGene007285, KlCYCD5like1b = KlGene029636, KlCYCD5like2a = KlGene015011, KlCYCD5like2b = KlGene029355), *Arabidopsis thaliana* (AtCYCD5;1 = AT4G37630).

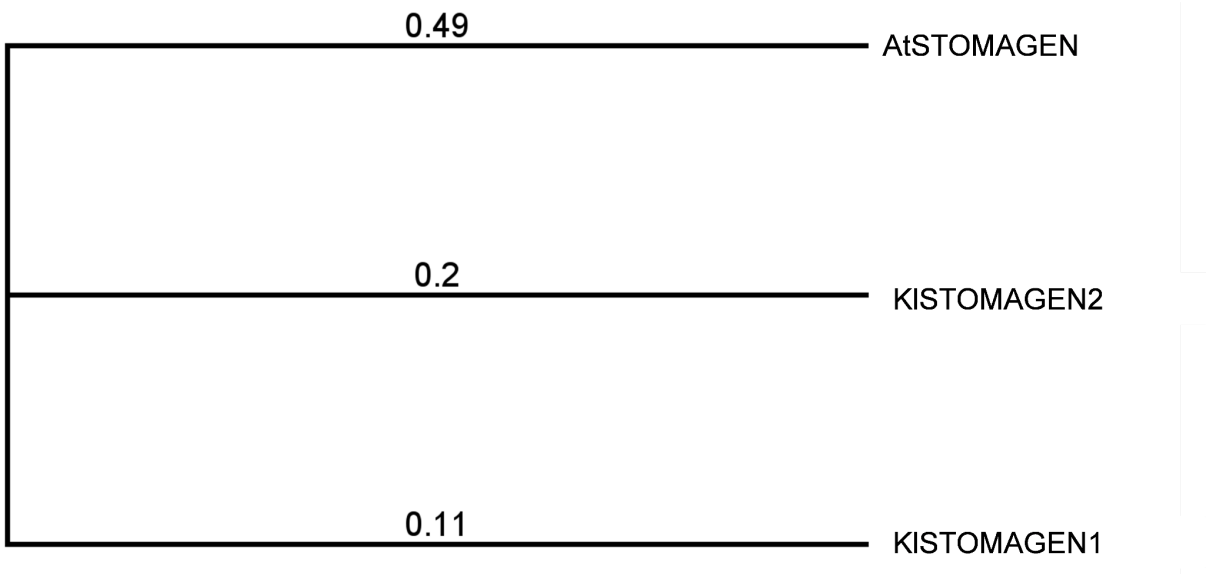

Figure S7. Phylogenetic tree of STOMAGEN in *Kalanchoë laxiflora* and *Arabidopsis thaliana*.
The whole amino acid sequence of each gene was used for the alignment. The phylogenetic tree was built by neighbor-joining, and no outgroup was set up. Sequences are from Kalanchoë laxiflora (KlSTOMAGEN2 = KlGene012723, KlSTOMAGEN1 = KlGene023262) and *Arabidopsis thaliana* (AtSTOMAGEN = AT4G12970).

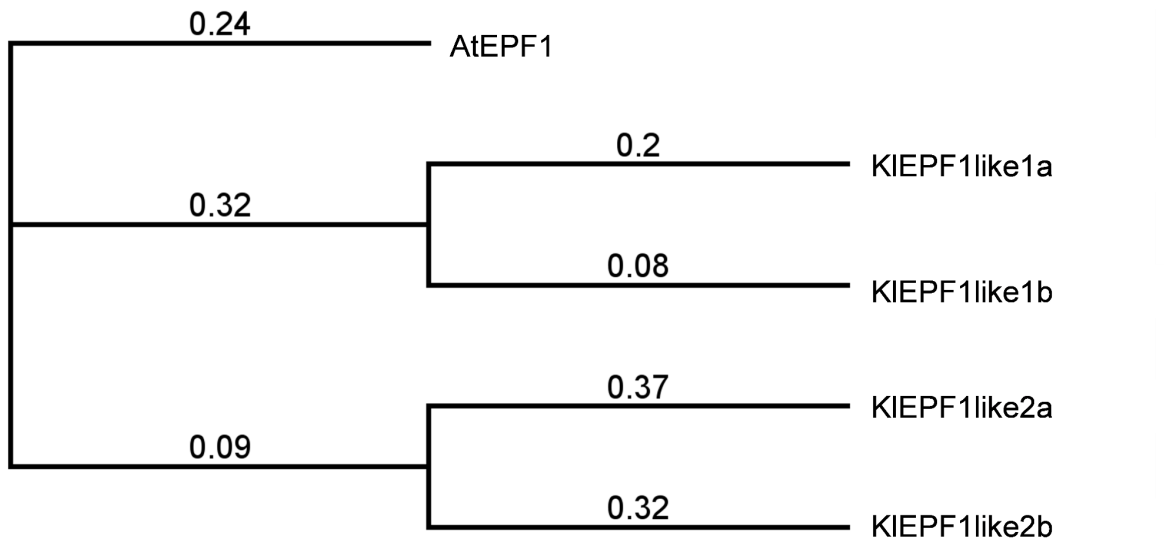

Figure S8. Phylogenetic tree of EPF1 in *Kalanchoë laxiflora* and *Arabidopsis thaliana*. The whole amino acid sequence of each gene was used for the alignment. The phylogenetic tree was built by neighbor-joining, and no outgroup was set up. Sequences are from: *Kalanchoë laxiflora* (KlEPF1like1a = KlGene006950, KlEPF1like1b = KlGene021413, KlEPF1like2a = KlGene003486, KlEPF1like2b = KlGene022175) and *Arabidopsis thaliana* (AtEPF1 = AT2G20875).

Figure S9. Phylogenetic tree of YDA in *Kalanchoë laxiflora* and *Arabidopsis thaliana*. The whole amino acid sequence of each gene was used for the alignment. The phylogenetic tree was built by neighbor-joining, and no outgroup was set up. Sequences are from Kalanchoë laxiflora (KlYDA1 = KlGene012364, KlYDA2 = KlGene019451) and *Arabidopsis thaliana* (AtYDA = AT1G63700).

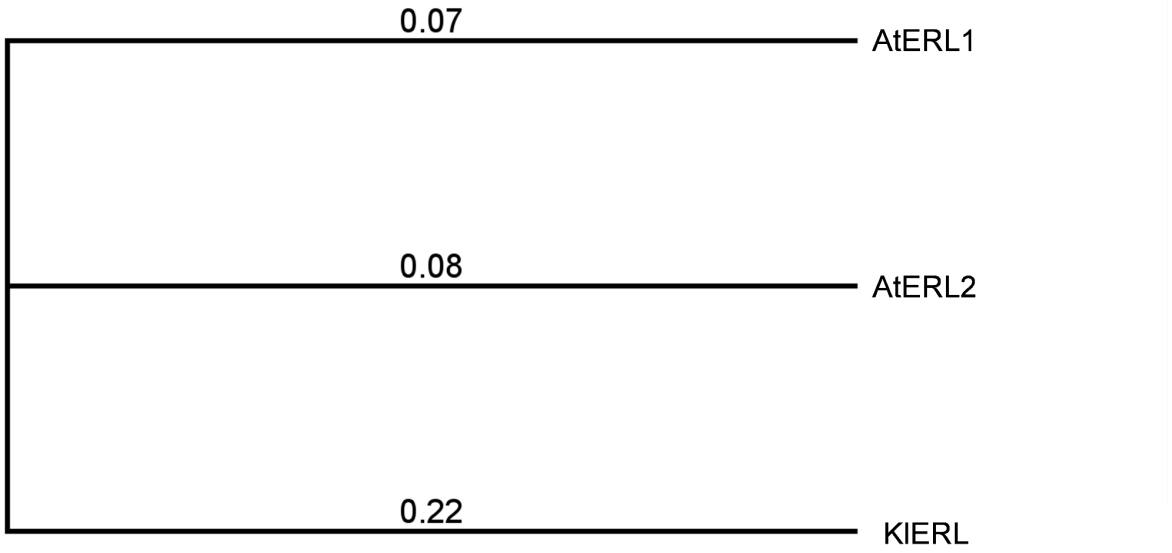

Figure S10. Phylogenetic tree of ERECTA-like members in *Kalanchoë laxiflora* and *Arabidopsis thaliana*.
The whole amino acid sequence of each gene was used for the alignment. The phylogenetic tree was built by neighbor-joining, and no outgroup was set up. Sequences are from Kalanchoë laxiflora (KlERL = KlGene028039) and *Arabidopsis thaliana* (AtERL1 = AT5G62230, AtERL2 = AT5G07180).

2. Supplementary Tables

Supplementary Table 1- DEG analysis of homologs of key stomatal transcription factors described in *Arabidopsis thaliana*

gene_name	gene_id	baseMean	log2FoldChange	lfcSE	stat	pvalue	padj
SCRM1	KlGene000465	318.2687	0.614297725	0.2639087	2.32769051	0.0199285	0.060682361
SCRM2	KlGene009864	1338.076	1.086176007	0.4266984	2.54553597	0.010911	0.037715396
FLP	KlGene010226	5173.932	-0.727765	0.236656	-3.07520229	0.0021036	0.010106928
FAMA1b	KlGene012763	24.12661	-1.080194177	0.6155527	-1.75483622	0.0792873	0.174215895
FAMA2	KlGene012781	38.6537	-1.213667249	0.3992646	-3.03975647	0.0023677	0.011104272
MUTE1	KlGene012921	13896.9	17.30615787	1.1158079	15.5099801	2.97E-54	1.11E-50
SPCH1	KlGene017537	1.529718	3.276832221	2.3650112	1.38554617	0.1658855	0.298534986
MUTE2	KlGene023418	34.04447	5.34683025	2.1868126	2.44503359	0.0144839	0.047339157
SPCH2	KlGene027982	62.38003	0.393281614	0.4533179	0.86756243	0.3856339	0.542576265

Supplementary Table 2- DEG analysis of homologs of key stomatal genes involved in cell polarity and cell divisions described in *Arabidopsis thaliana*

gene_name	gene_id	baseMean	log2FoldChange	lfcSE	stat	pvalue	padj
CYCD3like2	KlGene000830	301.137281	6.056539929	0.7001679	8.65012485	5.14E-18	6.90E-16
CYCD3like1b	KlGene001946	1.86974978	0.937190085	1.363537	0.68732282	0.4918793	0.639879
POLARlike1	KlGene004239	32.6396346	1.547017042	0.5289201	2.92485987	0.0034461	0.015055
CYCD5like1a	KlGene007285	0.4125107	0.88315237	3.767716	0.23439993	0.8146745	NA
CYCD3;1a	KlGene007307	95.7380516	1.55500342	0.6847457	2.27092102	0.0231518	0.068103
CYCD3like1c	KlGene008989	0.96617527	2.45615275	2.0876656	1.17650678	0.2393924	NA
CYCD3;2/3a	KlGene012173	70.0307743	-0.073966318	0.5213428	-0.1418766	0.8871775	0.931422
CYCD5like2a	KlGene015011	10.1701874	4.7860661	1.0559115	4.53263952	5.83E-06	6.79E-05
CYCD3;2/3c	KlGene015034	31.6472947	-1.024147307	0.4943065	-2.0718873	0.038276	0.100864
POLAR	KlGene016326	126.509597	0.325876836	0.2364565	1.37816802	0.1681514	0.301339
CYCD3;2/3b	KlGene019573	52.1842007	-0.109402901	0.5424185	-0.2016946	0.8401555	0.900888
BRXL2	KlGene020240	88.7365232	0.778316858	0.3634974	2.14118983	0.0322587	0.088171
CYCD3like1a	KlGene025540	0.87568985	-1.188570201	2.778221	-0.427817	0.6687844	NA
CYCD5like2b	KlGene029355	52.5520876	1.949460275	0.5559004	3.50685198	0.0004534	0.002836
CYCD3;1b	KlGene029624	20.2828025	0.985528658	0.9018776	1.09275209	0.2745027	0.42743
CYCD5like1b	KlGene029636	19.3954118	-1.161496056	0.5139847	-2.259787	0.0238345	0.069696

Supplementary Table 3- DEG analysis of homologs of key genes involved in stomata patterning described in *Arabidopsis thaliana*

gene_name	gene_id	baseMean	log2FoldChange	lfcSE	stat	pvalue	padj
TMM	KlGene003728	522.02919	-0.304228404	0.195173	-1.55876266	0.119053	0.2353
CHALLAH	KlGene005008	139.93267	1.100635717	0.377048	2.9190882	0.003511	0.015275
ER	KlGene005407	1746.4498	2.33641304	0.512215	4.56139103	5.08E-06	6.06E-05
EPF1like1a	KlGene006950	18.929421	-1.355820041	0.633368	-2.1406516	0.032302	0.088193
YDA1	KlGene012364	969.11758	-0.060356897	0.142043	-0.4249192	0.670896	0.781862
STOMAGEN2	KlGene012723	75.400574	0.329694101	0.732754	0.44993846	0.652755	0.768518
SDD1	KlGene014073	2.8314232	-4.942003363	1.6537	-2.98845233	0.002804	0.012768
EPF2	KlGene018971	1.1753303	2.811671299	2.500465	1.12445929	0.260818	0.412517
YDA2	KlGene019451	1471.2148	0.451260104	0.14619	3.08680175	0.002023	0.009801
EPF1like1b	KlGene021413	35.562545	-2.162393116	0.608117	-3.55588378	0.000377	0.002441
STOMAGEN1	KlGene023262	128.29445	0.049046808	0.359269	0.13651823	0.891412	0.934072
ERlike	KlGene028039	452.37303	0.593609412	0.583818	1.01677078	0.309262	0.464568

Supplementary Table 4-Murashige and Skoog medium for *Kalanchoë laxiflora* and *Arabidopsis thaliana*

medium	recipe(per liter)
1/2MS(for *K.laxiflora*)	2.2 g MS (including Gamborg's B5 vitamins) (Duchefa: M0231), 30 g sucrose (Fisher Scientific: BP220), pH adjusted to 5.8 using 1 M NaOH, then add 8 g Phytoagar (Duchefa: P1003).
Callus induction medium (CIM)(co-culture)	4.41 g MS (including Gamborg's B5 vitamins) (Duchefa: M0231), 30 g Sucrose (Fisher Scientific: BP220), pH adjusted to 5.7 using 1M NaOH), then add 8 g Phytoagar(Duche- fa: P1003), after autoclaving, add 1 mg/ L TDZ (Duchefa: T0916) and 0.2 mg/ L IAA (Duchefa: I0901) and 100 μM Acetosyringone (Sigma-Aldrich).
Callus induction medium (CIM)	4.41 g MS (including Gamborg's B5 vitamins) (Duchefa: M0231), 30 g Sucrose (Fisher Scientific: BP220), pH adjusted to 5.3 using 1M NaOH, then add 8 g Phyto- agar (Duchefa: P1003), after autoclaving, add 1 mg/L TDZ (Duchefa: T0916), 0.2 mg/L IAA (Duchefa: I0901), 100 mg/ L Kanamycin (Carl- Roth: T832) and 300 mg/L Timentin (Duchefa: T0190).
Shoot Induction Medium (SIM)	4.41g MS (including Gamborg's B5 vitamins) (Duchefa: M0231), 30 g Sucrose (Fisher Scientific: BP220), pH adjusted to 5.1 using 1M NaOH, then add 8 g Phytoagar (Duchefa: P1003), after autoclaving, add 1 mg L-1 BAP (Duchefa: B0904), 0.2 mg/L IAA (Duchefa: I0901), 100 mg/L Kanamycin (CarlRoth: T832) and 300 mg/L Timentin (Duchefa: T0190).
Root Induction Medium (RIM)	4.41g MS (including Gamborg's B5 vitamins)(Duchefa: M0231), 30 g Sucrose (Fisher Scientific: BP220), pH adjusted to 5.2 using 1M NaOH), then add 8 g Phytoagar (Duchefa: P1003), after autoclaving, add 50 mg/L Kanamycin (CarlRoth: T832) and 300 mg/L Timentin(Duchefa: T0190).
1/2MS(for *A. thaliana*)	2.15g MS (Duchefa: M0221), 30 g sucrose(Fisher Scientific: BP220), pH adjusted to 5.8 using 1M NaOH, then add 8g Phytoagar (Duchefa: P1003), after autoclaving, add 50 mg/L Kanamycin (CarlRoth: T832).

Supplementary Table 5- Soil for plant growth

soil	recipe
seedling substrate	Klasmann-Deilman GmbH, Germany, Article # 455433
Kalanchoë soil	"Landerde" (Ricoter, Switzerland):peat:white sand=5:4:1

Supplementary Table 6- 2X CTAB buffer recipe for DNA extraction

Component	Stocking concentration	Working concentration	100 mL in total
EDTA	20 mM	0.5 M	4 mL
Tris-HCl (PH 8.0)	100 mM	1 M	10 mL
NaCl	5 M	1.4 M	28 ml
CTAB			2 g
ddH_2O			up to 100 mL

Supplementary Table 7- Q5 PCR amplification setup and thermocycling conditions

Component	50ul reaction	Temperature	Time	Number of cycles
5xQ5 buffer	10 µL	98°C	30 s	1
(5*Q5 GC enhancer)	(10 µL)	98°C	10 s	30 Cycles
10mM dNTP)	1 µL	58°C	20 s	
10 µM Forward primer	2.5 µL	72°C	30s/kb	
10 µM Reward primer	2.5 µL	72°C	2 min	1
Q5 High-Fidelity DNA Polymerase (NEB)	0.5 µL	4°C	hold	
DNA	variable			
ddH_2O	up to 50 µL			

Supplementary Table 8- Taq PCR amplification setup and thermocycling conditions

Component	25µL/50uL reaction	Temperature	Time	Number of cycles
5xTaq buffer	5 µL/ 10 µL	95°C	30 s	1
10mM dNTPs	0.5µL/1 µL	95°C	30 s	30-35 cycles
10 µM Forward primer	0.5µL/1 µL	58°C	30 s	
10 µM Reward primer	0.5µL/1 µL	68°C	1min/kb	
one-Taq DNA polymerse	0.125µL/0.25 µL	68°C	5min	1
DNA	1 µL	4°C	hold	
ddH_2O	17.375µL/35.75µL			

Supplementary Table 9- Greengate reaction setup and thermocycling conditions

Component	20uL reaction	Temperature	Time	Number of cycles
promoter(module A)	1.5uL	37°C	5min	30 cycles
N-tag(module B)	1.5uL	16°C	2min	
CDS(module C)	1.5uL	50°C	5min	1
C-tag(module D)	1.5uL	80°C	5min	1
Terminator(module E)	1.5uL			
Resistance(module F)	1.5uL			
Destination Vector	1uL			
10x restriction buffer	2uL			
10mM ATP	2uL			
T4 DNA ligase	0.5uL			
BsaI	0.5uL			
ddH_2O	5uL			

Supplementary Table 10- Plasmids used in this thesis

Plasmid number	Plasmid Name	Creator
pXC01	pENTR-KIMUTE1-F1	Xin Cheng
pXC02	pENTR-KIMUTE1-F2	Xin Cheng
pXC05	p01178-AtCAS9-AtU6_26-KIMUTE1	Xin Cheng
pXC06	p01178-AtCAS9-AtU6_26-KIMUTE2	Xin Cheng
pXC07	p01178-AtCAS9-AtU6_26-KIMUTE	Xin Cheng
pXC08	pK7GWIWG2(II)-KIMUTE1-F1	Xin Cheng
pXC09	pK7GWIWG2(II)-KIMUTE1-F2	Xin Cheng
pXC10	pGGA000-KIMUTE1-promoter	Xin Cheng
pXC11	pGGC000-KIMUTE1-CDS(with stop codon)	Xin Cheng
pXC12	pGGA000-KIMUTE2-promoter	Xin Cheng
pXC13	pGGC000-KIMUTE2-CDS(with stop codon)	Xin Cheng
pXC14	pGGZ004_KIMUTE1 pro_mCitrine_KIMUTE1 CDS(with stop codon)	Xin Cheng
pXC15	pGGZ004_KIMUTE2 pro_mCitrine_KIMUTE2 CDS(with stop codon)	Xin Cheng
pXC16	pGGZ004_KIMUTE1 pro_mCitrine_GFP_NLS	Xin Cheng
pXC17	pGGZ004_KIMUTE2 pro_mCitrine_GFP_NLS	Xin Cheng
pXC18	pGGZ004_35S_mCitrine_KIMUTE1 CDS(with stop codon)	Xin Cheng
pXC19	pGGZ004_35S_mCitrine_KIMUTE2 CDS(with stop codon)	Xin Cheng
pXC21	pGGZ004_35S_mCitrine_AtMUTE CDS(with stop codon)	Xin Cheng
pYBG01	pGGZ003_35S_mCherry_AtPIP1;4	Yiğit Berkay Gündoğmuş

Supplementary Table 11-Antibiotics and plant hormones used in this study

Antibiotic	Stock concentration	Work concentration	Solvent	Catalogue
Ampicillin	100 mg/mL	100 mg/L	ddH_2O	Sigma-Aldrich
Spectinomycin	50 mg/mL	50 mg/L	ddH_2O	Sigma-Aldrich
Kanamycin	50 mg/mL	50 mg/L(cloning or *A. thaliana* screening)/100 mg/L(*K.laxiflora* screening)	ddH_2O	ROTH
Carbenicillin	50 mg/mL	50 mg/L	ddH_2O	ROTH
Rifampicin	50 mg/mL	50 mg/L	DMSO	Sigma-Aldrich
Gentamicin	25 mg/mL	25 mg/L	ddH_2O	Sigma-Aldrich

Supplementary Table 12-Organisms used in this study

Organism	Strain/Genotype
Escherichia coli	DH5α
Agrobacterium tumefaciens	GV3101
Kalanchoë laxiflora	Oxford Botanical Garden(OBG)
Arabidopsis thaliana	Col-0

Supplementary Table 13-Primers used in this thesis

Primer name	sequence [5'-3']	description
priXC1	caccGTTTGAGTCCCAGCCCAAA	FP to amplify KlMUTE1 KlGene012921 specific domain for RNAi and dropping into pENTR-D-TOPO -> KD of both KlMUTE homologs
priXC2	CCTCTCCAACTCGCTGACTA	RP to amplify KlMUTE1 KlGene012921 specific domain for RNAi and dropping into pENTR-D-TOPO -> KD of both KlMUTE homologs
priXC3	GTGTCTTCCATGCTGCTGAT	RP to amplify KlMUTE1 KlGene012921 specific domain for RNAi and dropping into pENTR-D-TOPO -> KD of both KlMUTE homologs
priXC4	AACAGGTCTCA**GGCT**CCATGTCT CACATAGCTGTGGAGC	FP to amplify KlMUTE1 KlGene012921 CDS as C module
priXC5	AACAGGTCTCA**CTGA**CTATAAGT GATGAGCAAGCAGTGAG	RP to amplify KlMUTE1 KlGene012921 CDS as C module
priXC6	AACAGGTCTCA**ACCT**TACCGTCG ACTTTGTGTGAC	FP to amplify KlMUTE1 KlGene012921 promoter as A module
priXC7	AACAGGTCTCA**TGTT**GTTTGACTA TGGCAGGCAGAA	RP to amplify KlMUTE1 KlGene012921 promoter as A module
priXC8	AACAGGTCTCA**GGCT**CCATGTCT CACATAGCGGTGGA	FP to amplify KlMUTE2 KlGene023418 CDS as C module
priXC9	AACAGGTCTCA**CTGA**CTATAAGTA GTTTGCAAGCAGTGTG	RP to amplify KlMUTE2 KlGene023418 CDS as C module
priXC11	AACAGGTCTCA**TGTT**GCTCGGCT GAATGGCAG	RP to amplify KlMUTE2 KlGene023418 promoter as A module
priXC12	AACAGGTCTCA**CTTA**GTTGGCGA GCTAAAGTGC	RP to mutate BsaI site in KlMUTE2 KlGene023418 CDS_used with priXC8
priXC13	AACAGGTCTCA**TAAG**AGTTATTGA TACCAGCAAGT	FP to mutate BsaI site in KlMUTE2 KlGene023418 CDS_used with priXC9
priXC14	attggTCAAGGATCGAAGGACTTTG	FP Guide2 for KlMUTE1
priXC15	aaacCAAAGTCCTTCGATCCTTGAc	RP Guide2 for KlMUTE1
priXC18	attggTGACAGTTTGGCTTCCACGT	FP Guide1 for KlMUTE2
priXC19	aaacACGTGGAAGCCAAACTGTCA c	RP Guide1 for KlMUTE2

priXC24	attgGATCAGGCTTCAATCATAGG	FP Guide2 for both KIMUTE homologs
priXC25	aaacCCTATGATTGAAGCCTGATC	RP Guide2 for both KIMUTE homologs
priXC28	GAAAAATAGAGAGAGATAGATTTGTAGAGAG	FP for detecting sequence betwwen attB1-attB2 site in pK7GWIWG2(II)
priXC29	GCCGTAAGAAGAGGCAAGAGT	FP for detecting sequence betwwen attB2-attB1 site in pK7GWIWG2(II)
priXC30	GAAGAGAAGCAGGCCCATTTATA	FP for detecting guide sequence in p01178(CRISPR-CAS9)
priXC31	ACGTAAGGGATGACGCACA	FP for detecting mcherry tag in pYBG1_pGGZ003_35S_mCherry-GSL_AtPIP1;4_KanR
priXC32	GGTTCTGTCAGTTCCAAACGTAA	FP for detecting the T35S motif in the pK7GWIWG2(II)
priXC33	AAACGCTCTTTTCTCTTAGGTTTAC	RP for detecting the p35S motif in the pK7GWIWG2(II)
priXC34	CGCGAAAATGACATCAAAAACG	FP for detecting the "T" deletion on the backbone in the p01178
priXC35	GGGGAAGAAGTGGCTGATCT	FP for amplifying the mutation and deletion on the backbone in the pK7GWIWG2(II)
priXC36	GCAACTGACTGAAATGCCTC	RP for amplifying of the mutation and deletion on the backbone in the pK7GWIWG2(II)
priXC37	TAACGGAATAATGGGCTATCTACATG	FP for continue sequencing the plasmid pXC10(middle primer)
priXC38	GTGGTCTTGAGAATTGTTTGCAG	FP for continue sequencing the plasmid pXC13(middle primer)
priXC41	TTTGTGAGACTGGGGCATATAGA	FP for continue sequencing the plasmid pXC12(middle primer 3)
priXC42	GGCTCCTTCCATCCTCGTA	FP for continue sequencing the plasmid pXC12(middle primer 4)
priXC44	GCCCAAGACTGCTGGAAG	FP for continue sequencing the plasmid pXC11(middle primer)
priXC54	AACTACACTCCCACGTCTGA	FP for clony PCR of pXC14
priXC55	GATGGGGTCAAGGATCGAAG	RP for clony PCR of pXC14
priXC59	AACAGGTCTCA**ACCT**GTACAACCGCAAGCAGTTTC	FP to amplify KIMUTE2 KIGene023418 promoter as A module(~2kb)
priXC60	GAGGTGCTCATTCATCTGCC	RP for clony PCR of pXC15
priXC61	TTCGATCCTTGACCCCATCT	FP for KIMUTE1 genotyping(for crispr construct pXC07)
priXC74	GAGAAGAGCTGGAGTTGTGG	RP for KISPCH2(for RT-PCR)
priXC85	CTTCTTCCTGCAGTTGACGG	RP for KIUBQ10(reference gene for RT-PCR)
priXC86	ATTCCAGCCCTATCTTGATAACAAT	RP for KIMUTE2(for RT-PCR, cross 2,3 exon)
priXC87	TTCCAGCCCTATCTTGACAACAAA	RP for KIMUTE1(for RT-PCR, cross 2,3 exon)
priXC89	TCAATCCCAATCTTGATGGTGA	RP for KISPCH1(for RT-PCR, cross 2,3 exon)

priXC90	GAAGACCATCACGCTCGAG	FP for KlUBQ10(reference gene for RT-PCR)
priXC91	AGATTGAATCCTGTTGCCGG	FP for sequencing the kan(F) module and Z module
priXC94	TTCTACATCAAAAGGGGAGATCAGGCTTCA	FP for KlMUTE1(for RT-PCR, cross 1.2 exon)
priXC95	TTCTACATCAAAAAGGGAGATCAGGCTTCC	FP for KlMUTE2 (for RT-PCR, cross 1,2 exon)
priXC96	TATGTCAAAAAAGGTGACCAAGCG	FP for KlSPCH1(for RT-PCR, cross 1,2 exon)
priXC98	CTATGTTAAAAAAGGTGACCAAGCAT	FP for KlSPCH2(for RT-PCR, cross 1,2 exon)
priXC122	TCAATTTATGCGTCCGTGCT	FP for genotyping KlMUTE2 CRISPR mutant
priXC123	GTCTTCCATGCTGCTGATGT	RP for genotyping KlMUTE2 CRISPR mutant(work with priXC122)
priYBG4	GATGAGCAAGCAGTGAGTCA	RP amplifying KlMUTE1 on Exon 3 for RT-PCR
priYBG7a	GCGGTTGAGAGGAATAGAAGG	FP for RT-PCR for Klgene012761_KlFAMA1a with priYBG10
priYBG7b	ATAGCGGTTGAGAGAAATAGAAGA	FP for RT-PCR for Klgene012763_KlFAMA1b with priYBG8
priYBG8	GAGCTTGCTATGTCCTCTGC	RP for RT-PCR for Klgene012763_KlFAMA1b (with priYBG7b) & Klgene012781_KlFAMA2 (with priYBG9)
priYBG9	GAGATCAGGCTGCTGCATTA	FP for RT-PCR for Klgene012781_KlFAMA2 with priYBG8)
priYBG10	TGCACTATATCTGGTTTCACTTGA	RP for RT-PCR for Klgene012761_KlFAMA1a (with priYBG7a)

Supplementary Table 14 -Recipe of Toluidine blue staining solution

Step	Solution	Recipe
1	Acetate buffer	Dissolve 0.01g pectolyase in 84.7 mL 1M Acetic acid, then add distilled water up to 100 mL
2	Toluidine Blue	Dissolve 0.2 g Toluidine Blue O in 40 mL Acetate Buffer

Supplementary Table 15- Emission and excitation wavelength used for confocal microscopy

Fluorescence	Excitation (nm)	Emission (nm)
mCitrine	515	520-545
mCherry	549	575-640
FM4-64	549	575-640
Calcofluor white	401	420-450
PI	549	600-640
Direct Red 23	561	590-620

Bibliography

Abraham, P. E., Yin, H., Borland, A. M., Weighill, D., Lim, S. D., De Paoli, H. C., Engle, N., Jones, P. C., Agh, R., Weston, D. J., Wullschleger, S. D., Tschaplinski, T., Jacobson, D., Cushman, J. C., Hettich, R. L., Tuskan, G. A., & Yang, X. (2016). Transcript, protein and metabolite temporal dynamics in the CAM plant Agave. *Nature Plants*, *2*(12), 16178.

Abrash, E. B., & Bergmann, D. C. (2010). Regional specification of stomatal production by the putative ligand CHALLAH. *Development* , *137*(3), 447–455.

Abrash, E. B., Davies, K. A., & Bergmann, D. C. (2011). Generation of signaling specificity in Arabidopsis by spatially restricted buffering of ligand-receptor interactions. *The Plant Cell*, *23*(8), 2864–2879.

Akulova-Barlow, Z. (2009). Kalanchoe. *Cactus and Succulent Journal*, *81*(6), 268–276.

Balcerowicz, M., Ranjan, A., Rupprecht, L., Fiene, G., & Hoecker, U. (2014). Auxin represses stomatal development in dark-grown seedlings via Aux/IAA proteins. *Development* , *141*(16), 3165–3176.

Barrera Zambrano, V. A., Lawson, T., Olmos, E., Fernández-García, N., & Borland, A. M. (2014). Leaf anatomical traits which accommodate the facultative engagement of crassulacean acid metabolism in tropical trees of the genus Clusia. *Journal of Experimental Botany*, *65*(13), 3513–3523.

Belkhadir, Y., & Chory, J. (2006). Brassinosteroid signaling: a paradigm for steroid hormone signaling from the cell surface. *Science*, *314*(5804), 1410–1411.

Berger, D., & Altmann, T. (2000). A subtilisin-like serine protease involved in the regulation of stomatal density and distribution in Arabidopsis thaliana. *Genes & Development*, *14*(9), 1119–1131.

Bergmann, D. C., Lukowitz, W., & Somerville, C. R. (2004). Stomatal development and pattern controlled by a MAPKK kinase. *Science*, *304*(5676), 1494–1497.

Bergmann, D. C., & Sack, F. D. (2007). Stomatal development. *Annual Review of Plant Biology*, *58*(1), 163–181.

Bidhendi, A. J., Chebli, Y., & Geitmann, A. (2020). Fluorescence visualization of cellulose and pectin in the primary plant cell wall. *Journal of Microscopy*. *278*(3), 164−181.

Blanc-Mathieu, R., Dumas, R., Turchi, L., Lucas, J., & Parcy, F. (2024). Plant-TFClass: a structural classification for plant transcription factors. *Trends in Plant Science*, *29*(1), 40–51.

Boccalandro, H. E., Rugnone, M. L., Moreno, J. E., Ploschuk, E. L., Serna, L., Yanovsky, M. J., & Casal, J. J. (2009). Phytochrome B enhances photosynthesis at the expense of water-use efficiency in Arabidopsis. *Plant Physiology*, *150*(2), 1083–1092.

Borland, A. M., Barrera Zambrano, V. A., Ceusters, J., & Shorrock, K. (2011). The photosynthetic plasticity of crassulacean acid metabolism: an evolutionary innovation for sustainable productivity in a changing world: Tansley review. *The New Phytologist*, *191*(3), 619–633.

Borland, A. M., Griffiths, H., Hartwell, J., & Smith, J. A. C. (2009). Exploiting the potential of plants with crassulacean acid metabolism for bioenergy production on marginal lands. *Journal of Experimental Botany*, *60*(10), 2879–2896.

Borland, A. M., Hartwell, J., Weston, D. J., Schlauch, K. A., Tschaplinski, T. J., Tuskan, G. A., Yang, X., & Cushman, J. C. (2014). Engineering crassulacean acid metabolism to improve water-use efficiency. *Trends in Plant Science*, *19*(5), 327–338.

Boxall, S. F., Kadu, N., Dever, L. V., Kneřová, J., Waller, J. L., Gould, P. J. D., & Hartwell, J. (2020). *Kalanchoë* PPC1 Is Essential for Crassulacean Acid Metabolism and the Regulation of Core Circadian Clock and Guard Cell Signaling Genes. *The Plant Cell*, *32*(4), 1136–1160.

Cantón, F. R., & Quail, P. H. (1999). Both phyA and phyB mediate light-imposed repression of PHYA gene expression in Arabidopsis. *Plant Physiology*, *121*(4), 1207–1216.

Carretero-Paulet, L., Galstyan, A., Roig-Villanova, I., Martínez-García, J. F., Bilbao-Castro, J. R., & Robertson, D. L. (2010). Genome-wide classification and evolutionary analysis of the bHLH family of transcription factors in Arabidopsis, poplar, rice, moss, and algae. *Plant Physiology*, *153*(3), 1398–1412.

Cashmore, A. R., Jarillo, J. A., Wu, Y. J., & Liu, D. (1999). Cryptochromes: blue light receptors for plants and animals. *Science*, *284*(5415), 760–765.

Casson, S. A., Franklin, K. A., Gray, J. E., Grierson, C. S., Whitelam, G. C., & Hetherington, A. M. (2009). phytochrome B and PIF4 regulate stomatal development in response to light quantity. *Current Biology*, *19*(3), 229–234.

Casson, S. A., & Hetherington, A. M. (2014). phytochrome B Is required for light-mediated systemic control of stomatal development. *Current Biology*, *24*(11), 1216–1221.

Chaffey, N. J. (1983). Epidermal Structure in the Ligule of Rice (Oryza sativa L.). *Annals of Botany*, *52*(1), 13–21.

Chang, G., Ma, J., Wang, S., Tang, M., Zhang, B., Ma, Y., Li, L., Sun, G., Dong, S., Liu, Y., Zhou, Y., Hu, X., Song, C.-P., & Huang, J. (2023). Liverwort bHLH transcription factors and the origin of stomata in plants. *Current Biology*. *33*(13), 2806–2813.e6.

Chater, C. C., Caine, R. S., Tomek, M., Wallace, S., Kamisugi, Y., Cuming, A. C., Lang, D., MacAlister, C. A., Casson, S., Bergmann, D. C., Decker, E. L., Frank, W., Gray, J. E., Fleming, A., Reski, R., & Beerling, D. J. (2016). Origin and function of stomata in the moss Physcomitrella patens. *Nature Plants*, *2*, 16179.

Chater, C. C. C., Caine, R. S., Fleming, A. J., & Gray, J. E. (2017). Origins and Evolution of Stomatal Development. *Plant Physiology*, *174*(2), 624–638.

Chater, C., Peng, K., Movahedi, M., Dunn, J. A., Walker, H. J., Liang, Y.-K., McLachlan, D. H., Casson, S., Isner, J. C., Wilson, I., Neill, S. J., Hedrich, R., Gray, J. E., & Hetherington, A. M. (2015). Elevated CO2-induced responses in stomata require ABA and ABA signaling. *Current Biology*, *25*(20), 2709–2716.

Cheng, X., Lindner, H., Hoffmann, L., Filho, A. A. P., Duarte, P. R., Boxall, S. F., Gündogmus, Y. B., Pritchard, J. H., Haldenby, S., Gemmell, M., Darby, A., Läderach, M., Hartwell, J., & Raissig, M. T. (2024). MUTE drives asymmetric divisions to form stomatal subsidiary cells in Crassulaceae succulents. In *bioRxiv* (p. 2024.12.27.630159). https://doi.org/10.1101/2024.12.27.630159

Cheng, X., & Raissig, M. T. (2023). From grasses to succulents - development and function of distinct stomatal subsidiary cells. *The New Phytologist*, *239*(1), 47–53.

Chen, L., Wu, Z., & Hou, S. (2020). SPEECHLESS Speaks Loudly in Stomatal Development. *Frontiers in Plant Science*, *11*, 114.

Chua, L. C., & Lau, O. S. (2024). Stomatal development in the changing climate. *Development*, *151*(20), dev202681.

Clough, S. J., & Bent, A. F. (1998). Floral dip: a simplified method for Agrobacterium-mediated transformation of Arabidopsis thaliana. *The Plant Journal: For Cell and Molecular Biology*, *16*(6), 735–743.

Cockburn, W. (1979). Relationships between stomatal behavior and internal carbon dioxide concentration in Crassulacean acid metabolism plants. *Plant Physiology*, *63*(6), 1029–1032.

Croxdale, J., Smith, J., Yandell, B., & Johnson, J. B. (1992). Stomatal patterning in Tradescantia: an evaluation of the cell lineage theory. *Developmental Biology*, *149*(1), 158–167.

Cushman, J. C. (2001). Crassulacean acid metabolism. A plastic photosynthetic adaptation to arid environments. *Plant Physiology*, *127*(4), 1439–1448.

Cushman, J. C., & Bohnert, H. J. (1999). CRASSULACEAN ACID METABOLISM: Molecular genetics. *Annual Review of Plant Physiology and Plant Molecular Biology*, *50*(1), 305–332.

Deng, G., Zhou, L., Wang, Y., Zhang, G., & Chen, X. (2020). Hydrogen sulfide acts downstream of jasmonic acid to inhibit stomatal development in Arabidopsis. *Planta*, *251*(2), 42.

Dever, L. V., Boxall, S. F., Kneřová, J., & Hartwell, J. (2015). Transgenic perturbation of the decarboxylation phase of Crassulacean acid metabolism alters physiology and metabolism but has only a small effect on growth. *Plant Physiology*, *167*(1), 44–59.

Dewitte, W., Scofield, S., Alcasabas, A. A., Maughan, S. C., Menges, M., Braun, N., Collins, C., Nieuwland, J., Prinsen, E., Sundaresan, V., & Murray, J. A. H. (2007). Arabidopsis CYCD3 D-type cyclins link cell proliferation and endocycles and are rate-limiting for cytokinin responses. *Proceedings of the National Academy of Sciences of the United States of America*, *104*(36), 14537–14542.

Dodd, A. N., Borland, A. M., Haslam, R. P., Griffiths, H., & Maxwell, K. (2002). Crassulacean acid metabolism: plastic, fantastic. *Journal of Experimental Botany*, *53*(369), 569–580.

Dong, J., MacAlister, C. A., & Bergmann, D. C. (2009). BASL controls asymmetric cell division in Arabidopsis. *Cell*, *137*(7), 1320–1330.

Draper, J., Mur, L. A., Jenkins, G., Ghosh-Biswas, G. C., Bablak, P., Hasterok, R., & Routledge, A. P. (2001). Brachypodium distachyon. A new model system for functional genomics in grasses. *Plant Physiology*, *127*(4), 1539–1555.

Duclercq, J., Sangwan-Norreel, B., Catterou, M., & Sangwan, R. S. (2011). De novo shoot organogenesis: from art to science. *Trends in Plant Science*, *16*(11), 597–606.

Eggli, U., & Nyffeler, R. (2009). Living under temporarily arid conditions - succulence as an adaptive strategy. *Bradleya*, *27*(27), 13–36.

Esau, K. (2006). *Anatomy of the Seed Plants, 3rd edition* (R. F. Evert (ed.)). John Wiley & Sons, Inc.

Evert, R. F. (2006). *Esau's Plant Anatomy: Meristems, Cells, and Tissues of the Plant Body: Their Structure, Function, and Development*. John Wiley & Sons.

Fischer-Parton, S., Parton, R. M., Hickey, P. C., Dijksterhuis, J., Atkinson, H. A., & Read, N. D. (2000). Confocal microscopy of FM4-64 as a tool for analysing endocytosis and vesicle trafficking in living fungal hyphae. *Journal of Microscopy*, *198*(3), 246–259.

Franks, P. J., & Farquhar, G. D. (2007). The mechanical diversity of stomata and its significance in gas-exchange control. *Plant Physiology*, *143*(1), 78–87.

Gallagher, K., & Smith, L. G. (2000). Roles for polarity and nuclear determinants in specifying daughter cell fates after an asymmetric cell division in the maize leaf. *Current Biology*, *10*(19), 1229–1232.

Gao, Y., Wu, M., Zhang, M., Jiang, W., Liang, E., Zhang, D., Zhang, C., Xiao, N., & Chen, J. (2018). Roles of a maize phytochrome-interacting factors protein ZmPIF3 in regulation of drought stress responses by controlling stomatal closure in transgenic rice without yield penalty. *Plant Molecular Biology*, *97*(4-5), 311–323.

Garcês, H. M. P., Champagne, C. E. M., Townsley, B. T., Park, S., Malhó, R., Pedroso, M. C., Harada, J. J., & Sinha, N. R. (2007). Evolution of asexual reproduction in leaves of the genus Kalanchoë. *Proceedings of the National Academy of Sciences of the United States of America*, *104*(39), 15578–15583.

Garcês, H. M. P., Koenig, D., Townsley, B. T., Kim, M., & Sinha, N. R. (2014). Truncation of LEAFY COTYLEDON1 protein is required for asexual reproduction in Kalanchoë daigremontiana. *Plant Physiology*, *165*(1), 196–206.

Garcês, H., & Sinha, N. (2009). The "mother of thousands" (*Kalanchoë daigremontiana*): a plant model for asexual reproduction and CAM studies. *Cold Spring Harbor Protocols*, *2009*(10), pdb.emo133.

Geisler, M., Nadeau, J., & Sack, F. D. (2000). Oriented asymmetric divisions that generate the stomatal spacing pattern in arabidopsis are disrupted by the too many mouths mutation. *The Plant Cell*, *12*(11), 2075–2086.

Gong, Y., Dale, R., Fung, H. F., Amador, G. O., Smit, M. E., & Bergmann, D. C.

(2023). A cell size threshold triggers commitment to stomatal fate in *Arabidopsis*. *Science Advances*, *9*(38), eadf3497.

Gray, A., Liu, L., & Facette, M. (2020). Flanking Support: How Subsidiary Cells Contribute to Stomatal Form and Function. *Frontiers in Plant Science*, *11*, 881.

Griffiths, H., Cousins, A. B., Badger, M. R., & von Caemmerer, S. (2007). Discrimination in the dark. Resolving the interplay between metabolic and physical constraints to phosphoenolpyruvate carboxylase activity during the crassulacean acid metabolism cycle. *Plant Physiology*, *143*(2), 1055–1067.

Griffiths, H., & Males, J. (2017). Succulent plants. *Current Biology*, *27*(17), R890–R896.

Gudesblat, G. E., Schneider-Pizoń, J., Betti, C., Mayerhofer, J., Vanhoutte, I., van Dongen, W., Boeren, S., Zhiponova, M., de Vries, S., Jonak, C., & Russinova, E. (2012). SPEECHLESS integrates brassinosteroid and stomata signalling pathways. *Nature Cell Biology*, *14*(5), 548–554.

Hachez, C., Ohashi-Ito, K., Dong, J., & Bergmann, D. C. (2011). Differentiation of Arabidopsis guard cells: analysis of the networks incorporating the basic helix-loop-helix transcription factor, FAMA. *Plant Physiology*, *155*(3), 1458–1472.

Han, S.-K., Herrmann, A., Yang, J., Iwasaki, R., Sakamoto, T., Desvoyes, B., Kimura, S., Gutierrez, C., Kim, E.-D., & Torii, K. U. (2022). Deceleration of the cell cycle underpins a switch from proliferative to terminal divisions in plant stomatal lineage. *Developmental Cell*, *57*(5), 569–582.e6.

Han, S.-K., Qi, X., Sugihara, K., Dang, J. H., Endo, T. A., Miller, K. L., Kim, E.-D., Miura, T., & Torii, K. U. (2018). MUTE Directly Orchestrates Cell-State Switch and the Single Symmetric Division to Create Stomata. *Developmental Cell*, *45*(3), 303–315.e5.

Han, S.-K., & Torii, K. U. (2016). Lineage-specific stem cells, signals and asymmetries during stomatal development. *Development* , *143*(8), 1259–1270.

Han, X., Hu, Y., Zhang, G., Jiang, Y., Chen, X., & Yu, D. (2018). Jasmonate Negatively Regulates Stomatal Development in Arabidopsis Cotyledons. *Plant Physiology*, *176*(4), 2871–2885.

Hara, K., Kajita, R., Torii, K. U., Bergmann, D. C., & Kakimoto, T. (2007). The secretory peptide gene EPF1 enforces the stomatal one-cell-spacing rule. *Genes & Development*, *21*(14), 1720–1725.

Hara, K., Yokoo, T., Kajita, R., Onishi, T., Yahata, S., Peterson, K. M., Torii, K. U., & Kakimoto, T. (2009). Epidermal cell density is autoregulated via a secretory peptide, EPIDERMAL PATTERNING FACTOR 2 in Arabidopsis leaves. *Plant & Cell Physiology*, *50*(6), 1019–1031.

Harrison, E. L., Arce Cubas, L., Gray, J. E., & Hepworth, C. (2019). The influence of stomatal morphology and distribution on photosynthetic gas exchange. *The Plant Journal: For Cell and Molecular Biology*. *101*(4), 768–779.

Hartwell, J. (2007). The circadian clock in CAM plants. In *Endogenous Plant Rhythms* (pp. 211–236). Blackwell Publishing Ltd.

Hartwell, J., Dever, L. V., & Boxall, S. F. (2016). Emerging model systems for functional genomics analysis of Crassulacean acid metabolism. *Current Opinion in Plant Biology*, *31*, 100–108.

Hatfield, J. L., & Dold, C. (2019). Water-Use Efficiency: Advances and Challenges in a Changing Climate. *Frontiers in Plant Science*, *10*, 103.

Haworth, M., Marino, G., Loreto, F., & Centritto, M. (2021). Integrating stomatal physiology and morphology: evolution of stomatal control and development of future crops. *Oecologia*. *197*(4), 867–883.

Heim, M. A., Jakoby, M., Werber, M., Martin, C., Weisshaar, B., & Bailey, P. C. (2003). The basic helix-loop-helix transcription factor family in plants: a genome-wide study of protein structure and functional diversity. *Molecular Biology and Evolution*, *20*(5), 735–747.

Heyduk, K. (2022). Evolution of Crassulacean acid metabolism in response to the environment: past, present, and future. *Plant Physiology*, *190*(1), 19–30.

Horst, R. J., Fujita, H., Lee, J. S., Rychel, A. L., Garrick, J. M., Kawaguchi, M., Peterson, K. M., & Torii, K. U. (2015). Molecular Framework of a Regulatory Circuit Initiating Two-Dimensional Spatial Patterning of Stomatal Lineage. *PLoS Genetics*, *11*(7), e1005374.

Houbaert, A., Zhang, C., Tiwari, M., Wang, K., de Marcos Serrano, A., Savatin, D. V., Urs, M. J., Zhiponova, M. K., Gudesblat, G. E., Vanhoutte, I., Eeckhout, D., Boeren, S., Karimi, M., Betti, C., Jacobs, T., Fenoll, C., Mena, M., de Vries, S., De Jaeger, G., & Russinova, E. (2018). POLAR-guided signalling complex assembly and localization drive asymmetric cell division. *Nature*, *563*(7732), 574–578.

Hronková, M., Wiesnerová, D., Šimková, M., Skůpa, P., Dewitte, W., Vráblová, M.,

Zažímalová, E., & Šantrůček, J. (2015). Light-induced STOMAGEN-mediated stomatal development in Arabidopsis leaves. *Journal of Experimental Botany*, *66*(15), 4621–4630.

Hughes, J., Hepworth, C., Dutton, C., Dunn, J. A., Hunt, L., Stephens, J., Waugh, R., Cameron, D. D., & Gray, J. E. (2017). Reducing Stomatal Density in Barley Improves Drought Tolerance without Impacting on Yield. *Plant Physiology*, *174*(2), 776–787.

Hunt, L., & Gray, J. E. (2009). The signaling peptide EPF2 controls asymmetric cell divisions during stomatal development. *Current Biology: CB*, *19*(10), 864–869.

Huq, E., Al-Sady, B., Hudson, M., Kim, C., Apel, K., & Quail, P. H. (2004). Phytochrome-interacting factor 1 is a critical bHLH regulator of chlorophyll biosynthesis. *Science*, *305*(5692), 1937–1941.

Ikeuchi, M., Favero, D. S., Sakamoto, Y., Iwase, A., Coleman, D., Rymen, B., & Sugimoto, K. (2019). Molecular mechanisms of plant regeneration. *Annual Review of Plant Biology*, *70*(1), 377–406.

Jewer, P. C., Incoll, L. D., & Howarth, G. L. (1981). Stomatal responses in isolated epidermis of the crassulacean acid metabolism plant Kalanchoe daigremontiana Hamet et Perr. *Planta*, *153*(3), 238–245.

Jezek, M., & Blatt, M. R. (2017). The Membrane Transport System of the Guard Cell and Its Integration for Stomatal Dynamics. *Plant Physiology*, *174*(2), 487–519.

Kamle, M., Bajpai, A., Chandra, R., Kalim, S., & Kumar, R. (2011). Somatic embryogenesis for crop improvement. *GERF Bull Biosci*, *2*(1), 54–59.

Kanaoka, M. M., Pillitteri, L. J., Fujii, H., Yoshida, Y., Bogenschutz, N. L., Takabayashi, J., Zhu, J.-K., & Torii, K. U. (2008). SCREAM/ICE1 and SCREAM2 specify three cell-state transitional steps leading to arabidopsis stomatal differentiation. *The Plant Cell*, *20*(7), 1775–1785.

Kang, C.-Y., Lian, H.-L., Wang, F.-F., Huang, J.-R., & Yang, H.-Q. (2009). Cryptochromes, phytochromes, and COP1 regulate light-controlled stomatal development in Arabidopsis. *The Plant Cell*, *21*(9), 2624–2641.

Kellogg, E. A. (2015). Brachypodium distachyon as a Genetic Model System. *Annual Review of Genetics*, *49*, 1–20.

Khan, F., Yousaf, Z., Ahmed, H., Arif, A., Rehman, H., Younas, A., Rashid, M., Tariq, Z., & Raiz, N. (2014). Stomatal patterning: An important taxonomic tool for systematical studies of tree species of angiosperm. *Annual Research & Review*

in Biology, *4*(24), 4034–4053.

Khan, M., Rozhon, W., Bigeard, J., Pflieger, D., Husar, S., Pitzschke, A., Teige, M., Jonak, C., Hirt, H., & Poppenberger, B. (2013). Brassinosteroid-regulated GSK3/Shaggy-like kinases phosphorylate mitogen-activated protein (MAP) kinase kinases, which control stomata development in Arabidopsis thaliana. *The Journal of Biological Chemistry*, *288*(11), 7519–7527.

Kim, E.-D., Dorrity, M. W., Fitzgerald, B. A., Seo, H., Sepuru, K. M., Queitsch, C., Mitsuda, N., Han, S.-K., & Torii, K. U. (2022). Dynamic chromatin accessibility deploys heterotypic cis/trans-acting factors driving stomatal cell-fate commitment. *Nature Plants*, *8*(12), 1453–1466.

Kim, E.-D., & Torii, K. U. (2024). Stomatal cell fate commitment via transcriptional and epigenetic control: Timing is crucial. *Plant, Cell & Environment*, *47*(9), 3288–3298.

Kim, E.-J., Zhang, C., Guo, B., Eekhout, T., Houbaert, A., Wendrich, J. R., Vandamme, N., Tiwari, M., Simon-Vezo, C., Vanhoutte, I., Saeys, Y., Wang, K., Zhu, Y., De Rybel, B., & Russinova, E. (2023). Cell type-specific attenuation of brassinosteroid signaling precedes stomatal asymmetric cell division. *Proceedings of the National Academy of Sciences of the United States of America*, *120*(36), e2303758120.

Kim, T.-W., Michniewicz, M., Bergmann, D. C., & Wang, Z.-Y. (2012). Brassinosteroid regulates stomatal development by GSK3-mediated inhibition of a MAPK pathway. *Nature*, *482*(7385), 419–422.

Kim, T.-W., & Wang, Z.-Y. (2010). Brassinosteroid signal transduction from receptor kinases to transcription factors. *Annual Review of Plant Biology*, *61*(1), 681–704.

Klermund, C., Ranftl, Q. L., Diener, J., Bastakis, E., Richter, R., & Schwechheimer, C. (2016). LLM-domain B-GATA transcription factors promote stomatal development downstream of light signaling pathways in Arabidopsis thaliana hypocotyls. *The Plant Cell*, *28*(3), 646–660.

Kluge, M., Brulfert, J., Ravelomanana, D., Lipp, J., & Ziegler, H. (1991). Crassulacean acid metabolism in Kalanchoë species collected in various climatic zones of Madagascar: a survey by δ13C analysis. *Oecologia*, *88*(3), 407–414.

Koornneef, M., & Meinke, D. (2010). The development of Arabidopsis as a model plant. *The Plant Journal: For Cell and Molecular Biology*, *61*(6), 909–921.

Krämer, U. (2015). Planting molecular functions in an ecological context with *Arabidopsis thaliana*. *eLife*, *4*, e06100.

Kumari, A., Jewaria, P. K., Bergmann, D. C., & Kakimoto, T. (2014). Arabidopsis reduces growth under osmotic stress by decreasing SPEECHLESS protein. *Plant & Cell Physiology*, *55*(12), 2037–2046.

Lai, L. B., Nadeau, J. A., Lucas, J., Lee, E.-K., Nakagawa, T., Zhao, L., Geisler, M., & Sack, F. D. (2005). The Arabidopsis R2R3 MYB proteins FOUR LIPS and MYB88 restrict divisions late in the stomatal cell lineage. *The Plant Cell*, *17*(10), 2754–2767.

Lampard, G. R., & Bergmann, D. C. (2007). A shout-out to stomatal development: How the bHLH proteins SPEECHLESS, MUTE and FAMA regulate cell division and cell fate. *Plant Signaling & Behavior*, *2*(4), 290–292.

Lampard, G. R., Lukowitz, W., Ellis, B. E., & Bergmann, D. C. (2009). Novel and expanded roles for MAPK signaling in Arabidopsis stomatal cell fate revealed by cell type-specific manipulations. *The Plant Cell*, *21*(11), 3506–3517.

Lampard, G. R., Macalister, C. A., & Bergmann, D. C. (2008). Arabidopsis stomatal initiation is controlled by MAPK-mediated regulation of the bHLH SPEECHLESS. *Science*, *322*(5904), 1113–1116.

Lampropoulos, A., Sutikovic, Z., Wenzl, C., Maegele, I., Lohmann, J. U., & Forner, J. (2013). GreenGate---a novel, versatile, and efficient cloning system for plant transgenesis. *PloS One*, *8*(12), e83043.

Lange, O. L., & Medina, E. (1979). Stomata of the CAM plant Tillandsia recurvata respond directly to humidity. *Oecologia*, *40*(3), 357–363.

Lau, O. S., & Bergmann, D. C. (2012). Stomatal development: a plant's perspective on cell polarity, cell fate transitions and intercellular communication. *Development* , *139*(20), 3683–3692.

Lau, O. S., Davies, K. A., Chang, J., Adrian, J., Rowe, M. H., Ballenger, C. E., & Bergmann, D. C. (2014). Direct roles of SPEECHLESS in the specification of stomatal self-renewing cells. *Science*, *345*(6204), 1605–1609.

Lau, O. S., Song, Z., Zhou, Z., Davies, K. A., Chang, J., Yang, X., Wang, S., Lucyshyn, D., Tay, I. H. Z., Wigge, P. A., & Bergmann, D. C. (2018). Direct Control of SPEECHLESS by PIF4 in the High-Temperature Response of Stomatal Development. *Current Biology*, *28*(8), 1273–1280.e3.

Lawson, T., & Blatt, M. R. (2014). Stomatal size, speed, and responsiveness impact

on photosynthesis and water use efficiency. *Plant Physiology*, *164*(4), 1556–1570.

Lee, E., Lucas, J. R., & Sack, F. D. (2014). Deep functional redundancy between FAMA and FOUR LIPS in stomatal development. *The Plant Journal: For Cell and Molecular Biology*, *78*(4), 555–565.

Lee, J.-H., Jung, J.-H., & Park, C.-M. (2017). Light Inhibits COP1-Mediated Degradation of ICE Transcription Factors to Induce Stomatal Development in Arabidopsis. *The Plant Cell*, *29*(11), 2817–2830.

Lee, J. S. (2010). Stomatal Opening Mechanism of CAM Plants. *Journal of Plant Biology = Singmul Hakhoe Chi*, *53*(1), 19–23.

Lee, J. S., Hnilova, M., Maes, M., Lin, Y.-C. L., Putarjunan, A., Han, S.-K., Avila, J., & Torii, K. U. (2015). Competitive binding of antagonistic peptides fine-tunes stomatal patterning. *Nature*, *522*(7557), 439–443.

Lee, J. S., Kuroha, T., Hnilova, M., Khatayevich, D., Kanaoka, M. M., McAbee, J. M., Sarikaya, M., Tamerler, C., & Torii, K. U. (2012). Direct interaction of ligand-receptor pairs specifying stomatal patterning. *Genes & Development*, *26*(2), 126–136.

Le, J., Liu, X.-G., Yang, K.-Z., Chen, X.-L., Zou, J.-J., Wang, H.-Z., Wang, M., Vanneste, S., Morita, M., Tasaka, M., Ding, Z.-J., Friml, J., Beeckman, T., & Sack, F. (2014). Auxin transport and activity regulate stomatal patterning and development. *Nature Communications*, *5*, 3090.

Leprince, O., Pellizzaro, A., Berriri, S., & Buitink, J. (2017). Late seed maturation: drying without dying. *Journal of Experimental Botany*, *68*(4), 827–841.

Li, J., Kong, D., Ke, Y., Zeng, W., & Miki, D. (2024). Application of multiple sgRNAs boosts efficiency of CRISPR/Cas9-mediated gene targeting in Arabidopsis. *BMC Biology*, *22*(1), 6.

Lima, J. F., Leite, K. R. B., Clark, L. G., & de Oliveira, R. P. (2019). Leaf micromorphology in Poaceae subtribe Olyrinae (Bambusoideae) and its systematic implications. *Botanical Journal of the Linnean Society. Linnean Society of London*, *192*(1), 184–207.

Lind, C., Dreyer, I., López-Sanjurjo, E. J., von Meyer, K., Ishizaki, K., Kohchi, T., Lang, D., Zhao, Y., Kreuzer, I., Al-Rasheid, K. A. S., Ronne, H., Reski, R., Zhu, J.-K., Geiger, D., & Hedrich, R. (2015). Stomatal guard cells co-opted an ancient ABA-dependent desiccation survival system to regulate stomatal closure.

Current Biology, *25*(7), 928–935.

Lindner, H., Kessler, S. A., Müller, L. M., Shimosato-Asano, H., Boisson-Dernier, A., & Grossniklaus, U. (2015). TURAN and EVAN mediate pollen tube reception in Arabidopsis Synergids through protein glycosylation. *PLoS Biology*, *13*(4), e1002139.

Li, Q.-H., & Yang, H.-Q. (2007). Cryptochrome signaling in plants. *Photochemistry and Photobiology*, *83*(1), 94–101.

Li, S., Yan, J., Chen, L.-G., Meng, G., Zhou, Y., Wang, C.-M., Jiang, L., Luo, J., Jiang, Y., Li, Q.-F., Tang, W., & He, J.-X. (2024). Brassinosteroid regulates stomatal development in etiolated Arabidopsis cotyledons via transcription factors BZR1 and BES1. *Plant Physiology*, *195*(2), 1382–1400.

Liu, D., Chen, M., Mendoza, B., Cheng, H., Hu, R., Li, L., Trinh, C. T., Tuskan, G. A., & Yang, X. (2019). CRISPR/Cas9-mediated targeted mutagenesis for functional genomics research of crassulacean acid metabolism plants. *Journal of Experimental Botany*, *70*(22), 6621–6629.

Liu, T., Ohashi-Ito, K., & Bergmann, D. C. (2009). Orthologs of *Arabidopsis thaliana* stomatal bHLH genes and regulation of stomatal development in grasses. *Development* , *136*(13), 2265–2276.

Love, M. I., Huber, W., & Anders, S. (2014). Moderated estimation of fold change and dispersion for RNA-seq data with DESeq2. *Genome Biology*, *15*(12), 550.

Lucas, J. R., Nadeau, J. A., & Sack, F. D. (2006). Microtubule arrays and Arabidopsis stomatal development. *Journal of Experimental Botany*, *57*(1), 71–79.

Lu, J., He, J., Zhou, X., Zhong, J., Li, J., & Liang, Y.-K. (2019). Homologous genes of epidermal patterning factor regulate stomatal development in rice. *Journal of Plant Physiology*, *234-235*, 18–27.

Lundgren, M. R., Mathers, A., Baillie, A. L., Dunn, J., Wilson, M. J., Hunt, L., Pajor, R., Fradera-Soler, M., Rolfe, S., Osborne, C. P., Sturrock, C. J., Gray, J. E., Mooney, S. J., & Fleming, A. J. (2019). Mesophyll porosity is modulated by the presence of functional stomata. *Nature Communications*, *10*(1), 2825.

Lupanga, U., Röhrich, R., Askani, J., Hilmer, S., Kiefer, C., Krebs, M., Kanazawa, T., Ueda, T., & Schumacher, K. (2020). The Arabidopsis V-ATPase is localized to the TGN/EE via a seed plant-specific motif. *eLife*, *9*, e60568.

Lüttge, U. (2004). Ecophysiology of crassulacean Acid Metabolism (CAM). *Annals of*

Botany, *93*(6), 629–652.

MacAlister, C. A., & Bergmann, D. C. (2011). Sequence and function of basic helix-loop-helix proteins required for stomatal development in Arabidopsis are deeply conserved in land plants. *Evolution & Development*, *13*(2), 182–192.

MacAlister, C. A., Ohashi-Ito, K., & Bergmann, D. C. (2007). Transcription factor control of asymmetric cell divisions that establish the stomatal lineage. *Nature*, *445*(7127), 537–540.

Mahoney, A. K., Anderson, E. M., Bakker, R. A., Williams, A. F., Flood, J. J., Sullivan, K. C., & Pillitteri, L. J. (2016). Functional analysis of the Arabidopsis thaliana MUTE promoter reveals a regulatory region sufficient for stomatal-lineage expression. *Planta*, *243*(4), 1–12.

Males, J., & Griffiths, H. (2017). Stomatal Biology of CAM Plants. *Plant Physiology*, *174*(2), 550–560.

McAusland, L., Vialet-Chabrand, S., Davey, P., Baker, N. R., Brendel, O., & Lawson, T. (2016). Effects of kinetics of light-induced stomatal responses on photosynthesis and water-use efficiency. *The New Phytologist*, *211*(4), 1209–1220.

McKown, K. H., Anleu Gil, M. X., Mair, A., Xu, S.-L., Raissig, M. T., & Bergmann, D. C. (2023). Expanded roles and divergent regulation of FAMA in Brachypodium and Arabidopsis stomatal development. *The Plant Cell*, *35*(2), 756–775.

McKown, K. H., & Bergmann, D. C. (2018). Grass stomata. *Current Biology*, *28*(15), R814–R816.

Meinke, D. W., Cherry, J. M., Dean, C., Rounsley, S. D., & Koornneef, M. (1998). Arabidopsis thaliana: a model plant for genome analysis. *Science*, *282*(5389), 662, 679–682.

Meng, X., Chen, X., Mang, H., Liu, C., Yu, X., Gao, X., Torii, K. U., He, P., & Shan, L. (2015). Differential Function of Arabidopsis SERK Family Receptor-like Kinases in Stomatal Patterning. *Current Biology*, *25*(18), 2361–2372.

Meyerowitz, E. M. (2001). Prehistory and history of Arabidopsis research. *Plant Physiology*, *125*(1), 15–19.

Moseley, R. C., Tuskan, G. A., & Yang, X. (2019). Comparative Genomics Analysis Provides New Insight Into Molecular Basis of Stomatal Movement in Kalanchoë fedtschenkoi. *Frontiers in Plant Science*, *10*, 292.

Mott, K. A., Gibson, A. C., & O'leary, J. W. (1982). The adaptive significance of

amphistomatic leaves. *Plant, Cell & Environment*, *5*(6), 455–460.

Muroyama, A., Gong, Y., & Bergmann, D. C. (2020). Opposing, Polarity-Driven Nuclear Migrations Underpin Asymmetric Divisions to Pattern Arabidopsis Stomata. *Current Biology*, 4467–4475.e4.

Muroyama, A., Gong, Y., Hartman, K. S., & Bergmann, D. C. (2023). Cortical polarity ensures its own asymmetric inheritance in the stomatal lineage to pattern the leaf surface. *Science*, *381*(6653), 54–59.

Nadeau, J. A., & Sack, F. D. (2002a). Control of stomatal distribution on the Arabidopsis leaf surface. *Science*, *296*(5573), 1697–1700.

Nadeau, J. A., & Sack, F. D. (2002b). Stomatal development in Arabidopsis. *The Arabidopsis Book / American Society of Plant Biologists*, *1*, e0066.

Ni, M., Tepperman, J. M., & Quail, P. H. (1999). Binding of phytochrome B to its nuclear signalling partner PIF3 is reversibly induced by light. *Nature*, *400*(6746), 781–784.

Nunes, T. D. G., Zhang, D., & Raissig, M. T. (2020). Form, development and function of grass stomata. *The Plant Journal: For Cell and Molecular Biology*, *101*(4), 780–799.

O'Brien, T. P., Feder, N., & McCully, M. E. (1964). Polychromatic staining of plant cell walls by toluidine blue O. *Protoplasma*, *59*(2), 368–373.

Ochatt, S. J., & Sangwan, R. S. (2008). In vitro shortening of generation time in Arabidopsis thaliana. *Plant Cell, Tissue and Organ Culture*, *93*(2), 133–137.

Ogburn, R. M., & Edwards, E. J. (2009). Anatomical variation in Cactaceae and relatives: Trait lability and evolutionary innovation. *American Journal of Botany*, *96*(2), 391–408.

Ohashi-Ito, K., & Bergmann, D. C. (2006). Arabidopsis FAMA controls the final proliferation/differentiation switch during stomatal development. *The Plant Cell*, *18*(10), 2493–2505.

Ohki, S., Takeuchi, M., & Mori, M. (2011). The NMR structure of stomagen reveals the basis of stomatal density regulation by plant peptide hormones. *Nature Communications*, *2*, 512.

Ortega, A., de Marcos, A., Illescas-Miranda, J., Mena, M., & Fenoll, C. (2019). The Tomato Genome Encodes SPCH, MUTE, and FAMA Candidates That Can Replace the Endogenous Functions of Their Arabidopsis Orthologs. Frontiers in plant science, 10, 1300.

Pant, D. D. (1965). On the Ontogeny of Stomata and Other Homologous Structures. *Plant Sci. Ser.*, *1*, 1024.

Parkhurst, D. F. (1978). The adaptive significance of stomatal occurrence on one or both surfaces of leaves. *The Journal of Ecology*, *66*(2), 367.

Patel, J. D., Raju, E. C., Fotedar, R. L., Kothari, I. L., & Shah, J. J. (1975). Structure and histochemistry of stomata and epidermal cells in five species of Polypodiaceae. *Annals of Botany*, *39*(3), 611–619.

Pemadasa, M. A. (1979). Movements of abaxial and adaxial stomata. *The New Phytologist*, *82*(1), 69–80.

Pérez-López, A. V., Lim, S. D., & Cushman, J. C. (2023). Tissue succulence in plants: Carrying water for climate change. *Journal of Plant Physiology*, *289*(154081), 154081.

Perveen, A., Abid, R., & Fatima, R. (2008). Stomatal types of some dicots within flora of Karachi , Pakistan. *Pakistan Journal of Botany*. *39*(4): 1017-1023.

Peterson, K. M., Rychel, A. L., & Torii, K. U. (2010). Out of the mouths of plants: the molecular basis of the evolution and diversity of stomatal development. *The Plant Cell*, *22*(2), 296–306.

Piccinini, L., Nirina Ramamonjy, F., & Ursache, R. (2024). Imaging plant cell walls using fluorescent stains: The beauty is in the details. *Journal of microscopy*, *295*(2), 102–120.

Pillitteri, L. J., Bemis, S. M., Shpak, E. D., & Torii, K. U. (2007). Haploinsufficiency after successive loss of signaling reveals a role for ERECTA-family genes in Arabidopsis ovule development. *Development*, *134*(17), 3099–3109.

Pillitteri, L. J., & Dong, J. (2013). Stomatal development in Arabidopsis. *The Arabidopsis Book / American Society of Plant Biologists*, *11*, e0162.

Pillitteri, L. J., Peterson, K. M., Horst, R. J., & Torii, K. U. (2011). Molecular profiling of stomatal meristemoids reveals new component of asymmetric cell division and commonalities among stem cell populations in Arabidopsis. *The Plant Cell*, *23*(9), 3260–3275.

Pillitteri, L. J., Sloan, D. B., Bogenschutz, N. L., & Torii, K. U. (2007). Termination of asymmetric cell division and differentiation of stomata. *Nature*, *445*(7127), 501–505.

Pillitteri, L. J., & Torii, K. U. (2012). Mechanisms of stomatal development. *Annual Review of Plant Biology*, *63*, 591–614.

Pires, N., & Dolan, L. (2010). Origin and diversification of basic-helix-loop-helix proteins in plants. *Molecular Biology and Evolution*, *27*(4), 862–874.

Prabhakar, M. (2004). Structure, Delimitation, Nomenclature and Classification of Stomata. *Acta Botanica Sinica*, *46*(2), 242–252.

Qi, X., Han, S.-K., Dang, J. H., Garrick, J. M., Ito, M., Hofstetter, A. K., & Torii, K. U. (2017). Autocrine regulation of stomatal differentiation potential by EPF1 and ERECTA-LIKE1 ligand-receptor signaling. *eLife*, *6*, 447.

Qi, X., & Torii, K. U. (2018). Hormonal and environmental signals guiding stomatal development. *BMC Biology*, *16*(1), 21.

Raissig, M. T., Abrash, E., Bettadapur, A., Vogel, J. P., & Bergmann, D. C. (2016). Grasses use an alternatively wired bHLH transcription factor network to establish stomatal identity. *Proceedings of the National Academy of Sciences of the United States of America*, *113*(29), 8326–8331.

Raissig, M. T., Matos, J. L., Anleu Gil, M. X., Kornfeld, A., Bettadapur, A., Abrash, E., Allison, H. R., Badgley, G., Vogel, J. P., Berry, J. A., & Bergmann, D. C. (2017). Mobile MUTE specifies subsidiary cells to build physiologically improved grass stomata. *Science*, *355*(6330), 1215–1218.

Raissig, M. T., & Woods, D. P. (2022). The wild grass *Brachypodium distachyon* as a developmental model system. *Current topics in developmental biology*, *147*, 33–71.

Raitskin, O., & Patron, N. J. (2016). Multi-gene engineering in plants with RNA-guided Cas9 nuclease. *Current Opinion in Biotechnology*, *37*, 69–75.

Ran, J.-H., Shen, T.-T., Liu, W.-J., & Wang, X.-Q. (2013). Evolution of the bHLH genes involved in stomatal development: implications for the expansion of developmental complexity of stomata in land plants. *PloS One*, *8*(11), e78997.

Raschke, K., & Fellows, M. P. (1971). Stomatal movement in Zea mays: Shuttle of potassium and chloride between guard cells and subsidiary cells. *Planta*, *101*(4), 296–316.

Redkar, A., Jaeger, E., & Doehlemann, G. (2018). Visualization of growth and morphology of fungal hyphae in planta using WGA-AF488 and propidium iodide co-staining. *Bio-Protocol*, *8*.

Rhee, S. Y., Beavis, W., Berardini, T. Z., Chen, G., Dixon, D., Doyle, A., Garcia-Hernandez, M., Huala, E., Lander, G., Montoya, M., Miller, N., Mueller, L. A., Mundodi, S., Reiser, L., Tacklind, J., Weems, D. C., Wu, Y., Xu, I., Yoo, D., …

Zhang, P. (2003). The Arabidopsis Information Resource (TAIR): a model organism database providing a centralized, curated gateway to Arabidopsis biology, research materials and community. *Nucleic Acids Research*, *31*(1), 224–228.

Richter, R., Behringer, C., Müller, I. K., & Schwechheimer, C. (2010). The GATA-type transcription factors GNC and GNL/CGA1 repress gibberellin signaling downstream from DELLA proteins and PHYTOCHROME-INTERACTING FACTORS. *Genes & Development*, *24*(18), 2093–2104.

Rout, G. R., Debata, B. K., & Das, P. (1991). Somatic embryogenesis in callus cultures of Rosa hybrida L. cv. Landora. *Plant Cell, Tissue and Organ Culture*, *27*(1), 65–69.

Rowe, M. H., Dong, J., Weimer, A. K., & Bergmann, D. C. (2019). A Plant-Specific Polarity Module Establishes Cell Fate Asymmetry in the Arabidopsis Stomatal Lineage. In *bioRxiv* (p. 614636). https://doi.org/10.1101/614636

Rudall, P. J., Hilton, J., & Bateman, R. M. (2013). Several developmental and morphogenetic factors govern the evolution of stomatal patterning in land plants. *The New Phytologist*, *200*(3), 598–614.

Sage, R. F., Gilman, I. S., Smith, J. A. C., Silvera, K., & Edwards, E. J. (2023). Atmospheric CO2 decline and the timing of CAM plant evolution. *Annals of Botany*, *132*(4), 753–770.

Saibo, N. J. M., Vriezen, W. H., Beemster, G. T. S., & Van Der Straeten, D. (2003). Growth and stomata development of Arabidopsis hypocotyls are controlled by gibberellins and modulated by ethylene and auxins. *The Plant Journal*, *33*(6), 989–1000.

Samakovli, D., Tichá, T., Vavrdová, T., Ovečka, M., Luptovčiak, I., Zapletalová, V., Kuchařová, A., Křenek, P., Krasylenko, Y., Margaritopoulou, T., Roka, L., Milioni, D., Komis, G., Hatzopoulos, P., & Šamaj, J. (2020). YODA-HSP90 module regulates phosphorylation-dependent inactivation of SPEECHLESS to control stomatal development under acute heat stress in Arabidopsis. *Molecular Plant*, *13*(4), 612–633.

Schlereth, A., Möller, B., Liu, W., Kientz, M., Flipse, J., Rademacher, E. H., Schmid, M., Jürgens, G., & Weijers, D. (2010). MONOPTEROS controls embryonic root initiation by regulating a mobile transcription factor. *Nature*, *464*(7290), 913–916.

Scholthof, K.-B. G., Irigoyen, S., Catalan, P., & Mandadi, K. K. (2018).

Brachypodium: A Monocot Grass Model Genus for Plant Biology. *The Plant Cell*, *30*(8), 1673–1694.

Serna, L. (2020). The Role of Grass MUTE Orthologues During Stomatal Development. *Frontiers in Plant Science*, *11*, 55.

Serna, L., & Fenoll, C. (1996). Ethylene induces stomata differentiation in Arabidopsis. *The International Journal of Developmental Biology*, *Suppl 1*, 123S – 124S.

Sharma, N. (2017). Leaf clearing protocol to observe stomata and other cells on leaf surface. *Bio-Protocol*, *7*(17).

Shpak, E. D., McAbee, J. M., Pillitteri, L. J., & Torii, K. U. (2005). Stomatal patterning and differentiation by synergistic interactions of receptor kinases. *Science*, *309*(5732), 290–293.

Simmons, A. R., Davies, K. A., Wang, W., Liu, Z., & Bergmann, D. C. (2019). SOL1 and SOL2 regulate fate transition and cell divisions in the Arabidopsis stomatal lineage. *Development* , *146*(3), dev171066.

Soulhat, C., Wehbi, H., Fierlej, Y., Berquin, P., Girin, T., Hilson, P., & Bouchabké-Coussa, O. (2023). Fast-track transformation and genome editing in Brachypodium distachyon. *Plant Methods*, *19*(1), 31.

Spalding, M. H., Stumpf, D. K., Ku, M. S. B., Burris, R. H., & Edwards, G. E. (1979). Crassulacean acid metabolism and diurnal variations of internal CO_2 and O_2 concentrations in Sedum praealtum DC. *Functional Plant Biology: FPB*, *6*(4), 557.

Sparkes, I., Runions, J., Kearns, A., & Hawes, C. (2006). Rapid, transient expression of fluorescent fusion proteins in tobacco plants and generation of stably transformed plants. *Nature Protocols*, *1*, 2019–2025.

Spiegelhalder, R. P., Berg, L. S., Nunes, T. D. G., Dörr, M., Jesenofsky, B., Lindner, H., & Raissig, M. T. (2024). Dual role of BdMUTE during stomatal development in the model grass Brachypodium distachyon. *Development*, *151*(20), dev.203011.

Spiegelhalder, R. P., & Raissig, M. T. (2021). Morphology made for movement: formation of diverse stomatal guard cells. *Current Opinion in Plant Biology*, *63*, 102090.

Stebbins, G. L., & Shah, S. S. (1960). Developmental Studies of Cell Differentiation in the Epidermis of Monocotyledons. II. Cytological Features of Stomatal

Development in the Gramineae. *Developmental Biology*, *2*, 477–500.

Stubblefield, S., & Banks, H. P. (1978). The cuticle of Drepanophycus spinaeformis, a long‐ranging Devonian lycopod from New York and eastern Canada. *American Journal of Botany*, *65*(1), 110–118.

Sun, T.-X., Edwards, D., & Li, C.-S. (2005). The stomatal apparatus of Lycopodium japonicum and its bearing on the stomata of the Devonian lycophyte Drepanophycus spinaeformis. *Botanical Journal of the Linnean Society. Linnean Society of London*, *149*(2), 209–216.

Takata, N., Yokota, K., Ohki, S., Mori, M., Taniguchi, T., & Kurita, M. (2013). Evolutionary relationship and structural characterization of the EPF/EPFL gene family. *PloS One*, *8*(6), e65183.

Tallman, G., Zhu, J., Mawson, B. T., Amodeo, G., Nouhi, Z., Levy, K., & Zeiger, E. (1997). Induction of CAM in Mesembryanthemum crystallinum abolishes the stomatal response to blue light and light-dependent zeaxanthin formation in guard cell chloroplasts. *Plant & Cell Physiology*, *38*(3), 236–242.

Tameshige, T., Ikematsu, S., Torii, K. U., & Uchida, N. (2017). Stem development through vascular tissues: EPFL–ERECTA family signaling that bounces in and out of phloem. *Journal of Experimental Botany*, *68*(1), 45–53.

Tanaka, Y., Nose, T., Jikumaru, Y., & Kamiya, Y. (2013). ABA inhibits entry into stomatal-lineage development in Arabidopsis leaves. *The Plant Journal: For Cell and Molecular Biology*, *74*(3), 448–457.

Taylor, S. H., Franks, P. J., Hulme, S. P., Spriggs, E., Christin, P. A., Edwards, E. J., Woodward, F. I., & Osborne, C. P. (2012). Photosynthetic pathway and ecological adaptation explain stomatal trait diversity amongst grasses. *The New Phytologist*, *193*(2), 387–396.

Toledo-Ortiz, G., Huq, E., & Quail, P. H. (2003). The Arabidopsis basic/helix-loop-helix transcription factor family. *The Plant Cell*, *15*(8), 1749–1770.

Torii, K. U. (2012). Mix-and-match: ligand-receptor pairs in stomatal development and beyond. *Trends in Plant Science*, *17*(12), 711–719.

Torii, K. U. (2021). Stomatal development in the context of epidermal tissues. *Annals of Botany*, *128*(2), 137–148.

Ursache, R., Andersen, T. G., Marhavý, P., & Geldner, N. (2018). A protocol for combining fluorescent proteins with histological stains for diverse cell wall

components. *The Plant Journal: For Cell and Molecular Biology*, *93*(2), 399–412.

Van Cotthem, W. (1973). The classification of morphological and ontogenetic types of stomata. *The Botanical Review; Interpreting Botanical Progress*, *3*.

Vargas, A., Herrera, I., Nualart, N., Guézou, A., Gómez-Bellver, C., Freire, E., Jaramillo Díaz, P., & López-Pujol, J. (2022). The genus Kalanchoe (crassulaceae) in Ecuador: From gardens to the wild. *Plants*, *11*(13), 1746.

Vatén, A., Soyars, C. L., Tarr, P. T., Nimchuk, Z. L., & Bergmann, D. C. (2018). Modulation of Asymmetric Division Diversity through Cytokinin and SPEECHLESS Regulatory Interactions in the Arabidopsis Stomatal Lineage. *Developmental Cell*, *47*(1), 53–66.e5.

Vera-Estrella, R., Barkla, B. J., Amezcua-Romero, J. C., & Pantoja, O. (2012). Day/night regulation of aquaporins during the CAM cycle in Mesembryanthemum crystallinum. *Plant, Cell & Environment*, *35*(3), 485–501.

Veselý, P., Šmarda, P., Bureš, P., Stirton, C., Muasya, A. M., Mucina, L., Horová, L., Veselá, K., Šilerová, A., Šmerda, J., & Knápek, O. (2020). Environmental pressures on stomatal size may drive plant genome size evolution: evidence from a natural experiment with Cape geophytes. *Annals of Botany*, *126*(2), 323–330.

von Caemmerer, S., & Griffiths, H. (2009). Stomatal responses to CO_2 during a diel Crassulacean acid metabolism cycle in Kalanchoe daigremontiana and Kalanchoe pinnata. *Plant, Cell & Environment*, *32*(5), 567–576.

Von Groll, U., Berger, D., & Altmann, T. (2002). The subtilisin-like serine protease SDD1 mediates cell-to-cell signaling during Arabidopsis stomatal development. *The Plant Cell*, *14*(7), 1527–1539.

Voznesenskaya, E. V., Koteyeva, N. K., Edwards, G. E., & Ocampo, G. (2010). Revealing diversity in structural and biochemical forms of C4 photosynthesis and a C3–C4 intermediate in genus Portulaca L. (Portulacaceae). *Journal of Experimental Botany*, *61*(13), 3647–3662.

Wallner, E.-S., Dolan, L., & Bergmann, D. C. (2023). Arabidopsis stomatal lineage cells establish bipolarity and segregate differential signaling capacity to regulate stem cell potential. *Developmental Cell*, *58*(18), 1643–1656.e5.

Wall, S., Vialet-Chabrand, S., Davey, P., Van Rie, J., Galle, A., Cockram, J., & Lawson, T. (2022). Stomata on the abaxial and adaxial leaf surface contribute

differently to leaf gas exchange and photosynthesis in wheat. *The New Phytologist*, *235*(5), 1743–1756.

Wang, H., Guo, S., Qiao, X., Guo, J., Li, Z., Zhou, Y., Bai, S., Gao, Z., Wang, D., Wang, P., Galbraith, D. W., & Song, C.-P. (2019). BZU2/ZmMUTE controls symmetrical division of guard mother cell and specifies neighbor cell fate in maize. *PLoS Genetics*, *15*(8), e1008377.

Wang, H., Ngwenyama, N., Liu, Y., Walker, J. C., & Zhang, S. (2007). Stomatal development and patterning are regulated by environmentally responsive mitogen-activated protein kinases in Arabidopsis. *The Plant Cell*, *19*(1), 63–73.

Wang, L., Zhou, C.-M., Mai, Y.-X., Li, L.-Z., Gao, J., Shang, G.-D., Lian, H., Han, L., Zhang, T.-Q., Tang, H.-B., Ren, H., Wang, F.-X., Wu, L.-Y., Liu, X.-L., Wang, C.-S., Chen, E.-W., Zhang, X.-N., Liu, C., & Wang, J.-W. (2019). A spatiotemporally regulated transcriptional complex underlies heteroblastic development of leaf hairs in *Arabidopsis thaliana*. *The EMBO Journal*, *38*(8), e100063.

Wang, S., Zhou, Z., Rahiman, R., Lee, G. S. Y., Yeo, Y. K., Yang, X., & Lau, O. S. (2021). Light regulates stomatal development by modulating paracrine signaling from inner tissues. *Nature Communications*, *12*(1), 3403.

Wang, X., Chen, X., Cheng, Q., Zhu, K., Yang, X., & Cheng, Z. (2019). Agrobacterium–mediated Transformation of *Kalanchoe laxiflora*. *Horticultural Plant Journal*, *5* (5): 221–228.

Weng, X., Zhu, L., Yu, S., Liu, Y., Ru, Y., Zhang, Z., He, Z., Zhou, L., & Chen, X. (2022). Carbon monoxide promotes stomatal initiation by regulating the expression of two EPF genes in Arabidopsis cotyledons. *Frontiers in Plant Science*, *13*, 1029703.

Willert, D. J., Eller, B. M., Werger, M. J. A., & Brinckmann, E. (1990). Desert succulents and their life strategies. *Vegetatio*, *90*(2), 133–143.

Willmer, C., Fricker, M. (1996). The mechanics of stomatal movements. In: Stomata. Springer, Dordrecht.

Winter, K. (2019). Ecophysiology of constitutive and facultative CAM photosynthesis. *Journal of Experimental Botany*, *70*(22), 6495–6508.

Winter, K., & Smith, J. A. C. (1996). An Introduction to Crassulacean Acid Metabolism. Biochemical Principles and Ecological Diversity. In: Winter, K., Smith, J.A.C. (eds) Crassulacean Acid Metabolism. Ecological Studies, vol 114.

Springer, Berlin, Heidelberg.

Woodward, F. I. (1987). Stomatal numbers are sensitive to increases in CO2 from pre-industrial levels. *Nature*, *327*, 617.

Wu, Z., Chen, L., Yu, Q., Zhou, W., Gou, X., Li, J., & Hou, S. (2019). Multiple transcriptional factors control stomata development in rice. *The New Phytologist*, *223*(1), 220–232.

Wyka, T. P., Duarte, H. M., & Lüttge, U. E. (2005). Redundancy of Stomatal Control for the Circadian Photosynthetic Rhythm in *Kalanchoë daigremontiana* Hamet et Perrier. *Plant Biology*, *7*(2), 176–181.

Xie, Z., Lee, E., Lucas, J. R., Morohashi, K., Li, D., Murray, J. A. H., Sack, F. D., & Grotewold, E. (2010). Regulation of cell proliferation in the stomatal lineage by the Arabidopsis MYB FOUR LIPS via direct targeting of core cell cycle genes. *The Plant Cell*, *22*(7), 2306–2321.

Yamaguchi, N., Wu, M.-F., Winter, C. M., Berns, M. C., Nole-Wilson, S., Yamaguchi, A., Coupland, G., Krizek, B. A., & Wagner, D. (2013). A molecular framework for auxin-mediated initiation of flower primordia. *Developmental Cell*, *24*(3), 271–282.

Yamori, W., Hikosaka, K., & Way, D. A. (2014). Temperature response of photosynthesis in C3, C4, and CAM plants: temperature acclimation and temperature adaptation. *Photosynthesis Research*, *119*(1-2), 101–117.

Yang, K., Wang, L., Le, J., & Dong, J. (2020). Cell polarity: Regulators and mechanisms in plants. *Journal of Integrative Plant Biology*, *62*(1), 132–147.

Yang, K.-Z., Jiang, M., Wang, M., Xue, S., Zhu, L.-L., Wang, H.-Z., Zou, J.-J., Lee, E.-K., Sack, F., & Le, J. (2015). Phosphorylation of Serine 186 of bHLH Transcription Factor SPEECHLESS Promotes Stomatal Development in Arabidopsis. *Molecular Plant*, *8*(5), 783–795.

Yang, X., Cushman, J. C., Borland, A. M., Edwards, E. J., Wullschleger, S. D., Tuskan, G. A., Owen, N. A., Griffiths, H., Smith, J. A. C., De Paoli, H. C., Weston, D. J., Cottingham, R., Hartwell, J., Davis, S. C., Silvera, K., Ming, R., Schlauch, K., Abraham, P., Stewart, J. R., … Holtum, J. A. M. (2015). A roadmap for research on crassulacean acid metabolism (CAM) to enhance sustainable food and bioenergy production in a hotter, drier world. *The New Phytologist*, *207*(3), 491–504.

Yu, H., Chen, X., Hong, Y.-Y., Wang, Y., Xu, P., Ke, S.-D., Liu, H.-Y., Zhu, J.-K.,

Oliver, D. J., & Xiang, C.-B. (2008). Activated expression of an Arabidopsis HD-START protein confers drought tolerance with improved root system and reduced stomatal density. *The Plant Cell*, *20*(4), 1134–1151.

Zhang, D., Spiegelhalder, R. P., Abrash, E. B., Nunes, T. D. G., Hidalgo, I., Anleu Gil, M. X., Jesenofsky, B., Lindner, H., Bergmann, D. C., & Raissig, M. T. (2022). Opposite polarity programs regulate asymmetric subsidiary cell divisions in grasses. *eLife*, *11*, e79913.

Zhang, J.-Y., He, S.-B., Li, L., & Yang, H.-Q. (2014). Auxin inhibits stomatal development through MONOPTEROS repression of a mobile peptide gene STOMAGEN in mesophyll. *Proceedings of the National Academy of Sciences of the United States of America*, *111*(29), E3015–E3023.

Zhang, Y., Wang, P., Shao, W., Zhu, J.-K., & Dong, J. (2015). The BASL polarity protein controls a MAPK signaling feedback loop in asymmetric cell division. *Developmental Cell*, *33*(2), 136–149.

Zhao, L., & Sack, F. D. (1999). Ultrastructure of stomatal development in Arabidopsis (Brassicaceae) leaves. *American Journal of Botany*, *86*(7), 929–939.

Zoulias, N., Harrison, E. L., Casson, S. A., & Gray, J. E. (2018). Molecular control of stomatal development. *Biochemical Journal*, *475*(2), 441–454.

Zuch, D. T., Herrmann, A., Kim, E.-D., & Torii, K. U. (2023). Cell cycle dynamics during stomatal development: Window of MUTE action and ramification of its loss-of-function on an uncommitted precursor. *Plant & Cell Physiology*, *64*(3), 325−335.